THE EFFECTS OF FLOTATION VARIABLES ON THE BUBBLE SIZE, MIXING CHARACTERISTICS AND FROTH BEHAVIOUR IN COLUMN FLOTATION CELLS

BY

CRAIG MICHAEL GOODALL

DEPARTMENT OF CHEMICAL ENGINEERING

A dissertation submitted to the Faculty of Engineering, University of Cape Town, in fulfillment of the requirements for the Degree of Doctor of Philosophy.

August 1992

DECLARATION

I hereby declare that, unless otherwise indicated, all the work in this dissertation was done by myself and that this dissertation has not been submitted to this or any other institution of learning in support of an application for any other degree or qualification.

Signed

C. M. Goodall

August 1992

DEDICATION

To my parents, Rob and Evol, for their love, support and friendship.

ACKNOWLEDGEMENTS

The author would like to express his sincere thanks to the following people:

Prof. Cyril O'Connor, my supervisor, for hours of invaluable discussions, numerous helpful suggestions, and for proofreading this dissertation. His energy and enthusiasm were a great inspiration;

Mr Bill Randall of the Chemical Engineering Department for designing and building the bubble sizing equipment used in this study;

Mr Tony Barker and Mr Rob Senekal of the Chemical Engineering Department for making most of the equipment used in this study;

The column flotation group at the University of Cape Town for their input into this project;

Dr Wolter te Riele of Mintek for his suggestions and keen interest.

The President of Mintek for allowing me to do this project and for providing financial support.

Mr Schalk Smith and the staff of the Atomic Energy Corporation for their help in conducting the residence time distribution studies;

Prof Tony Bryson of the University of the Witwatersrand for his suggestions about the mathematical modelling;

My family for their continued interest, encouragement and all the opportunities they have given me.

SYNOPSIS

Column flotation has only come into vogue in the last decade, and in the last five years there has been a dramatic increase in the number of plant installations on mines throughout the world. Due to the heightened interest in this technology it is important that the factors influencing the performance of column flotation cells be properly quantified. Most of the column studies to date have focused on the pulp zone, while far less work has been done on the froth zone. There are conflicting views about the importance of various froth parameters. For example, some researchers hold that froth depth is of little importance, while others have found it to be crucial. The aim of this study was to examine the processes occurring in the column as a whole, but to put special emphasis on the froth zone.

With respect to the pulp zone, a system was developed for measuring the bubble size distribution in the pulp. It involved detecting about 3000 bubbles as they were sucked up a glass capillary tube past two optical detectors. The accuracy of the system was found to be excellent, and the number of bubbles sized made the distributions statistically meaningful. Bubble size tests were conducted in a small laboratory column cell in both water and pulp. The trends for the two- and three-phase systems were the same, although the bubbles in the pulp tests were generally bigger than those in water. It was found that factors which led to a decrease in the viscosity or surface tension in the pulp resulted in smaller bubbles. This was because the size of a bubble is determined by the rate at which a film of water can form around a pocket of air, which is directly influenced by the viscosity and surface tension of the pulp.

Residence time distribution studies of the collection zone were conducted in a laboratory column flotation cell using both liquid and solid tracers. The liquid tracer studies showed that the residence time distributions in the pulp zone were hardly affected by the presence of solids in the column. When the solid tracer was used, however, it was found that there was a significant difference between the residence time distributions of the solid and liquid phases. The solids were significantly more mixed than the liquid and they had a shorter mean residence time. It was found that the residence time distributions in the pulp could be adequately modelled using a simple tanks-in-series model. The axial dispersion model was not used because

some of the D/uL values found in this study were too large for the model assumptions to be valid. It was generally found that flotation parameters which led to an increase in the mean residence time in the pulp also led to a decrease in the degree of mixing in the column.

The effects of various flotation parameters on the behaviour of the froth zone were examined using froth stability tests and by splitting the froth at various levels. The stability of the froth was determined by the maximum froth height achieved in a small batch column. A system was developed to split the froth into four horizontal segments so that the froth could be examined at different levels. This system was used on both a batch and a continuous column and it allowed data to be obtained on the grade, the recovery, the solids and water mass pull, the air hold-up, and the particle size distribution as a function of height in the froth.

The froth stability tests showed that it is a combination of the particle size and hydrophobicity that determine the stability of the froth. The stability of the froth increased as the particle size decreased because there were more particles available to inhibit froth drainage and bubble coalescence. It was also found that the froth stability passed through a maximum as the xanthate collector dosage was increased. The optimum collector dosage depended on the collector chain length and the particle size. The hydrophobicity of the particles increased as the collector chain length and dosage increased. As the particle size increased the particles needed to be more hydrophobic to produce the same froth stability.

A fine synthetic ore comprising 90 percent quartz and 10 percent pyrite was used in the batch froth splitting tests. It was found that the coarser pyrite tended to float first with little entrained material reporting to the top of the froth, and the amount of entrained material in the froth increased towards the bottom of the froth. Ultra-fine pyrite (<10 μm) was concentrated at the bottom of the froth indicating that this material was either entrained or slow floating. It was again found that there was an optimum collector type and concentration to achieve the best grades and recoveries caused by poor collection on one hand and the froth being too tightly packed for selective flotation on the other hand. It was found that froth stability played an important role in determining the final grades and recoveries. If the froth was too stable then elutriation of entrained material from the froth was

difficult, and if it was not stable enough then floated material was lost due to bubble coalescence in the froth.

In the continuous froth cutting tests the synthetic pyrite/quartz ore was again used along with a real gold bearing pyrite ore. The tests were conducted with and without wash water. It was found that the trends observed in the batch tests were generally repeated in the continuous tests with no wash water. Where differences were observed, these could be ascribed to the depletion of pyrite in the batch tests which did not occur in the continuous tests. The addition of wash water made a significant difference to the characteristics of the froth. The froth was stable at much lower frother concentrations and the amount of bubble coalescence was greatly reduced. There was a far more uniform grade profile through the froth and a significant reduction in the amount of entrained material in all levels of the froth, especially near the bottom.

Residence time distribution studies of the froth zone were conducted using an isotopically labelled flotable solid tracer and a salt solution liquid tracer. The liquid tracer showed that very little of the water in the feed reported to the concentrate. The solid tracer studied showed that the froth zone could not be modelled adequately using a one parameter model and thus a two parameter model was chosen. The model consisted of a perfect plug flow reactor with a recycle stream. The model was chosen because it could model any situation from a completely mixed system to a perfect plug flow system. It was found that the mean residence time in the froth and the plug flow reactor's residence time could be related, and the degree of mixing in the froth and the reactor recycle ratio were also related. These relationships further validated the choice of model because the model parameters could be directly linked to the residence time distribution in the froth. It was again found that factors that increased the mean residence time in the froth also decreased the extent of mixing in the froth. There was a linear increase in the concentrate grade and a linear decrease in concentrate mass pull as the mean residence time in the froth increased. The recovery remained virtually constant. This indicates that the froth zone is responsible to a large extent for the grade in the column, and that longer froth residence times helped reduce the levels of entrained material in the concentrate.

An examination of the effects of flotation parameters on the metallurgical performance of the column showed that the mean residence time in the pulp was most affected by the pulp density and the air rate had the biggest effect in the froth. The volumetric feed rate and the wash water rate had the biggest influence in the degree of mixing in the pulp and froth respectively. The concentrate grade was most affected by the air rate, while the volumetric feed rate had the biggest effect on the mass pull to the concentrate. The recovery tended to pass through an optimum, with the frother concentration having the biggest effect on recovery. The wash water rate had a large effect on the mean particle size in the concentrate.

TABLE OF CONTENTS.

LIST OF FIGURES.

LIST OF TABLES.

LIST OF PUBLICATIONS.

GOODALL, C.M. BARKER, A.M. and O'CONNOR, C.T., 1988. *Investigation of a Pyrite-Quartz Flotation Froth by use of a Novel Froth Splitting Apparatus.*, Int. J. Miner. Process., Vol. 24, pp 307 - 317.

GOODALL, C.M., RANDALL, E.W. and O'CONNOR, C.T., 1988. *The Effect of Physical and Chemical Variables on Bubble Sizes in a Laboratory Column Cell.*, S. Afr. Instn. Chem. Engrs. Meeting., Johannesburg, South Africa, August.

RANDALL, E.W., GOODALL, C.M., FAIRLAMB, P.M., DOLD, P.L. and O'CONNOR, C.T., 1989. *A Method of Measuring the Sizes of Bubbles in Two- and Three-Phase Systems.*, J. Phys. E. Sci. Instrum., Vol. 22, pp 827 - 832.

GOODALL, C.M. and O'CONNOR, C.T., 1989. *Residence Time Distribution Studies of the Solid and Liquid Phases in a Laboratory Column Flotation Cell., Developments in Froth Flotation.*, S. Afr. Instn. Min. Metall. Int. Colloq., Vol. 2, Gordon's Bay, Cape Town.

O'CONNOR, C.T. RANDALL, E.W. and GOODALL, C.M., 1990. *Measurement of the Effects of Physical and Chemical Variables on Bubble Size.*, Int. J. Miner. Process., Vol. 28, pp 139 - 149.

GOODALL, C.M. and O'CONNOR, C.T., 1990. *Residence Time Distribution Studies of the Solid and Liquid Phases in a Laboratory Column Flotation Cell.*, SME Annual Meeting, Salt Lake City, Utah, February 26 - March 1, Preprint No. 90-609.

RANDALL, E.W., GOODALL, C.M. and O'CONNOR, C.T., 1990. *The Measurement of Bubble Size in an Air Agitated System.*, Minerals, Materials and Industry, 14th CMMI Cong., London, July, pp 103 - 107.

GOODALL, C.M. and O'CONNOR, C.T., 1991. *Pulp-Froth Interactions in a Laboratory Column Flotation Cell.*, Miner. Engng., Vol. 4., Nos. 7 - 11, pp 951 - 958.

GOODALL, C.M. and O'CONNOR, C.T., 1991. *Residence Time Distribution Studies in a Flotation Column. Part I : The Modelling of Residence Time Distributions in a Laboratory Column Flotation Cell.*, Int. J. Miner. Process., Vol. 31, pp 97 - 113.

GOODALL, C.M. and O'CONNOR, C.T., 1992. *Residence Time Distribution Studies in a Flotation Column. Part II : The Relationship Between Solids Residence Time Distribution and Metallurgical Performance.*, Int. J. Miner. Process., In Press.

Chapter 1

INTRODUCTION

1.1 BACKGROUND TO COLUMN FLOTATION

Several different flotation machines have been classified as "column flotation cells". These include:

- the conventional or Canadian column (Boutin and Wheeler, 1967);
- the Bahr cell (Bahr, 1982);
- the Flotaire column (Zipperian and Svenssen, 1988);
- the packed column (Yang, 1988);
- the WEMCO/Leads column (Degner and Sabey, 1988);
- the Jameson column (Jameson, 1988);
- the Hydrochem column (Schneider and Van Weert, 1988); and
- the air sparged hydrocyclone (Ye et al., 1988).

In this study only conventional column cells are considered. The flotation column concept (Canadian or conventional column) was patented in the early 1960s by Boutin and Tremblay (Canadian patents 680,575 and 694,547). A diagramatic layout of this type of column is shown in Figure 1.1. Column cells were initially used to separate silica from iron ore by reverse flotation, and later to recover sulphides in copper flotation (Wheeler, 1988). The initial attempts at scale-up were unsuccessful and resulted in the mining industry being sceptical about the viability of column cells.. This caused a temporary halt in column flotation research due to lack of funds. In 1980, after many years of research, Mines Gaspé were persuaded to order two columns for use on their by-product molybdenum circuit. These columns had diameters of 46 and 91 cm and proved to be very successful. This success led to several other mines installing flotation columns. Table 1.1

details some of the column applications in various places throughout the world. It can be seen that the use of columns is widespread and covers many different flotation operations. Canada is the leading user of columns in the world at the moment, probably because columns were developed in Canada. The mining industry is conservative by nature, and it is only in the last few years that columns have been proven. From Table 1.1 it is evident that there has been a large increase in the number of full scale columns being used on mines from 1988 to 1991 and column circuits are beginning to replace conventional installations in some applications.

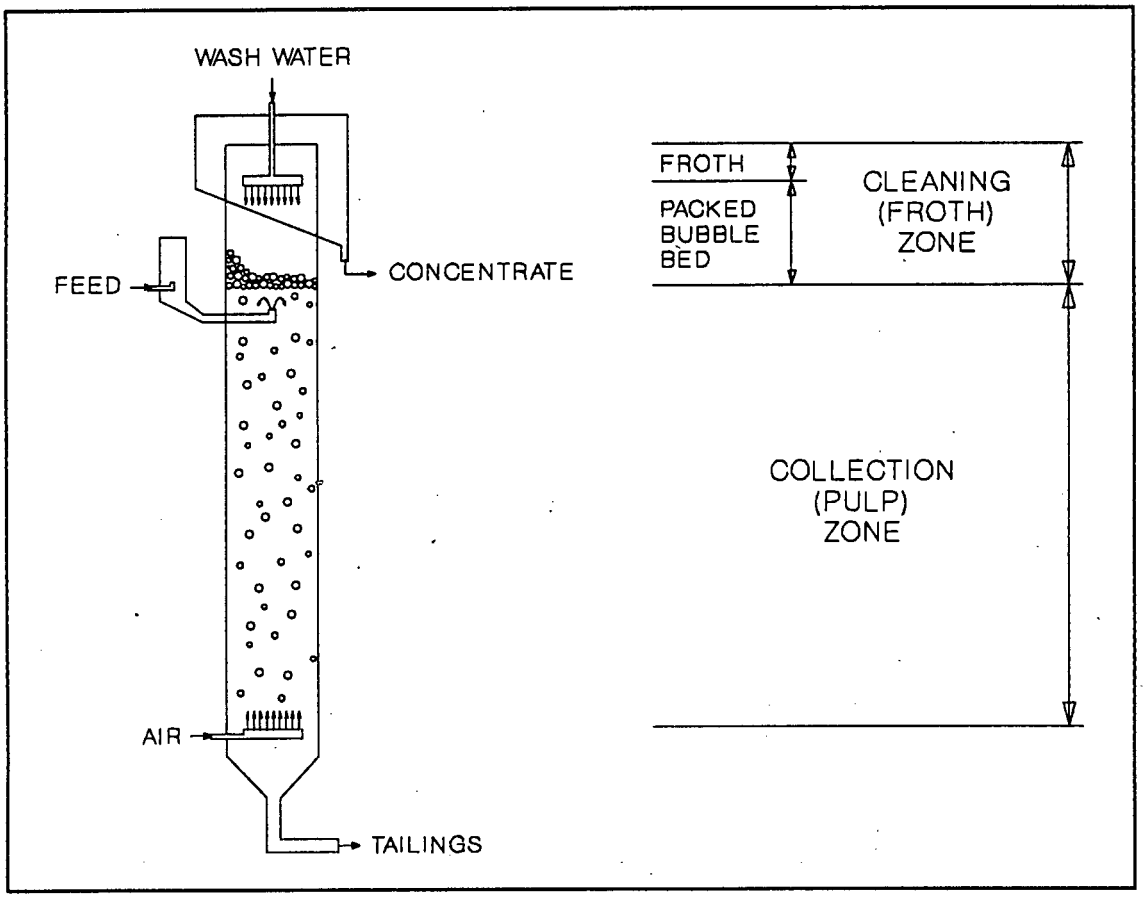

FIGURE 1.1 : Diagramatic Layout of a Column Flotation Cell.

A diagram of a column flotation cell is shown in Figure 1.1. Flotation columns are characterized by two main zones, the collection (pulp) zone and the cleaning (froth) zone. In the collection zone there is counter-current contact between the bubble swarm from the bottom of the column and the feed which is introduced about one third of the way down the column. The floatable material is collected by the bubble swarm and is carried into the cleaning zone and the tailings leave through the bottom of the column. The

TABLE 1.1 : Some Column Applications

COUNTRY/MINE/INSTITUTION	MINERAL	COLUMN DIAMETER	SCALE	REFERENCE
AUSTRALIA				
Riverside Mine	Coal	1.70 m	Plant	Nicol et al. (1988)
Harbour Lights	Gold Sulphide	0.11 m	Pilot	Subramanian et al. (1988)
Mount Isa Mines	Copper/Lead/ Zinc	0.05 m	Pilot	Espinosa-Gomez et al. (1988)
Peak Gold	Sulphide Ore	0.10 m	Pilot	Alford et al. (1991)
Mount Isa Mines	Copper/Lead/ Zinc	2.50 m	Plant	Espinosa-Gomez et al. (1991)
BRAZIL				
Carbonifera Criciuma	Coal	0.05 m	Pilot	Oliveira and Peres (1991)
Samarco Mineração S.A.	Iron Ore	3.65 m	Plant	Viana et al. (1991)
Mineração Mantati Ldda.	Copper	0.60 m	Plant	Reis and Peres (1991)
CANADA				
Mines Gaspé	Moly	0.91 m	Plant	Wheeler (1988)
Gibraltar Mines Ltd.	Moly	0.51 m	Plant	Moon and Sirois (1988)
Brunswick Mining and Smelting Corp. Ltd.	Zinc	1.80 m	Plant	Moon and Sirois (1988)
GECO, Manitouwadge	Copper	0.90 m	Plant	Moon and Sirois (1988)
Polaris	Zinc/Lead	0.60 m	Plant	Egan et al. (1988)
Sulivan Mine	Zinc/Lead	0.30 m	Pilot	Egan et al. (1988)
Falconbridge Strathcona	Copper/Nickel	0.15 m	Pilot	Furey and Moon (1991)
Highland Valley	Copper	0.15 m	Pilot	Furey and Moon (1991)
Falconbridge Strathcona	Copper/Nickel	2.10 m	Plant	Huls et al. (1991)
Les Mines Selbaie	Copper/Zinc	0.05 m	Pilot	Del Villar et al. (1991)
Les Mines Camchib Inc.	Copper	0.06 m	Pilot	Laohapanit et al. (1991)
Ruttan Operation, Hudson Bay Mining	Zinc	0.91 m	Pilot	Webber at al. (1991)
Matagami	Copper/Zinc	1.20 m	Pilot	Ounpuu and Tremblay (1991)
Coal Research Laboratories	Coal	0.76 m	Pilot	Salama et al. (1991)
Faro, Curragh Resources Inc.	Lead/Zinc	3.60 m	Plant	Beaumont et al. (1991)
Sulivan Mine	Zinc/Lead	2.40 m	Plant	Bromley et al. (1991)
CHILLE				
Cia Minera Punta del Talca	Gold	0.05 m	Pilot	Ugarte and Reinoso (1991)
Cuajone	Copper/Moly	1.22 m	Pilot	Amelunxen et al. (1988)
Las Cenizas	Copper	0.10 m	Pilot	Bergh and Yianatos (1991)
Compañía Minera Disputada de Les Condes	Pyrite	0.91 m	Plant	Yianatos and Bergh (1991)
FRANCE				
Chessy	Copper/Zinc	0.06 m	Pilot	Morizot et al. (1991)
JAPAN				
Toyoha Mines	Lead/Zinc	2.70 m	Plant	Hirajima et al. (1991)
INDIA				
Bhojudih Washery	Coal	0.22 m	Lab	Narasimhan et al. (1988)
NORWAY				
Sydvaranger at Kirkens	Silica	2.45 m	Plant	Sandvik et al. (1991)
SOUTH AFRICA				
Durnacol	Coal	0.30 m	Pilot	Gorzitzke and MacPhail (1989)
Unisel	Pyrite	0.05 m	Lab	Goodall and O'Connor (1989)
Rooiberg	Tin	0.09 m	Pilot	Harris and Franzidis (1989)
University of Cape Town	Coal	0.10 m	Pilot	Franzidis et al. (1991)
University of Cape Town	Gold Residues	0.10 m	Pilot	Franzidis et al. (1991)
University of Cape Town	Platinum	0.10 m	Pilot	Franzidis et al. (1991)
Northam Platimum Mine	Platinum	1.0 m	Plant	O'Connor (1991)
Pering Mine	Lead/Zinc	1.2 m	Plant	Norton (1991)
President Steyn Mine	Gold	1.0 m	Plant	O'Connor (1991)
Palaborwa Mining Company	Copper	0.5 m	Pilot	O'Connor (1991)
Mintek	Gold Residue	0.15 m	Pilot	Burger (1991)
SPAIN				
Apirsa	Zinc	2.40 m	Plant	Bolin and Söderberg (1991)
SWEDEN				
Laisvall	Zinc	0.45 m	Pilot	Bolin and Söderberg (1991)
Aitik	Copper	3.00 m	Plant	Bolin and Söderberg (1991)
Boliden	Zinc	1.70 m	Plant	Bolin and Söderberg (1991)
TURKEY				
Etibank Üçköprü	Chromite	0.07 m	Pilot	Güney et al. (1991)
USA				
Red Dog	Zinc/Lead	0.10 m	Pilot	Egan et al. (1988)
Elkhorn	Coal	0.05 m	Lab	Luttrell et al. (1988)
Oracle Peak	Copper	1.52 m	Plant	Olsen and Meik (1991)
Red Dog	Zinc	2.70 m	Plant	Bromley et al. (1991)
ZAMBIA				
Nchanga Mine	Copper	1.83 m	Plant	Chowdhury et al. (1991)
Zambia Consolidated Mines	Copper	0.05 m	Pilot	Smithson et al. (1991)

cleaning zone consists of an expanded bubble bed below the wash water system and a conventional froth above it. The wash water creates a downward (positive) bias in the froth zone which prevents hydraulic entrainment of gangue material into the concentrate. The wash water also stabilizes the froth zone. Column flotation cells often produce better grades than mechanical flotation cells due to this froth washing (Yianatos, 1989).

Flotation columns are distinguished from mechanical flotation cells by three major differences, viz: firstly the wash water system, secondly the aeration system and thirdly there is no mechanical agitation.

Column flotation cells owe their popularity to a number of factors (Yianatos, 1989), viz:

- they are easy to maintain as there are no moving parts to wear and the spargers can usually be replaced without shutting down the column;
- they are cheaper to run than mechanical cells because there is no power required to agitate the pulp and often the same results can be achieved at lower reagent dosages;
- one column may often achieve the same, or better results than a whole bank of mechanical cells;
- the floor space required for columns is considerably less than that required for a comparable mechanical installation;
- columns are generally better controlled than mechanical cells because good control is essential if columns are to produce good results;
- column cells can be used to treat systems with fine particles and high pulp densities because of their efficient cleaning action;
- the design and construction of columns is relatively simple leading to savings in capital costs; and
- scale-up from pilot plant to plant scale columns is far easier than with mechanical cells because there is a single three-dimensional froth and steady state laboratory tests are possible.

1.2 REVIEW OF COLUMN FLOTATION TECHNOLOGY

Column flotation technology can be classified into three main groups, viz: column variables, column modelling and scale-up and column control.

1.2.1 COLUMN VARIABLES

Possibly the most important group of column variables are those associated with the generation of the bubbles because almost all of the column parameters are affected by these variables. The two major variables in this group are the air rate and the sparger system. The air rate is usually given as a superficial velocity for easy comparison between columns of different sizes.

The medium of transport of particles from the pulp into the concentrate is the surface of the bubbles. The amount of bubble surface area available for flotation is determined by a combination the bubble size and the air flow rate. The bubble size is influenced by the air flow rate and the sparger type. Dobby and Finch (1986a, 1986b) have shown that there is optimum air flow rate for the collection of particles, and this is the air rate at which the carrying capacity of the column is at its maximum. Low air rates lead to a decrease in total bubble surface area. Clingan and McGregor (1987) have shown that grade and recovery can be adversely affected at high air flow rates. Espinosa-Gomez et al. (1988) found that the air rate had little effect on the performance of the column over a wide range of superficial air velocities (1.5 - 3.5 $cm \cdot s^{-1}$).

Bubble size is of critical importance to the performance of the column since it affects the gas hold-up, the fluid flow regime in column and the collection efficiency of the bubbles (Dobby and Finch, 1986b). Luttrell et al. (1988) have shown that small bubbles improve the performance of column cells. Bubble sizes have been measured in column cells (Tucker et al., 1991; Zhou et al, 1991) and it has been found that frother concentration has a significant effect on both bubble size and bubble rise velocity. An optimum bubble size for column cells of between 0.4 and 0.8 mm has been suggested by Dobby and Finch (1986a).

Column spargers can be divided into two groups, internal (e.g. filter cloth sparger) and external (e.g. US Bureau of Mines sparger) spargers. More detail about these sparger types is given in section 2.2.3. The external spargers are generally better because the bubble size can be controlled independently of the air flow rate. With the internal spargers the bubble size increases as the air rate increases. Dobby and Finch (1986a) state that column spargers should be designed to produce small bubbles at high velocities.

Air hold-up in the collection zone is important because it affects the residence time of the particles and the collection efficiency. Factors which affect air hold-up are the air rate, the bubble size, the pulp density and the bubble loading (Yianatos, 1989).

Wash water is added near the top of the froth to maintain a positive bias in the column and to stabilize the deep froth. The net downward flow of water through the froth has been shown to be very effective in reducing hydraulic entrainment of gangue (Yianatos et al., 1987). Typical superficial wash water rates are about 0.3 to 0.5 $cm \cdot s^{-1}$. Lower wash water rates lead to poor froth washing with a resultant decrease in grade and higher wash water rates are counter-productive because they lead to increased mixing in the froth with severe channelling and recirculation. Yianatos et al. (1986a) state that it is important to maintain an even distribution of water across the whole froth and to avoid jetting. In order to achieve this the design of the wash water distributor is very important. The wash water distributor may be located above or just below the surface of the froth. If it is located above the froth surface then an increased wash water rate is required to maintain the downward bias because much of the water reports directly to the concentrate, but it is easy to achieve a gentle, even distribution of water. Wash water distributors located below the froth surface require less wash water but distribution is more difficult and the distributor may interfere with the flow of froth (Finch and Dobby, 1990). The increased water hold-up in the froth caused by the addition of wash water stabilizes the froth by inhibiting bubble coalescence.

The height of the column determines the retention time of the slurry in the column (Ynchausti et al., 1988b) and Luttrell et al. (1988) have shown that increasing the column height leads to better column performance. The

fluid flow regime in the collection zone is determined to a large extent by the column height-to-diameter ratio. Yianatos et al. (1988b) show that there is an optimum column height-to-diameter ratio. Below this value the increase in mixing in the collection zone limits the recovery and above this value the carrying capacity of the column becomes limiting and no benefit is gained from the increased height. Ounpuu and Tremblay (1991) state that column heights are often determined by arbitrary constraints like the roof or crane height and hence many columns are taller than necessary. Large columns are generally baffled vertically into several sections which effectively increases their height-to-diameter ratio and decreases the extent of mixing in the collection zone (Moys et al., 1991).

The carrying capacity of a column is determined mainly by the froth zone and can be defined, for a given set of conditions, as the solids rate entering the froth at which maximum rate of concentrate production occurs. Column carrying capacity is defined in units of mass per unit area and has been found to be relatively independent of column size for columns up to 1 m in diameter (Finch and Dobby 1990). For larger columns the lip loading capacity (maximum rate of concentrate production per unit length of column lip) becomes limiting and it is often necessary to install internal launders to increase the lip length of the column (Amelunxen, 1991). The major factors that affect the carrying capacity of a column are the particle size and pulp density. Air rate has been found to have a relatively small affect on carrying capacity because an increase in air rate is usually accompanied by an increase in bubble size. These two effects cancel each other out and there is little change in bubble surface area (Finch and Dobby, 1990). Espinosa-Gomez et al. (1988) found the froth depth had a significant effect on the carrying capacity of a column, with a decrease in recovery being observed as froth height increased.

The froth zone in a column is usually much deeper and more hydrated than the froths found in mechanical cells. No general rules regarding froth depth seem to have been developed, except that they are usually deeper than 1 m in industrial scale columns (Yianatos, 1989). Again the froth height-to-column diameter ratio is important in determining the degree of mixing in this zone with deeper froths having a more plug flow behaviour (Yianatos, 1987). Ynchausti et al. (1988b) have found that most of the cleaning in the column occurs at the pulp-froth interface due to the downward

bias in the column and the sudden deceleration of the bubbles at the bottom of the froth.

The stability of the froth increases as the liquid hold-up in the froth increases. Woodburn et al. (1989) showed that froth stability was a strong function of residual surfactant concentration, and Yianatos et al. (1986) showed that liquid hold-up in the froth was affected by wash water rate, liquid drainage rate and froth bubble size. Pal and Masliyah (1990) showed that the froth drainage flux in the froth was a function of the liquid hold-up in the froth.

Models for the processes occurring in column froths are generally modifications of models proposed for conventional froths. Yianatos et al. (1988a) propose a procedure for quantifying the froth based on the model proposed by Moys (1984) and Ross and Van Deventer (1988) have extended their computer model of mass transport in the froth (Ross, 1988) to cover the deeper more hydrated froths found in columns. Temperature profiles were used by Moys and Finch (1988) and by Fairweather and Egan (1991) to quantify mixing in the froth phase. Falutsu and Dobby (1989) used a modified column to isolate the froth phase and measure froth dropback.

A list of typical column flotation design and operating conditions are given below (Finch and Dobby, 1990):

Superficial Air Rate	: 1 - 3 $cm \cdot s^{-1}$
Superficial Pulp (Slurry) Rate	: 0.3 - 1.2 $cm \cdot s^{-1}$
Superficial Wash Water Rate	: 0 - 0.4 $cm \cdot s^{-1}$
Superficial Bias Rate	: -0.05 - 0.2 $cm \cdot s^{-1}$
Froth Depth	: 50 - 120 cm
Average Bubble Size	: 0.05 - 0.2 cm
Height-to-Diameter Ratio	: $\geq$ 10:1

1.2.2 COLUMN MODELLING AND SCALE-UP

Luttrell et al. (1988) states that the three most important factors in the scale-up process are the mixing characteristics of the column, the residence time of the particles in the column and the kinetic rate constants. In the

first attempt to model the column flotation cell Sastry and Fuerstenau (1970) used an axial dispersion model to account for the mixing of both the air and the slurry. The model was of limited value because the froth phase was not considered and no wash water addition was taken into account. Dobby and Finch (1986b) developed the first useful scale-up methodology considering both the collection and cleaning zones. Kinetic data is obtained from laboratory column tests and the mixing in the collection zone is accounted for using the axial dispersion model. This model accounts for both the collection zone and the cleaning zone recoveries as well as the effects of overloading the bubbles.

Much work has been done on the mixing in the collection zone. In most cases the mixing of the solids and the liquid are assumed to be equivalent. Laplante at al. (1988) improved on Dobby and Finch's (op. cit.) model by taking into account the solids concentration. Xu and Finch (1991b) further improved on this model by accounting for the superficial liquid velocity, and Xu and Finch (1991a) reviewed the use of the axial dispersion model and found that it is an appropriate model for the collection zone as long as the boundary conditions are correctly identified.

Goodall and O'Connor (1989, 1991) used a flotable isotopically labelled tracer in a laboratory column and found that the mixing in the collection zone could be modelled using a tanks-in-series model. Mavros et al. (1989) modelled the collection zone using a tanks-in-series model with backmixing between stages and found that the dispersion coefficient was too high to use the axial dispersion model. Mills and O'Connor (1990) in their review of mixing in column cells found that many of the early correlations used for flotation columns were based on the mixing characteristics found in bubble columns under different conditions and hence are not applicable. They also found that the solid and liquid phase mixing were not equivalent. Yianatos and Bergh (1991) conducted a series of tests in an industrial scale column cell using isotopically labelled gangue of different particle sizes and a radio-active solution as tracers. They found that the mixing in the collection zone was a function of particle size. More detail on the mixing in the collection zone is given in section 2.2.5.

The column diameter is chosen to accommodate the required feed flow rate and the column length to achieve the required residence time in the

collection zone. The air hold-up is also important in determining the particle residence time as it affects the effective volume of the column. The hindered settling velocity of the particles (a function of particle size and density) combined with the effective volume of the collection zone, the liquid mixing and tailings flowrate are generally used to estimate the residence time of the particles (Yianatos, 1989a).

Dobby and Finch (1986b) attempted to measure collection zone rate constants by running the column at a very high bias with a very shallow froth thus eliminating the cleaning zone and preventing entrainment and the drop-back of floated particles into the collection zone. The collection zone recovery was then found and an estimate of the cleaning zone recovery was made to arrive at the recovery for the overall system. The recovery in the cleaning zone was generally estimated to be 100 %. Two shortcomings of this method were that the high bias was not effective in eliminating hydraulic entrainment and the recovery in the cleaning zone was difficult to measure.

In subsequent studies Yu and Finch (1990) have estimated the froth zone recovery from the collection zone recovery and the overall recovery. They found froth zone recoveries of less than 50 %. Falutsu and Dobby (1989) used a different method to estimate the recovery in the froth zone and got similar results.

The other common method used to estimate the rate constants in the column is to use the recovery of the column as a whole as the collection zone recovery. This gives conservative values for the rate constants. Scale-up parameters and methodology for the froth zone are still not well defined (Yianatos 1989a).

Contini et al. (1988) have developed a method for estimating the rate constants for a particular flotation system in a laboratory column cell. A combination of co-current and counter-current tests are used to obtain the rate constant for flotation. Mular and Musara (1991) use a batch recycle column in which the tailings are continuously recycled to the feed to measure flotation rate constants. Burger (1989) has developed a model for the air hold-up and concentration profiles of flotable and non-flotable species in the

collection zone for different particle sizes and densities. This model could be used to estimate rate constants.

The recovery in a column cell is generally estimated as a function of the mixing characteristics in the column, the mean particle residence time and the kinetics of flotation. The kinetics of flotation are generally assumed to be first order (Finch and Dobby, 1990).

Another important consideration in scale-up is the carrying capacity of the column and the lip loading capacity. In the sizing of full scale columns it is vital to ensure that these limits are not exceeded (Amelunxen 1991).

A number of column simulators have been developed for single columns and for column circuits (e.g. Del Villar, 1988; Wilson and Stratton Crawley, 1991; Castillo and Dobby, 1991). These models generally use first order kinetics for particle collection process and correlations for the column carrying capacity, column mixing, particle residence time and other parameters derived from experimental data.

1.2.3 COLUMN CONTROL

In order to achieve efficient cleaning in column flotation cells it is important that there be a net downward flow (positive bias) of water in the froth zone. This is achieved by ensuring that the tailings flowrate is greater than the feed flowrate. There are two ways of achieving this, viz: either maintain a constant positive bias (tailings rate - feed rate) or maintain a constant bias ratio (tailings rate / feed rate) which is greater than 1. Bias ratios of between 1.01 and 1.15 are recommended (Yianatos, 1989). A major problem in setting the bias in the column correctly is the detection of the bias in the froth zone. Moys and Finch (1988) utilised a temperature difference between the feed water and wash water to measure temperature profiles in the froth and from these profiles they could infer the bias in the froth. Bergh and Yianatos (1991) expanded on these tests to include conductivity as a method of obtaining froth profiles.

The other important variable in column control is the level of the pulp-froth interface. It is important to be able to detect and control this level because

it affects the depth of the froth. Several methods of monitoring this level have been used, including floats (Finch and Dobby, 1990), pressure measurements (Kosick et al, 1991), temperature profiles (Moys and Finch, 1988) and conductivity measurements (Moys, 1989). Moys and Finch (1988) suggest that temperature or conductivity measurements are the best methods of detecting the level in the column because they are not affected by changes in air hold-up and pulp density. The level is usually controlled by varying the tailing flowrate. Moys (1989) describes a multi-point conductivity sensor with reference points. in the pulp to account for changes in the feed conductivity (e.g. pH or pulp density). This system would also allow conductivity profiles and hence the froth bias to be measured. This system is superior to temperature measurements because no difference in the feed and wash water temperatures is required and it can easily be incorporated into an overall control strategy.

Several computer based expert systems for column control and simulation have been developed (e.g. Ynchausti et al., 1988a; Sastry and Lofftus, 1988; Lee et al., 1991; Hirajima, 1991; Kossick et al., 1991). These systems are based on correlations obtained from experimental studies or on operator experience and heuristic rules. There is still much work to be done in measuring column variables and understanding their interactions before complete models can be produced. Ynchausti et al. (1988a) point out that process simulation is useful for supervisory control, but the concept of a self controlling column is not feasible at present.

1.3 OBJECTIVES OF RESEARCH

The aims of this study were:

- to quantify the effects of common flotation variables on the sizes of bubbles produced in a column flotation cell, and then to relate the effects of bubble size to the behaviour of both the pulp and froth zones;
- to derive models for the fluid flow regimes in both the pulp and froth zones and to compare these models to the existing models for these zones;

- to compare the mixing of the solid and liquid phases and to determine if the liquid phase mixing could be used to predict the mixing of the solid phase in the collection zone;
- to examine the effects of common flotation variables on the residence time distributions of the solids in both the collection and the cleaning zones;
- to quantify the effects of the residence time distributions of the pulp and froth zones on flotation parameters such as grade, recovery and particle size;
- to identify the processes occurring at different levels in the froth by splitting the froth into four horizontal segments and examining froth parameters such as grade, recovery, air hold-up and particle size as a function of height in the froth;
- to quantify the effects of flotation variables on the structure of the froth; and
- to identify interactions between the pulp and froth zones.

Chapter 2

PULP ZONE EFFECTS

2.1 INTRODUCTION

Of the three zones in flotation columns, the collection zone, the cleaning zone and the froth zone, the most research has been conducted on the collection zone (pulp zone). The processes occurring in this zone are similar to those occurring in conventional flotation cells, and there are the same particle-bubble attachment and entrainment mechanisms. The biggest differences are that the system is less turbulent and there is counter-current contact between the solids and the air.

This chapter addresses two main topics:

- The determination of bubble size in the pulp for both two- and three-phase systems.
- The modelling of the residence time distributions of the liquid and solid phases of the pulp zone.

The aim of the bubble size measurements was to quantify the effects of various common flotation variables such as air rate, pulp density, etc. on the size of bubbles formed in columns and to relate this data to the performance of the flotation system. The bubble size is known to have a significant effect on the attachment of particles to bubbles (Ahmed and Jameson, 1985), the degree of mixing in the system (Finch and Dobby, 1990), the kinetics of flotation (Dobby and Finch, 1987) and the stability of the froth (Ross, 1988).

The aim of the residence time distribution modelling was to propose models for the solid and liquid phases in the collection zone. Several residence time distribution models have been proposed for this zone and most of them estimate the residence time distribution of the solids from that of the liquid

(e.g. Dobby and Finch, 1986b; Yianatos, 1987; Espinosa-Gomez, 1987; Miszczak, 1987). The validity of this assumption is examined, together with the suitability of the existing models.

A discussion of the literature on bubble size and residence time distribution models is followed by a description of the equipment used in these studies and the experimental methods. The results are discussed and a summary of the findings of this section complete the chapter.

2.2 THEORY

2.2.1 BUBBLE SIZE

The importance of bubble size in the efficiency of the flotation process is well known (Dobby and Finch, 1987). Small bubbles are needed to float fine particles. Dobby and Finch (1986a) showed that bubble size was an important variable in flotation column performance. Smaller bubbles led to an increase in the overall bubble surface area, a more stable froth zone and an increase in column carrying capacity. They found that bubbles of the order of 1 mm diameter were optimum.

Bubble size and stability are determined by a stress balance at the air-liquid interface (Jameson, 1984). The factors which contribute to the stresses on a bubble include the liquid viscosity and surface tension. There is often no shape for which the surface forces and the surface tension gradients are in static equilibrium and hence the bubble's form may be constantly changing. For this reason it is difficult to resolve the forces on a bubble into a single resultant force as is possible with a solid particle. This makes the behaviour of the bubbles difficult to predict.

Figure 2.1 shows the changes in the rise velocity of bubbles in water as the diameter of the bubbles changes. It can be seen that the presence of contaminants (surface active materials) even in low concentrations results in a decrease in bubble rise velocity. This effect is most pronounced at small bubble sizes.

The shape of the bubbles changes as the bubble size changes. Small bubbles (< 1 mm) are spherical in appearance and rise with a steady rectilinear motion. From 1 mm to about 18 mm the bubbles are ellipsoidal in appearance and rise in either a helical or zigzag pattern. These irregular patterns result in a decrease in bubble rise velocity because the bubbles have further to travel. The ellipsoidal shape of these bubbles is caused by the inertia of the oncoming liquid which tends to flatten the bubbles. For large bubbles (> 18 mm) the bubbles have a spherical cap with the bottom of the bubble being either flat (in water) or slightly concave (in more viscous liquids). The shape of these bubbles is due to the slightly lower pressure in the bubble wake and the drag forces on the sides of the bubble.

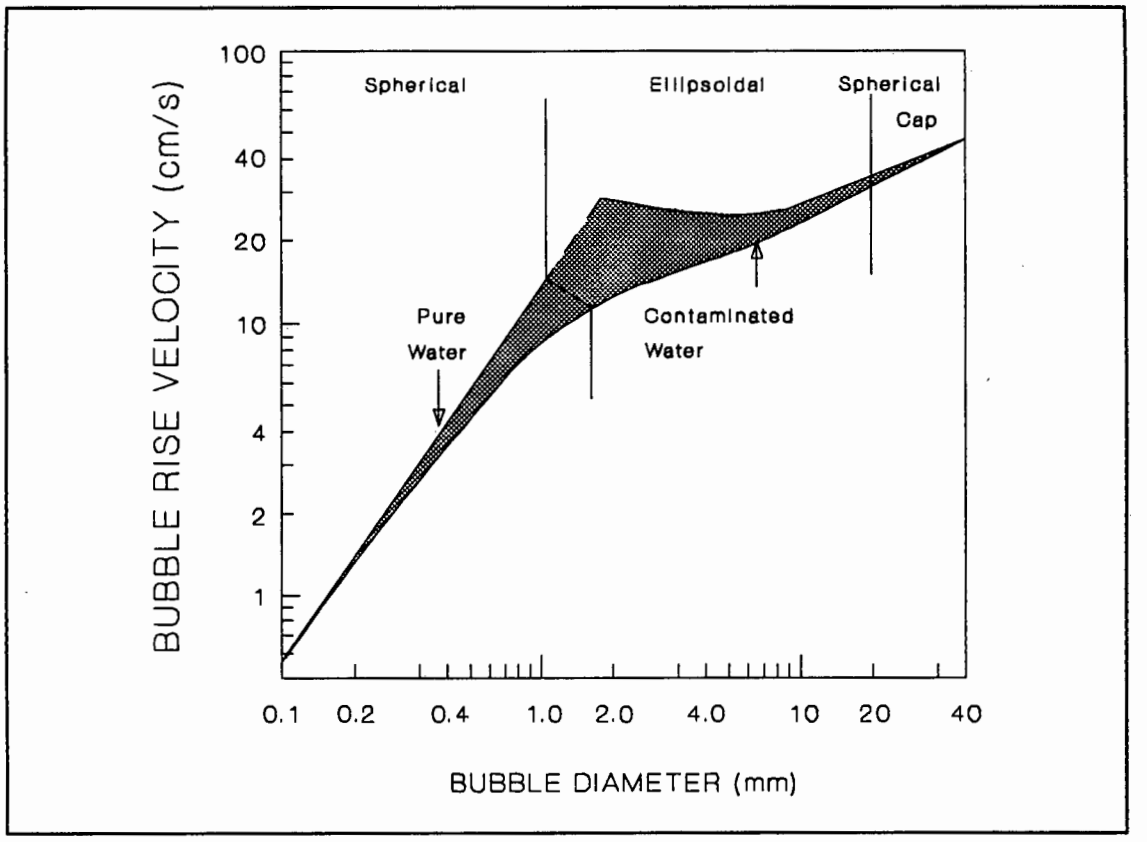

FIGURE 2.1 : The Terminal Velocity of Air Bubbles in Water at 20°C (After Jameson, 1984)

The size of a bubble formed at an orifice in a quiescent system is determined by a balance between the buoyancy forces pulling the bubble up, the surface tension forces holding it at the orifice and the force needed to displace the liquid into which the bubble grows. In more turbulent systems the solution to the force balance becomes more complicated as lateral forces have to be included. Davidson and Schuler (1960a) propose that the bubble volume (V) is a function of the gas flow rate (Q) and the acceleration due to gravity (g) if the surface tension forces are neglected.

$$V = 1.378 \cdot Q^{1.2}/g^{0.6}$$

This equation works well at low flow rates in liquids with low viscosities. As the liquid viscosity (μ) increases the viscous drag plays an increasingly important role until it replaces the inertial term and the equation becomes (Davidson and Schuler, 1960b):

$$V = (4\pi/3)^{1/3} \cdot (15\mu Q/2g)^{3/4}$$

Pryor (1965) states that bubbles of less than 0.5 mm diameter are indiscriminate in their adhering power and tend to promote too stable a froth. If the bubbles are extremely small, they remain in the pulp and cannot lift themselves. An upper limit to the size of the bubbles for efficient flotation is about 3 mm.

In general the size of a bubble in the pulp phase is influenced mainly by the following factors:

- the size of the aperture from which it emerges;
- the hydrostatic head against which it is compressed;
- the surface tension of the air-liquid interface at the point where the bubble is formed;
- the speed of emergence, and the volume and pressure of gas behind it;
- the turbulence of the surrounding pulp.

When a frother is added to the pulp, the surface tension is lowered and the power requirement in mechanical cells is reduced. Bubbles generated in mechanical cells tend to lie between 0.05 and 1.5 mm diameter with the bulk being around 1 mm. Pneumatic spargers (sintered discs, porous rubber mats, filter cloth etc.), without frother, generate bubbles averaging 2.5 to 3 mm diameter.

2.2.2 BUBBLE SIZING METHODS

A number of methods have been described for determining the size of bubbles in two- and three-phase systems. These include, inter alia, photographic techniques, (Miller, 1985) electroresistivity measurements, (Yasumishi et al., 1986), calculations using empirical or semi-empirical correlations, etc. (e.g. Sada et al., 1978; Tsunge et al., 1981).

The most common method of sizing bubbles in column flotation cells is by drift flux analysis (Dobby et al., 1989). The mean bubble size is calculated from the superficial gas and liquid rates (J_g and J_l), the gas hold-up (ε), and the liquid density and viscosity (ρ_l and μ). The case of a two-phase

system is shown below. The bubble size is varied until the velocity of the gas relative to the liquid (u_{sg}) is equal for the two equations below:

$$u_{sg} = \frac{J_g}{\varepsilon} \pm \frac{J_l}{(1 - \varepsilon)}$$

$$u_{sg} = \frac{g \cdot d_b^2 \cdot \rho_l (1 - \varepsilon)^{m-1}}{18 \cdot \mu (1 + 0.15 \cdot Re_{bs}^{0.687})}$$

i.e.

$$\frac{J_g}{\varepsilon} \pm \frac{J_l}{(1 - \varepsilon)} = \frac{g \cdot d_b^2 \cdot \rho_l (1 - \varepsilon)^{m-1}}{18 \cdot \mu (1 + 0.15 \cdot Re_{bs}^{0.687})}$$

where

$$m = [4.45 + 18(d_b/d_c)] \cdot Re_b^{-0.1} \qquad 1 < Re_b < 200$$

$$m = 4.45 \cdot Re_b^{-0.1} \qquad 200 < Re_b < 500$$

and

$$Re_b = \frac{d_b \cdot u_b \cdot \rho_l}{\mu} \quad \text{and} \quad Re_{bs} = \frac{d_b \cdot u_{sg} \cdot \rho_l}{(1-\varepsilon_g)\mu}$$

This is an iterative procedure because u_{sg} is part of the bubble-slurry Reynolds number (Re_{bs}).

Dunne et al. (1976) pioneered the method used in this work. Bubbles are sucked via a capillary tube inserted into the pulp through a block containing optical sensors. With the aid of a computer, bubble size distributions may be determined in two- and three-phase systems.

2.2.3 BUBBLE GENERATION IN COLUMN CELLS

The sparger systems used in column flotation cells can be broadly classified into two groups, viz: internal and external systems (Finch and Dobby, 1990).

With internal sparger systems the sparger is located inside the column cell. These systems can be classified into two main groups; viz: porous spargers such as sintered glass discs and filter cloth and multinozzle spargers such as perforated steel or rubber plates. Part of the sparger is located outside the column with external sparger systems. These include the US Bureau of Mines (USBM) sparger (McKay et al., 1988), the Cominco Sparger (Tucker et al., 1991) and venturi systems (Sanchez-Pino and Moys, 1991).

Internal sparger systems are generally inferior to the external systems because they can block up with solids and require the column to be shut down for their maintenance. Internal spargers produce a larger range of bubble sizes, they are generally more difficult to control and the mean bubble size is larger for internal sparger systems than for external sparger systems.

The USBM sparger and the Cominco sparger operate on the same principle. Air and water are combined at about 4 bar pressure in some sort of T-piece arrangement and are then introduced into the column via a pipe with a series of small holes (1/16" for the Cominco sparger). High sheer is created at these holes by the shock of the sudden pressure reduction resulting in small bubbles being produced (< 1 mm in diameter). The bubble size produced can be controlled by varying the pressure and the water flow rate to the sparger. Venturi aerators and orifice plates can also be used to produce small bubbles and are commonly used on Jameson Cells (Sanches-Pino and Moys, 1991). These aerators can be used to promote high intensity contact between the air and the slurry and hence increase the rate of flotation. External aerators are generally easy to maintain, and can be removed without shutting the column down.

2.2.4 BUBBLE-PARTICLE INTERACTIONS

The interaction of particles with bubbles can be thought of as two separate systems: Firstly the formation of the bubble-particle agglomerates in the pulp and their subsequent rise into the froth. Secondly the processes occurring in the froth which affects the stability of these agglomerates. These two systems are affected to different degrees by the various flotation conditions.

There are three phases in the attachment of a particle to a bubble (Schulse 1977):

- The approach of the particle to the bubble.
- The thinning of the liquid film between the particle and the bubble.
- The receding of the liquid film to give a solid-air interface.

In general the film thinning stage is the rate determining step.

Jowett (1980) observed that ultra-fine particles (< 10 µm) and coarse particles (> 200 µm) give very poor flotation rates and ultimate recoveries (Figure 2.2). The reasons for this give some insight into the processes occurring in the pulp.

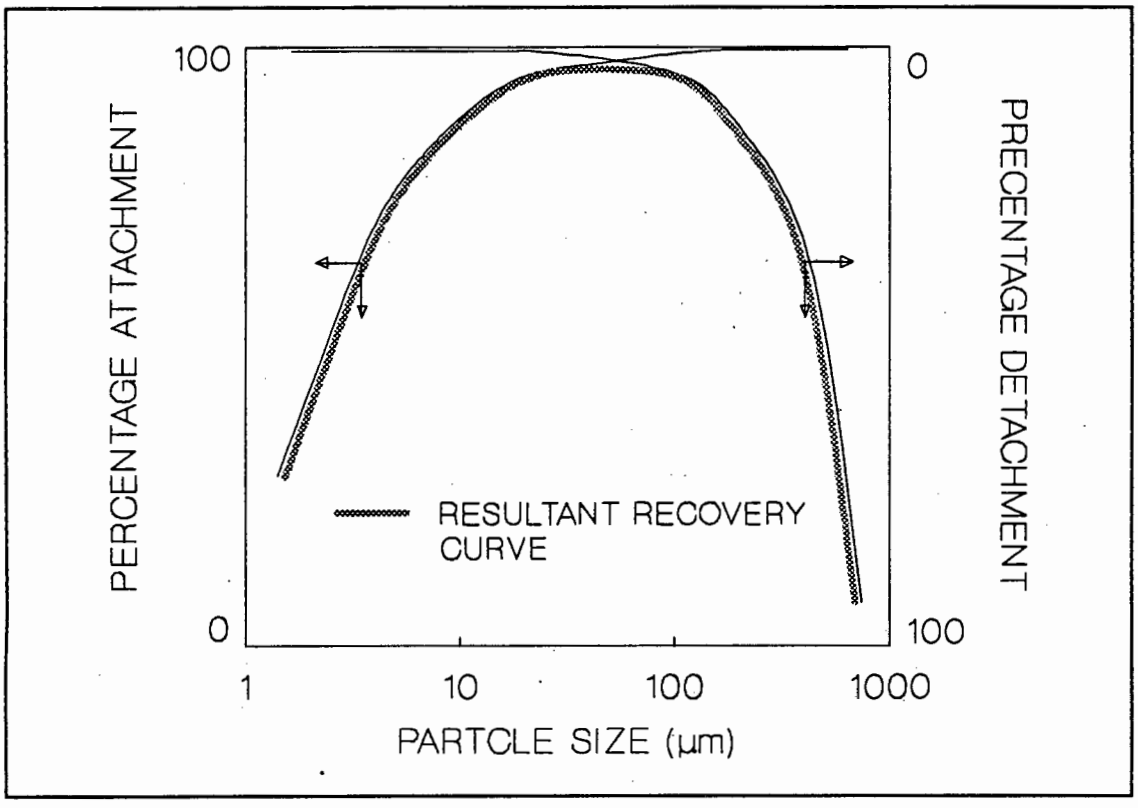

FIGURE 2.2 : Hypothetical Particle-Bubble Attachment and Detachment Curves in Flotation (After Jowett, 1980)

It is generally accepted (King, 1982; Ewers, 1984) that the poor rate of flotation of ultra-fine particles (< 10 µm) is due to decreased opportunity for collision. This is due mainly to the increasing influence of streamlines as the particle size decreases. The ultra-fine particles have little momentum and thus when the fluid stream-lines curve around a bubble the fine particles

remain in these streams and do not come into contact with the surface of the bubble. Since these streamlines are far more pronounced in Stoke's law flow regime than in turbulent conditions and because increasing the turbulence increases the momentum of the particles and bubbles, more turbulent conditions lead to better recovery of these ultra-fine particles.

Several researchers (e.g. Schulze, 1977; King, 1982) have proposed that coarse particles (> 200 μm) have low rates of flotation due to the disruption of the bubble-particle agglomerates by the inertial forces associated with turbulence. Therefore decreasing the turbulence of the system aids the flotation of coarse particles. The best conditions for the flotation of coarse particles on the basis of this proposal are therefore when there is just sufficient agitation to suspend the particles.

It was felt by Kirchberg and Topfer (1964) that a more significant reason for the poor flotation of coarse particles is that few bubble-particle bonds occur on collision of these particles with bubbles. By means of high speed photography Kirchberg and Topfer found that these collisions were elastic. The particles have a relatively high kinetic energy causing the bubbles to deform on collision. The bubbles tend to regain their stable spherical shape almost immediately and the particles rebound preventing a solid-air interface from forming. More turbulent conditions would enhance this effect. It is probable that both the breaking of the bubble-particle agglomerate and the elastic collision mechanisms contribute to the poor recovery of these coarse particles.

The elastic collision mechanism was supported by Ahmed and Jameson (1985) who studied three pure materials all with similar particle sizes: Latex (density 1050 $kg \cdot m^{-3}$), quartz (density 2650 $kg \cdot m^{-3}$) and zircon (density 4560 $kg \cdot m^{-3}$). It was found that the degree of turbulence had a large influence on the rate of flotation of the particles. Increasing the speed of agitation had a far larger effect on the kinetic energy of the zircon particles than the latex particles (a factor of 4.4). It was found that the best rates of flotation for zircon were achieved at low agitation speeds, intermediate speeds were best for quartz and high agitation speeds gave the best results for latex.

Jowett (1980) did a series of tests using galena, sphalerite, pyrite and pentlandite. He disputed the accepted theories for the poor flotation rate of coarse and ultra-fine particles on the basis of his results which are shown in Figure 2.3.

The differences between the recovery of coarse galena and pyrite particles can be attributed to differences in density (galena 7500 $kg \cdot m^{-3}$ and pyrite 5000 $kg \cdot m^{-3}$). This cannot, however, be used as an explanation for the differences in the pentlandite and pyrite systems which have very similar densities. It is also difficult to reconcile the differences in the recovery of fine minerals in terms of the differences in the frequency of bubble-particle collisions caused by the differences in density. Sphalerite (density 4000 kg m^{-3}) has a similar fines recovery to galena in spite of the large density difference, while pentlandite and pyrite have far lower fines recoveries than sphalerite. Density is the only obvious physical property of the minerals that might affect the formation and disruption of bubble-particle agglomerates.

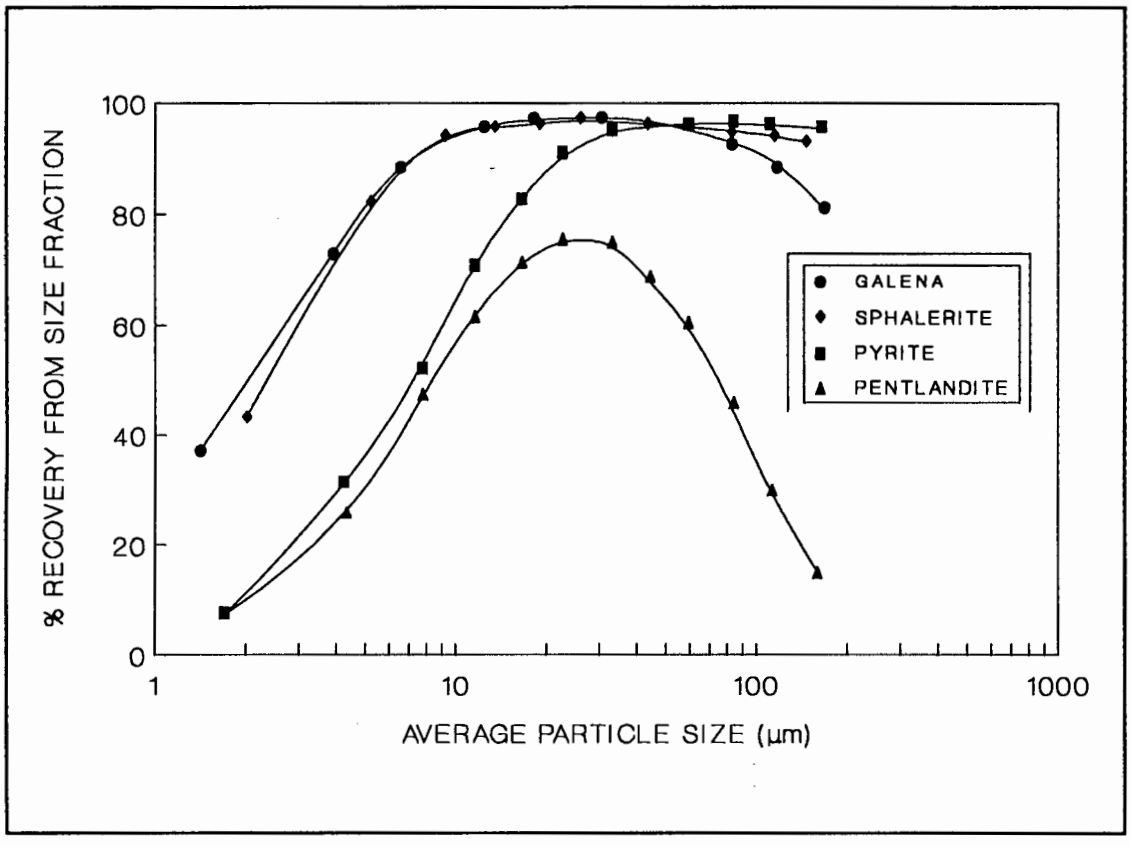

FIGURE 2.3 : Size-by-Size Recovery of some Sulphide Minerals after 60 seconds Flotation in Timed Batch Tests (After Jowett, 1980)

This led Jowett to the conclusion that it is surface chemical factors that determine the potential for bubble-particle agglomerate formation. Induction time is an obvious measure of the potential for the formation of agglomerates. The induction time can be defined as the time taken for a bubble to form a three-phase contact at a solid surface after the initial bubble-particle collision. The shorter the induction time the greater the potential for agglomerate formation. Good induction times are of the order of 10 ms.

The obvious surface chemical factor is the hydrophobicity of the mineral. This is determined, to a large extent, by the interaction of the collector with the mineral. The role of the collector is to render the mineral particle hydrophobic. The induction time is obviously determined mainly by the hydrophobicity of the mineral particle, but very little work has been done to quantify this relationship (Jowett 1980).

The step that controls the induction time is the rate at which the liquid film between the particle and the bubble thins. Derjaguin and Dukhin (1961) point out that induction time phenomena are difficult to analyse mathematically based on the thinning and rupture of water films. This is because these quantities are difficult to measure and are determined by several other variables.

The induction time is dependent on physical factors to some extent. The two main physical factors are particle size and liquid viscosity. Small particles have little effect on the induction time, while large particles increase the induction time because the extent of the three-phase contact that must be formed is increased. The liquid viscosity (and hence the temperature and pulp density) affect the rate of thinning of the film between the bubble and the particle. The higher the viscosity, the longer the induction time. Inertial effects due to system turbulence also play a part in determining the induction time.

In an attempt to quantify the effect of streamlines on fine particles, Flint and Howarth (1970) defined the collision efficiency (E):

$$E = N_B/N_T$$

where N_B is the number of particles that actually collide with bubbles and

N_T is the number of particles that would collide with bubbles if the fluid streamlines were not diverted by the bubbles.

Jiang and Holtham (1986) produced a correlation for E based on the particle size (d_p) and the bubble size (d_b):

$$E = k[d_p/d_b]^n$$

where k and n are constants dependent on the bubble size, the value of n being less than 1.

Flint and Howarth assumed a bubble-particle collision to be a collision between two spheres and hence could be modelled by a collision between any two spheres. They used a system where particles were modelled by 0.5 mm glass beads and bubbles by 13 mm nylon balls. The nylon balls were kept stationary and the glass beads circulated around them. It was found that there is a critical bubble-particle size factor ($k_{b\text{-}pC}$) below which bubble-particle collisions cannot occur. In theory increasing $k_{b\text{-}p}$ should increase the collision efficiency. In practice this is observed up to a certain point, but generally it is found that smaller bubbles improve fine particle flotation. This anomaly arises because the calculations are not strictly valid for a flotation system.

Ahmed and Jameson (1985) studied the effect of bubble size on the rate of flotation of spherical latex, zircon and quartz particles. Bubbles of a known size were generated by introducing the air through glass sintered discs of known porosity. It was found that there was an increase of up to 100 fold when the bubble size was decreased from 655 μm to 75 μm for all three materials.

The main reasons for the increased rate of flotation of fine particles with small bubbles are:

- As the bubble size decreases the bubble surface area per unit volume of air increases and the rate at which the bubbles rise decreases. This increases the probability of bubble-particle collisions.

- Smaller bubbles have more linear streamlines which affect the particles less.
- Smaller bubbles are more stable because they are less susceptible to the internal stresses caused by the turbulence of the system.

Frothers have the effect of lowering the surface tension of the liquid aiding in the formation of bubbles. Generally larger bubbles are stable at low frother concentrations and smaller bubbles are stable at high frother concentrations (Sutherland and Wark, 1955). Due to the lowering of the surface tension the frother also aids in the formation of a three-phase boundary and thus bubble-particle agglomerates (Leja and He, 1984).

2.2.5 RESIDENCE TIME DISTRIBUTION MODELLING

The two basic residence time distribution models are the plug flow reactor in which no mixing occurs and the completely-stirred-tank-reactor (CSTR) in which complete mixing occurs. To model situations between these extremes, models based on one or other of these base cases are used.

The axial dispersion model (ADM) is based on the plug flow model with a dispersion coefficient (D) being introduced to account for mixing (Levenspiel, 1972). The model is described by an unsteady state material balance equation for the tracer:

$$\partial C/\partial t + u/(1-\varepsilon)\cdot\partial C/\partial x_p = D\cdot\partial^2 C/\partial x_p^2$$

where C is the tracer concentration, t is the time, u is the superficial velocity, ε is the gas holdup and x_p is the axial distance along the column. The dispersion coefficient allows for mixing patterns anywhere between plug flow (D = 0) and mixed flow (D = ∞). The exit age distribution function [E(θ)] for this model depends on the boundary conditions of the system. The simplest case, the open-open system where the tracer input and measurement does not affect the mixing in the vessel:

$$E(\theta) = \frac{1}{2\sqrt{\pi\theta(D/uL)}}\cdot\exp\left[-\frac{(1-\theta)^2}{[\,4\theta(D/uL)]}\right]$$

where θ is the normalised time (t/τ), where τ = volume of the vessel/volumetric flow rate. For this system the normalised variance (σ_θ^2) is given by:

$$\sigma_\theta^2 = \sigma^2/\tau^2 = 2\cdot(D/uL) + 8\cdot(D/uL)^2$$

where σ^2 is the variance.

This model has been expanded to include an axial and a radial dispersion coefficient, which allows diffusion of material in all directions along the column (Eissa et al. 1971). This model yields the following unsteady state mass balance for the tracer:

$$u\cdot\partial C/\partial t = D_x\cdot\partial C^2/\partial x_p^2 + D_r(1/r_p\cdot\partial C/\partial r_p + \partial^2 C/\partial r_p^2)$$

where x_p is the axial position and r_p is the radial position and D_x and D_r are the axial and radial dispersion coefficients respectively.

The tanks-in-series model accounts for incomplete mixing by having a series of perfectly mixed zones with N = 1 for a CSTR and N = ∞ for a plug flow reactor (Levenspiel, 1972). The equation for this model is:

$$E(\theta) = [N\cdot(N\cdot\theta)^{N-1}/(N-1)!]\cdot\exp(-N\theta)$$

where N is the number of tanks-in-series, θ is the normalised time (t/τ) where τ = volume of the vessel/volumetric flow rate and $E(\theta)$ is the exit age distribution function. The normalised variance (σ_θ^2) for this model is:

$$\sigma_\theta^2 = \sigma^2/\tau^2 = 1/N$$

Buffham and Gibilaro (1968) point out that since the model has no physical significance there is no reason why only integer values of N should be allowed. They, therefore, propose a generalized equation to include positive real values as well:

$$E(\theta) = [N\cdot(N\cdot\theta)^{N-1}/\Gamma(N)]\cdot\exp(-N\theta)$$

where $\Gamma(N)$ is the gamma function:

$$\Gamma(N) = {}_0\int^{\infty} \exp(-x)\cdot x^{N-1}\, dx$$

The tanks-in-series model may be expanded to cover residence time distributions which are not well modelled by only a series of well mixed zones. This is achieved by adding backmixing, bypassing or dead volume to the model.

Numerous methods of interrelating the model parameters of the tanks-in-series model (N) and the axial dispersion model (D/uL) have been proposed (e.g. Kramers and Alberda, 1953; Trambouze, 1960). Levenspiel (1961) points out that the shapes of the E curves for these two models are not the same and simply matching the maxima and variances of the $E(\theta)$ curves for these models can lead to errors. Riquarts (1981) has shown that N and D/uL are formally equivalent if the simplifying assumptions for the ADM discussed below are made.

The most common model for the study of the residence time distributions of the collection (pulp) zone in column flotation cells is the axial dispersion plug flow model (Finch and Dobby, 1990). This model assumes:

- No radial mixing occurs.
- Flows caused by axial mixing can be represented by a diffusion type mechanism, and the diffusivity does not vary along the length of the reactor.
- Fluid flow is in one direction (axial) only.
- The fluid flow conditions are at steady state along the length of reactor under consideration ('infinitely' long reactor).

Due to the boundary condition assumptions the model becomes invalid at larger values D/uL values. It has been suggested that D/uL value should not exceed 0.2 (Bischoff and Levenspiel, 1962).

Levenspiel (1979) states that there is a large deviation from plug flow at D/uL values of 0.01 or larger, and under these conditions it is very important to identify correctly the proper boundary conditions at the input and outlet points of the tracer. The axial dispersion model has been adapted to deal with different boundary conditions, and equations for the variance (σ_θ) are

available for systems with open or closed ends, or a combination of open and closed ends. If these conditions are not identified correctly then there can be a significant variation between the actual and the calculated D/uL values. It is often difficult to identify these conditions and they vary with the position of the detectors and the way in which the tracer is introduced (e.g. through the wall measurements as with isotopic tracers (open end), or conductivity of the tailing as with salt tracers (closed end); tracer introduced directly into the column (open end) or into the feed line (closed end), etc. Figure 2.4 shows some of the many possible boundary conditions that can arise with the axial dispersion model. It has also not been possible to obtain an analytical solution for the exit age distribution curve [E(θ)] for any of the systems except the one with both an open inlet and an open outlet. For other boundary conditions the E(θ) curve must be determined numerically (Levenspiel, 1972). These problems do not arise with the tanks-in-series model.

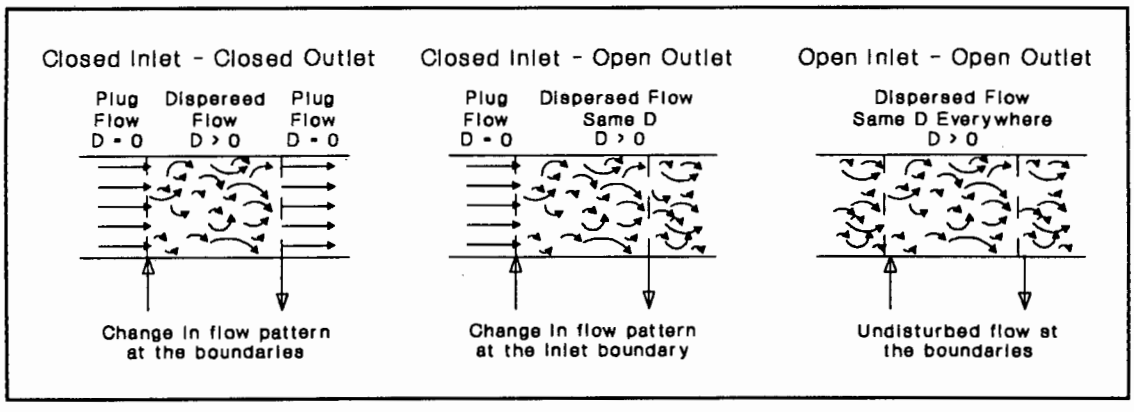

FIGURE 2.4 : Some of the Many Possible Boundary Conditions for the Axial Dispersion Model (After Levenspiel, 1972)

Levenspiel (1979) also states that "If the flow deviates greatly from plug (D/uL large) chances are that the real vessel doesn't meet the assumptions of the model (a lot of independent random fluctuations). Here it becomes questionable whether the model should even be used. I hesitate when D/uL > 1". He also questions the use of the model on non-symmetrical curves.

Furthermore, the assumption that no radial mixing occurs is unlikely to be true at larger Reynolds numbers (Re) where more turbulent conditions exist. This makes the axial dispersion model unsuitable for scale-up purposes since:

$$Re = \rho u d_c / \eta$$

where ρ = fluid density, u = fluid velocity, d_c = column diameter and η = fluid viscosity. If it is assumed that all the conditions in Re except for the column diameter remain constant, then the turbulence in the column, and consequently the radial mixing, will increase as the column diameter increases.

2.2.5.i RESIDENCE TIME DISTRIBUTION MODELS IN BUBBLE COLUMNS

Mills and O'Connor (1990) have presented an in depth review of column flotation modelling. They question the validity of column flotation models based on the axial dispersion model because the conditions found in the bubble columns that these models are based on differ significantly from those in column flotation cells.

2.2.5.ia TWO-PHASE BUBBLE COLUMNS

The dispersion model has been used to model bubble columns in both co-current and counter-current modes. Generally the gas and liquid rates in these columns are significantly higher than those of flotation columns, with the bubbles being an order of magnitude larger than those found in flotation columns. Flotation columns usually run with bubbles in the 0.5 to 3 mm size range and with superficial gas velocities between 1 and 3 $cm \cdot s^{-1}$ (Laplante et al., 1988).

Laplante et al. (1988) categorised the work done on bubble columns into three sections according to superficial gas velocity (J_g):

- $J_g < 0.5$ $cm \cdot s^{-1}$
- $0.5 < J_g < 3.0$ $cm \cdot s^{-1}$
- $J_g > 3.0$ $cm \cdot s^{-1}$

At low gas velocities (< 0.5 $cm \cdot s^{-1}$) the bubbles tended to rise in a plume at the centre of the column (Ulbrecht and Baykara, 1981). The bubbles were small and the dispersion coefficient was proportional to the rise velocity of the liquid associated with these bubbles. This result is to be expected because the laminar flow associated with these conditions prevents any significant radial mixing. Hence the dispersion model is a good model for these conditions.

Ohki and Inoue (1970) conducted a series of tests in columns from 4 to 16 cm in diameter and found that, at high superficial gas velocities ($5 < J_g < 25$ $cm \cdot s^{-1}$), the coefficient of dispersion (D) was directly proportional the gas velocity. Reith et al. (1968) determined dispersion coefficients in bubble columns with large superficial gas velocities ($10 < J_g < 45$ $cm \cdot s^{-1}$) in columns with diameters ranging from 5 to 29 cm. They found that D was proportional to both J_g and d_c. It was also observed that slug flow occurred in this region and the system would therefore alternate between gas-dispersed and liquid-dispersed modes. Under these conditions the assumption of the axial dispersion model would definitely not hold.

In the intermediate range where columns operate diffusion coefficients have been determined by several researchers (Baird and Rice, 1975; Joshi and Sharma, 1979 and Joshi, 1980). Baird and Rice analysed several previous studies and showed that, for unbaffled columns, an isotropic turbulence model for D applies where the axial dispersion occurred by eddy diffusivity:

$$D = K_c \cdot l^{4/3} \cdot P_m^{1/3} \qquad \text{(Isotropic Turbulence Model).}$$

$$P_m = u_d \cdot (1 - \rho_d/\rho_c) \cdot g \qquad \rho_d/\rho_c \cong 0$$

$$D = 0.35 \cdot d_c^{4/3} \cdot J_g^{1/3} \cdot g \qquad \text{(Bubble Column Model).}$$

$$= 3.43 \cdot d_c^{4/3} \cdot J_g^{1/3}$$

where K_c = dimensionless constant, l = primary length parameter, P_m is the specific energy dissipation rate, u_d = the velocity of the dispersed phase, ρ_d = density of the dispersed phase, ρ_c = density of the continuous phase, and g = the acceleration due to gravity. The models developed by the other researchers in this field are in good agreement with this model.

2.2.5.ib THREE-PHASE BUBBLE COLUMNS

Three-phase bubble column systems have been studied by several researchers (e.g. Cova, 1966; Suganuma and Yamanishi, 1966; Imafuku et al. 1968).

Cova obtained the dispersion coefficient for a two-phase system at various superficial gas velocities. Using this information together with the terminal settling velocity of single particles in a stagnant liquid he predicted a coefficient of dispersion for the solid phase. This study had several flaws which make its validity dubious:

- The solid phase was assumed to behave in the same way as the liquid phase at similar gas velocities.
- It was assumed that there was no interaction between the solid particles in the system.
- The liquid in the bubble column was not stagnant and so the flow regime that the terminal solid settling velocity was based on was incorrect.
- Insufficient experimental data was given to backup the assumptions made.

An empirical correlation predicting the concentration distribution of solid particles in bubble columns with continuously circulating flow of liquid has been presented by Suganuma and Yamanishi. This study is, however, of limited value because the settling velocity and dispersion coefficient of the particles were not determined.

Imafuku et al. studied continuous co-current flow in 5, 10 and 20 cm pachuca tanks. High superficial velocities of both liquid and gas (2 - 10 $cm \cdot s^{-1}$) were used to ensure that the solids remained suspended. Large particle (60 - 180 μm) were used, and the high gas rate caused the bubbles formed to be big (> 1 cm). For these conditions Imafuku et al. concluded that:

- It was valid to apply the axial dispersion model to the slurry phase because there was a uniform radial distribution of solid particles

- The axial dispersion coefficient was the same for both the solid and liquid phases at the same gas velocity.

The axial dispersion model is probably well suited to this system because in a co-current system with high liquid rates there should only be a small difference between the liquid and gas superficial velocities and hence little radial mixing.

The presence of radial mixing in bubble columns is confirmed by Joshi and Sharma (1979), who postulate the presence of circulation cells within the column. Their model is based on a series of well mixed regions, with backmixing between the regions.

Deckwer and Schumpe (1987) in their review of models in bubble columns also question the use of the ADM in the light of the fluid mechanics in these columns. The ADM is a continuous gradient model and presupposes that turbulent eddies are small in comparison with the column diameter. This fluid flow regime is unlikely to be valid for the conditions found in a column with turbulent churning flow (column flotation cells), especially if there is a range of bubble sizes present. The ADM and other single parameter models (tanks-in-series) cannot reflect the current state of knowledge of the fluid mechanics in bubble columns.

2.2.5.ii RESIDENCE TIME DISTRIBUTION STUDIES IN COLUMN FLOTATION CELLS

The early residence time distribution models for flotation columns were based on studies of bubble columns. Axial dispersion models were used and it was assumed that the dispersion coefficients for the solid (D_p) and liquid (D_l) phases were equivalent.

Dobby and Finch (1985) used two 13 m columns, with diameters of 46 and 91 cm to conduct the first investigation of the mixing characteristics of column flotation cells. The conditions used were typical of those found in flotation columns except for the pulp density, which was 2 - 3% solids. Fluorescein was used to trace the liquid phase, and manganese dioxide

(non-floatable) the solid phase. From these studies they concluded that the axial dispersion model could be used to model the collection zone, and there was little difference between the dispersion coefficients of the liquid and solid phases. It is probable that no difference was observed between the solid and liquid dispersion coefficients because the solids concentration was too low, and not typical of normal column conditions. Based on these studies and those done on bubble columns it was proposed that:

$$D_p = D_l = 0.063 \cdot d_c$$

This correlation was valid for columns larger than 20 cm in diameter operating at superficial gas velocities of between 1 and 3 $cm \cdot s^{-1}$. This model was subsequently extended using bubble column theory to cover columns of all diameters (Dobby and Finch, 1986b);

$$D_p = D_l = 0.063 \cdot d_c \cdot (J_g/1.6)^{0.3}$$

In subsequent residence time distribution studies (Yianatos, 1987; Espinosa-Gomez, 1987; Miszczak, 1987), it has been assumed that the dispersion coefficients for the solid and liquid phases are equivalent, and due to the difficulty of obtaining solid phase dispersion coefficients tests have been based on liquid phase studies.

Yianatos et al. (1986b) in their study of apparent hindered settling of particles in a countercurrent gas-liquid-solid column quantified the residence times of different sized particles in a flotation column. They quote the following ratios of the solids-to-liquid residence times (τ_p/τ_l) based on the study by Dobby and Finch (1985):

d_p (μm)	44	63	88	125
τ_p/τ_l	0.77	0.71	0.58	0.48

For small extents of dispersion (Levenspiel, 1972):

$$\sigma^2/\tau^2 = 2 \cdot (D/uL)$$

and from Dobby and Finch (1985):

$\tau_p/\tau_l = u_l/(u_l + u_p)$ where $u_l + u_p$ is the particle superficial velocity.

thus if $D_p = D_l$ and L is constant then:

$$\sigma_p^2/\tau_p^2 \cdot \tau_l^2/\sigma_l^2 = u_l/(u_l + u_p) = \tau_p/\tau_l = (D/uL)_{part}/(D/uL)_{liq}$$

or

$$(D/uL) \propto \tau$$

Thus the assumption that the D values for the solids and the liquid are equal ($D_p = D_l$) implies that the degree of mixing in the pulp zone is directly proportional to the residence time in the pulp zone. Thus the degree of mixing should decrease as the particle size of the solids increases. This is in sharp disagreement with the work of Yianatos and Bergh (1991) who found the opposite trend.

Laplante et al. (1988) developed an empirical correlation for the dispersion coefficient in column flotation cells including the solids concentration (S):

$$D = 2.98 \cdot d_c^{1.31} \cdot J_g^{0.33} \cdot \exp(0.025 \cdot S)$$

This correlation was based on liquid phase data from a number of workers (Dobby and Finch, 1985; Yianatos, 1987; Espinosa-Gomez, 1987; Miszczak, 1987). The result is very similar to that developed by Baird and Rice (1975) if the solids concentration is ignored. For the first time, the solids concentration is one of the parameters in the correlation, implying that $D_p \neq D_l$. A minor flaw in this model is that it predicts the largest dispersion coefficient with no solids present. This is clearly not the case as it has been found that two-phase systems give lower dispersion coefficients than three-phase systems (Yianatos and Bergh, 1991). This implies that there should be a low solids concentration which gives the largest dispersion coefficient.

Xu and Finch (1991a) propose the following correlation for the vessel dispersion number (D/uL):

$$D/uL = 0.56 \cdot \{(d_c/L_c) \cdot (J_g/J_l) \cdot [(J_g/\varepsilon) + (J_l/(1 - \varepsilon)]\}^{0.41}$$

where d_c is the column diameter, L_c is the column height, ε is the gas hold-up and J_g and J_l are the superficial velocities of gas and liquid respectively.

This correlation includes a correction for the gas hold-up (ε) in the system which is a definite improvement because the gas hold-up can be correlated to bubble size, which must be one of the parameters affecting the degree of mixing in the column. It is also recognised that the mixing is dependent on the aspect ratio of the column, and not merely its diameter. The differences in the solid and liquid phase mixing are, however, again ignored, and this assumption is questionable. It is also pointed out in the paper that, while the correlation holds well for laboratory scale columns, the fit becomes progressively worse as the column diameter increases, although a good fit is claimed for D/uL values ranging from 0.08 to 1.1.

Xu and Finch (1991b) in their review of the use of the axial dispersion model in column flotation point out that care must be exercised when using this model at larger degrees of dispersion. Significant errors can arise if the boundary conditions are not correctly identified, or if the model assumptions are exceeded. They point out, however, that the model generally provides a good basis for scale-up, and that no better models are available for this purpose.

Yianatos and Bergh (1991) have studied the effects of different particle sizes on the degree of mixing in an industrial column flotation cell (0.91 m in diameter by 12 m high) using isotopically labelled tracers. They found that there was an increase in D/uL with increasing particle size, and that there was little difference in the degree of mixing between the liquid and the fine (- 38 μm) solids. They also found that the mean residence time of the solids in the column decreased as the particle size increased. This is probably due to increased gravitational forces. Examination of the data in this paper reveals D/uL values of 1.0 for the unsized feed, and 10 for the coarse particle sizes (75 μm < d_p < 150 μm). These values are clearly outside the range where the axial dispersion model holds.

Mills et al. (1992) have correlated the data obtained by Yianatos and Bergh (op. cit.) and some laboratory scale column tests which they conducted, and have found that there was an exponential relationship between the particle size and the D/uL value in the collection zone. They also propose that the following models should be used for the collection zone:

$d_c < 0.1$ m	Either the tanks-in-series, or the axial dispersion model - Little mixing.
0.1 m $< d_c <$ 1.5 m	Axial dispersion model - Better fit.
1.5 m $< d_c$	One CSTR - Well mixed zone.

Mavros et al. (1989) proposed a tanks-in-series model with backmixing between the tanks. This model is similar to that proposed by Joshi and Sharma (1980). They postulate the following correlation between the vessel dispersion number and their model.

$$(1+2\lambda)/2N = D/uL$$

where λ is the backmixing parameter and N is the number of tanks-in-series. This would allow these parameters to be calculated from the variance of the response curve in a similar fashion to the vessel dispersion number.

This is a more appropriate model to use for a column because it allows for internal recycling in the column. Although they do not propose any scale-up methodology using this model, they point out that by overlaying information about the solids concentration, gas hold-up and bubble size, a full scale model could be obtained.

If a dispersion model is to be used then the model with both axial and radial dispersion should provide a better model for the processes occurring in the column. An analytical solution for this model is provided by Eissa et al. (1971):

$$C/C_0 = (P/2S')\exp[-P\cdot(S'-Z)]$$

where

$$S' = [(2r_p/d_c)^2 + Z^2]^{1/2}$$

$$P = ud_c/4(D_x\cdot D_r)^{1/2}$$

$$Z = (2x_p/d_c)\cdot(D_r/D_x)^{1/2}$$

C and C_0 are the concentration and the initial concentration respectively, D_r and D_x and the radial and axial dispersion coefficients respectively, r_p and x_p are the radial and axial positions respectively, u is the superficial pulp velocity and d_c is the column diameter.

The bubble size in the collection zone is ignored in most of the collection zone models, and it is likely to have a significant effect on the mixing in this zone due to the different rise rates and residence time distributions of different sized bubbles. Generally in scale-up the bubble size remains similar to that in the test column while the column diameter is increased. Yianatos and Levy (1989) points out that the degree of mixing that occurs with small bubbles in large columns is significantly larger than the degree of mixing that occurs in smaller columns with the same size bubbles. Thus large columns tend to have more mixed collection zones than small columns. This often leads to industrial scale flotation columns not performing to their design specifications.

2.3 EXPERIMENTAL METHODS

2.3.1 BUBBLE SIZING SYSTEM

A diagram of the system used to measure the bubble sizes is shown in Figure 2.5. The tests were conducted in the batch laboratory column cell used in the froth cutting tests which is described in section 3.4.2. The cell consisted of a perspex cylinder (25 cm x 6 cm) with a temperature jacket and a magnetic stirrer-propeller system. The bubbles were generated using a sintered glass frit (porosity 2, pore diameter 40 - 90 μm) located near the base of the cell using air that had been presaturated with water.

The bubble sizing system consists of a capillary tube with a belled end passing between two pairs of photo-cell - diode detectors. These detectors are mounted exactly 5 mm apart at right angles to each other. Bubbles are drawn up the tube under vacuum and are transformed from near-spheres into cylinders. As the bubbles pass the detectors they are monitored as a change in light intensity. This change arises from the different refractive indices and optical densities of the air-glass and liquid-glass boundaries. In order to obtain an accurate bubble size distribution about 3000 bubbles are sized. The bubbles are then collected in a gas burette so that the total volume of bubbles is known.

Pulses are generated by the passage of the bubbles past the detectors. Due to the leading and trailing edges of the bubbles, these pulses are not sharp, but have rounded edges. To correct this, the pulses are fed into a circuit which generates sharp up-going and down-going spikes. These spikes are then used to generate square waves equivalent to the bubble velocity and the bubble length. The square waves are sent to the data capture system.

The data capture system is based on the Motorola 6809 processor which controls the operation of a M6845 programmable timer. This timer has three independent channels, which are used to time the run, the length pulses and the velocity pulses. The length and velocity pulses are stored in memory along with the time at which they occurred. The capture system can have up to 56 kilobytes of memory (RAM) allowing about 7000 bubbles to be processed although the system used for these tests only had enough memory

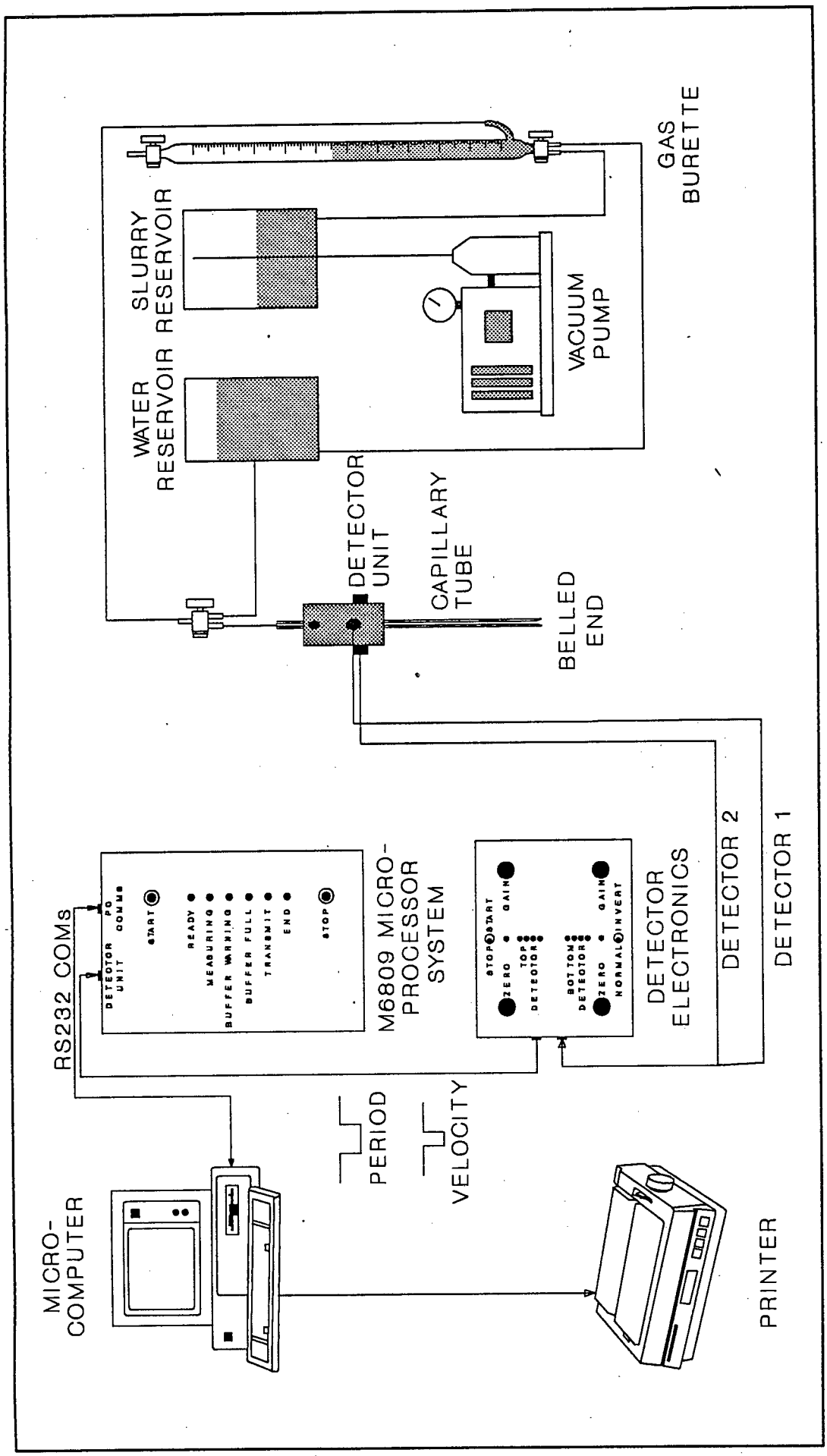

FIGURE 2.5 : Bubble Sizing System.

for 4000 bubbles. It has been found that the system is capable of processing more than 50 bubbles per second. This speed is far in excess of typical operating conditions (about 20 bubbles per second). Details of the entire system are given in Appendix 1.

At the end of a run the data is downloaded from the buffers of the data capture system to a micro-computer. The programme which is used to process the data calculates the bubble volume from the velocity and length data for each bubble. .The bubble volumes are then normalised with respect to the total volume collected. Since the total bubble volume is measured at normal pressure, the bubble diameters obtained are at atmospheric pressure. If the diameter is required at a given pressure then the gas law must be used to obtain it. This normalisation is necessary because a thin film of water coats the inside of the capillary making the effective capillary diameter difficult to calculate. The thickness of this film varies with the size of the bubble in the capillary, smaller bubbles and more viscous slurries have thicker films.

Dunne et al. (1976) found that the applied vacuum and the geometry of the capillary bell can be critical factors in obtaining an accurate bubble-size distribution. If either of these parameters is incorrect bubble coalescence or breakage can occur in the capillary. A further explanation of these extreme conditions can be found in Appendix 1.

A portable version of the system with a submersible detector unit has been built. This unit has successfully been used to monitor the bubble size in several different systems including batch flotation cells, continuous flotation cells, column flotation cells, waste water treatment reactors and bacterial leach pachucas. With slight modification the dissolved oxygen can be logged at the same time as the bubble size is being measured (Randall et al., 1989). This allows mass transfer coefficients to be calculated as a function of bubble size. Bubbles have been measured in pulp densities of up to 30% solids. By changing the bore of the capillary a large range of bubble sizes have been measured (0.5 - 10 mm).

2.3.2 RESIDENCE TIME DISTRIBUTION STUDIES

A schematic diagram of the laboratory column flotation cell used in the solids residence time distribution tests is shown in Figure 2.6. The perspex column had a diameter of 5.4 cm and a height of 230 cm. A sintered glass frit of porosity 2 (pore diameter 40 - 90 μm) was used as the air distributor and micro-jets were used for the wash water. Variable speed peristaltic pumps were used to control the flow rates of the feed, tailings and wash water, while the air passed through a rotameter with a needle valve.

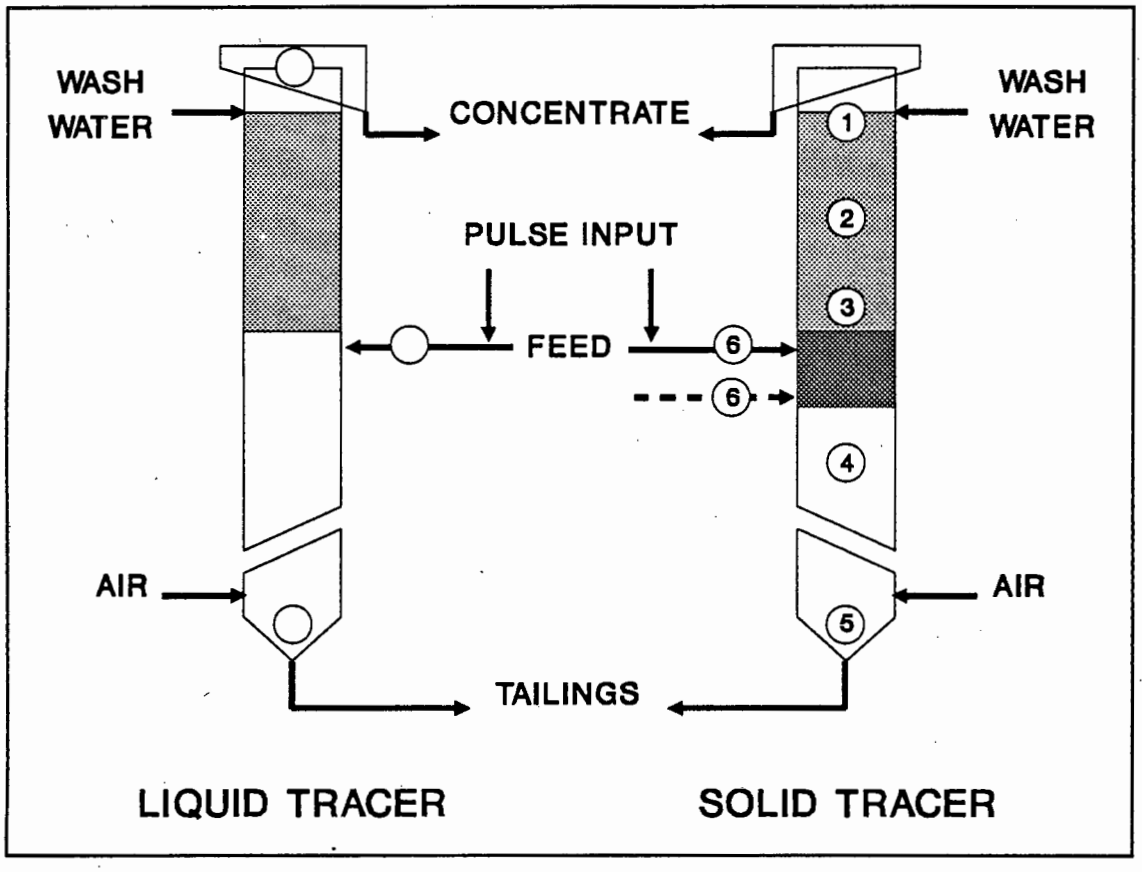

FIGURE 2.6 : Schematic Diagram of the Equipment used in the Pulp-Phase Residence Time Distribution Studies

Throughout the three-phase tests a gold-bearing pyritic ore from a South African gold mine (Unisel) was used. The collector used was sodium mercaptobenzothiazole (SMBT, 50 g/ton) and the frother Dowfroth 200 (a polypropylene glycol with a molecular weight of about 200, 25 ppm). Frother was added to both the wash water and the pulp. A reagent conditioning time of 10 minutes was allowed, and the pulse injected after a further twenty minutes to allow the column to reach steady state (Schommarz, 1991).

The Unisel ore had a mean particle size (d_{50}) of 18.1 μm and a sulphur grade of 1.9 %.

In the liquid studies both two- and three-phase systems were examined. The liquid tracer that was used was a 20 cm^3 pulse of 3.50 molar sodium chloride solution. Conductivity cells located on the feed line, the concentrate line and the tailings outlet were used as detectors.

The solid tracer was isotopically labelled gold present in the ore. The $^{89}Au_{191}$ isotope was chosen because it has a convenient half-life of about 68 hours. The ore was irradiated a week before it was used to allow the short-life isotopes to decay to negligible levels. Each pulse consisted of 7 g of ore at a pulp density of 50% solids and was introduced into the feed line using a syringe 20 cm before the feed point to the column. The isotopically labelled tracer pulses were conditioned in the same way as the feed slurry.

Six geiger-counters were used as detectors, five on the column and one on the feed line. The detectors on the column were labelled from 1 to 5 with 1 at the top and 5 at the bottom (Figure 2.4). Detector 6 was located on the feed line. The signals from these detectors was logged directly to a personal computer.

Samples of the concentrate and tailings were taken for each run just before the tracer was introduced to determine the grade, recovery and mass pull for the run. Once the tracer had been injected it was not possible to take any further samples due to radio-active contamination. This contamination also made it impossible to do any tracer mass balances.

It should be noted that the liquid tracer studies were conducted a few weeks after the solid tracer studies. The solid tracer studies were conducted in Pretoria and the liquid studies in Cape Town. It is therefore possible that some of the conditions (e.g. water quality, temperature, etc.) were not identical for both sets of runs. The differences between the solids and liquid behaviour reported in section 2.4.2, however, are far greater than the aforementioned differences.

Several different flotation parameters were studied and these are shown in Table 2.1.

TABLE 2.1 : Solids RTD Experimental Conditions

RUN NO	PARAMETER VARIED	FEED RATE (cm/s)	PULP DENSITY (% sol)	WASH WATER RATE (cm/s)	AIR FLOW RATE STP (cm/s)	FEED FROM TOP (mm)	FROTHER CONC (ppm)	FROTH DEPTH (mm)
1		**0.93**	20	0.25	2.31	760	25	650
2	FEED	**0.84**	20	0.25	2.31	760	25	650
3	RATE	**0.73**	20	0.25	2.31	760	25	650
4		**0.63**	20	0.25	2.31	760	25	650
5		**0.53**	20	0.25	2.31	760	25	650
6		0.73	20	**0.29**	2.31	760	25	650
7	WASH	0.73	20	**0.27**	2.31	760	25	650
8	WATER	0.73	20	**0.25**	2.31	760	25	650
9	RATE	0.73	20	**0.23**	2.31	760	25	650
10		0.73	20	**0.20**	2.31	760	25	650
11		0.73	20	0.25	**5.07***	760	25	650
12	AIR	0.73	20	0.25	**7.08**	760	25	650
13	RATE	0.73	20	0.25	**4.51**	760	25	650
14		0.73	20	0.25	**2.31**	760	25	650
15		0.73	20	0.25	**1.69**	760	25	650
16		0.73	20	0.25	2.31	760	**25**	650
17	FROTHER	0.73	20	0.25	2.31	760	**20**	650
18	CONC	0.73	20	0.25	2.31	760	**15**	650
19		0.73	20	0.25	2.31	760	**10**	650
20	PULP	0.73	**20**	0.25	2.31	760	25	650
21	DENSITY	0.73	**15**	0.25	2.31	760	25	650
22		0.73	**10**	0.25	2.31	760	25	650
23	REPEATS	**0.93**	20	0.25	2.31	760	25	650
24		0.73	20	**0.20**	2.31	760	25	650
25	FROTH	0.73	20	0.25	2.31	**980**	25	**910**
26	HEIGHT	0.73	20	0.25	2.31	**980**	25	**780**
27		0.73	20	0.25	2.31	**980**	25	**680**

* FILTER CLOTH SPARGER

2.4 RESULTS AND DISCUSSION

2.4.1 BUBBLE SIZE MEASUREMENTS

Unless otherwise stated the values of the various parameters in this study were as follows:

Air rate: 1.6 $l \cdot min^{-1}$
Axial position: 5 cm from frit
Radial Position: Centre
Air Pressure: Atmospheric
Temperature: 20°C
pH: Approximately 7
Particle size: 70% < 75 µm
Gas hold-up: 0.08

Frother type: None
Frother dosage: None
Collector type: None
Collector dosage: None
Liquid: Tap water
Solids: A pyritic ore
Pulp density: 10% solids

2.4.1.i REPRODUCIBILITY

Two- and three-phase reproducibility studies were carried out to establish the precision of the results (Table 2.2). In an air-water system the mean bubble diameter was found to be 2.82 mm with an average standard deviation of 0.80 mm while in an air-water-quartz system the mean bubble size was 3.09 mm with an average standard deviation of 0.92 mm. The standard deviation gives an indication of the distribution of bubble sizes. It was found that the reproducibility was excellent. In six repeat experiments for the two-phase system a mean bubble size of 2.822 mm (σ = 0.015 mm) was recorded. The accuracy of this data is indicated by its proximity to the values expected for pneumatic spargers (Pryor, 1965).

Tests were also carried out to establish the effect of the axial and radial position of the capillary in the cell on bubble size (Table 2.2). It was found that, for the column cell being used, these effects were negligible. There was a slight increase in size as the distance from the liquid surface decreased and this is ascribed to a bubble size gradient in the cell. The bubble rise rate is a function of the bubble size and thus bubbles of different sizes would have different residence times in the cell. The effects of coalescence appeared to be negligible.

TABLE 2.2 : Effect of Capillary Position on Bubble Size

	PARAMETER	VALUE	2-PHASE		3-PHASE	
			MEAN SIZE (mm)	STD. DEV. (%)	MEAN SIZE (mm)	STD. DEV. (%)
A	REPRODUCIBILITY *	run 1	**2.84**	28.5	**3.08**	29.5
		run 2	**2.83**	28.6	**3.10**	30.0
		run 3	**2.81**	28.5	**3.06**	29.1
		run 4	**2.82**	28.4	**3.11**	30.5
		run 5	**2.80**	28.2	**3.09**	30.4
		run 6	**2.83**	28.6	**3.08**	29.9
B	RADIAL POSITION *	r (side)	**2.84**	28.9	**3.08**	30.8
		1/2 r	**2.80**	27.5	**3.11**	30.5
		0 (centre)	**2.81**	27.8	**3.06**	29.1
		1/2 r	**2.83**	27.9	**3.09**	30.1
		r (side)	**2.82**	28.7	**3.07**	29.6
C	AXIAL POSITION	5 cm from liquid surface	**2.89**	28.0	**2.93**	31.7
		10 cm from liquid surface	**2.85**	28.4	**2.91**	31.6
		15 cm from liquid surface	**2.82**	28.0	**2.91**	31.3

* Solids fraction used was quartz (70 % < 75 μm)

2.4.1.ii EFFECT OF PHYSICAL PARAMETERS ON BUBBLE SIZE

Table 2.3 shows the effect of various physical variables on the bubble size. In Table 2.3(A) the influence of air flow rate (superficial gas velocity J_g) on bubble size can be seen. As the air flow rate increases the bubble size increases. The relationship between superficial air velocity and bubble size (d_b) was found to fit a simple power law relationship:

$$d_b = kJ_g^x$$

where k = constant and x = 0.40 and x = 0.47 for the two- and three-phase systems respectively. Dobby and Finch (1986a) found a similar relationship.

Table 2.3(B) shows the effect of using quartz of different particle sizes. In general the presence of the solid phase produced slightly larger bubbles. Fine particles (- 38 μm) produced bubbles smaller than those observed in the presence of coarse particles (+ 106 μm). These results are consistent with the findings of Dobby and Finch (1989). Hansford et al. (1976) showed that, for pyritic ores, viscosity increased as particle size increased. This

was due to increased shear between the particles and the liquid. Similar results were found by Marsden (1962). Clift (1991) points out that larger particles may cause bubble coalescence at the point of bubble formation. If a particle was located between two bubbles a sharp local curvature in the bubble surfaces would result, causing the water film to rupture and the bubbles to coalesce.

TABLE 2.3 : Effect of Physical Parameters on Bubble Size

	PARAMETER	VALUE			2-PHASE		3-PHASE	
					MEAN SIZE (mm)	STD. DEV. (%)	MEAN SIZE (mm)	STD. DEV. (%)
A	AIR FLOW RATE	0.59 cm/sec			**2.36**	25.8	**2.34**	31.2
		0.71 cm/sec			**2.54**	26.0	**2.54**	31.5
		0.82 cm/sec			**2.70**	26.3	**2.73**	33.0
		0.94 cm/sec			**2.84**	28.2	**2.91**	33.0
		1.06 cm/sec			**2.97**	30.0	**3.07**	32.6
		1.18 cm/sec			**3.10**	31.0	**3.22**	33.2
B	PARTICLE SIZE	unsized					**3.08**	28.8
		+ 106 µm					**4.00**	30.5
		75 - 106 µm					**3.63**	30.3
		53 - 75 µm					**3.15**	30.8
		38 - 53 µm					**2.95**	29.2
		- 38 µm					**2.71**	29.2
C	ORE TYPE	quartz					**3.08**	29.5
		pyrite					**2.98**	29.2
		pyritic gold ore					**2.91**	29.2
D	LIQUID VISCOSITY AND SURFACE TENSION	*Liquid*	*Viscosity*	*Surface Tension*				
		methanol	0.60 cP	22.61 dynes/cm	**2.38**	26.1		
		benzene	0.65 cP	28.85 dynes/cm	**2.50**	26.0		
		water	1.03 cP	72.75 dynes/cm	**2.83**	28.6		
		ethanol	1.20 cP	22.75 dynes/cm	**3.15**	31.1		
		n-propanol	2.20 cP	23.78 dynes/cm	**3.53**	35.5		
		n-butanol	2.95 cP	24.60 dynes/cm	**3.69**	32.5		
		analine	4.40 cP	42.90 dynes/cm	**4.05**	31.6		
E	PULP DENSITY *	*Density*	*Viscosity*					
		0 %	1.03 cP				**2.83**	28.6
		10 %	1.13 cP				**3.08**	29.5
		15 %	1.20 cP				**3.37**	29.1
		20 %	1.29 cP				**3.75**	30.1
		30 %	1.54 cP				**4.50**	34.6
F	PULP TEMPERATURE, SURFACE TENSION AND VISCOSITY	*Temp.*	*Water Surface Tension*	*Viscosity* 2-Phase	*Viscosity* 3-Phase			
		16°C	73.3 dynes/cm	1.11 cP	1.28 cP	**2.90**	29.7	**3.00**	33.4
		20°C	72.7 dynes/cm	1.03 cP	1.15 cP	**2.83**	28.6	**2.93**	30.3
		30°C	71.2 dynes/cm	0.80 cP	0.90 cP	**2.74**	27.0	**2.91**	22.6
		40°C	69.5 dynes/cm	0.65 cP	0.73 cP	**2.61**	27.6	**2.86**	21.8

* Solids fraction used was quartz (70 % < 75 µm)

Table 2.3(C) shows the effect of using different ores. The pyrite and pyritic ore were finer than the quartz (pyrite: 75% < 15 μm; pyritic ore: 75% < 20 μm; and quartz: 75% < 53 μm). The differences between the quartz and the other two ores can be ascribed to a particle size effect, but the pyritic ore and the pyrite are almost the same size. Since the pyrite ore consists mainly of quartz (2% sulphur), it is likely that the differences in bubble size between the pyrite and the pyritic ore are due to surface charge effects. The point of zero charge (PZC) of quartz occurs at a pH of about 2 while the PZC of pyrite is around a pH of 7. Hansford et al. (1976) postulated the presence of an 'ionic cloud' around the particles which increased the effective diameter of the particles and hence the viscosity. The size of this cloud increased as pH increased. It is probable that the size of this 'ionic cloud' is a function of the particle surface charge, and this would change for different minerals.

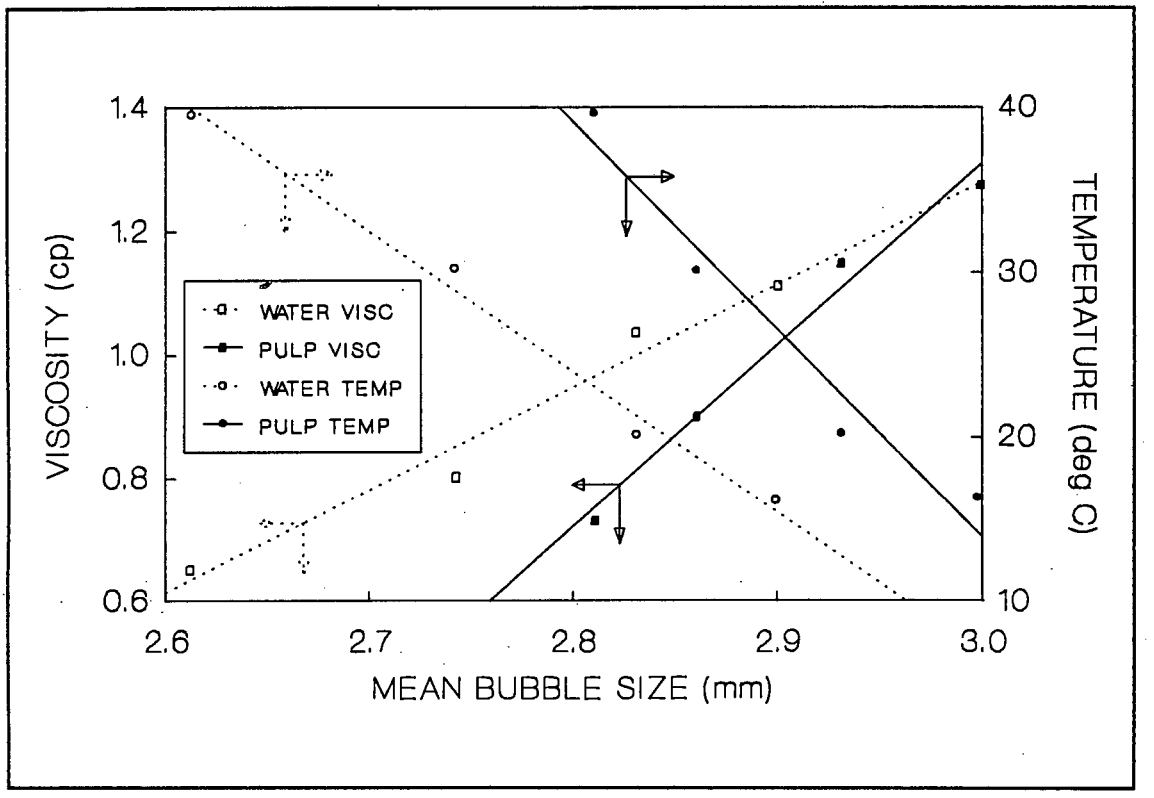

FIGURE 2.7 : Effect of Viscosity and Temperature on Bubble Size

The effect of liquid viscosity (η) on bubble size can be seen in Tables 2.3(D) and 2.3(F) and Figures 2.7 and 2.8. All the tests using liquids of different viscosities were carried out at 20°C, while the water viscosity was changed by changing the temperature. Also given in these tables are the

surface tensions for the liquid in contact with air. It has generally been found that low viscosities and surface tensions produce small bubbles, and in this case it is clear that as viscosity increased, larger bubbles were produced. This may be a result of liquid films forming faster at the point of bubble formation as viscosity decreases, trapping less air in each bubble and thus forming smaller bubbles. Dobby and Finch (1986a) showed that the bubble size (d_b) increases with the viscosity (η) of the liquid according to a power law:

$$d_b \propto \eta^x$$

It was found in this study that this correlation between bubble size and viscosity for liquids was in good agreement with that proposed by Dobby and Finch (op. cit.) (this study: x = 0.26; Dobby and Finch: x = 0.25) but the value of x was significantly higher (x = 1.22) for the three-phase system. Clearly there are factors which affect the bubble size in three-phase systems other than pulp density and viscosity.

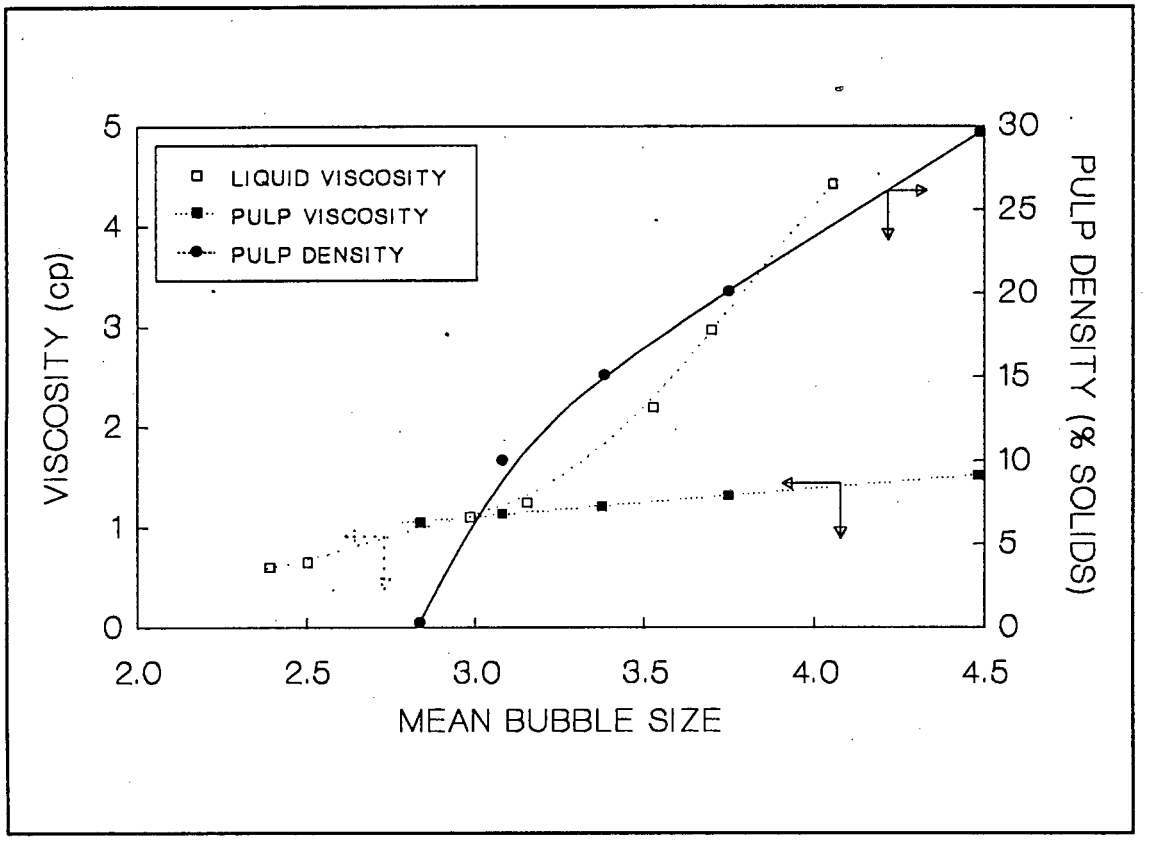

FIGURE 2.8 : Effect of Viscosity and Pulp Density on Bubble Size

It has been shown (Weast, 1982) that the surface tension can be related to the viscosity for water, in the temperature range 0 - 100°C, by:

$$\eta = \frac{0.0231 + 0.00083\gamma}{1 - 0.0126\gamma}$$

where γ = surface tension. From the above correlation it is obvious that η increases as γ increases. From the liquid viscosity and surface tension data in Table 2.3(D) it is clear that the viscosity has the dominant effect in determining bubble size. Water has by far the highest surface tension of any of the liquids studied, and yet it produces relatively small bubbles. Surface tension does, however play a role in determining bubble size as is evident if benzene at 20°C and water at 40°C are compared. Both liquids have the same viscosity (0.65 cP), but water has a higher surface tension and gives larger bubbles. The addition of frother also results in smaller bubbles by reducing the surface tension of the water without changing the viscosity [Table 2.4(A)]. Harris (1992) points out that it is the dynamic surface tension that has an effect on bubble size and that most surface tension measurements are made under static conditions. Care must therefore be exercised when relating static surface tension measurements to bubble sizes. It is, however, apparent that bubble size is a function of both the liquid viscosity and surface tension.

Table 2.3(E) shows the influence of pulp density on bubble size. The viscosity of the pulp as calculated from Mooney's correlation (1951) is also shown. These results are plotted in Figure 2.8. For this system the following relationship between the bubble size and the pulp density was found:

$$d_b = 2.814 + 0.0185 \cdot \rho_p + 0.00128 \cdot \rho_p^2$$

where d_b is the bubble size and ρ_p is it pulp density.

Table 2.3(F) shows that the bubble size decreased as temperature increased for both the two- and three-phase systems. Since surface tension, like viscosity, decreases as temperature increases, the decrease in bubble size with increasing temperature seen in Figure 2.7 is expected. The data for the bubble size and viscosity of the water at different temperatures fits the bubble size - liquid viscosity relationship proposed above well.

2.4.1.iii EFFECT OF CHEMICAL PARAMETERS ON BUBBLE SIZE

Table 2.4 shows the effect of chemical parameters on the sizes of bubbles. Figure 2.9 and Table 2.4(A) show that the presence of frother (Dowfroth 250) reduces the size of the bubbles. This is due to a lowering of the surface tension by the frother. No surface tension data could be obtained for polyoxypropylene glycols (Dowfroth 200, 250, etc.), but the trends shown in Figure 2.10 for polyoxyethylene derivatives should be analogous to those of polyoxypropylene derivatives. Dowfroth 250 contains 3 oxypropylene groups. If Figures 2.9 and 2.10 are compared it can be seen that there is a marked correlation between the trends seen in the surface tension of the solution and the bubble size as the frother concentration increases.

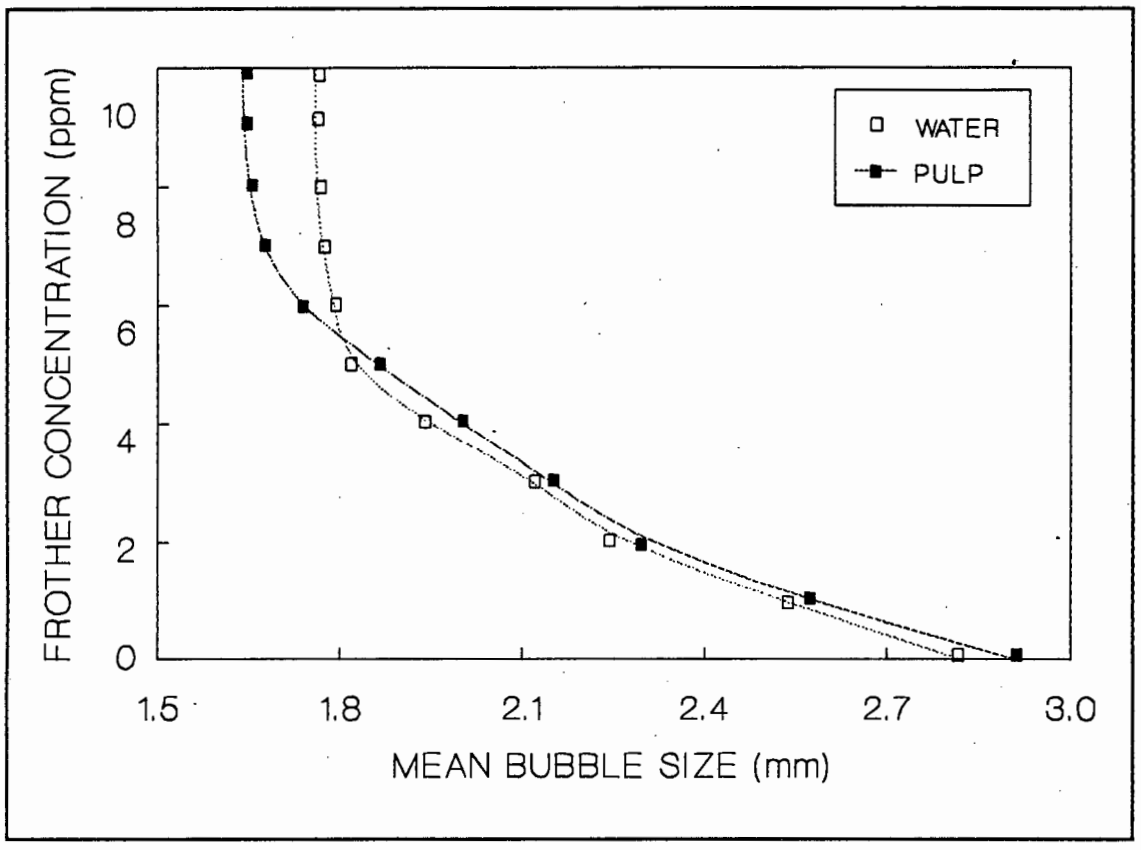

FIGURE 2.9 : Effect of Frother Concentration on Bubble Size

Tables 2.4(B) and 2.4(C) indicate that neither collector type nor dosage has an effect on the bubble size. This was expected because the xanthate collectors used in this study have no frothing properties (Leja, 1982a). Table 2.4(D) shows that the presence of frother was the dominant factor in determining bubble size when frother and collector were mixed with ore.

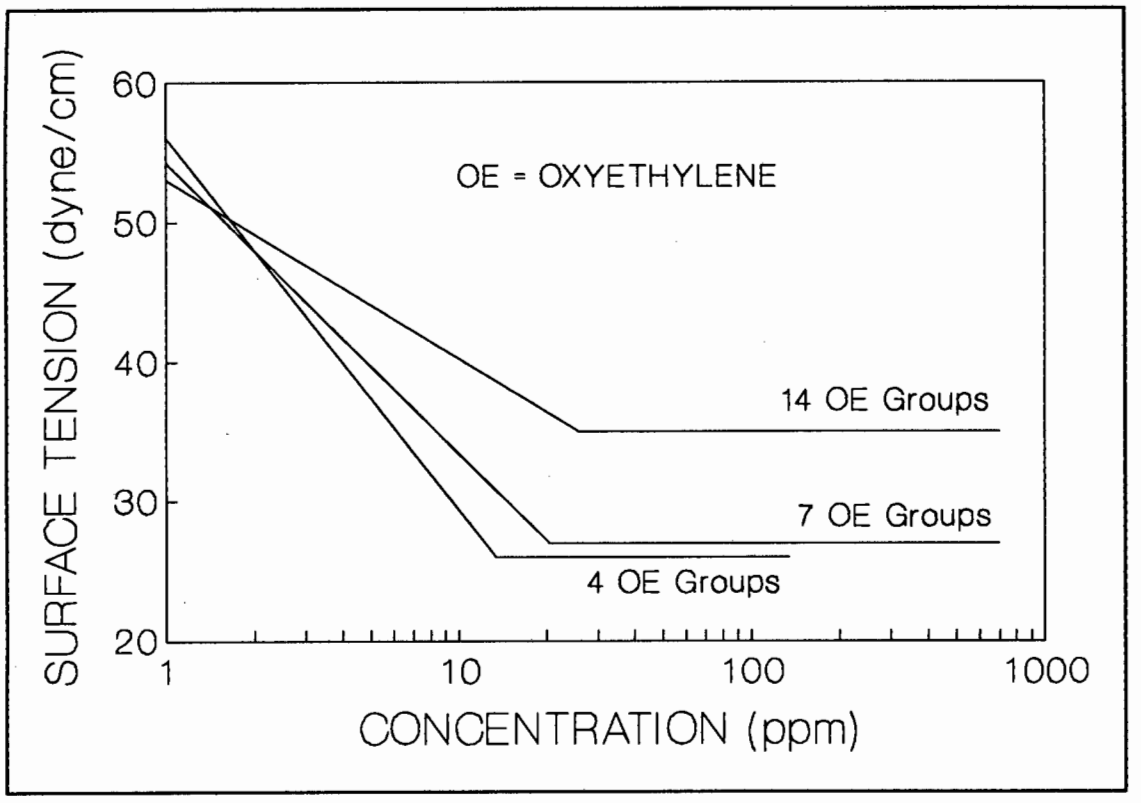

FIGURE 2.10 : Concentration vs Surface Tension for Aqueous Solutions of n-Dodecyl Polyoxyethylene (After Leja, 1982b)

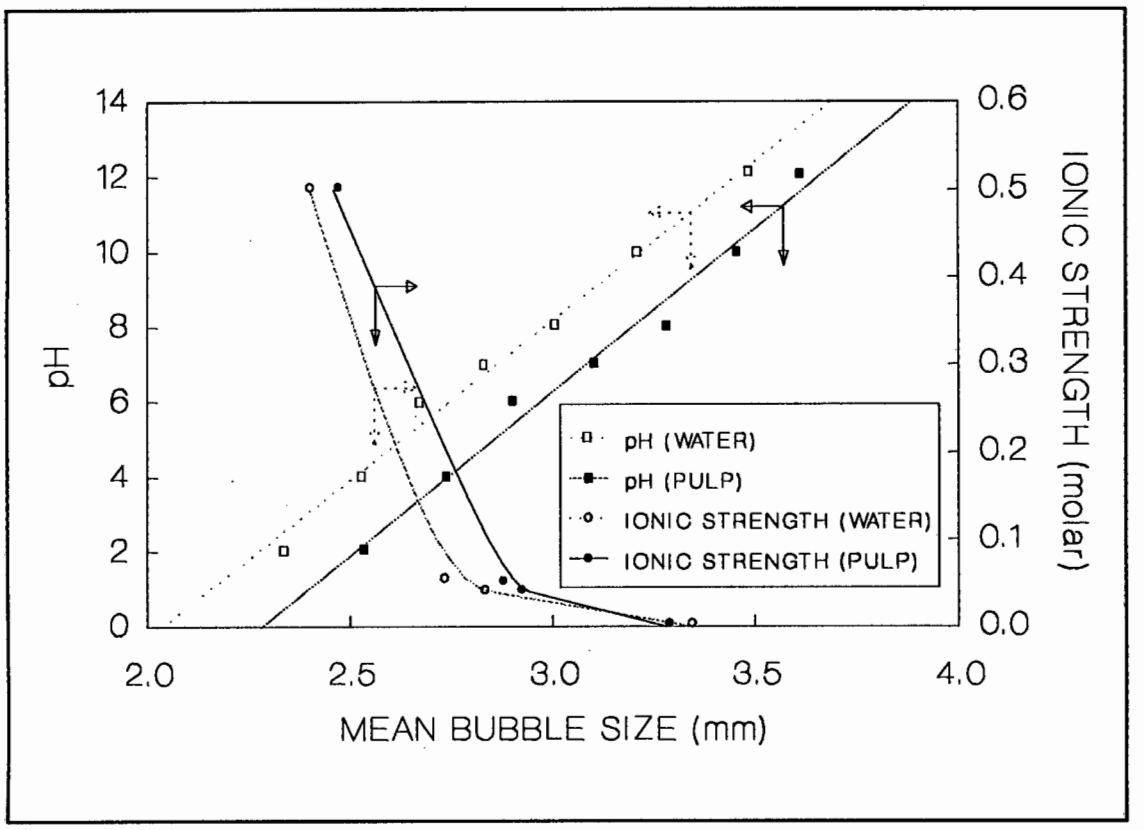

FIGURE 2.11 : Effect of pH and Ionic Strength on Bubble Size

TABLE 2.4 : Effect of Chemical Parameters on Bubble Size

	PARAMETER	VALUE		2-PHASE		3-PHASE	
				MEAN SIZE (mm)	STD. DEV. (%)	MEAN SIZE (mm)	STD. DEV. (%)
A	FROTHER CONCENTRATION (DOWFROTH 250)	0 ppm		**2.82**	29.1	**2.91**	31.3
		1 ppm		**2.58**	27.9	**2.53**	29.2
		2 ppm		**2.28**	25.9	**2.21**	28.1
		3 ppm		**2.19**	24.2	**2.15**	27.0
		4 ppm		**2.04**	23.0	**2.00**	24.0
		5 ppm		**1.81**	19.3	**1.86**	21.5
		6 ppm		**1.79**	17.9	**1.75**	19.4
		7 ppm		**1.77**	18.1	**1.70**	20.6
		8 ppm		**1.76**	17.0	**1.65**	20.0
		9 ppm		**1.76**	17.0	**1.64**	20.1
		10 ppm		**1.76**	17.0	**1.64**	20.1
B	COLLECTOR TYPE (0.5 mmol/litre)	Sodium ethyl xanthate (SEX)		**2.83**	27.6	**2.91**	30.9
		Potassium amyl xanthate (PAX)		**2.81**	28.8	**2.89**	32.2
		Sodium n-octyl xanthate (SOX)		**2.84**	28.9	**2.88**	31.3
C	COLLECTOR CONCENTRATION (PAX)	0.0 mmol/litre		**2.83**	27.6	**2.91**	31.3
		0.5 mmol/litre		**2.81**	28.8	**2.88**	32.3
		1.0 mmol/litre		**2.82**	29.1	**2.91**	31.3
D	PULP CONDITIONING	None		**2.83**	27.6	**2.89**	31.5
		PAX		**2.81**	28.8	**2.91**	32.0
		10 ppm Dowfroth 250		**1.76**	17.0	**1.63**	20.2
		PAX + Dowfroth 250		**1.76**	17.0	**1.62**	20.4
E	pH (SULPHURIC ACID) (SODIUM HYDROXIDE)	2		**2.33**	28.8	**2.53**	29.2
		4		**2.52**	27.8	**2.73**	30.8
		6		**2.66**	28.9	**2.90**	31.0
		±7		**2.83**	27.6	**3.10**	29.4
		8		**3.00**	28.0	**3.28**	30.2
		10		**3.21**	28.0	**3.45**	31.9
		12		**3.48**	28.7	**3.60**	33.9
F	IONIC STRENGTH	Solution	Ionic Strength				
		Distilled water	0.00	**3.34**	30.8	**3.28**	36.9
		Tap water	0.04	**2.83**	28.6	**2.91**	29.2
		0.1 molar KCl	0.05	**2.70**	28.5	**2.87**	31.4
		1.0 molar KCl	0.50	**2.40**	29.6	**2.46**	33.3

The effect of pH on bubble size is shown in Figure 2.11 and Table 2.4(E). It can be seen that an increase in pH causes the bubble size to increase. It has been shown (Hoh et al., 1986; Weast, 1982) that surface tension increases as pH increases. Hansford et al. (1976) have shown that viscosity increases as pH increases due to the 'ion cloud' effect. This result is consistent with the observation that, in the case of pyrite, recovery decreased

at higher pH's (Fuerstenau, 1982; Dimou, 1986). Apart from the other effects associated with surface adsorption of the collector at these pH's it is also possible that the lower recoveries are due to the smaller total surface area and lower collection efficiencies (Anfruns and Kitchener, 1976).

Table 2.4(F) shows that an increase in ionic strength leads to a decrease in bubble size. It has been shown that increasing the ionic strength increases the surface tension, but decreases the kinematic viscosity (Weast, 1982). This seems to be anomalous with the observation that increasing the surface tension increases the bubble size, but Sutherland and Wark (1955) state that salt solutions have weak frothing properties. They also state that it is impossible to form froths in pure solutions. This is probably because ions are necessary to stabilize the bubble once it has formed. It has, however, also been observed that high salt concentrations destroy the froth. Thus, it appears that, the presence of ions in solution in low concentrations leads to smaller bubbles with a larger bubble surface area and hence to a better collection efficiency. It can be seen from Figure 2.11 that increasing the ionic strength has the largest effect on bubble size at low ionic strengths, and this trend decreases and may even be reversed at higher ionic strengths. These observations are consistent with the findings of Barker (1986), who found that in many instances increasing the ionic strength increased the final recoveries in a pyrite-quartz system.

Table 2.5 shows the effect of adding various ions to a solution containing potassium butyl xanthate. In these tests a sintered disc with smaller porosity (porosity 4, pore diameter 9 - 15 μm) was used, so the results cannot be directly compared with the other results in this study. Copper and lead ions lead to an increase in bubble size. This is thought to be due to the formation of ultra-fine hydrophobic precipitates of copper or lead xanthates which lead to bubble coalescence due to increased contact angle. The presence of zinc and iron ions led to a decrease in bubble size. This decrease can be ascribed to the presence of ions in solution. These results compare well with those of Livshitz and Dudenkov (1965) who studied the same variables using a nephelometric and photographic method.

TABLE 2.5 : Effect of Cation-Collector Interactions on Bubble Size

POTASSIUM BUTYL XANTHATE CONCENTRATION (mg/l)	MEAN BUBBLE DIAMETER (mm)			
	Cu (2+) (50 ppm)	Pb (2+) (50 ppm)	Zn (2+) (50 ppm)	Fe (2+) (50 ppm)
0	1.70	1.70	1.69	1.67
5	1.84	1.73	1.31	1.32
10	1.84	1.77	1.24	1.28
20	1.88	1.84	1.21	1.21
30	1.99	1.90	1.20	1.24
40	2.14	1.96	1.19	1.21
50	2.24	2.04	1.19	1.21

2.4.1.iv SUMMARY OF BUBBLE SIZE EFFECTS

The relative effects of an increase in the various flotation parameters on bubble size are summed up in Figure 2.12. The values in this figure are approximate, because some of the parameters do not display linear effects on bubble size, and are only meant to give a qualitative picture of these effects.

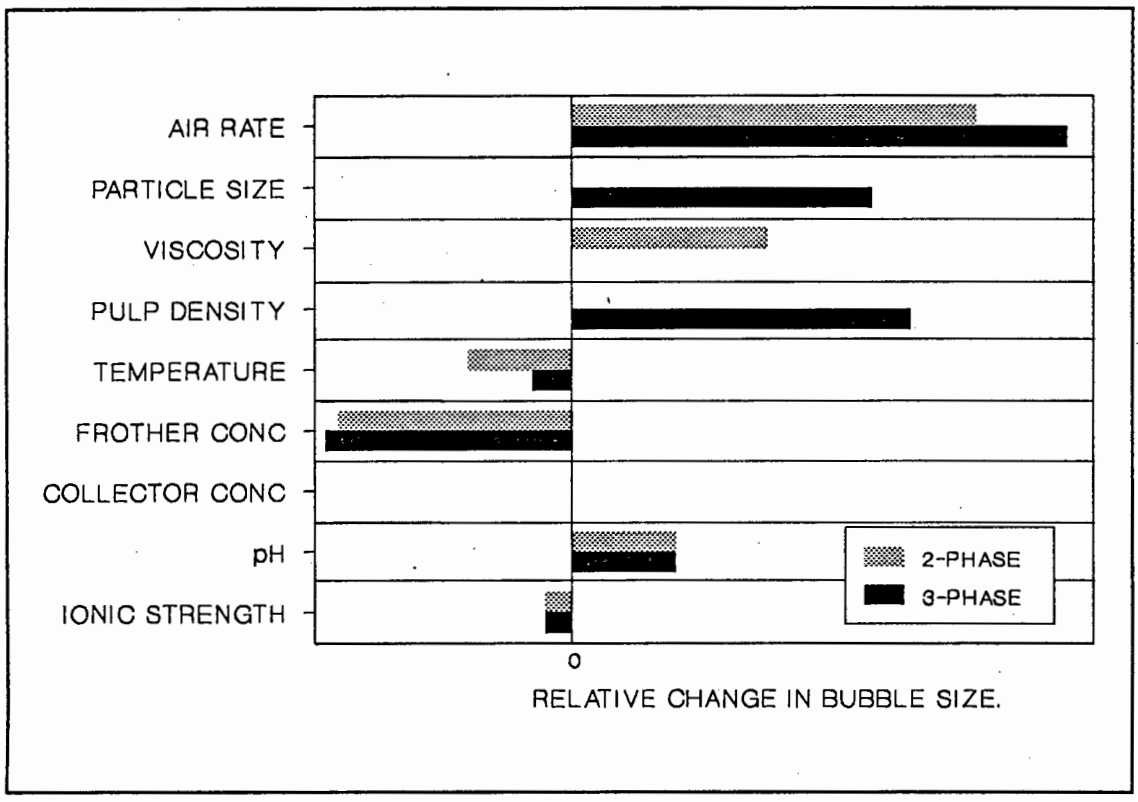

FIGURE 2.12 : Effect of Flotation Parameters on Bubble Size

It can be seen that air rate has the greatest effect on the bubble size. Factors which affect the viscosity (particle size, pulp density, temperature, pH) play a large role in determining bubble size. The frother concentration affects the bubble size by lowering the surface tension and making smaller bubbles more stable, although the magnitude of this effect, like that of ionic strength, decreases as the concentration increases.

2.4.2 RESIDENCE TIME DISTRIBUTION MODELLING

Both solid and liquid tracer studies were carried out on three-phase systems and liquid tracer studies on two-phase systems. The primary aim of this study was to develop a residence time distribution model for the solid phase in a column flotation cell. Having developed this model, the solid phase behaviour was compared to that of the liquid phase and to existing models of the pulp zone in flotation columns. The model development was therefore based entirely on solid tracer data in three-phase systems, and the liquid tracer tests were carried out purely for comparative purposes.

2.4.2.i SOLID TRACER STUDIES

A unique problem is posed when comparing a flotation column to a chemical reactor because there is one inlet and two outlets to the column. Classical chemical reactor models are not designed to handle this situation. It was thus decided to consider three independent systems, viz., the pulp zone, the froth zone and an unknown zone between them. Due to the unusual nature of the system it was difficult to carry out a mass balance of the tracer. This was because the concentrate and tailings became radioactive and could not be handled. Each detector also had its own sensitivity making it difficult to calibrate the detectors relative to each other. In order to overcome this problem the signals at each detector were simply normalised to give exit age distribution, E(t), curves.

$$E(t) = \text{Signal}(t)/\Sigma\text{Signal}(t)$$

This method is widely applied in industrial use of isotopic tracers to characterise flow patterns (Smith, 1989).

In choosing froth and pulp models it was important to note that only models with two or fewer model parameters could be used. Using more parameters would have over-specifying the system and made the parameters virtually meaningless. The reason for this was that the residence time distribution curves only had two measurable characteristics, viz., the peak height and the decay rate.

The pulp zone was modelled using a standard tanks-in-series model (Figure 2.13). A tanks-in-series (T-I-S) model with a bypass stream on each tank provided a slightly better fit than the T-I-S model as did a tanks-in-series model with backmixing between tanks (the Mavros et al., 1989 model), with a decrease in the error of 0.4% or less. It was not felt that this slight increase in precision warranted the complication of adding an extra parameter. It is probable that a one parameter model provided a good fit because a small diameter column was used. A bigger column would be better fitted by a two parameter model (Deckwer and Schumpe, 1987).

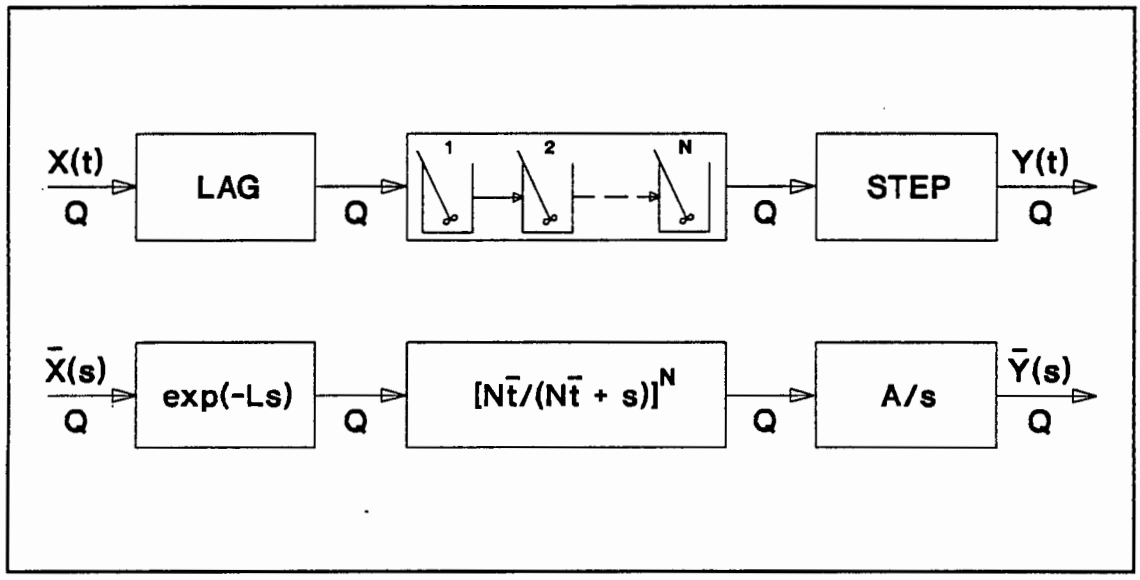

FIGURE 2.13 : Pulp Phase Model

It was necessary to include two constant terms in the model; viz., a time lag and a step change (Figure 2.13). The time lag accounts for the period between the time the tracer pulse was injected into the line and the beginning of the output signals. This lag was caused by the necessity to introduce the tracer about 20 cm from the feed point to the column so that the tracer input point could be well shielded from the other detectors on the column. The step change was required because slight contamination of the column

occurred during the course of each run preventing the detector output signals from returning to their base levels. This contamination was constant at the end of a run, but increased slightly with each successive run because the walls of the column picked up a small radioactivity from the tracer.

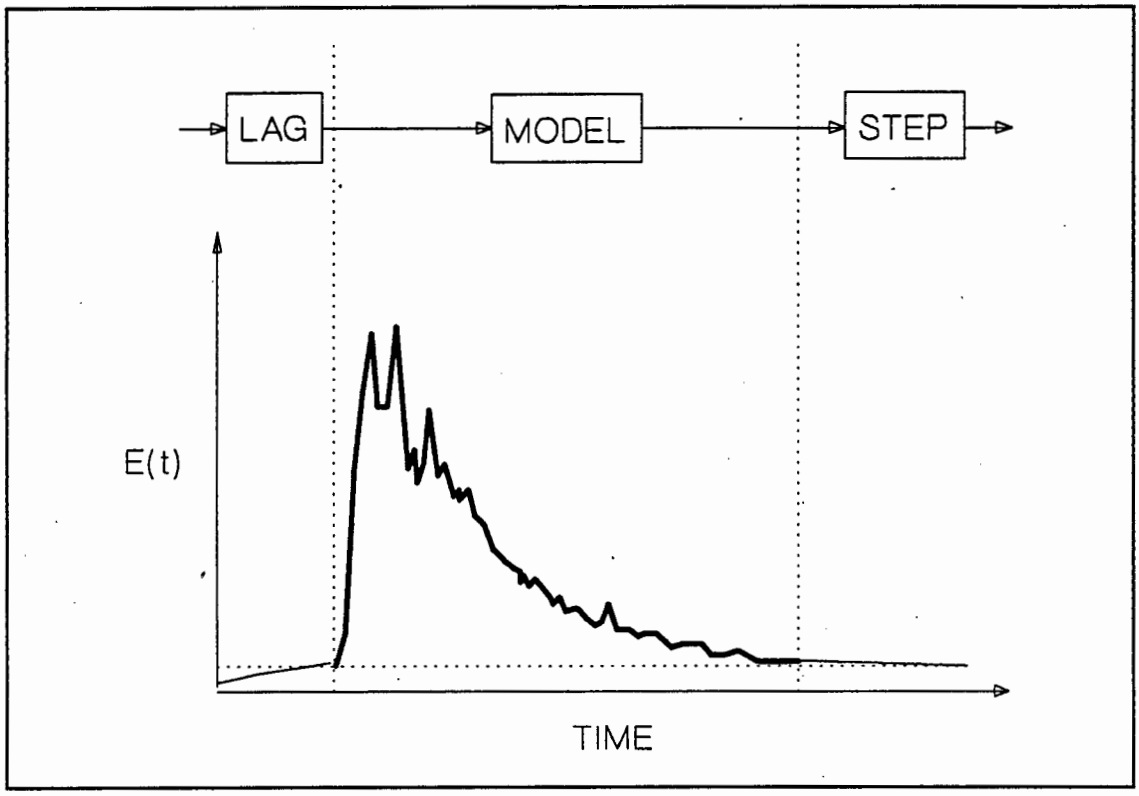

FIGURE 2.14 : A Schematic Representation of the Residence Time Distribution Model

The distortion of the residence time distribution of a system by a long tail is a problem often encountered in tracer studies. To overcome this problem a data manipulation technique suggested by Bryson (1970) was used. Since the data fits an exponential decay curve for some time period after the peak, a plot of the log of the E(t) data against time (t) will yield a straight line for this time period. The equation of this straight line is:

$$\ln[E(t)] = k_r t + \ln(k)$$

where k_r and k are constants. After this time period there will be a deviation from the straight line due to the tail. In order to eliminate the increase in variance due to this tail, the data for the tail region is discarded and is replaced by the calculated data using the equation for the straight line above. This technique is shown graphically in Figure 2.15.

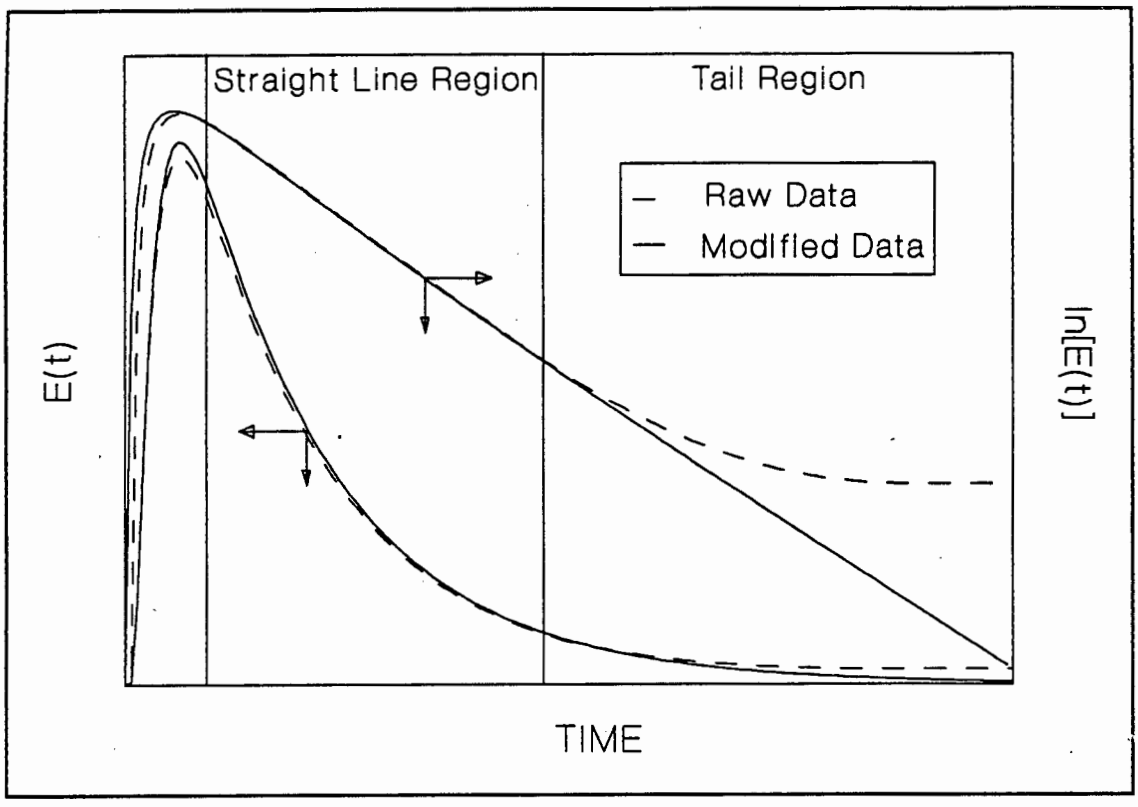

FIGURE 2.15 : The Elimination of a Long Tail Using an Exponential Function

2.4.2.ia Calculation of Model Parameters

The value of the pulp-zone model parameter (N, the number of tanks-in-series) was calculated using the standard reactor design theory as shown below. The mean residence time in the reactor (τ) and the variance (σ^2) were calculated from the concentration (C) and time (t) data.

$$\tau = \Sigma(C \cdot t)/\Sigma(C)$$

and

$$\sigma^2 = \Sigma(C \cdot t^2)/\Sigma(C) - \tau^2$$

The vessel dispersion number (D/uL) and number of tanks-in-series (N) were calculated from the relationships (closed inlet, open outlet vessel):

$$\sigma_\theta^2 = \sigma^2/\tau^2 = 1/N \cong 2(D/uL) + 3(D/uL)^2$$

This relationship is for fairly small extents of mixing (D/uL < 1) (Levenspiel, 1979).

The exit age distribution curve E(θ) for the model was calculated from the equations given in section 2.2.5, and the error between the experimental data and the model could then be found.

Buffham and Gibilaro (1968) point out that using the variance of the E(θ) curve to obtain N is sensitive to experimental error and using the normalised peak time (t_{peak}) is more accurate. If the equation for E(θ) in section 2.2.5 is differentiated then:

$$N = 1/(1 - t_{peak}) \qquad N \geq 1$$

If N < 1 then the response at a fixed normalised time may be used to estimate N. It was found in this study that the use of the variance technique produced very similar values of N to the techniques described above.

2.4.2.ib Choice of Tracer

Levenspiel (1972) points out that any material that can be detected and does not disturb the flow pattern in the reactor may be used as a tracer. Ideally the tracer should perform in exactly the same way as the bulk material being measured and should not be absorbed by the walls of the reactor. If only the flow regime in the reactor is to be measured, then the tracer should not interact with any other phases in the system, or else the combination of the interactions and the flow regime is measured.

Unfortunately it it not possible to measure only the flow regime in a column because the phases do interact. There is a liquid film around both bubbles and particles and particles may either become attached to, or be entrained by bubbles. This does not detract from the validity of the experiments since it is the actual behaviour of the particles in the real system that is of interest. Thus it is the combination of the phase interactions and the flow regime that should be measured.

The tracer chosen for these tests should be representative of the behaviour of the material leaving the column in the tailings. This will be a combination of floatable and non-floatable material, with the bulk being non-floatable particles. For this reason labelling the gangue would provide the best approximation to the behaviour of the solids in the collection zone.

If, however, it is assumed that there is little detachment of floated material from bubbles then the behaviour of the hydrophobic and the hydrophillic material should be similar at the bottom of the column. At the conditions of these tests with low bubble loadings and small bubbles Ross (1988) found that there was little detachment of floated particles from bubbles. The only other mechanism of bubble-particle interaction is entrainment which should affect all particles of the same size in a similar manner because entrainment is unselective. This of course does not account for the effects of density. Although pyrite is about twice as dense as quartz, the particle size is small enough for the density effects not to be very significant. The hydrophobic tracer should, therefore, provide a reasonable approximation of the behaviour of solids in the collection zone.

This has recently been found to be the case by Mills et al. (1992) at the University of Cape Town. In some recent column residence time distribution studies isotopically labelled tracers of hydrophobic, hydrophilic, and liquid material were used (Table 2.6).

TABLE 2.6 : Comparison Between Hydrophobic, Hydrophilic and Liquid Tracer RTDs (Mills et al., 1992)

	$\bar{t}$ (sec)	D/uL	N
HYDROPHOBIC TRACER	117	0.038	12.34
HYDROPHILIC TRACER	97	0.041	11.62
LIQUID TRACER	198	0.026	18.20

There is a small difference between the hydrophobic and the hydrophilic tracers but this is probably due to the density difference between the pyrite (hydrophobic material) and the quartz (hydrophillic material). It is however, evident that the liquid RTD is very different to that of the solids.

2.4.2.ic Tracer Studies

The pulse input in the feed line was assumed to be a δ function input signal for the pulp zone. The actual input signal into the pulp would have a longer tail than the column feed signal due to the elutriation of entrained material from the froth, but this difference was assumed to be small due to the recycling of these particles within the column (section 3.4.2). It would be possible to use the output signal from detector 4 (half way down the pulp zone) as the input for detector 5 at the bottom of the column, but the same problem of internal recycling would exist, and the information about the top half of the pulp zone would be lost.

Five runs were done at the standard conditions (run 3) to determine the reproducibility of the tracer studies. In all cases the mean absolute deviation (MAD) between the experimental response curves and mean response curve for all the runs was less than 9% (Table 2.7).

TABLE 2.7 : Reproducibility Tests

TEST NO.	DETECTOR 3				DETECTOR 4				DETECTOR 5			
	$\bar{t}$ (sec)	MAD (%)	VAR	MAD (%)	$\bar{t}$ (sec)	MAD (%)	VAR	MAD (%)	$\bar{t}$ (sec)	MAD (%)	VAR	MAD (%)
1	**70**	4.5	**1.507**	5.0	**83**	1.2	**0.754**	6.5	**136**	1.4	**0.427**	2.8
2	**69**	3.0	**1.555**	2.0	**87**	3.6	**0.762**	5.5	**131**	5.1	**0.454**	9.4
3	**63**	6.0	**1.671**	5.3	**81**	3.6	**0.864**	7.2	**143**	3.6	**0.380**	8.4
4	**61**	9.0	**1.719**	8.3	**83**	1.2	**0.852**	5.7	**145**	5.1	**0.396**	4.6
5	**72**	7.5	**1.484**	6.5	**86**	2.4	**0.798**	1.0	**135**	2.2	**0.417**	0.4
AVE	**67**	6.0	**1.587**	5.4	**84**	2.4	**0.806**	5.2	**138**	3.5	**0.415**	5.1

$\bar{t}$ = MEAN RESIDENCE TIME MAD = MEAN ABSOLUTE DEVIATION VAR = VARIANCE

From Table 2.8 it is evident that the calculation of the number of tanks-in-series often yields values of less than 1 near the feed point (detector 3). This implies that some short circuiting is occurring and the region should be modelled as a mixed tank with dead volume. This would result in an increase in the volume of the tank and consequently an increase in τ. This would lead to an increase in N because σ^2 remains unchanged.

The values of N in Table 2.8 show that the column was well mixed near the feed point (detector 3) and the flow regime tended towards plug flow near the bottom of the column (detector 5). It can also be seen that as

the mean residence time in the column decreased the degree of mixing (1/N) increased.

TABLE 2.8 : Pulp Phase Model Data

RUN NO	DETECTOR 3			DETECTOR 4			DETECTOR 5		
	$\bar{t}$ (sec)	D/uL	N	$\bar{t}$ (sec)	D/uL	N	$\bar{t}$ (sec)	D/uL	N
1	44	0.556	0.49	61	0.326	1.03	101	0.187	2.09
2	57	0.507	0.56	73	0.308	1.11	118	0.174	2.28
3	67	0.467	0.63	84	0.283	1.24	138	0.166	2.41
4	81	0.433	0.70	91	0.273	1.30	163	0.160	2.52
5	91	0.400	0.78	102	0.261	1.38	180	0.152	2.68
6	47	0.564	0.48	58	0.370	0.87	107	0.199	1.94
7	64	0.520	0.54	77	0.331	1.01	133	0.193	2.01
8	67	0.467	0.63	84	0.283	1.24	138	0.166	2.41
9	71	0.412	0.75	91	0.253	1.43	142	0.144	2.86
10	76	0.390	0.81	96	0.233	1.59	150	0.128	3.27
11	49	0.608	0.43	65	0.370	0.87	105	0.211	1.80
12	16	0.808	0.28	72	0.344	0.96	131	0.179	2.20
13	38	0.549	0.50	83	0.310	1.10	135	0.173	2.30
14	67	0.467	0.63	84	0.283	1.24	138	0.166	2.41
15	85	0.383	0.83	86	0.267	1.34	150	0.130	3.21
16	67	0.467	0.63	84	0.283	1.24	138	0.166	2.41
17	64	0.442	0.68	80	0.298	1.16	132	0.169	2.36
18	61	0.416	0.74	78	0.331	1.01	129	0.175	2.26
19	60	0.412	0.75	81	0.319	1.06	123	0.176	2.24
20	67	0.467	0.63	84	0.283	1.24	138	0.166	2.41
21	22	0.638	0.40	43	0.336	0.99	98	0.234	1.58
22	16	0.808	0.28	40	0.364	0.89	81	0.273	1.30
23	48	0.549	0.50	64	0.331	1.01	106	0.182	2.16
24	80	0.390	0.81	97	0.237	1.56	153	0.127	3.30
25	160	0.344	0.96	25	0.495	0.58	97	0.283	1.24
26	89	0.393	0.80	22	0.478	0.61	98	0.263	1.36
27	68	0.467	0.63	20	0.472	0.62	100	0.271	1.31

$\bar{t}$ = Mean Residence Time D/uL = Vessel Dispersion Number

N = Number of Tanks in Series

Figures 2.16 and 2.17 show the age distribution curves in the pulp, which are based on detectors 4 and 5 respectively. Also shown are the E(t) curves predicted by the model. The mean absolute deviation of the model from actual behaviour of the pulp was less than 5% in all cases.

It was concluded from the values of the vessel dispersion numbers in Table 2.8 that the axial dispersion model was not the best model for the

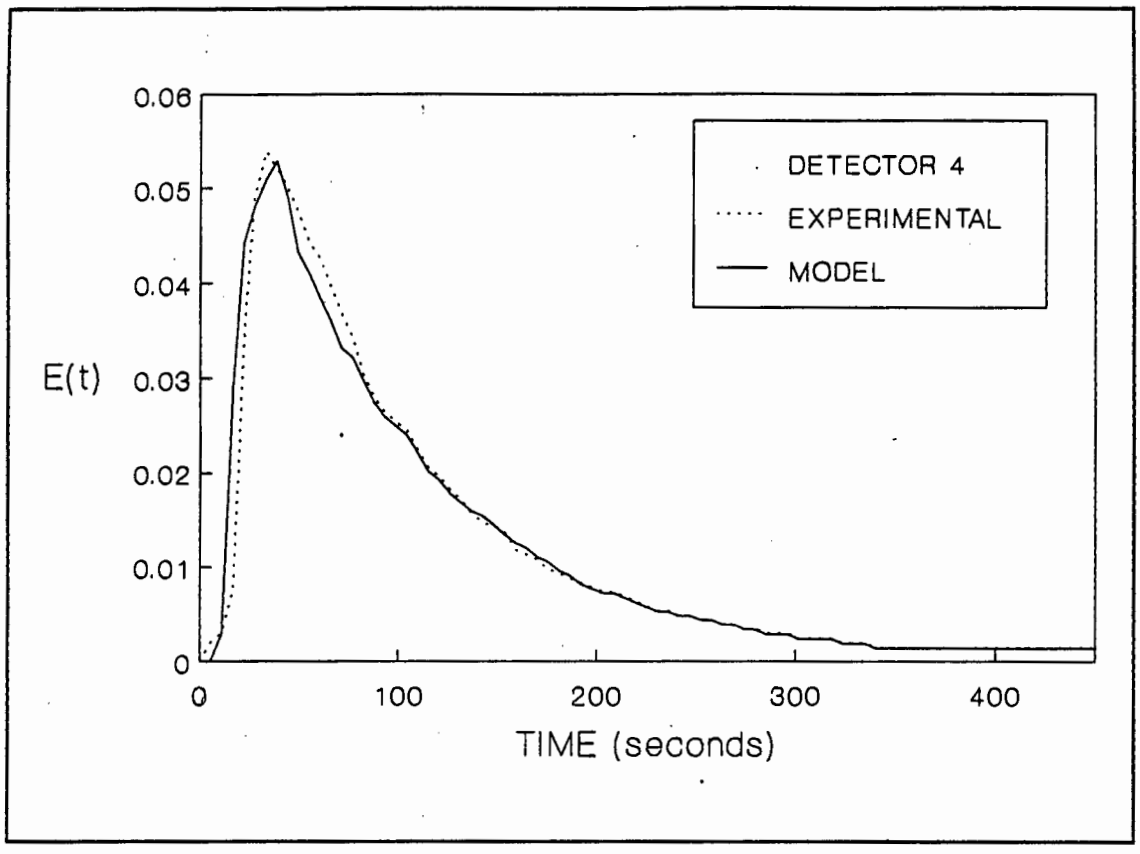

FIGURE 2.16 : E(t) Curve for Detector 4

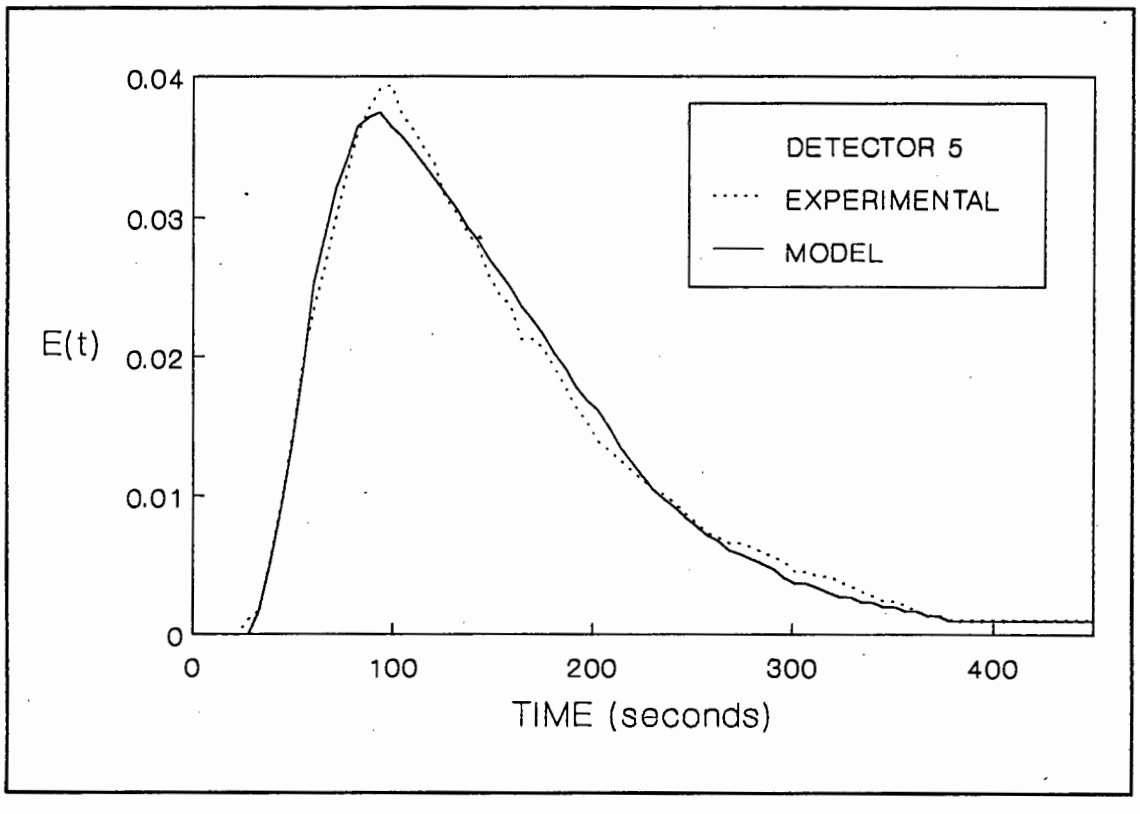

FIGURE 2.17 : E(t) Curve For Detector 5

pulp zone. The reason for this is that, while the vessel dispersion numbers at the tailings exit are generally well within the recommended limits (0.2, Bischoff and Levenspiel, 1962), the value half way down the column are significantly higher and often greater than the recommended values. It appears, as expected, that the length to diameter ratio (L_c/d_c) of the column has a large effect on the mixing in the column. This implies that on large scale columns the high degree of mixing that would be encountered in the pulp zone would invalidate this model. Most of the values of D/uL quoted by Laplante et al. (1988) are greater than 0.2 with the maximum being 0.97. These values are for liquid tracer studies in columns up to 1.03 m in diameter. In this study it has been found that the D/uL values for liquid are significantly lower than those for the solids, implying that the D/uL values in plant scale columns could often be larger than 1.

The tanks-in-series model does not suffer from the limitations of the axial dispersion model and, moreover, it describes the residence time distributions found in the pulp zone well. Future models for the pulp zone should therefore be based on the tanks-in-series model rather than the axial dispersion model.

Joshi and Sharma (1979) in their study of the fluid flow regime in bubble columns found that the circulation in a column did not extend over the whole length of the column, but was broken down into circulation cells in the axial direction (Figure 2.18 A). These circulation cells can be viewed as a series of well mixed zones, or tanks-in-series. The height of each circulation cell was determined by seeking the minimum eddy intensity and was found to be equal to the diameter of the column (d_c). This was true for a wide range of column diameters, column heights and gas flow rates.

It is dangerous to make direct comparisons between bubble columns and flotation columns because the conditions in the two types of column are usually quite different (gas rates are generally much higher, flow is usually cocurrent, etc. in bubble columns). The concept of the number of mixed regions in the pulp zone being related to the column diameter, however, should hold for flotation columns and would provide a good basis for scale-up using a tanks-in-series model. The column diameter is already used as one of the parameters for scale-up with the axial dispersion model (Finch and Dobby, 1990).

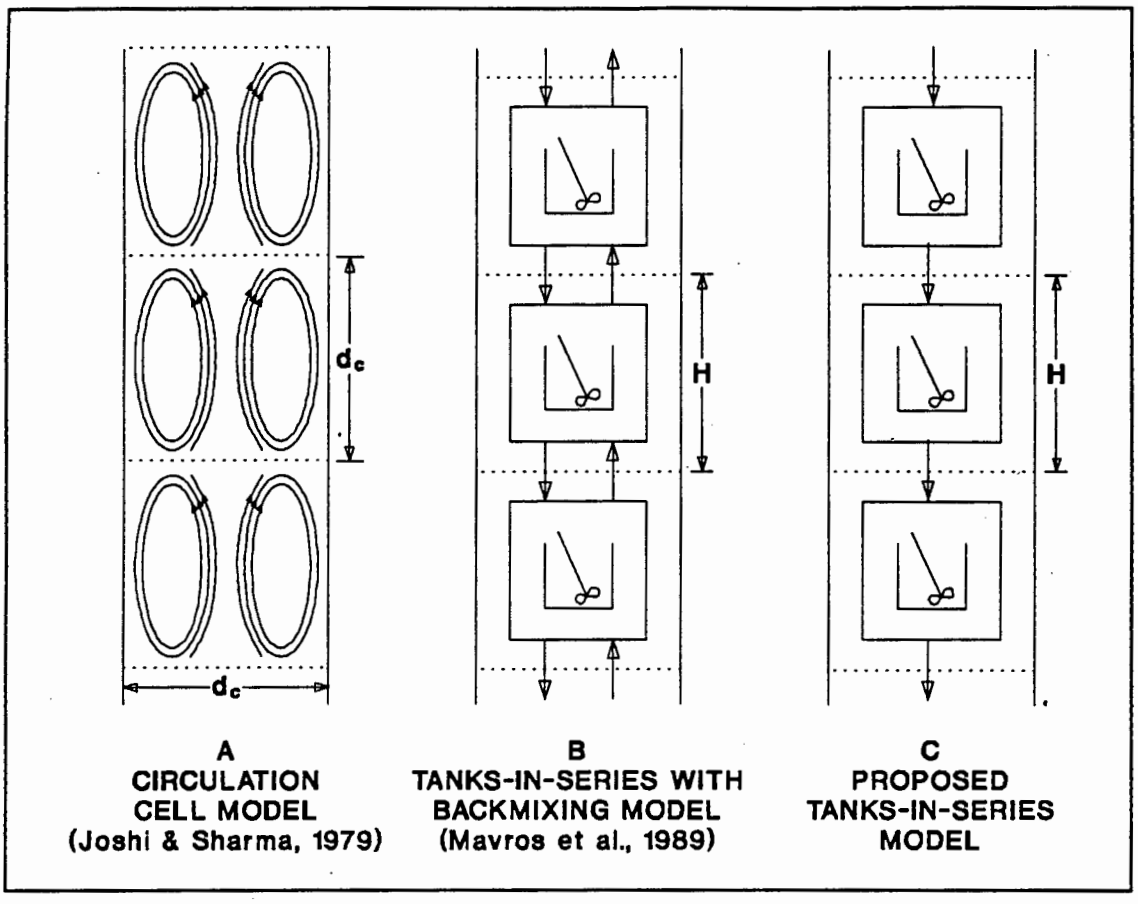

FIGURE 2.18 : Mixed Flow Models for the Pulp Zone of a Column Flotation Cell

The model proposed by Mavros et al. (1989) uses a series of well mixed zones with backmixing between adjacent zones (Figure 2.18 B) to describe the mixing found in the pulp zone. Deckwer and Schumpe (1987) found that it was not possible to describe the fluid flow regime in large bubble columns using a single parameter model, and this is also likely to be true for larger flotation columns. Thus the model proposed by Mavros et al. (op. cit.) is likely to provide a better fit for the data obtained from columns with larger diameters than a simple tanks-in-series model. The model parameters (N and λ) have been related to the vessel dispersion number (D/uL) by Mavros et al. so that the existing scale-up methodology can be applied. Since this effectively reduces the model back to a single parameter model, it is felt that a better way using the model for scale-up would be to relate the model parameters to the length and diameter of the column (L_c and d_c). A model based on a series of well mixed zones which incorporates air flow rate, pulp density, particle size, etc. analagous to the models proposed using the axial dispersion model could then be obtained.

TABLE 2.9 : Variation of Pulp Zone Mixing with Column Height

RUN NO	DETECTOR 4		DETECTOR 5		N_4/N_5
	$\bar{t}$ (sec)	Nd_c/L_p	$\bar{t}$ (sec)	Nd_c/L_p	
1	61	0.087	101	0.078	1.11
2	73	0.094	118	0.085	1.10
3	84	0.105	138	0.091	1.16
4	91	0.110	163	0.095	1.16
5	102	0.116	180	0.100	1.16
6	58	0.073	107	0.072	1.01
7	77	0.085	133	0.075	1.13
8	84	0.105	138	0.091	1.16
9	91	0.121	142	0.107	1.13
10	96	0.134	150	0.123	1.09
11	65	0.073	105	0.067	1.09
12	72	0.081	131	0.083	0.98
13	83	0.093	135	0.086	1.08
14	84	0.105	138	0.091	1.16
15	86	0.113	150	0.120	0.94
16	84	0.105	138	0.091	1.16
17	80	0.098	132	0.088	1.11
18	78	0.085	129	0.084	1.01
19	81	0.089	123	0.084	1.06
20	84	0.105	138	0.091	1.16
21	43	0.084	98	0.060	1.41
22	40	0.075	81	0.049	1.54
23	64	0.085	106	0.081	1.05
24	97	0.132	153	0.125	1.06
25	25	0.075	97	0.055	1.36
26	22	0.078	98	0.060	1.30
27	20	0.080	100	0.058	1.37

N = Number of Tanks-in-Series
N_4 = N for the Top Half of the Pulp Zone
N_5 = N for the Whole of the Pulp Zone
$\bar{t}$ = Mean Residence Time
d_c = Column Diameter
L_p = Length in the Column

Table 2.9 gives the number of tanks-in-series, normalised with respect to column length and diameter, for detectors 4 (half way down the column) and 5 (bottom of the column). From the ratio of the normalised N values for detectors 4 and 5 it can be seen that the degree of mixing is reasonably constant throughout the pulp phase under most conditions.

On the basis of the work done by Joshi and Sharma (1979), it is proposed that the length of the pulp zone should be converted into a dimensionless quantity by dividing it by the column diameter (i.e. L_p/d_c). The number of

tanks-in-series should then be divided by this new dimensionless length to obtain a new mixing parameter ($N \cdot d_c/L_p$) which is independent of the column diameter. This would allow the tanks-in-series model (Figure 2.18 C) to be used for scale-up purposes. More work using columns of different diameters needs be done to check that this new mixing parameter ($N \cdot d_c/L_p$) can be used to correlate the mixing in different size columns. Correlations using the tanks-in-series model as a measure of pulp zone mixing, analogous to those developed using the axial dispersion model (e.g. Laplante et al., 1988) could then be obtained, e.g.:

$$N = fn(d_c/L_p, J_g, \varepsilon, S, d_p)$$

It must be noted that while the ADM is not the best model to use for the pulp zone, it often fits the data well and to date provides the only scale-up methodology. The parameters in the tank-in-series model and the ADM are, furthermore, essentially equivalent.

2.4.2.ii LIQUID TRACER STUDIES

Two- and three-phase residence time distribution studies of the liquid phase were carried out using a liquid tracer (Mills and O'Connor, 1990). The results of these tests can be seen in Table 2.10 and Figures 2.19 and 2.20. It was found that a good δ function pulse input could be achieved and the reproducibility was excellent with mean absolute deviations between the pulses of less than 5%. Good reproducibility was also achieved in the RTD tests.

TABLE 2.10 : Comparison Betweem Solids and Liquid Residence Time Distributions (Mills and O'Connor, 1990)

PARAMETER	SOLIDS	LIQUID	
		2-PHASE	3-PHASE
MEAN RESIDENCE TIME (sec)	138	155	152
VARIANCE	0.41	0.12	0.13
VESSEL DISPERSION NEMBER (D/uL)	0.164	0.064	0.070
NUMBER OF TANKS IN SERIES (N)	2.41	8.33	7.98

No tracer was detected in the concentrate. This is to be expected because any feed water in the concentrate would have to be entrained, and the wash water should prevent this from happening to any significant extent.

The mean residence times and variances for the liquid phase in the pulp for two- and three-phase systems were very similar and it is probable that these differences lie within the bounds of experimental error. Slight differences may have been due to the increased settling rate of the solids compared to the liquid or to the volume of the solids in the pulp for the three-phase case. Only one pulp density (15% solids) was examined, but these values should only change slightly at other pulp densities (Laplante et al., 1988). In previous studies (e.g. Dobby and Finch, 1985, & 1986b) pulp density has not been included as a parameter in the correlations proposed.

From Table 2.10 and Figure 2.19 it can be seen that there are significant differences between the behaviour of the solid and liquid phases. Although there is little difference between the mean residence times of the solid and the liquid phases (about 10%), the shape of the E(t) curves are very different. The liquid flow regime is far closer to plug flow than that of the solids. This is to be expected because the bubbles interact with the particles causing them to become more mixed. Thus it is not possible to ascertain the residence time distribution of the solids by studying the liquid phase.

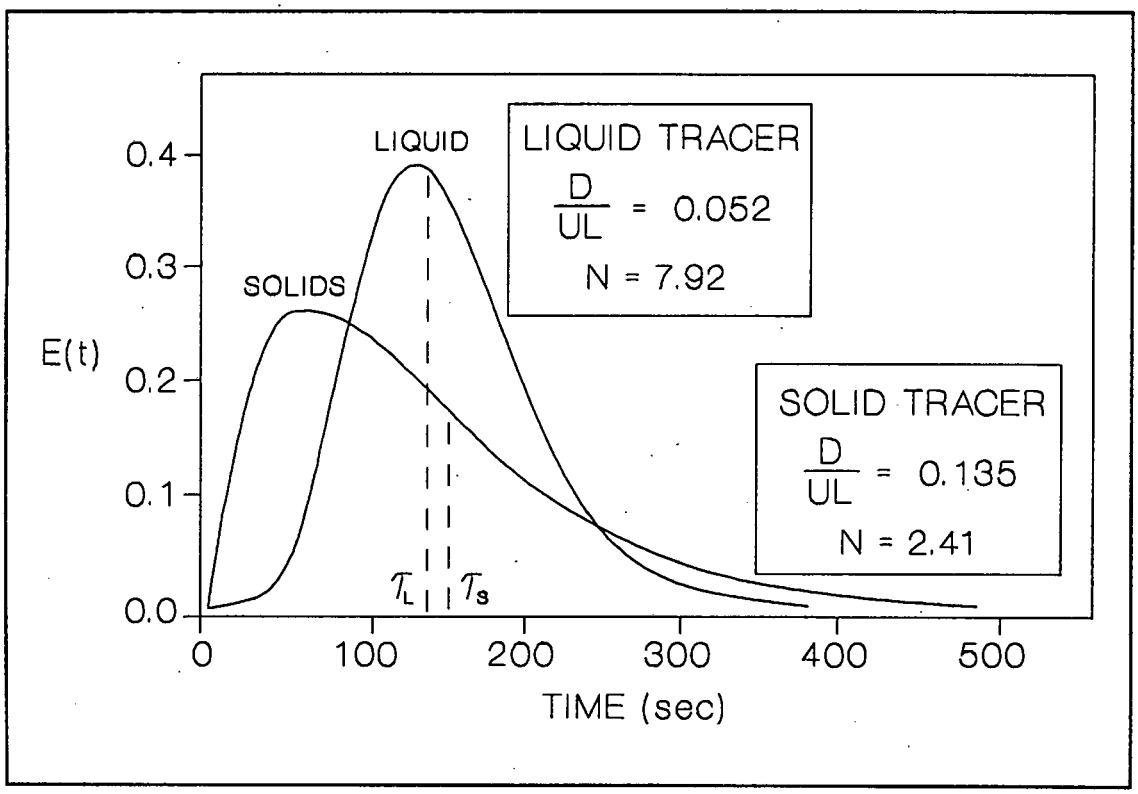

FIGURE 2.19 : Comparison Between the Residence Time Distributions of the Solid and Liquid Phases

2.4.2.iii COMPARISON WITH LITERATURE CORRELATIONS

Figures 2.20 and 2.21 show the trends in D/uL values with superficial air rate and pulp density respectively. It can be seen that the air rate has a far smaller effect on the liquid phase than on the solid phase. This reinforces the conclusion that it is bubble-particle interactions that are responsible for the differences in the degree of mixing between the solid and the liquid phases.

It can be seen that Dobby and Finch's (1985) initial correlation predicted the opposite trend to the results of this study because the air rate was not taken into account in the calculation of the vessel dispersion coefficient. As air rate increases D remains constant, but u increases because the effective area of the column (for liquid flow) decreases as the air hold-up increases and hence D/uL decreases.

The other correlations (Dobby and Finch, 1986 and Laplante et al., 1988) follow the same trend as the solid tracer study, and the differences observed may be due simply to different equipment and experimental conditions. Laplante's model provides the best fit for the data.

From Figure 2.20 it can be seen that neither of the correlations proposed by Dobby and Finch (1985, 1986b) show any change in the vessel dispersion number as the solids concentration changes. No significant change in D was observed in the liquid tracer studies as the pulp density increased from 0 to 15% solids indicating that the liquid phase is relatively unaffected by the presence of solids. Thus since Dobby and Finch's correlations are based on liquid phase data no change in the vessel dispersion number would be expected as the pulp density increased.

The correlation proposed by Laplante et al. (1988) gives the correct trend for higher pulp densities (> 10% solids), but predicts the highest values of D for the two-phase system. The data from this study indicates that the two-phase system has the lowest vessel dispersion number. It appears that there is a maximum value of D at a low pulp density, when there is maximum bubble-particle interaction. At higher pulp densities one of several effects may occur e.g.:

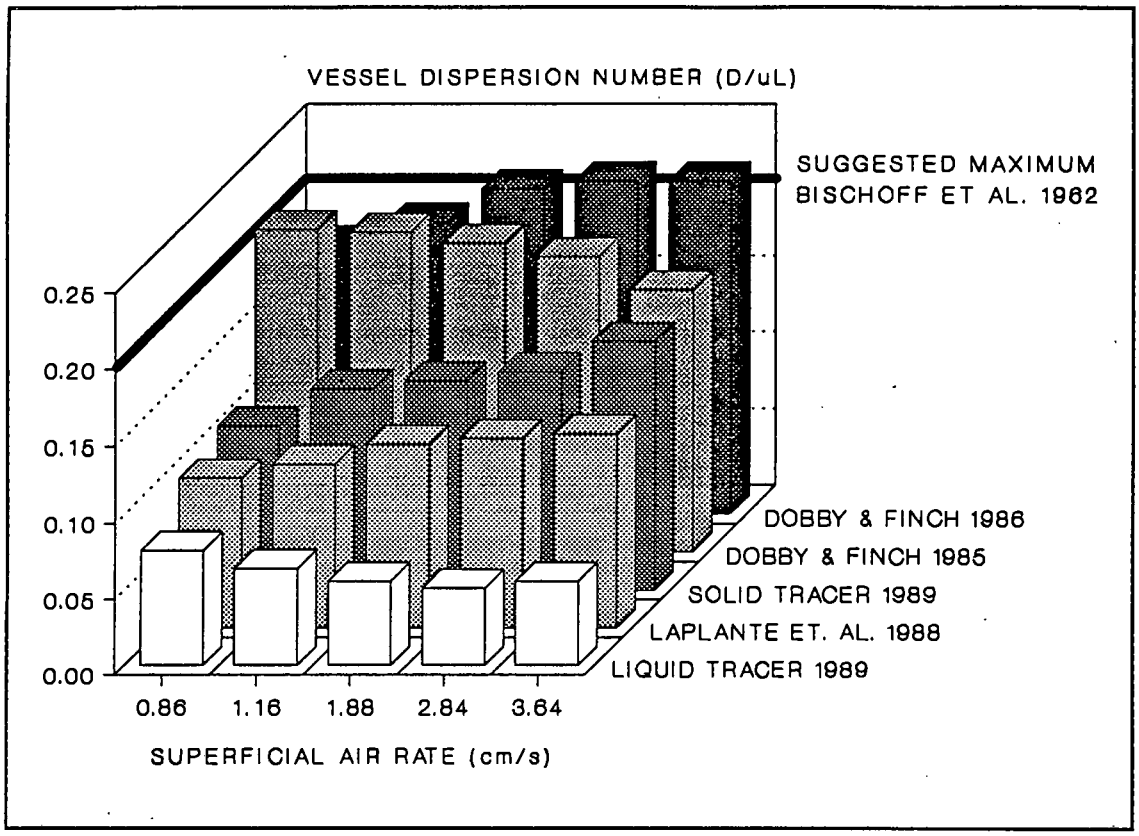

FIGURE 2.20 : Comparison of E(t) Curves for Superficial Air Rate

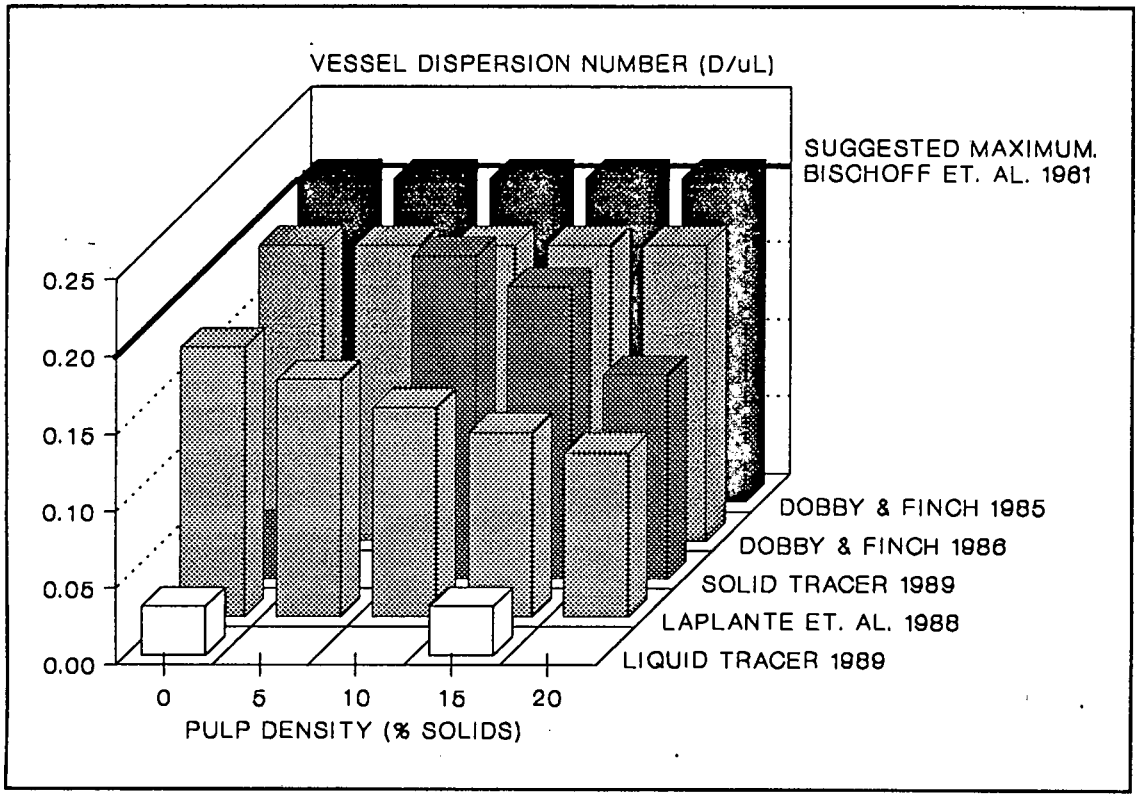

FIGURE 2.21 : Comparison of E(t) Curves for Pulp Density

- Inter-particle interactions hindering bubble-particle contacts.
- The increased viscosity slowing the formation of bubble-particle agglomerates.
- An increase in bubble loading, slowing the bubbles' rise velocity and decreasing the opportunity for entrainment.

2.4.3 EFFECTS OF FLOTATION PARAMETERS ON THE RESIDENCE TIME DISTRIBUTION IN THE PULP

Figure 2.22 gives a qualitative impression of the effects of increasing the flotation parameters considered in this study on the mean residence time and degree of mixing (1/N) in the pulp. Again, since many of the effects are not linear, this figure is merely designed to give an impression of the magnitude of the changes without putting any value to them.

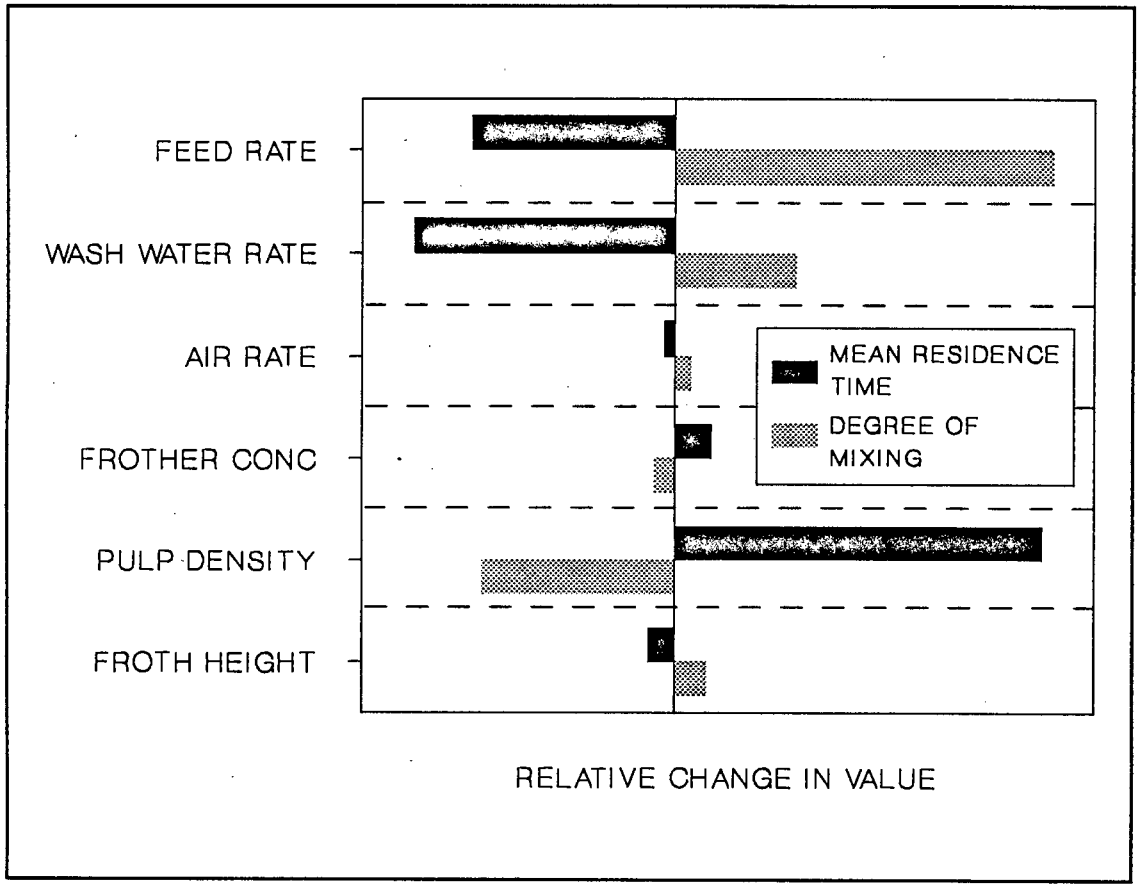

FIGURE 2.22 : Effect of Flotation Parameters on Residence Time

It can be seen that in all cases parameters which increase the mean residence time of the solids in the pulp decrease the degree of mixing in the pulp and often the relative magnitude of these effects are similar. A possible reason for this is the development of flow channels within the column which cause some short circuiting and mixing of the solids in the pulp zone. Short circuiting in a reactor implies that the reactor has some dead volume, and thus the effective volume of the reactor decreases. This decrease in effective volume obviously results in a decrease in mean residence time.

The decreases in the mean residence times of the solids in the pulp as the volumetric feed rate and the wash water rate increased were expected because of the increased downward bias in the column. The increased residence time of the solids as pulp density increased was probably due particles hindering each other, and to the increase in viscosity. These factors would also inhibit mixing. It can also be seen from Figure 2.12 that increasing the pulp density increases the bubbles size, thus decreasing the degree of mixing and gas hold-up and increasing the effective column diameter.

Only the solids feed rate changes when the pulp density changes, whereas feed rate and the wash water rate affect the volumetric feed rate to the column. The volumetric feed rate affects the solid and liquid feed rates without affecting the pulp density, while the wash water rate affects the feed rate of liquid and the pulp density without affecting the solid feed rate. These facts allow some conclusions to be drawn about the residence time distribution in the pulp zone of the column:

- If the residence time distribution of the solids and liquid were the same, then no change should be observed as the pulp density changes because the volumetric feed rate would remain constant. This is clearly not the case.
- It appears that the major effects that the wash water rate has on the pulp phase is to decrease the pulp density and increase the bias ratio. If the decrease in pulp density due to the additional wash water is considered, then the magnitudes of the changes to the mean residence time and degree of mixing cause by varying

these two factors are similar to those observed by changing the pulp density and increasing the volumetric feed rate.

- To achieve a given solid feed rate it is preferable to increase the pulp density rather than the volumetric feed rate (within certain limits) because this increases the residence of the solids in the column.
- A comparison of the feed rate and wash water rate trends shows that the degree of mixing of the solids in the column is most affected by the solids feed rate, while their residence time is determined to a large extent by the pulp density.

It can be seen that increasing the air rate has little effect on the residence time distribution in the pulp. Figure 2.11 shows that increasing the air rate has a significant affect on the bubble size. McKay et al. (1988), showed that the air rate had a far greater effect on the bubble size than on the gas holdup in columns using conventional spargers. This is because the increase in bubble volume is countered to a large extent by an increase in bubble rise rate and hence a decrease in bubble residence time. Larger bubbles tend to entrain more solids than small bubbles and hence would promote better mixing and longer residence times due to internal recycling. The changes observed in the residence time distribution as the air rate increases are probably due to a combination of these effects.

Figure 2.9 shows that increasing the frother concentration above 10 ppm has little effect on the bubble size. It is, therefore, expected that there should be little change in the residence time distribution as the frother concentration increases. The small changes observed are thus probably only due to a slight change in bubble size.

The changes observed in the pulp residence time when the froth height is increased are the result of decreasing the volume of the pulp zone and moving the feed point lower. The overall length of the column was not changed, thus the pulp zone was shorter and the L_p/d_c ratio of this section of the column decreased.

2.5 SUMMARY

A system has been developed to measure the sizes of bubbles in both two- and three-phase systems in a column flotation cell. The system provides statistically meaningful bubble size distributions with excellent reproducibility because about 3000 bubble are sized in each test.

It has been found that the bubble size in a column cell is primarily dependent on the viscosity and the surface tension of the system in which the bubbles are measured. These two factors are related, and affect the rate at which liquid films form around bubbles and the stability of these films. Increasing the viscosity or the surface tension, either directly or indirectly causes an increase in bubble size.

An increase in bubble size was caused by:

- An increase in air rate.
- An increase in particle size, and hence indirectly viscosity.
- An increase in viscosity.
- Changing the surface charge on the particles. This causes a change in viscosity due to ionic effects.
- A decrease in temperature.
- An increase in pulp density.
- A decreasing the frother concentration. This effect is most marked at low (< 5 ppm) frother concentrations.
- An increase in pH. This causes a change in viscosity due to ionic effects.
- A decrease in ionic strength. This is thought to make the bubbles unstable.
- The presence of ultra-fine metal-xanthate precipitates. These cause bubble coalescence.

Xanthate collectors were found to have no effect on bubble size.

The residence time distributions of the solid and liquid phases in the pulp zone of a column flotation cell have been studied using an isotopically labelled tracer for the solids and a salt solution to trace the liquid. The reproducibility of the system was good with a mean absolute deviation of less than 9% in all cases.

A tanks-in series model was found to provide a good fit for both the solid and liquid phases in the pulp zone with the mean absolute deviation between the experimental data and the model always less than 5%.

The axial dispersion model should not be used to model the solid phase in the pulp zone because the D/uL values are often too high for the assumptions made in the model to be valid. These D/uL values will increase as the L_c/d_c ratio of the column decreases causing errors in scale-up.

There was a significant difference between the residence time distributions of the solid and liquid phases with the solids being more mixed. Thus correlations predicting solid phase behaviour from liquid phase data should be avoided. For the liquid phase residence time distributions there was little difference between two- and three-phase systems.

It was found that factors which increased the mean residence time in the column decreased the degree of mixing in the column.

The pulp density tended to have the largest effect on the mean residence time in the collection zone of the column, while the solids feed rate had the biggest effect on the degree of mixing in this zone.

It was found that the air rate and frother concentration had little effect on the residence time distribution in the pulp zone of the column.

Chapter 3

FROTH ZONE EFFECTS

3.1 INTRODUCTION

In the early 1900s when froth flotation first came into vogue in the minerals industry the froth zone in flotation was thought to have little importance and was merely a medium of transportation for the concentrate from the pulp into the launder (Taggart, 1921). Concepts of the function of the froth have progressed markedly since then, but the froth still remains difficult to quantify, especially at the froth micro-kinetic (sub-process) level. Individual froth sub-processes are invariably difficult to distinguish and measure, and are often subtle or specific to one particular system.

When it comes to column flotation froths, matters are further complicated by the depth of the froth. Several different zones have been reported, and the addition of wash water is a variable not encountered in normal flotation processes. Due to the height of the froth it is very important to identify correctly the fluid flow regime in the froth and to distinguish between the behaviour of the various phases in froth.

The aim of this study was to better quantify the processes occurring in flotation froths, especially column flotation froths. This chapter describes and discusses the results of four studies:

- froth stability tests, in which maximum froth height is used as a method of determining the stability of the froth. These tests were aimed at quantifying the effects of flotation parameters, especially particle size and hydrophobicity on bubble coalescence and froth drainage;
- batch froth splitting tests in which the effects of flotation variables are quantified as a function of height in the froth to gain some insight into the processes occurring at different levels in the froth;

- continuous froth splitting tests designed to quantify froth effects while simulating more closely actual column operation. A further aim of these tests is to compare the froth in non steady-state (batch) and steady-state (continuous) operation; and
- residence time distribution studies of the froth phase in a laboratory column cell using a solid floatable tracer to determine the fluid flow regime of the solid phase in the froth and to compare it to the plug flow and completely mixed regimes postulated in the literature.

There are four sections in this chapter. In the first section the literature is discussed with special emphasis on the development of froth models. This is followed by a discussion of the apparatus and experimental methods used in each of the four tests programmes. The results are discussed, followed by a summary at the end of the chapter.

3.2 THEORY

3.2.1 THE FROTH PHASE OF FLOTATION

A flotation system consists of two basic interacting systems; the pulp zone and the froth zone. Much work has been done on the pulp zone (Moys, 1979). This includes investigation of physical factors such as cell dimensions and degree of turbulence and chemical factors like collector adsorption and pH. The froth zone however still presents an important area of potential investigation as little work has been done on this zone. Moys (1979) proposes two explanations for this: Firstly, the complexity of the sub-processes involved makes their investigation an unattractive proposition, best ignored, and secondly, the need to gain more insight into the equally important processes occurring in the pulp.

A good froth should be stable enough so as not to allow floated mineral particles to be dropped back into the pulp, but it must allow gangue drainage and must break readily for further treatment. A flotation froth is a complex, thermodynamically unstable, physico-chemical system. Its stability is determined by the rate and degree of liquid drainage from the inter-bubble films and subsequent bubble coalescence. This rate of thinning is influenced by a number of factors including liquid viscosity, particle size and hydrophobicity, bubble size and frother surface activity.

Most of the analyses performed thus far on flotation froths have been on a macro-kinetic level where the froth is examined as a whole, for example, the rate of concentrate production is assumed to be a function of the tailings concentration. Little understanding has so far been achieved on the micro-kinetic level because few methods exist for monitoring the sub-processes occurring in the froth. Most of the methods that do exist for quantifying the froth are complicated or require specialised equipment. For example Woodburn et al. (1989) used fibre optics and a high speed video camera linked to a powerful computer to analyse coal flotation froths.

The need to use assumptions of completely mixed or plug flow for the froth so that some degree of analysis can be performed tends to overshadow the effects of some of the parameters affecting the froth. In the words of Mika and Fuerstenau (1969): "The absence of a detailed representation of

froth sub-processes frustrates the attempts to arrive at a complete microscopic model of the overall flotation process...".

Models of flotation range from simple macro-kinetic models (Bushell, 1962) to more complex models (eg. King 1970). Here air rate, froth effects, particle size and composition and bubble loading are taken into account. Harris (1976) proposed an improvement to the ideal mixing assumption by introducing a recycle model. Woodburn et al. (1976), in his comprehensive review of flotation models proposed a complete model, but its complexity and the large number of variables involved make its analysis virtually impossible. It is, however, generally agreed that the processes occurring in flotation are linear and can best be represented by first order kinetics (Ball and Fuerstenau, 1974).

3.2.2 DEEP FROTH EQUIPMENT

Several pieces of equipment have been developed for sampling flotation froths. Most revolve around the concept of an 'equilibrium froth'. The froth is not removed from the cell as it is generated, but is allowed to build up. At a given time the froth is sampled or partitioned and then analysed. The purpose of these equilibrium froths was to allow the rate of transfer of material into and out of the froth to reach a steady-state, thus simplifying later analysis. Deep froths also allow the study of froth drainage and entrainment because these processes become more apparent as froth height increases. Using the equilibrium froths does not accurately simulate normal flotation because standard flotation froths do not have time to reach equilibrium. They do however provide a valuable insight into the factors affecting froth stability, especially those varying with froth height.

Watson and Grainger-Allen (1973) developed the 'equilibrium cell'. It consisted of a bottom driven batch flotation cell which was modified so that tall froths could be accommodated. The froth was allowed to build up until equilibrium was reached and then a slide was inserted between the froth and the pulp, thus separating the froth from the pulp. The froth and pulp were then removed and analysed.

This idea was continued and improved upon by Cutting and Devenish (1975). They split the froth into four horizontal segments by inserting three additional slides. This allowed the investigation of chosen parameters as a function of height in the froth.

Watson and Grainger-Allen's equilibrium cell concept was further developed by Cutting et al. (1981). Small sampling tubes were inserted into the froth and pulp at different levels. At a given time small samples could be withdrawn under vacuum for analysis using these tubes. This provided information about the froth at different levels, as well as locating the pulp-froth interface. This concept was extended to the non-equilibrium froths in conventional flotation systems.

Moys (1979) used a bottom driven cell with the high sides. The front of the cell was slotted and small strips of perspex could be inserted or removed to govern the froth height. Down one side of the cell was a series of holes sealed with rubber stoppers. These could be removed and small samples taken systematically starting from the top of the cell.

Ross (1988) used a similar system to Cutting and Devenish (op. cit.) in a batch cell to split the froth at various levels. He also used a sampling lance to sample the froth of full-scale cells at various levels. These techniques allowed him to develop froth profiles.

Both of the basic methods described above have advantages and shortcomings. In the methods where a small sample of froth is removed, the float can continue and the progress of the froth can be monitored with time. The disadvantage of this method is that the froth must be perfectly uniform at any froth depth to ensure a representative sample is obtained. This is unlikely to be the case, especially if the samples are taken near the walls (eg. Moys, op. cit.). The samples obtained from the froth splitting techniques are representative of the froth at that level because the whole layer of froth is removed, but the float must be stopped when the samples are taken. There are also practical problems involved with removing the froth. One advantage of this method is that it allows the total froth volume, including air, to be determined.

3.2.3 FROTH PHASE MODELS

Due to the complexity of the processes occurring in the froth phase of flotation and the variations encountered in different flotation systems, good froth phase models are difficult to obtain. Models either tend to be over simplifications, with their assumptions of ideality making them of little practical use, or the attempt to model the processes in a realistic fashion makes any analysis using these models difficult, if not impossible. For a model to be of value, however, it must incorporate the major sub-processes occurring in the froth. In order to do this, accurate methods of measuring froth variables are required. It is the lack of these methods that, to a large extent, have hindered the development of models for the froth phase.

A large number of froth models have been proposed (eg King, 1975; Woodburn et al. 1976; Sutherland, 1977; Ford and King, 1983; Green, 1984; and Smith 1984.). All these models rely on assumptions made about some of the parameters in the froth phase which are difficult to quantify. For example Green (op. cit.) placed constraints on the composition of certain streams in the simulation of flotation networks, and Woodburn et al. (op. cit.) used enhancement factors to simplify the solution of their model.

The more recent trend has been to shift the emphasis to models based on the measurement or more accurate estimation of froth variables. This has led to new and improved methods of characterising the froth. (eg Moys, 1978, 1984; Cutting et al, 1981, 1982, 1986; Ross, 1988.)

Early models include those of Bushell (1962) and Arbiter and Harris (1962). Bushell postulated a model in which the rate of return of particles into the pulp was proportional to the rate of particle entry into the froth phase. His model was of the form:

$$k' = k_p(1-k_f)$$

where k' is the effective rate of particle entry into the froth, k_p, the actual rate of particle entry into the froth, and k_f, the fraction of particles entering the froth that are returned to the pulp.

Arbiter and Harris (1962) proposed a model on which most further attempts at modelling the froth phase are based. They assumed perfect mixing in both the pulp and froth phases and that particle transfers between the phases could be modelled on first order kinetics.

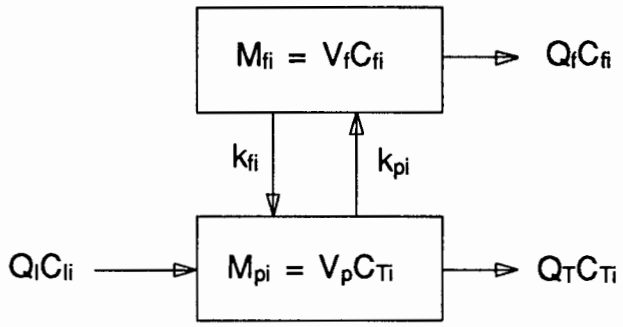

This gave the rate of flotation as:

$$Q_f C_{fi} = k_{pi} V_p C_{Ti} - k_{fi} V_f C_{fi}$$

where Q_f is the volumetric flow rate of froth, C_{fi} and C_{Ti} are the concentrations of particles of the ith component in the froth and pulp respectively, k_{pi} is the rate of particles entering the froth, and k_{fi} the rate of particles returning from the froth to the pulp. V_p and V_f are the volumes of pulp and froth respectively.

There are two main problems arising from this model: Firstly the assumption of a perfectly mixed froth is invalid due to the elutriation of gangue material from the froth, and the flow regime in the froth is likely to be somewhere between plug flow and perfectly mixed flow. The second difficulty is the measurement of the volumetric flow rate of the froth (Q_f). Since no methods of measuring the volumetric flow rate of froth (three-phase) had been developed, Q_f and V_f have to be defined on an air free basis. Most workers overcome this difficulty by assuming that the froth flow rate is constant over the range of conditions that they are working in. This is, however, only true over a small range and varying most flotation parameters would change the froth flow rate. If this assumption is made, however, the froth volume may be included in a new rate constant:

$$k_{fi}' = k_{fi} V_f$$

The notable exception to this approach is that used by Greaves and Allen (1974). They estimate V_f by assuming that all the components in the froth have the same residence time. Thus they get:

$$V_f = \frac{\text{(Volume of the froth zone)}}{(1 + G/Q_f)}$$

where G is the air flow rate.

This result is disputed by Moys (1979), who points out that the bubble rise rate is greater than that of the air free fraction, and there is a loss of air from the top of the froth due to bubble breakage. Moys, therefore, proposes that:

$$V_f = \frac{\text{(Volume of the froth zone)}}{(1 + \alpha_s G/Q_f)}$$

where α_s (<1) is the relative froth stability and is a function of the relative drainage rate of the froth. This, in turn, is a function of factors like the liquid viscosity, temperature, particle size, bubble size and bubble loading.

A major fault with Greaves and Allen's model is that generally Q_f is dependent on G and thus G/Q_f remains constant over a wide range of conditions. This implies that V_f is constant over this range, which is usually not the case.

Moys suggests that the model proposed by Harris and Rimmer (1966) can be used to obtain the air free volume of froth if it is assumed to be valid for both solids and water. Thus:

$$V_f = \Sigma(m_i/\rho_i)$$

where m_i and ρ_i are the mass and density respectively of the ith component.

Arbiter and Harris' model was used by Jowett et al. (1966) to interpret a large range of continuous coal flotation data. They found that this model gave a good fit for their data. The expression they used was:

$$\frac{C_T}{C_l C_f} = \frac{Q_f}{k_p' C_l} + \frac{k_f''}{k_p'}$$

where: $k_f'' = \frac{k_f}{V_f C_l}$ and $k_p' = \frac{k_p}{V_p}$

It was noted by Moys (1979) that the above equations resulted from the correlation of equilibrium data. Flotation froths are transient and hence the correlations obtained are not directly applicable. This is borne out by the studies of dynamic froth behaviour conducted by Greaves and Allen (1974) and Sadler (1973).

Several authors, including Ball and Fuerstenau (1974), have used and extended this model in both continuous and batch operations. Ball and Fuerstenau point out, however, that little insight can be gleaned from the model on even a macroscopic level due to the lack of a method of determining the particle return constant (k_f) with any accuracy.

Jowett (1966) described the effect of the froth phase on the recovery of hydrophillic gangue particles. He noted that the mechanism by which they were included in the froth was entrainment. The same basis was used for both gangue and floatable mineral recovery, but with different rate constants. Jowett postulated that the rate of gangue recovery due to entrainment was proportional to the gangue concentration in the pulp and the rate of water inclusion into the froth, the proportionality constant depending on the size fractions of the gangue involved.

This model was first quantified by Lynch et al. (1974) who proposed that the gangue recovery (R_g) could be obtained using the expression:

$$R_g = Q_w \Sigma (C_{Fi} C_{ti})$$

where Q_w is the flow rate of water in the concentrate and C_{ti} is the tailings concentration of gangue with particle size i. C_{Fi} is the classification function and is defined as:

$$C_{Fi} = \frac{\text{solids/water ratio of free gangue (size i) in conc}}{\text{solids/water ratio of free gangue (size i) in pulp}}$$

In a series of experiments in which particle density, pulp density and water recovery rate were varied, Bisshop and White (1976) defined a froth residence

time. They assumed that the air-free froth volume was proportional to the froth height and obtained:

$$\tau = V_f/Q_w = roh/Q_w$$

where τ is the froth residence time, V_f, the froth volume on an air free basis, h, the froth height and r_0, the proportionality constant. This would not however be true if certain flotation parameters, e.g. air rate, which affect the air hold-up in the froth were varied.

They then state that the rate of particles of size i entering the froth from the pulp (Q_i) is proportional to the rate of water entry into the froth (Q_{FW}) and to the concentration of particles of size i in the pulp (C_{pi}):

$$Q_i = k_{pi} \cdot Q_{FW} \cdot C_{pi}$$

where k_{pi} is a transfer factor. The rate of drainage (Q_D) from the froth is proportional to the mass in the froth (M). k_{fi} and k_{fw} are the proportionality constants.

$$Q_{Di} = k_{fi} \cdot M_i \qquad \text{and} \qquad Q_{DW} = k_{fw} \cdot M_w$$

They then assumed that the concentrate flow rate (Q_{Fi}) was proportional to the mass of gangue in the froth (M_i) and inversely proportional to the froth residence time. Thus:

$$Q_{Fi} = \frac{k_{ci} M_i}{\tau} = Q_i - Q_{Di}$$

Similarly:

$$Q_w = \frac{k_{cw} M_w}{\tau} = Q_{FW} - Q_{Dw}$$

Where k_{ci} and k_{cw} are the constants of proportionality. They then use the classification function proposed by Lynch et al. (1974) to get:

$$C_{Fi} = Q_{Fi}/(Q_W \cdot C_{pi})$$

Rearranging the above equations they get:

$$C_{Fi} = \frac{(1 + k_{fw}\tau/k_{cw})}{(1 + k_{fi}\tau/k_{ci})}$$

Moys (1979) points out that the values of k_{cw} and k_{ci} are close to 1 for dilute froths and can thus be ignored, thus:

$$C_{Fi} = \frac{(1 + k_{fw}\tau)}{(1 + k_{fi}\tau)}$$

Substituting the expression for τ above and including r_0 in the new proportionality constant they obtained:

$$Q_{Fi} = \frac{Q_w + k_{fw}"h}{Q_w + k_{fi}"h}$$

This allows easy analysis of the classification function because the froth height and water flow rate can both easily be controlled.

Woodburn et al. (1976) in their review of flotation kinetics developed a comprehensive model for flotation networks involving residence time distribution. They use enhancement factors to linearize computations of internal mass flow and they then use these mass flows together with knowledge of external effects such as chemical additions and cell operating parameters in an iterative process to redefine the enhancement factor matrix. Due to the complexity of the model it is impractical to use.

Moys (1979) made a significant contribution towards identifying sub-processes in equilibrium froths by using a first order kinetic model. He assumed that the rate of detachment of particles from bubbles was proportional to the concentration of the species in question. It was proposed that the mass flow rate of component i at height z was:

$$m_i(z) = m_i(0) \qquad z \leq z_{di}$$

$$= m_i(0)\exp[-k_i(z-z_{di})A_c/G] \qquad z > z_{di}$$

where $m_i(0)$ = mass flow rate of species i into the froth,
k_i = detachment rate constant,
z_{di} = level at which detachment starts,

G = aeration rate,
A_c = cross sectional area of the flotation cell.

A constant velocity difference (Δv_i) was assumed between the air and the downward flowing streams. This allowed a drainage velocity [$U_i(z)$] for species i to be calculated, and hence its mass fraction at any height.

$$U_i(z) = \Delta v_i - v(z)$$

where v(z) is the bubble rise velocity, which was assumed to be constant throughout the froth to simplify calculations. This clearly would not be the case because some bubble coalescence would occur as height in the froth increased.

Ross (1988) points out that this model has two limitations. Firstly, no estimate is provided of the height at which the detachment of entrained particles occurs. And secondly, a constant relationship is assumed between the drainage rate of water and entrained particles over the height of the froth. This is unlikely to be true because there would be an increasing degree of entrapment of particles as the water content of the froth decreases. Moys proposes the following equations for the flow rate of water (q_c) and particles (m_c) in the concentrate:

$$q_c = \alpha q_c(z_w)$$

and

$$m_c = \alpha[m_{fi}(z_w) + m_{ei}(z_w)]$$

where α = fraction of the froth removed in the concentrate,
$q_c(z_w)$ = water flow rate at the froth surface, z_w,
$m_{fi}(z_w)$ = mass flow rate of floated species at the froth surface,
$m_{ei}(z_w)$ = mass flow rate of entrained species at the froth surface.

These equations assume uniformity at the froth surface and no losses of water or particles in the removal of the froth. This is clearly not true. Cutting et al. (1981) introduced a cell efficiency factor (< 1) to account for the finite probability of particles in the froth being transferred into the concentrate.

Moys (1984) has expanded on his previous model to include froth flow in two dimensions. Residence time distribution studies were made of 'perfectly floatable' particles in the froth to predict froth mass flow rates. This model involves the numerical solution of two dimensional Laplace transforms. In it original form the equations are complex and difficult to solve. To facilitate the calculation of the model parameters the froth is divided into three stages. Stage one is a region at the back of the cell in which no froth movement towards the lip occurs, stage two is a region in which there is a linear increase in horizontal froth velocity as the distance from the lip decreases and stage three is a region near the lip in which only horizontal froth travel occurs. It was assumed that all material enters the froth from stages one and two.

Three shortcomings of this model are pointed out by Ross (1988). Firstly, the froth velocity was assumed to be independent of the froth depth, and only a function of the horizontal distance from the lip. Secondly, a uniform air distribution at the pulp-froth interface was assumed. And thirdly, no account was taken of the significant amount of vertical froth flow which occurs near the cell lip. The model is however a significant improvement on previous models and can deal with phenomena such as negative froth velocities (froth flow away from the lip) and the streamlines which occur in the froth.

Bascur and Herbst (1982) developed a population balance model in which particles are classified into four different groups, each group having its own rate constant. The groups were: particles free in the pulp, particles attached in the pulp, particles free in the froth, and particles attached in the froth. The balance of the particles and their rate constants were determined by the flotation conditions. Although the model worked in modelling the froths in a pilot plant, its parameters have little physical significance.

Meyer and Klimpel (1982) regard the froth as a kinetic species because it is a medium in which particles are carried. Their model describes the recovery (R_t) of particles after a time (t) in terms of the ultimate recovery (R) and a rate constant (k_r):

$$R_t = R - R\frac{1 - \exp(-k_r t)}{k_r t}$$

They also found that increasing the solids content in the froth led to a decrease in froth fluidity and concluded that the rate of removal of particles could be controlled by the characteristics of the froth as well as the rate phenomena occurring in the cell.

Frew and Trahar (1982) found in an investigation of rougher and cleaner banks on a plant that there is a significant difference between the rate constants for roughing and cleaning. They showed that batch flotation tests could predict the relative performance of the roughers and cleaners, but there were several factors like froth depth and mobility that could not be predicted from these tests.

Flynn and Woodburn (1987) used bubble surface flux and the thickness of the lamellae between bubbles at different heights in the froth to predict flotation performance. They showed that the inter-bubble lamellae are thicker in three-phase systems than in two-phase systems with the limiting thickness in a well drained froth correlating well with the d_{95} particle size. A major limitation of this model is that the thickness of inter-bubble lamellae is one of the parameters in the model and is very difficult to measure.

Ross (1988) points out that very little is known about the mechanism of transport of material near the top of the froth to the launder. This is a severe limitation in using the models discussed. Moys (1979) used high speed photographic techniques to examine the top of the froth, but his results were inconclusive because only the top layer of the froth could be seen and no information could be gleaned about the layers of froth just under the surface in which most of the transport of material to the launder occurs.

Ross (1988) has presented the most comprehensive picture of the sub-processes occurring in the froth to date. His models include sub-processes like the detachment of particles in the froth with allowances for possible re-attachment. The drainage of water and particles from the froth back to the pulp is also examined.

Models for both equilibrium (deep froths with no concentrate removal) and non-equilibrium froths are proposed. These are extensions of the models

proposed by Moys (1979, 1984) and overcome most of the shortcomings of these models. Provision is made for the uneven distribution of air at the pulp-froth interface, and the froth has been divided into four regions. A region of vertical plug flow has been added below the lip to account for the streamlines found in this region. A drawback of this model is that the assumption of plug flow in the froth is still retained. Bubble coalescence and froth drainage will inevitably lead to some mixing in the froth. It is likely that the fluid flow regime in the froth is one of the dominant factors in determining the behaviour of the froth, and a more realistic model should therefore be used. There are also no experimental techniques available to measure some of the parameters in the model, for example the re-attachment rate of hydrophobic particles to bubbles in the froth.

Again, as with all of the more comprehensive models discussed, the accurate modelling of the froth sub-processes carries the penalty of increased complexity. These models provide valuable insight into the processes occurring in the froth, but their application to flotation circuit design may be limited because of the difficulty in measuring or estimating some of the parameters required in the models.

3.2.4 FROTH EFFECTS

Generally, it has been found that fine particles have a stabilizing effect on the froth and often two-phase systems where no stable froths are formed are adequately stabilized by fine particles (Meyer and Klimpel, 1982; Woodburn and Wallin, 1984). Large particles do not directly destabilize froths, but they allow increased froth drainage, which may cause bubble coalescence. As the hydrophobicity of a particle increases it has a greater effect on the stability of the froth because it can hinder froth drainage, or cause bubble coalescence.

Dippenaar (1982a and 1982b) conducted a series of tests using particles of different sizes and hydrophobicities. He performed shaking tests in which a frother solution and particles were shaken together in a measuring cylinder and the froth volumes measured. He also used high speed photographic techniques to establish the mechanism of froth breakage.

Small hydrophobic particles with a contact angle of less than 90° stabilize the froth by bridging the inter-bubble lamellae and preventing liquid drainage from these lamellae, stopping the films from reaching rupture thickness.

Small hydrophobic particles with a contact angles of more than 90° were found to destabilize the froth by causing excessive thinning of the inter-bubble lamellae. A particle would attain its equilibrium contact angle in two adjacent bubbles and hence the bubbles would coalesce. This was also found with some particles with a contact angle of less than 90° if the three-phase boundaries are forced to migrate to the same discontinuity. A example of this is xanthated galena with a contact angle of 80°. Galena has a cubic structure with sheer faces and thus the three-phase boundaries are forced to migrate to the corners. When two bubbles meet at the same corner they coalesce.

The finely dispersed insoluble hydrophobic precipitates which result if xanthate collectors are mixed with certain metal ions decrease froth volume and stability (Livshitz and Dudenkov, 1965). This is due to accelerated coalescence of bubbles in both the pulp and the froth. The precipitate particles have a large contact angle and readily form bubble-particle agglomerates. When a particle in this agglomerate comes into contact with another bubble, rapid film thinning occurs causing the bubbles to coalesce. These precipitates increase the consumption of collector, which, in turn, leads to increased precipitate formation. This means that the frother dosage must be increased to achieve the desired froth stability. Depressants which either decrease the hydrophobicity of the precipitates or dissolve them can be used to control this effect.

It has been found that small bubbles produce more stable froths than large bubbles (Pal and Masliyah 1990) because they produce more hydrated froths, are less susceptible to coalescence due to inter-bubble film thinning and air diffuses out of small bubbles more slowly. These effects are due to the geometry of the bubbles, the smaller radius of curvature of the bubble surface, the more stable the film at the bubble surface.

The effect of other parameters on the rate of film thinning may be seen by studying the general equation for the rate of thinning of a vertical liquid film (Dippenaar, 1982a):

$$t = \frac{4\eta z_f}{\rho g d_f^2}$$

where t is the time, η, the viscosity of the liquid, z_f, the vertical height, ρ, the density of the liquid, g, the acceleration due to gravity, and d_f, the thickness of the film a distance z_f from the top of the film.

Thus increasing the viscosity of the liquid increases the film stability. The stability of the film is decreased by increasing the liquid density. Increasing the temperature has also been found to destabilize the froth because it causes the air to diffuse from the bubbles faster and it decreases the viscosity of the liquid.

3.2.5 COLUMN FLOTATION FROTHS

Little work has thus far been done to quantify the froth phase in column flotation cells. Yianatos et al. (1985) have proposed a method to measure the gas hold-up in the froth by estimating the tortuosity of the system using conductivity measurements.

This work was expanded to include bubble size distributions by Yianatos et al. (1986). Three regions are defined in the froth, viz: an expanded bubble bed, a packed bubble bed and a conventional froth. There is a trend for the gas hold-up to increase rapidly just above the interface (expanded bubble bed) and then level off at a value determined by flotation parameters (packed bubble bed) and then to increase again rapidly above the wash water distributor (conventional froth). Wash water was found to increase the stability of the lower two zones in the froth and help to reduce bubble coalescence. The major region in which bubble coalescence occurs is in the expanded bubble bed due to the sudden deceleration of the bubbles as they enter the froth. It is thought that a large part of the cleaning in the froth occurs at the pulp-froth interface due to this deceleration because entrained particles are dropped.

A model analogous to flow through a circular pipe was used to predict the behaviour of the expanded bubble bed. The bubbles in the packed bed

were found to be spherical and reasonably uniform in size. A cellular froth model provided a good fit for the behaviour of the packed bubble bed.

In a series of two-phase salt tracer tests Yianatos et al. (1987) showed that the use of wash water caused the rejection of practically all of the feed water within the first 10 cm of the froth. This implies that the downward bias achieved using wash water should be effective in reducing hydraulic entrainment of gangue material into the concentrate. An approach similar to that used for mass transfer in packed columns was used to describe the cleaning in the froth, with a number of transfer units being defined. An expression for the 'cleaning factor' A_{cf} was then defined:

$$A_{cf} = J_d/J_u$$

Where J_d and J_u are the downward and upward biases respectively.

Yianatos et al. (1988a) have proposed a model for selectivity in a column flotation froth. The model is based on the plug flow model developed by Moys (1978) and quantifies net particle detachment and washing rates in the froth. Although Moys (1984) has produced a two dimensional model for the froth in mechanical flotation cells, it was felt that a standard plug flow model would be well suited to a column because of the increased height to diameter ratio. While the models fit plant data for a Mo cleaning circuit well, no conclusions are drawn about the mechanisms of particle detachment and re-attachment due to their complexity. It is also pointed out that the froth depth has a significant effect on upgrading in the froth. Shallow froths (< 1 m) produce little upgrading because of increased mixing due to the closeness of the wash water entrance to the pulp-froth interface.

Pal and Masliyah (1990) measured the bubble size and liquid hold-up in the froth phase in a flotation column for a two-phase system. They found that there was little bubble coalescence in the froth and that the ratio of the froth drainage flux (J_{df}) to the terminal rise velocity of the bubbles was only a function of the liquid hold-up in the froth (α_f):

$$J_{df}/V_\infty = \alpha_f \cdot \exp[-2.4 + 2.5\alpha_f]$$

This value of J_{df}/V_∞ is analogous to the cleaning factor (A_{cf}) defined by Yianatos et al. (op. cit.).

Yu and Finch (1990) studied the recovery in the froth phase in a column cell by obtaining the overall recovery (R_{fc}) at different froth heights and extrapolating to a zero froth height. This gave the recovery in the collection zone (R_c) and hence the recovery in the froth zone (R_f) was found from the relationship:

$$R_{fc} = R_c \cdot R_f / [R_c \cdot R_f + (1-R_c)]$$

They found values of R_f of 50% or less. Falutsu and Dobby (1989) conducted a similar study using a different method and found similar results ($R_f < 60\%$).

Ross (1988), in his study of flotation froths, notes that the models developed in his thesis (discussed in section 3.2.3) are applicable to column flotation froths by merely taking the wash water into account.

3.3 EXPERIMENTAL METHODS

Four different sets of experiments were conducted to quantify froth effects. Froth height tests to determine froth stability, batch froth cutting tests to quantify froth effects as a function of height in the froth, continuous froth cutting tests to highlight any differences between steady-state and non steady-state systems, and residence time distribution studies to establish the flow patterns in the froth.

3.3.1 FROTH HEIGHT EQUIPMENT

The froth height equipment is shown in Figure 3.1. It consisted of a 250 by 50 mm graduated perspex cylinder with a sintered glass frit (porosity 4, pore diameter 9 - 15 μm) at the bottom through which the air was introduced. The pulp in the cylinder was agitated using a magnetic stirrer.

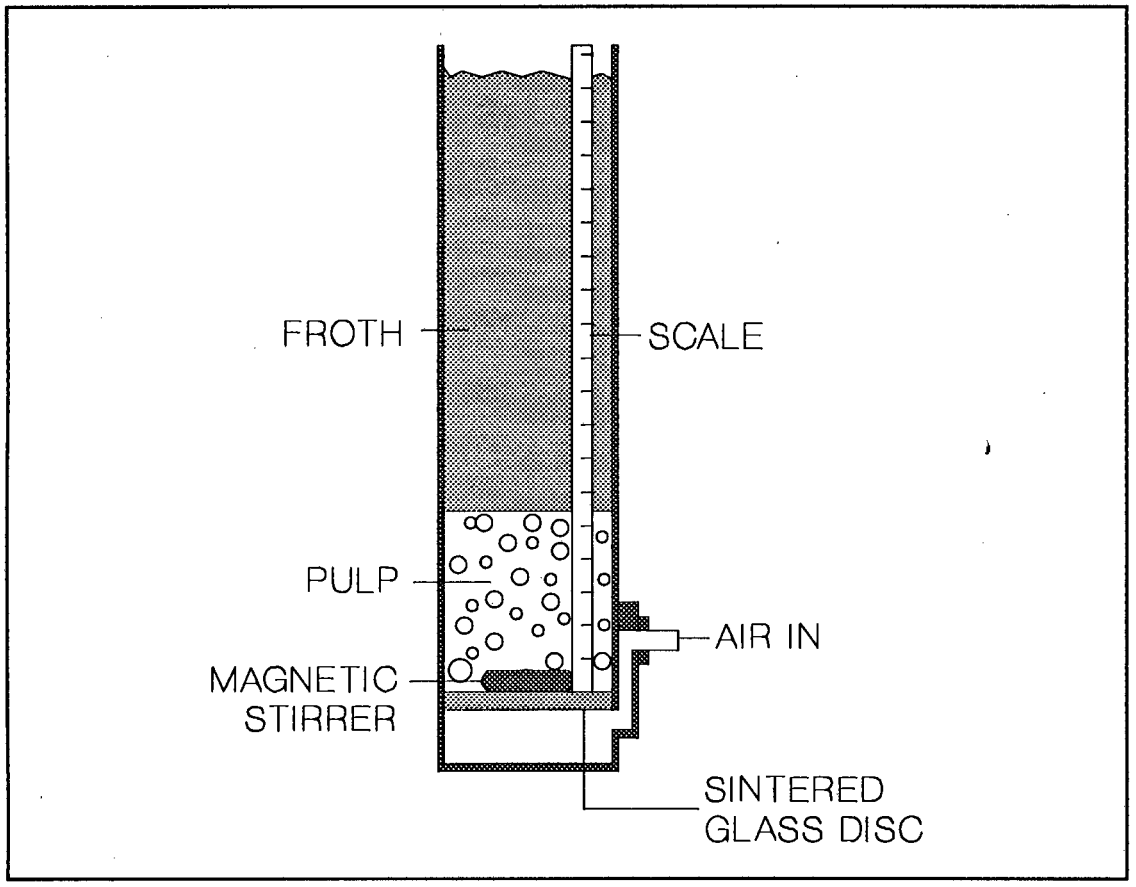

FIGURE 3.1 : Froth Height Equipment

Gravity concentrated pyrite was used to test the effects of oxidation state, xanthate collector type, and particle size on the stability of the froth. Surface oxidation was removed by an acid leach. The leached material was neutralised by repeated washing with water. The xanthate collectors used were both the normal- and iso-forms with chain lengths ranging from 2 to 8 carbon atoms. The particle size ranged from 16 to 106 μm.

The experimental conditions were as follows:

- Frother Type — Dowfroth 250
- Frother Dosage — 110 ppm
- Collector Dosage — 0.43 $mol \cdot ton^{-1}$ of dry solids
- Air Rate — 0.5 $cm \cdot s^{-1}$

For each test a slurry of 2 grams of pyrite in 180 ml of water was used. The collector conditioning time was 3 minutes and the frother was added one minute before the air was introduced. The froth was allowed to build up until a maximum was reached and this value was noted. This maximum value provided a measure of the stability of the froth. Each test was repeated three times with the average value being reported.

3.3.2 BATCH FROTH CUTTING EQUIPMENT

A diagram of the apparatus is depicted in Figure 3.2. The pulp was contained in a perspex column of height 250 mm and diameter 60 mm. The temperature of the pulp is controlled by the use of a water jacket which, together with the level controller, was fed from a water bath held at constant temperature. Air was introduced at the bottom of the column through a sintered glass frit. The size of the bubbles could be varied by the substitution of discs of different porosities, or by using different flotation conditions. Before it entered the column, the air was saturated with water at 20°C using two pre-saturators. The flowrate and pressure of the air were measured with a soap-bubble flow meter and a mercury manometer respectively. A magnetically stirred-propeller system with baffles was used to agitate the pulp and ensure good mixing without any swirling.

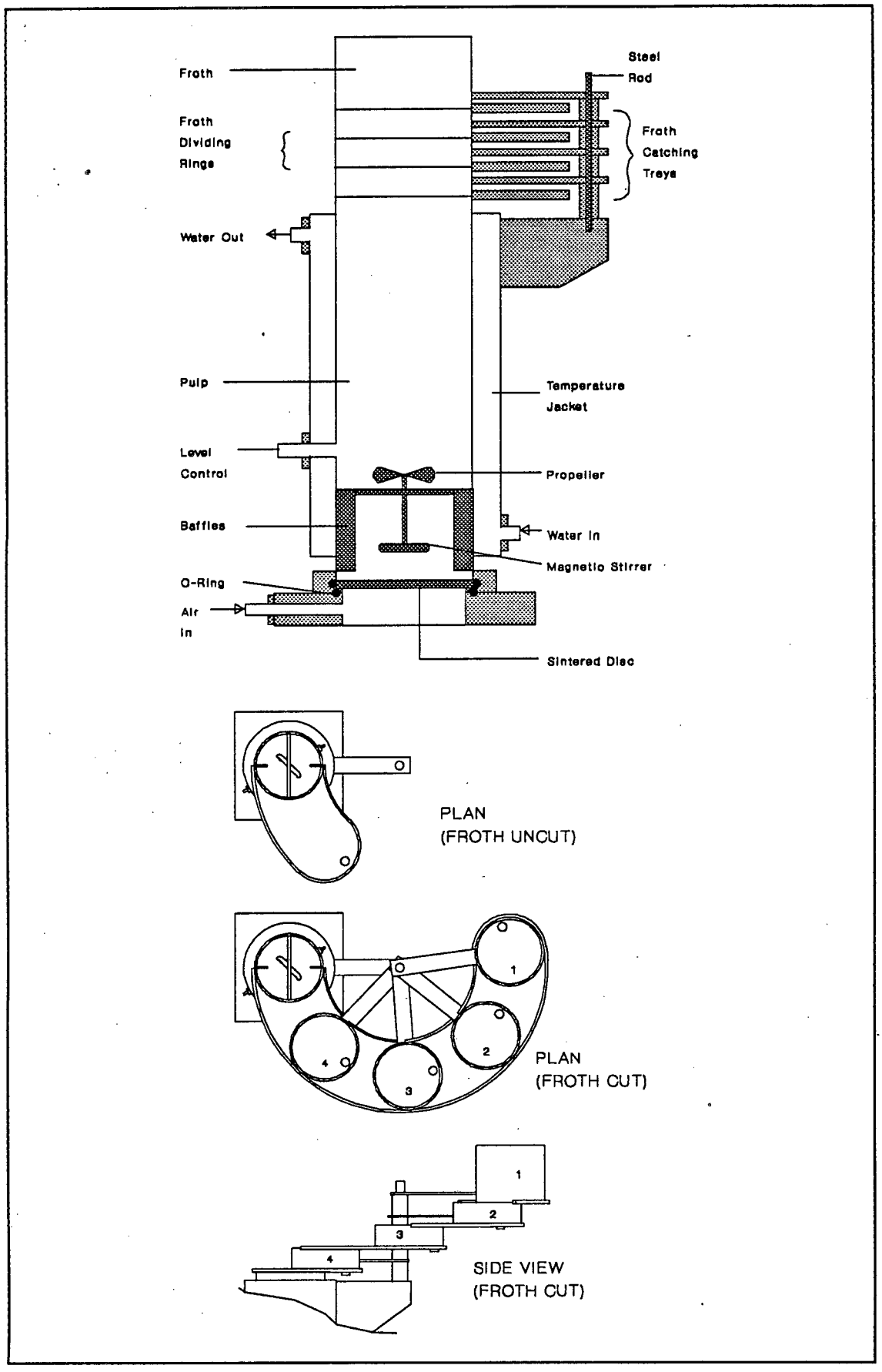

FIGURE 3.2 : Batch Froth Cutting Equipment

Four rings were used to divide the froth into four cylindrical segments above the pulp. The height of the lower three segments was 20 mm, while the top segment was 50 mm high. The froth was collected in trays that pivoted around a steel rod, allowing the froth to be cut into four horizontal sections. The arrangement of these trays in both the uncut and cut positions is shown in Figure 3.2.

Gravity concentrated pyrite from Durban Roodeport Deep Mine was used in the tests on the reproducibility of the results. A synthetic pyrite-quartz ore was used in all the other tests. The synthetic ore contained 10% pyrite milled to 75% smaller than 15 μm and 90% quartz (from a mine in the Delmas, Transvaal area) milled to 65% smaller than 38 μm. In both forms of feed the pyrite was leached for 2 hours in 8% hydrochloric acid, and then neutralised by washing and filtration.

Only a short conditioning time of 10 minutes was needed to ensure good mixing of the pulp and a uniform pulp temperature, since water of the desired temperature (usually 25°C) had been used. The solids content of the pulp was 5% (i.e. 35 grams of solids in 700 ml of pulp), which is lower than that typically found in column flotation cells (> 10%). This low solids content was used to allow the processes occurring in the froth to be seen more clearly and to control the total froth height. Other researchers (Dobby and Finch, 1985) have also used low solids concentrations in residence time distribution tests. A collector conditioning time of 2 minutes was allowed before the frother was added. Unless otherwise stated the collector used was 0.5 mol·ton^{-1} SEX (sodium ethyl xanthate) and the frother used was Dowfroth 250 (a polypropylene glycol with a molecular weight of about 250) at a dosage of 75 ppm. After a further minute the air was introduced. The air rate was generally 0.615 cm/s. When the froth had built up, filling the rings, the air was shut off and the froth cut simultaneously.

The collected froth was washed out of the collection trays into beakers with a known quantity of water and then the excess water on the trays was scraped into the beakers with a rubber scraper. After the froth in each segment had been weighed the concentrates were oven dried at 80°C and the masses of solids and water were calculated. The particle size distribution in each segment was obtained by the use of a Malvern particle size analyser, and the sulphur assayed using a Leco sulphur analyser.

3.3.3 CONTINUOUS FROTH CUTTING EQUIPMENT

A laboratory column cell with a froth cutting system similar to that used on the batch cell was used to extend the froth studies to a continuous system. A diagram of this column is shown in Figure 3.3. The column had a diameter of 60 mm and the collection zone height was 800 mm. Each of the froth collecting rings was 30 mm high with the top ring having the wash water system and the concentrate launder added to the top. Since the froth contained far more water than in the case of the batch cell, it was necessary to hold the froth rings down to prevent leaking. This was done using a system of rubber bands which were released just before the froth was cut.

The wash water system was a grid of 4 mm copper tubes with 1 mm holes in the bottom (Figure 3.3). This was fed via a variable speed peristaltic pump. The air sparge system was similar to that used on the batch cell with a sintered glass disc of porosity 4 (pore diameter 9 - 15 μm) being used to generate the bubbles.

The feed was slurried in a conditioning tank with reagents. The collector used was potassium normal butyl xanthate (PNAX) at a dosage of 0.5 mol/ton and the frother, 25 ppm of Dowfroth 200. Frother was added to both to feed and the wash water. A conditioning time of ten minutes was allowed before the feed was introduced into the column. The feed and tailings rate were controlled using peristaltic pumps. The feed rate was 1 cm/s, the wash water rate 0.33 cm/s and the superficial air rate 1 cm/s. Two different types of feed were used, the synthetic pyrite-quartz mix used in the batch tests and the gold bearing pyritic ore from Unisel mine in the Orange Free State which was used in the RTD studies.

The column was run for 10 minutes (7.5 residence times) to allow steady state to be reached and samples of the concentrate and tailings were then collected for 5 minutes. The air was shut off, the froth was cut into the various segments and the feed, wash water and tailings pumps were all stopped simultaneously. The removal of the froth from each segment was conducted in the same manner as for the batch system. The products were again analysed for sulphur and particle size.

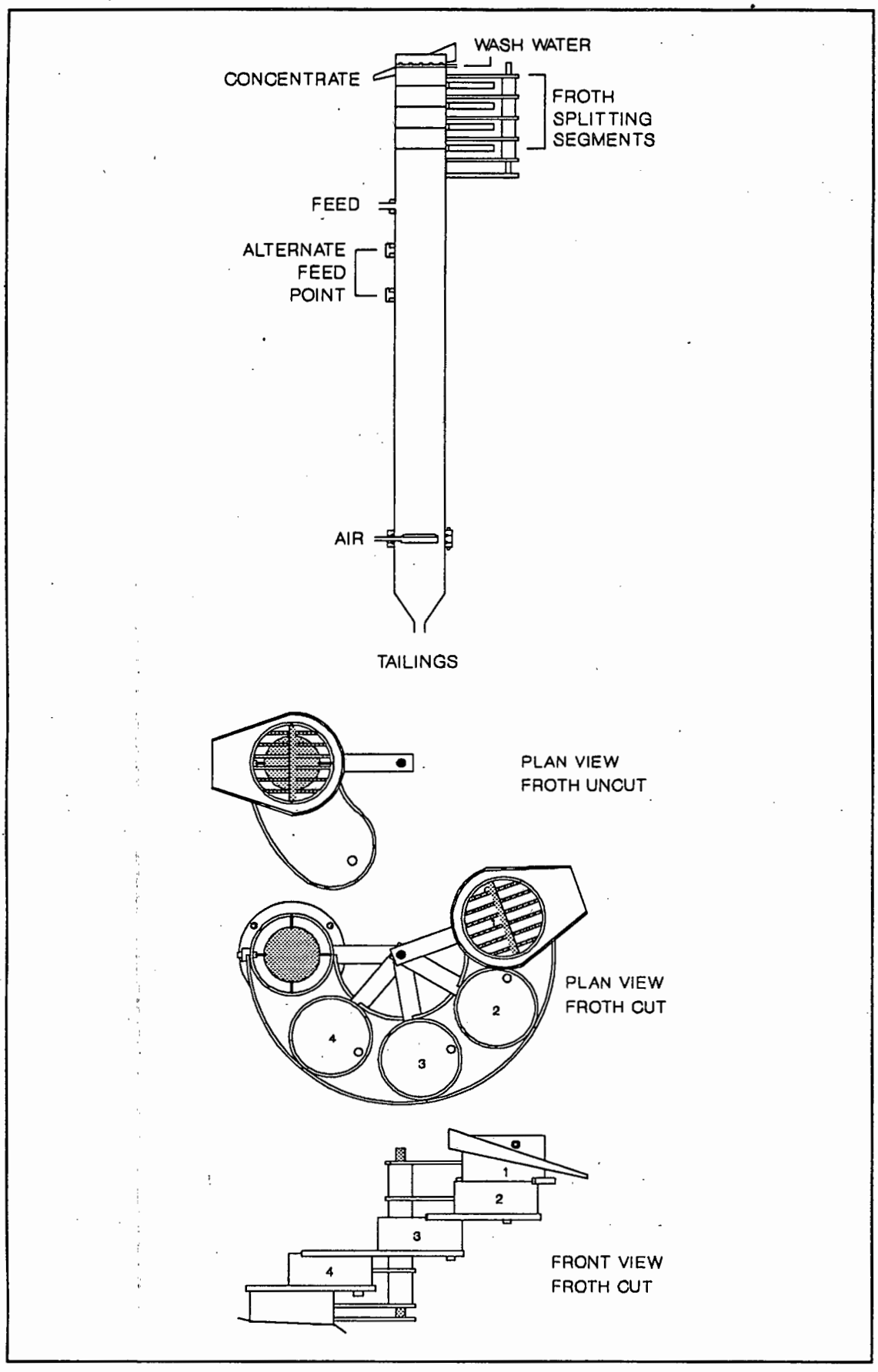

FIGURE 3.3 : Continuous Froth Cutting Column

3.3.4 RESIDENCE TIME DISTRIBUTION EQUIPMENT

The equipment used for the residence time distribution studies is shown in Figure 3.4. The details of the experimental conditions used for these tests can be found in Section 2.3.2, and the flotation parameters which were varied are given in Table 2.1.

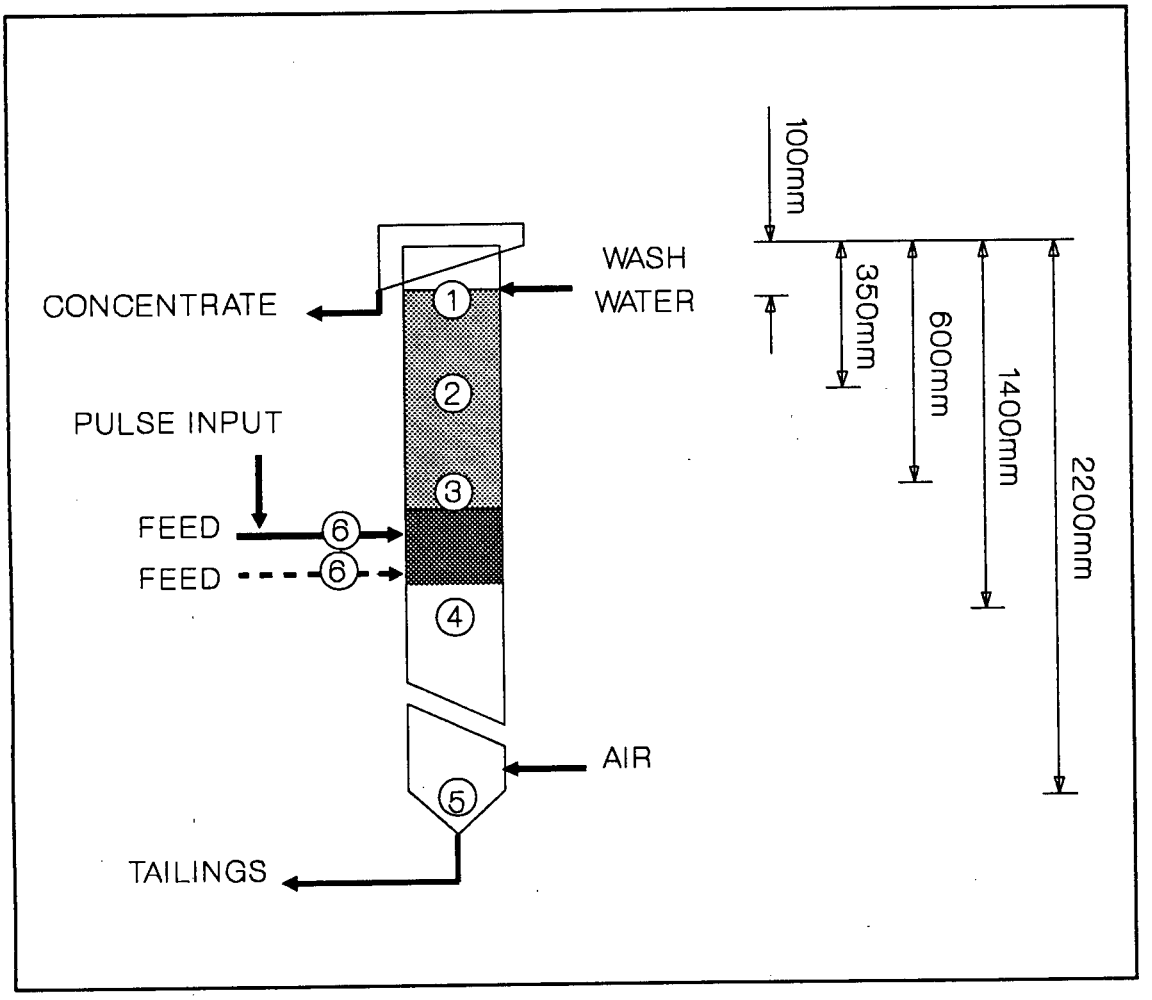

FIGURE 3.4 : Column Used in Solids RTD Tests

3.4 RESULTS AND DISCUSSION

3.4.1 FROTH STABILITY TESTS

3.4.1.i VARIATION OF XANTHATE CARBON CHAIN LENGTH

Tests were conducted using xanthate collectors to establish the effect of the carbon chain length and chain branching on the stability of the froth. The number of carbon atoms in the chain varied from 2 to 8 with both the normal- and iso-forms being used. The cation was sodium for the lower chain lengths and potassium for the higher chain lengths. It has been found that the potassium ion provides greater stability at high chain lengths than the sodium ion, but potassium xanthates with low chain lengths are difficult to make. Barker (1986) found that the cation in the xanthate has little effect on the performance of the xanthate.

The maximum froth height reached was used as a measure of the stability of the froth. Each test was repeated three times with the average value being reported.

Each of the collector types was tested under six different conditions, viz:

- without collector;
- with collector only;
- with collector and unleached pyrite (38 - 53 μm);
- with collector and unleached pyrite (75 - 106 μm);
- with collector and leached pyrite (38 - 53 μm);
- with collector and leached pyrite (75 - 106 μm);

The results of these tests are depicted in Figure 3.5 and the data are shown in Table 3.1. The major factor that affects the stability of the froth is the rate of bubble coalescence. Bubbles coalesce when the film of water between the bubbles thins to a critical value causing the film to rupture. Factors which retard the drainage of water from the froth increase its stability. Bubble-particle agglomerates with small particles can slow this water drainage by either forming a bridge between two bubbles and preventing rupture

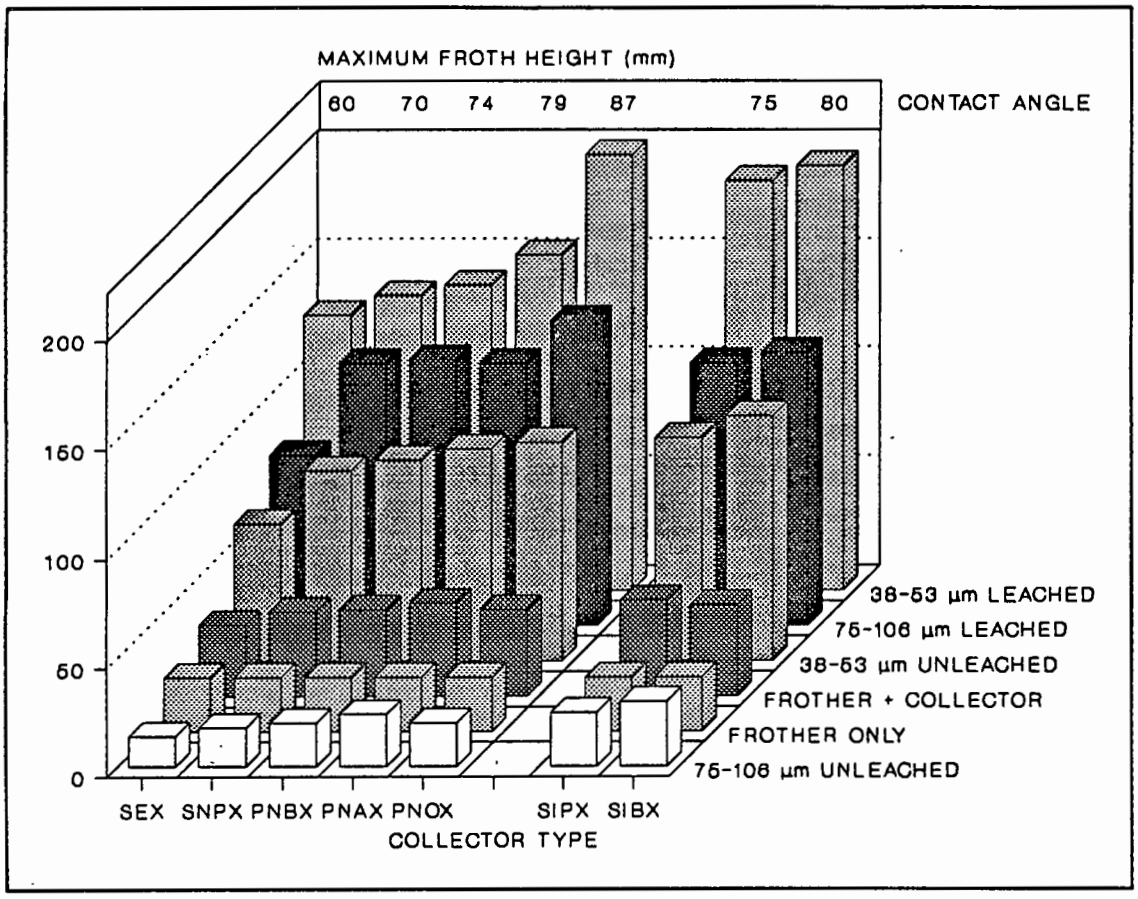

FIGURE 3.5 : Variation of Froth Height with Particle Size, Oxidation State and Collector Type

TABLE 3.1 : Effect of Particle Size and Conditioning on Froth Stability

ORE TYPE		MAXIMUM FROTH HEIGHT (mm)						
		SEX	**SNPX**	**PNBX**	**PNAX**	**PNOX**	SIPX	SIBX
FROTHER ONLY	MEAN	**25**	**25**	**25**	**25**	**25**	25	25
	RANGE	19-35	19-35	19-35	19-35	19-35	19-35	19-35
FROTHER + COLLECTOR	MEAN	**33**	**39**	**40**	**43**	**40**	44	42
	RANGE	31-35	38-40	34-50	38-50	35-43	36-50	33-52
75 - 106 µm UNLEACHED	MEAN	**14**	**18**	**20**	**24**	**20**	25	30
	RANGE	13-16	12-24	14-26	22-38	25-38	23-25	27-32
38 - 53 µm UNLEACHED	MEAN	**63**	**87**	**92**	**97**	**100**	102	112
	RANGE	59-72	84-91	85-100	90-103	89-108	100-145	109-106
75 - 106 µm LEACHED	MEAN	**78**	**120**	**122**	**120**	**140**	120	125
	RANGE	75-69	104-136	110-128	122-136	100-160	100-145	109-139
38 - 53 µm LEACHED	MEAN	**126**	**135**	**140**	**154**	**200+**	188	195
	RANGE	116-149	115-160	130-151	147-160	200+	183-193	182-205
CONTACT ANGLE (deg)		**60**	**70**	**74**	**79**	**87**	75	80

thickness from being reached, or by decreasing the effective area through which the water can drain. Large particles may have the opposite effect by keeping the bubbles to far apart and allowing excessive drainage of these films.

The addition of collector to the two-phase system appeared to stabilize the froth. This was possibly due to an ionic effect on the surface of the bubbles which caused a thicker film of water to be formed at the bubble surface. It is known that xanthates have no frothing properties (Sutherland and Wark, 1955).

It can be seen that leaching increased the stability of the froth. Leaching removes the layer of surface oxidation from the particles allowing better adsorption of the xanthate onto surface of the mineral. This renders the particle more hydrophobic, and hence more likely to form a bubble-particle agglomerate. Particles which have formed bubble-particle agglomerates are held at the bubble surface and are not free to drain from the froth with the water.

Decreasing the particle size increased the froth stability for two reasons: firstly, the fine particles help to slow inter-bubble film thinning by increasing the effective viscosity of the liquid, and secondly, the finer the particle size, the more particles per unit mass, and hence the more bubble-particle agglomerates that can form.

Figure 3.5 shows the equilibrium contact angles of the various collectors with pyrite (Sutherland and Wark, 1955). There was a high degree of correlation between the contact angle (hydrophobicity) of the particles and the stability of the froth, the higher the contact angle, the more stable the froth. It is also evident from Figure 3.5 that it was a combination of the size of a particle and its hydrophobicity that determined the stability of the froth. Fine hydrophobic particles (38 - 53 μm) helped to stabilize the froth, while larger particles (75 - 106 μm) with a lower hydrophobicity destabilized the froth. Ultra-fine hydrophobic particles have also been shown to destabilize the froth (e.g. metal-xanthate precipitates, Livshitz and Dudenkov, 1965).

3.4.1.ii VARIATION OF PARTICLE SIZE

Figure 3.6 and Table 3.2 show the effect of particle size on the stability of the froth. Six different particle size fractions were tested ranging from 16 µm to 106 µm. Froth heights of greater than 200 mm could not be measured because the total height of the cell was only 250 mm and the air had to be shut off to prevent the system from overflowing.

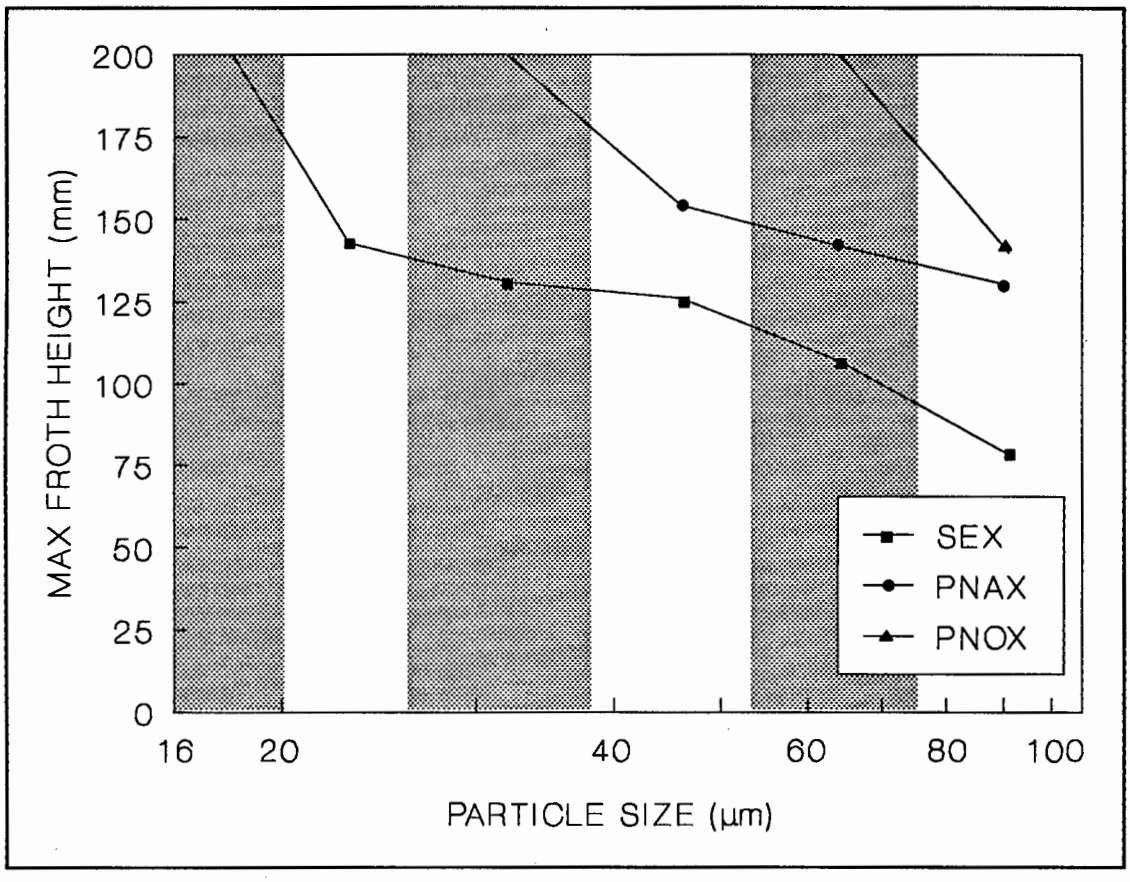

FIGURE 3.6 : Variation of Froth Height with Particle Size and Collector Type

TABLE 3.2 : Effect of Particle Size on Froth Stability

PARTICLE SIZE		SEX		PNAX		PNOX	
RANGE (µm)	MEAN (µm)	MEAN (mm)	RANGE (mm)	MEAN (mm)	RANGE (mm)	MEAN (mm)	RANGE (mm)
16 - 20	18	200+	200+	200+	200+	200+	200+
20 - 26	23	143	130-165	200+	200+	200+	200+
26 - 38	32	131	120-145	200+	200+	200+	200+
38 - 53	46	126	116-149	154	140-160	200+	200+
53 - 75	64	107	90-130	142	108-170	200+	200+
75 - 106	91	78	75-89	130	123-138	140	100-160

It has been found that ultra-fine (< 10 μm) and coarse (> 200 μm) particles give poor rates of flotation (Jowett, 1980). It is clear from Figure 3.6 that the stability of the froth decreased only as the particle size increased. The probable reason for this is that the smallest particle size range tested (16 - 20 μm) was above the range where poor flotation occurs. The classically accepted reason for poor flotation of ultra-fine particles is that the streamlines associated with the bubbles prevent the particles from coming into contact with the surface of the bubbles and hence bubble-particle agglomerates cannot be formed. In this apparatus the bubbles formed were extremely small and so this was not a significant factor. There is also a greater number of fine particles per unit mass than coarse particles and hence more bubble-particle agglomerates can be formed. Again it can be seen that the collector with the greatest contact angle (PNOX) provided the most stable froths with the larger particles.

3.4.2 BATCH FROTH CUTTING TESTS

Batch froth cutting tests were carried out to quantify the effects of certain flotation variables on the behaviour of the froth phase at different heights. Information was obtained about the following parameters as a function of height in the froth:

- the mass of solids,
- the mass of water,
- the volume of air,
- the particle size distribution,
- the grade, and
- the recovery.

3.4.2.i REPRODUCIBILITY

Six runs were carried out under identical conditions using gravity concentrated pyrite to establish the reproducibility of the results. These data are given in Table 3.3. The particle size distributions for the feed and at different heights in the froth (conc 1 at the top; conc 4 at the bottom) are shown in

TABLE 3.3 : Reproducibility : Batch Froth Cutting Tests

RUN	PARTICLE MASS (g)					
	1	2	3	4	TOTAL	MEAN
1	5.02	4.66	4.68	6.53	20.89	*5.22*
2	4.15	5.40	5.42	8.60	23.57	*5.89*
3	4.74	4.97	3.99	6.11	19.81	*4.95*
4	4.67	5.27	5.21	6.73	21.88	*5.47*
5	4.70	5.18	4.54	7.15	21.57	*5.39*
6	4.97	5.38	4.56	6.68	21.59	*5.40*
AVERAGE	4.71	5.14	4.73	6.97	21.55	*5.39*
STD. DEV.	6.57%	5.52%	10.86%	12.45%	5.24%	*8.85%*
SIGNIFICANT VARIATION (95% CONFIDENCE LIMIT)						**22.76%**
RUN	WATER MASS (g)					
	1	2	3	4	TOTAL	MEAN
1	2.78	3.39	3.65	3.56	13.56	*3.35*
2	2.55	5.00	4.12	4.79	16.46	*4.12*
3	3.40	3.25	4.76	5.28	16.69	*4.17*
4	2.65	3.93	4.83	4.27	15.68	*3.92*
5	3.18	3.55	3.69	3.63	14.05	*3.51*
6	3.28	4.47	3.91	5.08	16.74	*4.19*
AVERAGE	2.97	3.93	4.16	4.44	15.53	*3.88*
STD. DEV.	12.03%	17.38%	12.50 %	16.56%	9.00%	*14.62%*
SIGNIFICANT VARIATION (95% CONFIDENCE LIMIT)						**37.58%**
RUN	PARTICLE/WATER RATIO					
	1	2	3	4	TOTAL	MEAN
1	1.81	1.37	1.28	1.83	1.54	*1.56*
2	1.63	1.08	1.32	1.80	1.43	*1.43*
3	1.39	1.53	0.84	1.16	1.19	*1.19*
4	1.76	1.34	1.08	1.58	1.40	*1.40*
5	1.48	1.46	1.23	1.97	1.54	*1.53*
6	1.52	1.20	1.17	1.31	1.29	*1.29*
AVERAGE	1.60	1.33	1.15	1.61	1.40	*1.40*
STD. DEV.	10.24%	12.43%	15.23%	19.81%	9.95%	*10.23%*
SIGNIFICANT VARIATION (95% CONFIDENCE LIMIT)						**26.31%**
RUN	AIR HOLD-UP (%)					
	1	2	3	4	TOTAL	MEAN
1	93.3	92.4	91.9	91.4	92.2	*92.2*
2	94.0	89.2	90.8	88.5	90.6	*90.6*
3	92.3	92.5	90.2	88.5	90.9	*90.9*
4	93.7	91.2	89.6	90.1	91.1	*91.1*
5	92.7	91.9	91.9	91.1	91.9	*91.9*
6	92.4	90.2	91.5	88.7	90.7	*90.7*
AVERAGE	93.1	91.2	91.0	89.7	91.2	*91.2*
STD. DEV.	0.68%	1.29%	0.94%	1.35%	0.64%	*1.07%*
SIGNIFICANT VARIATION (95% CONFIDENCE LIMIT)						**2.74%**
RUN	PARTICLE SIZE (μm)					
	1	2	3	4	TOTAL	MEAN
1	56.0	55.2	28.1	27.4	41.7	*38.1*
2	57.7	51.5	27.2	26.9	40.8	*36.6*
3	56.2	54.7	27.2	27.2	41.3	*37.6*
4	56.4	54.5	28.1	27.9	41.7	*38.1*
5	55.3	56.4	27.8	27.2	41.7	*38.3*
6	54.1	51.2	27.8	27.0	40.0	*36.5*
AVERAGE	56.0	53.9	27.7	27.3	41.2	*41.2*
STD. DEV.	2.14%	3.89%	1.48%	1.31%	1.63%	*2.20%*
SIGNIFICANT VARIATION (95% CONFIDENCE LIMIT)						**5.66%**

Figure 3.7 and the air hold-up and solids-to-water ratio with error bars are given in Figure 3.9. The precision of these values was important because all subsequent analyses depended on the accuracy of these results. To facilitate direct comparison between the top segment (segment 1) and the lower segments (segments 2 to 4) the results for the top segment were normalised with respect to the height of the froth in each of the lower three segments. To do this it was assumed that all the characteristics of the froth were uniform throughout the froth in the top segment.

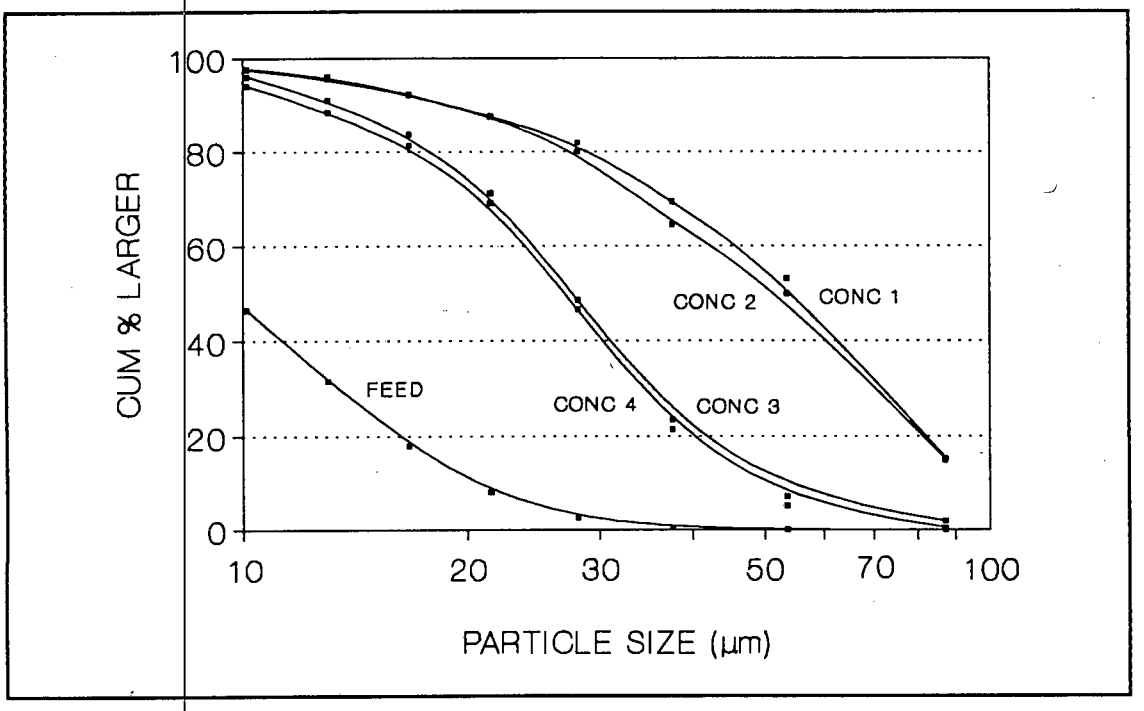

FIGURE 3.7 : Size Distribution for the Feed and the Froth

From Figure 3.7 it can be seen that the coarsest material was preferentially floated. This supports the theory that there is an optimum size for flotation and particles finer than the optimum tend to be entrained rather than floated (Jowett, 1980). Figure 3.8 shows the theoretical recovery by size curves for flotation and entrainment. The curves for segments 3 and 4 in Figure 3.7 seem to show a combination of the two theoretical curves, while the curves for the top two segments show the classical flotation trend. This indicates that the amount of entrained material in the froth increased towards the bottom of the froth. The other contributing factor to the shape of the curves for the bottom of the froth is that the coarser particles floated first and were found in the top of the froth, leaving fewer coarse particles to report to the bottom of the froth.

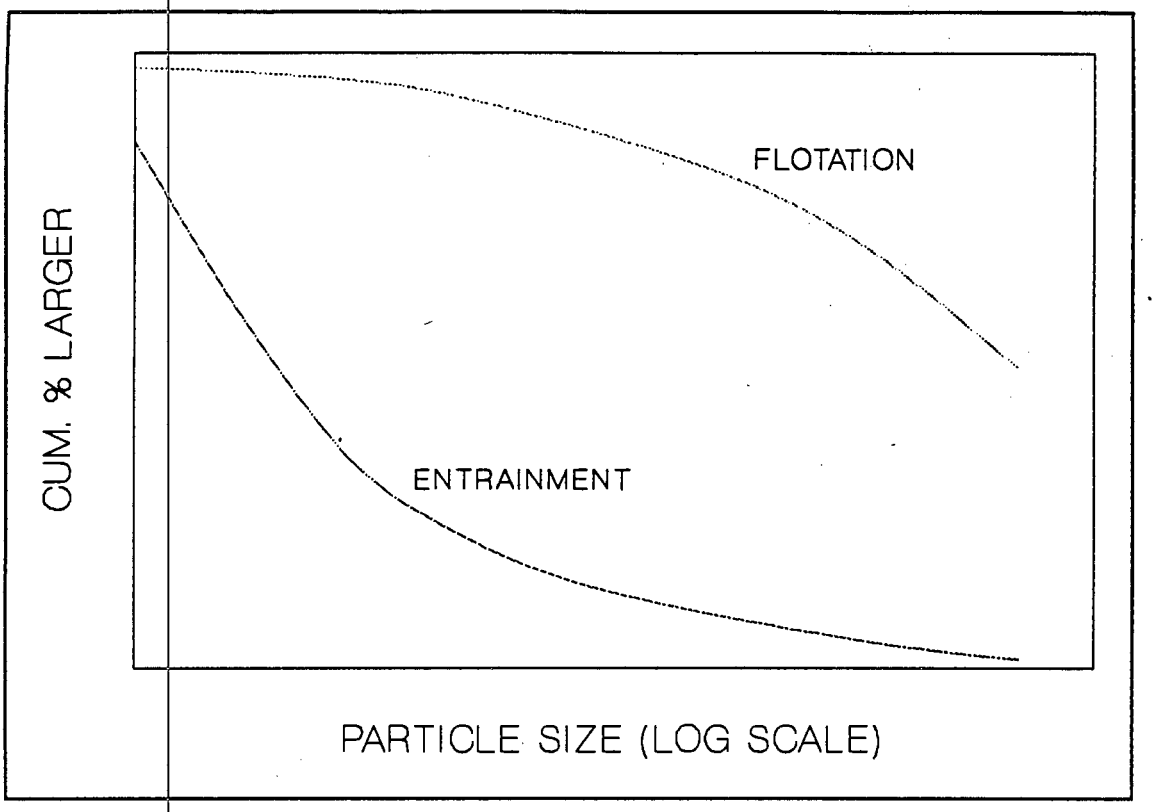

FIGURE 3.8 : Theoretical Recovery-by-Size Curves for Flotation and Entrainment

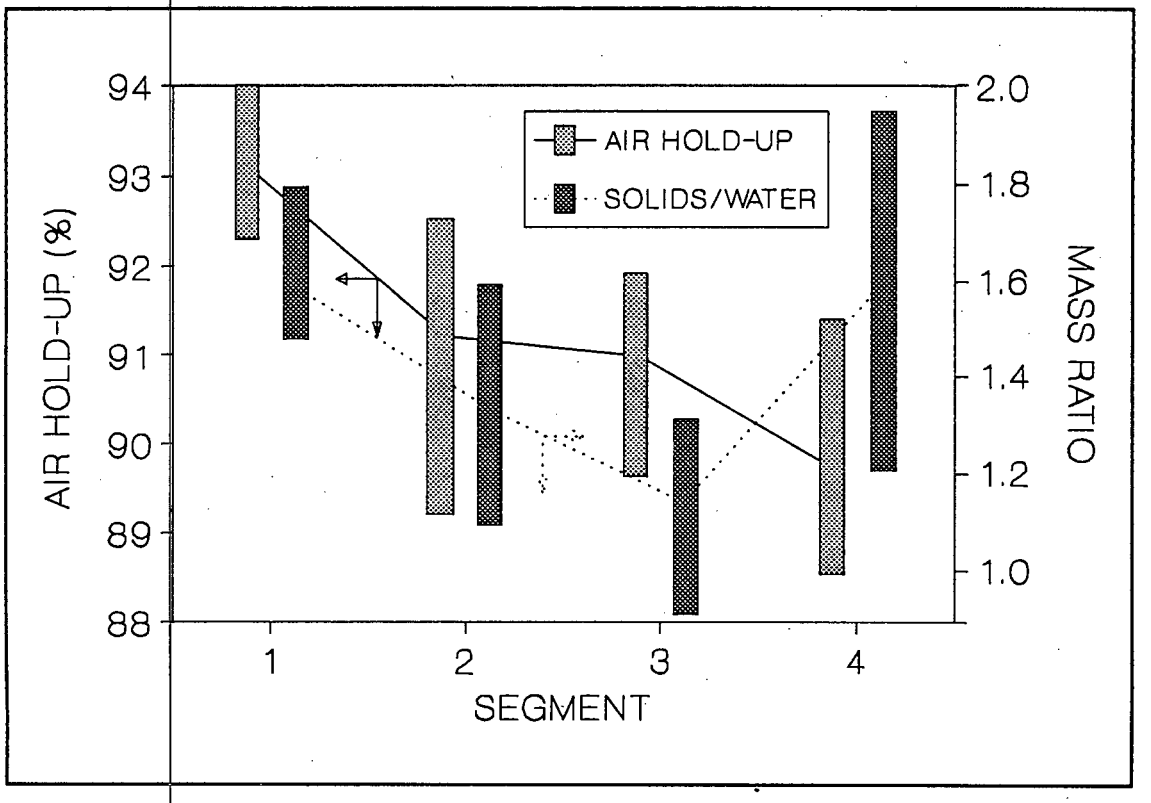

FIGURE 3.9 : Air Hold-up and Solids-to-Water Ratio at Different Heights in the Froth

Figure 3.9 shows the variation of air hold-up and solids-to-water ratio with height in the froth. The air hold-up provided information about the drainage of water from the froth. The higher the air hold-up, the better drained the froth. It can be seen that the froth was best drained at the top with froth drainage decreasing towards the bottom. The ratio of the masses of solids-to-water is a useful parameter when viewed with the air hold-up because it provides an indication of the extent of entrainment. It is reasonable to assume that the entrained material follows the water in the froth and hence the amount of entrained material increased with decreasing height in the froth.

There was a high solids-to-water ratio at the top of the froth because the froth was well drained, and most of the material at this level had been floated. The solids-to-water ratio decreased in segments 2 and 3 indicating an increase in the amount of water in the froth. The increase in the solids-to-water ratio at the bottom of the froth was probably due to a high proportion of the entrained material being rejected at this level due to the sudden deceleration of the bubbles at the pulp-froth interface. From the air hold-up profile it is clear that the water hold-up at this level did not decrease, therefore there must have been an increase in the amount of solids.

In all subsequent tests three identical runs were carried out under each set of conditions. For each run the concentrate from each segment was combined with the concentrates obtained from the same segment for the other two runs in the test. In this way enough concentrate was obtained for analysis of particle size and sulphur. The criterion for the acceptance of the results of a test was the extent of agreement of the masses of solids and water collected in each of the segments for the three runs in the test. On the basis of the results of the reproducibility tests (Tables 3.3 and 3.4) two criteria were set for the results of a test to be acceptable. The overall recovery of solids for a single run had to be within 13% of the mean, and the overall recovery of water within 22% of the mean, for the test. These values correspond to 1.5 standard deviations from the mean. The precision of the water recovery was low because the froth was scraped off the collection trays with a rubber scraper. This led to errors in the determination of the mass of water recovered.

TABLE 3.4 : Batch Froth Cutting Reproducibility Tests

SEGMENT			1	2	3	4	AVERAGE
SINGLE	SOLIDS MASS (g)	AVERAGE	4.71	5.14	4.73	6.97	*5.39*
		STD. DEV.	6.57%	5.52%	10.86%	12.45%	*8.85%*
		SIGNIFICANT VARIATION (95% CONFIDENCE LIMIT)					**22.76%**
	WATER MASS (g)	AVERAGE	2.97	3.93	4.16	4.44	*3.88*
		STD. DEV.	12.03%	17.38%	12.50%	16.56%	*14.62%*
		SIGNIFICANT VARIATION (95% CONFIDENCE LIMIT)					**37.58%**
	SOLIDS/ WATER RATIO	AVERAGE	1.60	1.33	1.15	1.61	*1.40*
		STD. DEV.	10.24%	12.43%	15.23%	19.81%	*10.23%*
		SIGNIFICANT VARIATION (95% CONFIDENCE LIMIT)					**26.31%**
	AIR HOLD-UP (%)	AVERAGE	93.1	91.2	91.0	89.7	*91.2*
		STD. DEV.	0.68%	1.29%	0.94%	1.35%	*1.07%*
		SIGNIFICANT VARIATION (95% CONFIDENCE LIMIT)					**2.74%**
	PARTICLE SIZE (µm)	AVERAGE	56.0	53.9	27.7	27.3	*41.2*
		STD. DEV.	2.14%	3.89%	1.48%	1.31%	*2.20%*
		SIGNIFICANT VARIATION (95% CONFIDENCE LIMIT)					**5.66%**

SEGMENT			1	2	3	4	AVERAGE
GROUPED	SOLIDS MASS (g)	AVERAGE	4.71	5.14	4.73	6.97	*5.39*
		STD. DEV.	1.24%	2.84%	0.85%	1.78%	*1.68%*
		SIGNIFICANT VARIATION (95% CONFIDENCE LIMIT)					**4.31%**
	WATER MASS (g)	AVERAGE	2.97	3.93	4.16	4.44	*3.88*
		STD. DEV.	2.33%	1.31%	0.44%	2.68%	*1.69%*
		SIGNIFICANT VARIATION (95% CONFIDENCE LIMIT)					**4.35%**
	SOLIDS/ WATER RATIO	AVERAGE	1.60	1.33	1.15	1.61	*1.40*
		STD. DEV.	0.80%	0.27%	0.63%	0.79%	*0.62%*
		SIGNIFICANT VARIATION (95% CONFIDENCE LIMIT)					**1.61%**
	AIR HOLD-UP (%)	AVERAGE	93.1	91.2	91.0	89.7	*91.2*
		STD. DEV.	0.14%	0.00%	0.02%	0.28%	*0.11%*
		SIGNIFICANT VARIATION (95% CONFIDENCE LIMIT)					**0.28%**
	PARTICLE SIZE (µm)	AVERAGE	56.0	53.9	27.7	27.3	*41.2*
		STD. DEV.	1.34%	0.24%	0.79%	0.40%	*0.69%*
		SIGNIFICANT VARIATION (95% CONFIDENCE LIMIT)					**1.78%**

In all subsequent tests a synthetic mixture of pyrite and quartz was used. The composition of this mixture is discussed in Section 3.3.2. From the particle size - grade curve shown in Figure 3.10 it can be seen that the pyrite was concentrated in the finer particle size fractions. The particle size - mass curve indicates that about 28% of the material had a particle size of less than 10 µm.

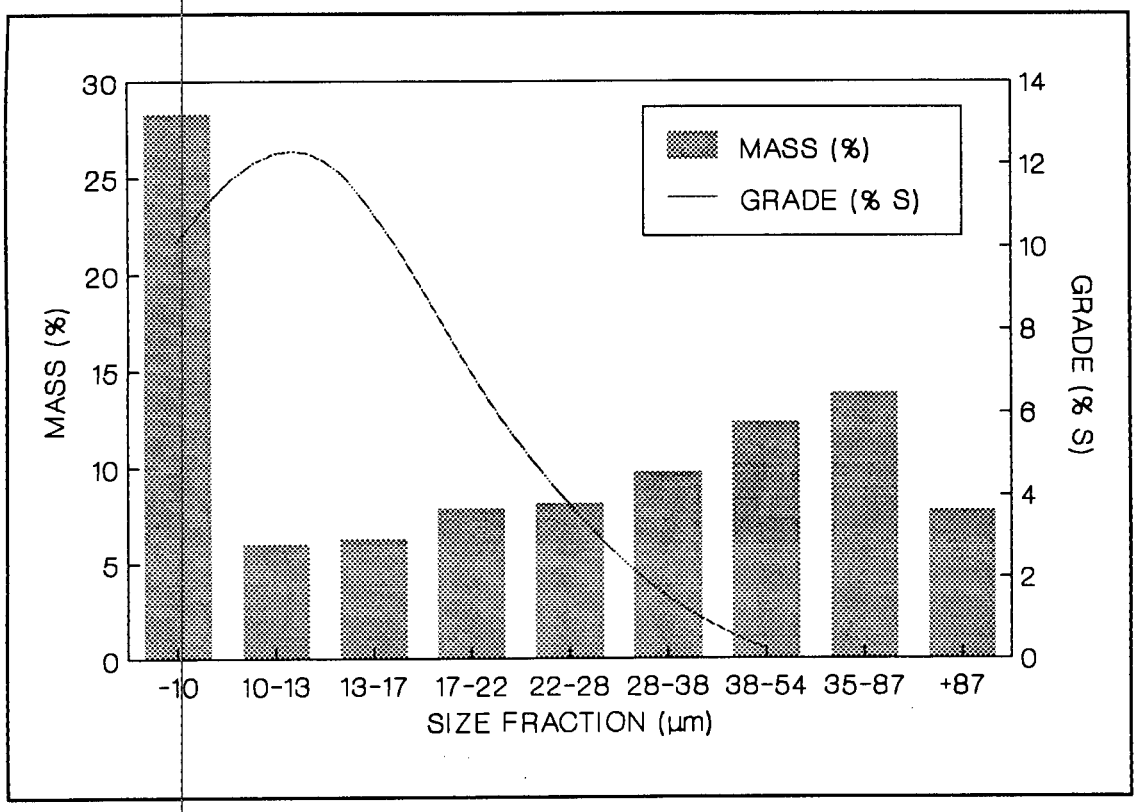

FIGURE 3.10 : Grade and Particle Size Distributions for the Synthetic Pyrite-Quartz Ore

3.4.2.ii TYPE AND CONCENTRATION OF COLLECTOR

The variation of particle size, air hold-up, grade and recovery with height in the froth as the collector type and concentration were varied are shown in Table 3.5 and Figures 3.11 - 3.15. These results are for a froth residence time of 90 seconds.

Figure 3.11 shows the proportion of coarse gangue (larger than 38 μm) in each froth segment. All of the pyrite in the feed was smaller than 38 μm. It can be seen that the coarse gangue material was slightly concentrated in segments 2 and 4. The gangue material in segment 2 was trapped in the froth and stabilized it by remaining in the inter-bubble water films. The water films were, hence, prevented from reaching the critical thickness at which the bubbles rupture. The size of this material made its elutriation from the froth with the entrained water difficult. The presence of gangue material in the bottom segment was due to elutriation from the top of the froth and entrainment from the pulp.

TABLE 3.5 : Batch Froth Cutting Tests
Collector Type and Concentration.

	SEGMENT	SEX		PNAX		PNOX	
		0.25 (mol/t)	0.5 (mol/t)	0.25 (mol/t)	0.5 (mol/t)	0.25 (mol/t)	0.5 (mol/t)
PARTICLE MASS (grams)	1	1.04	1.22	1.35	1.07	0.97	0.94
	2	0.70	0.82	0.79	0.76	0.75	0.70
	3	0.65	0.75	0.56	0.63	0.72	0.67
	4	1.37	1.57	1.44	1.38	1.34	1.29
	TOTAL	**3.76**	**4.36**	**4.14**	**3.84**	**3.78**	**3.60**
WATER MASS (grams)	1	8.2	7.6	6.5	5.3	5.6	5.4
	2	9.3	10.9	9.0	6.8	6.2	5.9
	3	9.8	12.0	10.8	8.9	6.9	6.6
	4	16.3	11.6	11.7	9.7	8.1	7.8
	TOTAL	**43.6**	**42.1**	**38.0**	**30.7**	**26.8**	**25.7**
PARTICLE/ WATER RATIO	1	0.127	0.161	0.208	0.202	0.173	0.174
	2	0.075	0.075	0.088	0.112	0.121	0.119
	3	0.066	0.063	0.052	0.071	0.104	0.102
	4	0.084	0.135	0.123	0.142	0.165	0.165
	AVERAGE	**0.086**	**0.104**	**0.109**	**0.125**	**0.141**	**0.140**
AIR HOLD-UP (%)	1	85.0	86.0	87.9	90.2	89.7	90.0
	2	83.2	80.3	83.7	87.6	88.7	89.2
	3	82.4	78.4	80.6	84.0	87.5	88.0
	4	70.5	78.7	78.6	82.2	85.0	85.6
	AVERAGE	**80.3**	**80.9**	**82.7**	**86.0**	**87.7**	**88.2**
GRADE (% S)	1	31.0	32.4	36.4	35.8	31.7	26.7
	2	29.3	25.5	32.6	31.3	24.0	25.3
	3	23.6	16.2	24.2	27.3	23.1	23.4
	4	26.1	17.7	20.1	25.2	18.5	20.8
	AVERAGE	**27.6**	**23.1**	**28.9**	**29.5**	**23.9**	**23.7**
RECOVERY (%)	1	20.9	25.7	31.9	24.9	20.0	16.3
	2	13.3	13.6	16.7	15.5	11.7	11.5
	3	10.0	7.9	8.8	11.2	10.8	10.2
	4	23.2	18.1	18.8	22.5	16.1	17.4
	TOTAL	**67.4**	**63.3**	**77.8**	**73.6**	**58.6**	**55.4**
PARTICLE SIZE (µm)	1	23.4	24.9	21.2	19.8	18.4	17.7
	2	27.1	31.0	20.1	19.9	21.4	21.7
	3	26.2	25.0	23.6	17.0	22.0	15.6
	4	28.3	29.2	25.6	21.7	25.0	21.1
	AVERAGE	**26.4**	**27.6**	**22.5**	**19.8**	**22.0**	**19.3**
FEED PART. SIZE (µm)		22.6	22.6	22.6	22.6	22.6	22.6
POOLED STD. DEV. (%)		6.5	12.4	6.6	12.1	12.3	4.2

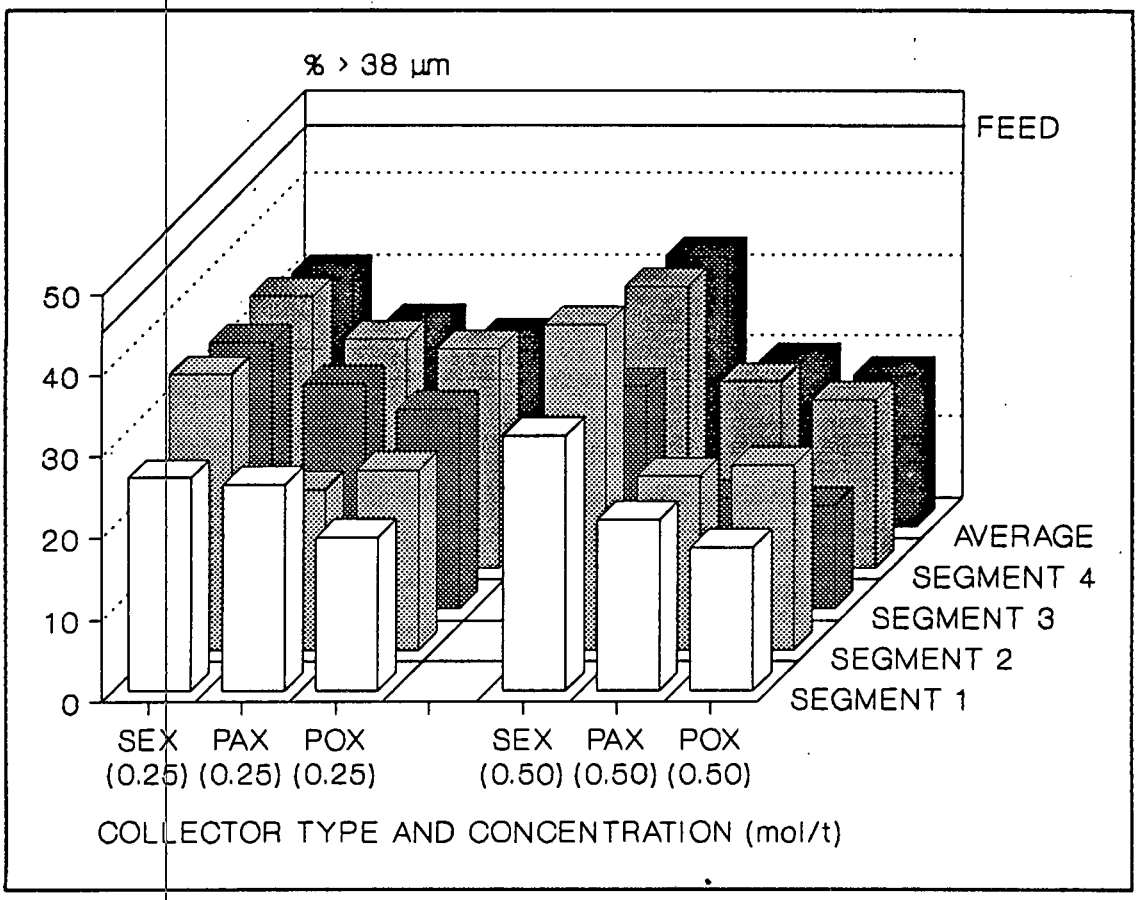

FIGURE 3.11 : Proportion of Gangue Material in Each Segment of the Froth for Different Collector Additions

The fact that less quartz was present in the top segment of the froth suggests that the coarsest pyrite particles were located in this segment. Figure 3.12 clearly shows that there was a large decrease in the size of the pyrite particles between segments 2 and 3. The mean particle size of the quartz decreased slightly as height in the froth increased, but the particle size distribution in the froth was far more uniform than that of the pyrite. The coarser pyrite particles stabilized the froth because they were able to attain their equilibrium contact angle in adjacent bubbles without causing excessive thinning of the water films between the bubbles.

Figure 3.13 indicates that the air hold-up increased from the bottom to the top of the froth. This implies that the water content, and hence the concentration of entrained material was lowest at the top of the froth and highest at the bottom of the froth.

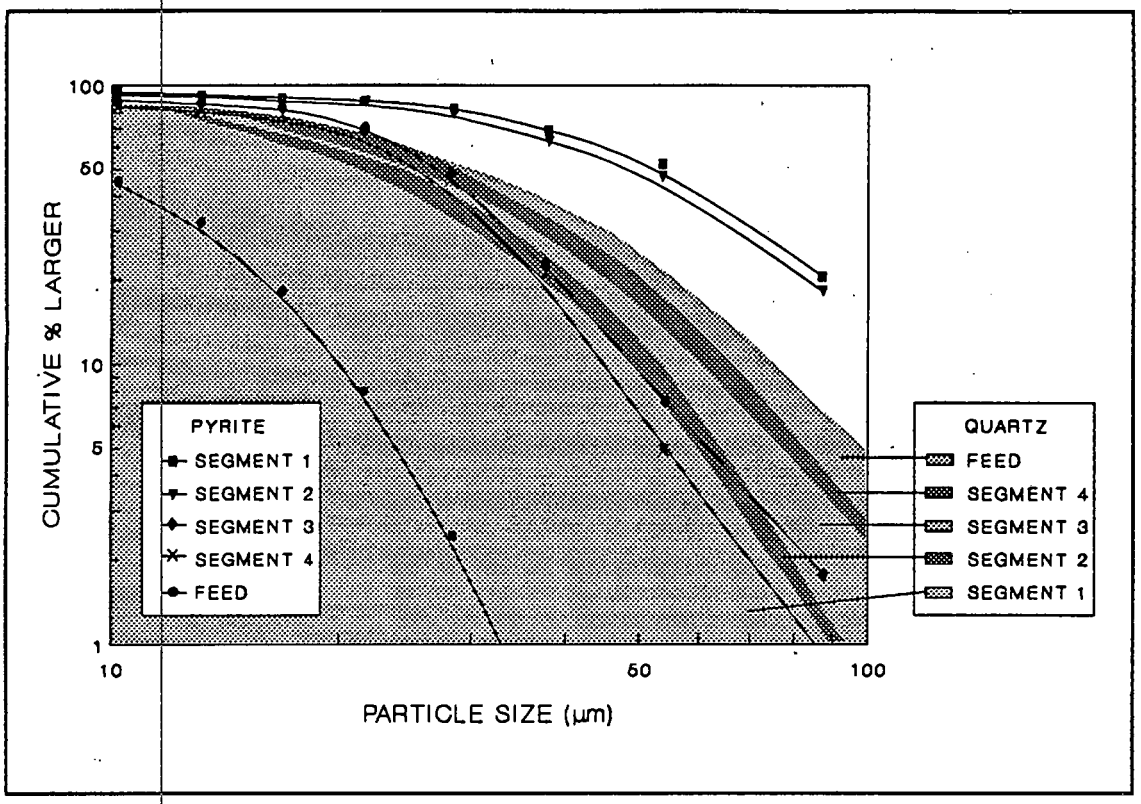

FIGURE 3.12 : Size Distribution of Pyrite and Quartz in the Froth

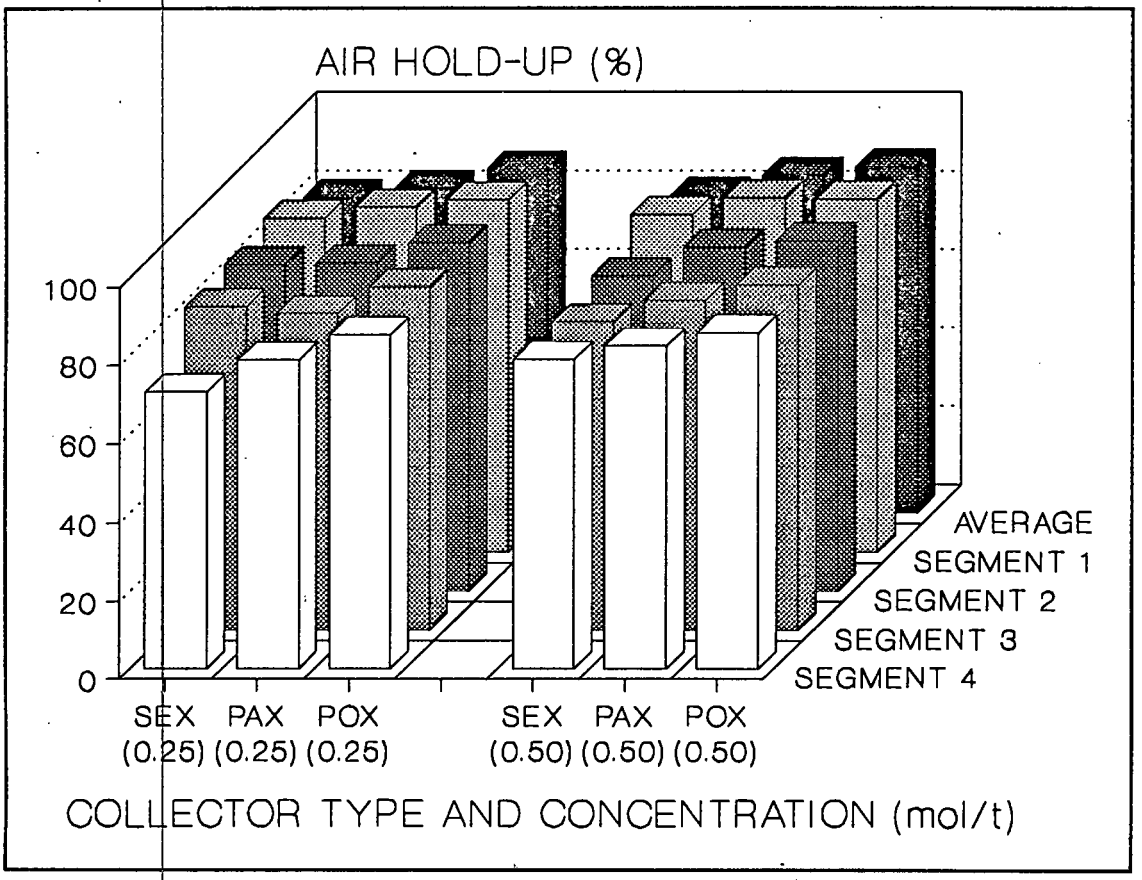

FIGURE 3.13 : Variation of Air Hold-up With Height in the Froth

Figure 3.14 shows that the recovery of pyrite decreased as the height in the froth decreased. The recovery in the bottom segment of the froth (segment 4) was, however, always greater than in segment 3. Figure 3.15 shows that the sulphur grade decreased with decreasing height in the froth. This trend was due to the elutriation of particles of gangue from the upper levels in the froth and the entrainment of quartz into the lower levels of the froth.

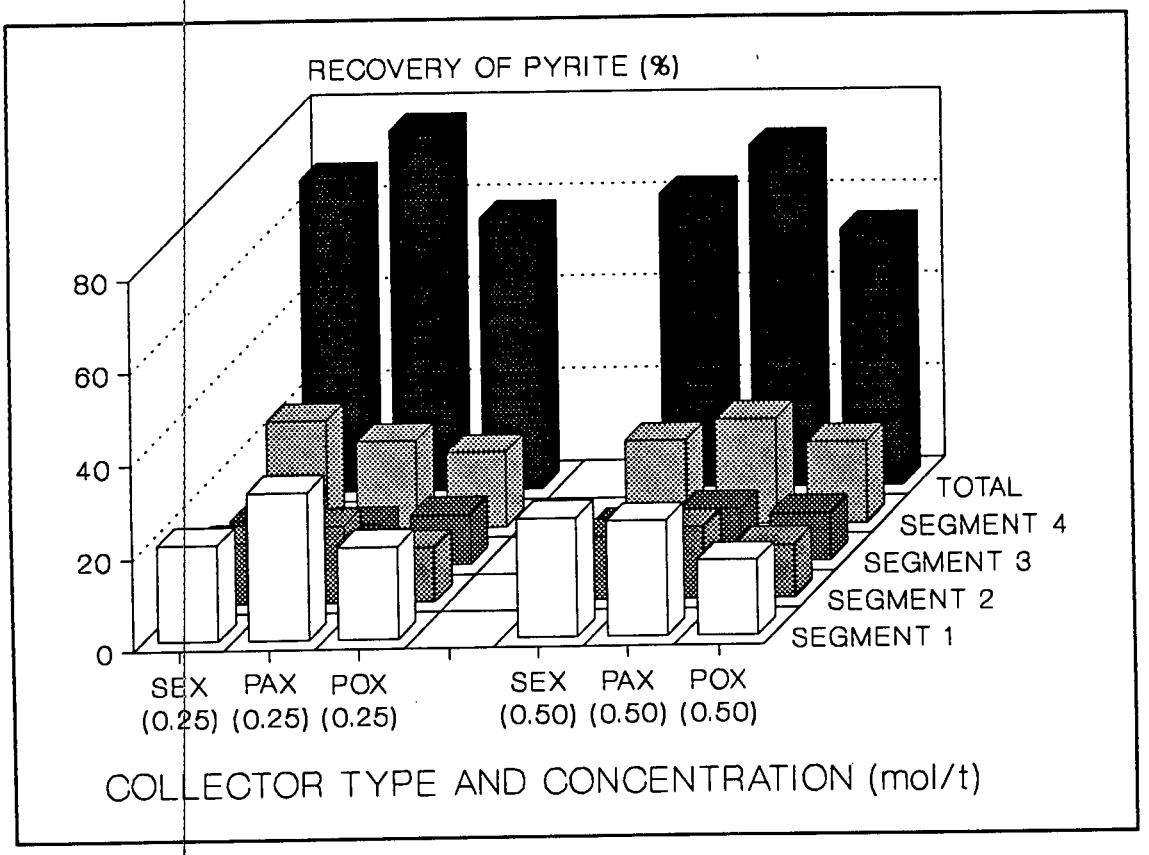

FIGURE 3.14 : Relationship Between Recovery of Pyrite and Height in the Froth

The above grade-recovery trend can be ascribed to two factors: A froth crowding effect at the pulp-froth interface, which prevented the pyrite from rising higher in the froth, and the recycling of ultrafine particles at the bottom of the froth. The recycling was due either to entrainment or to the bubble-breaking effect of this ultra-fine material. The bubble-breaking effect is caused by a particle attempting to attain its equilibrium contact angle in two adjacent bubbles, thus forcing the inter-bubble water film to thin excessively and rupture. This causes the ultra-fine particles at the bottom of the froth to be recycled, since the particles are floated, break the froth,

fall back into the pulp, and are refloated. However, it is likely that entrainment was the dominant effect, due to the size of the particles involved and the fact that the bottom of the froth was well hydrated.

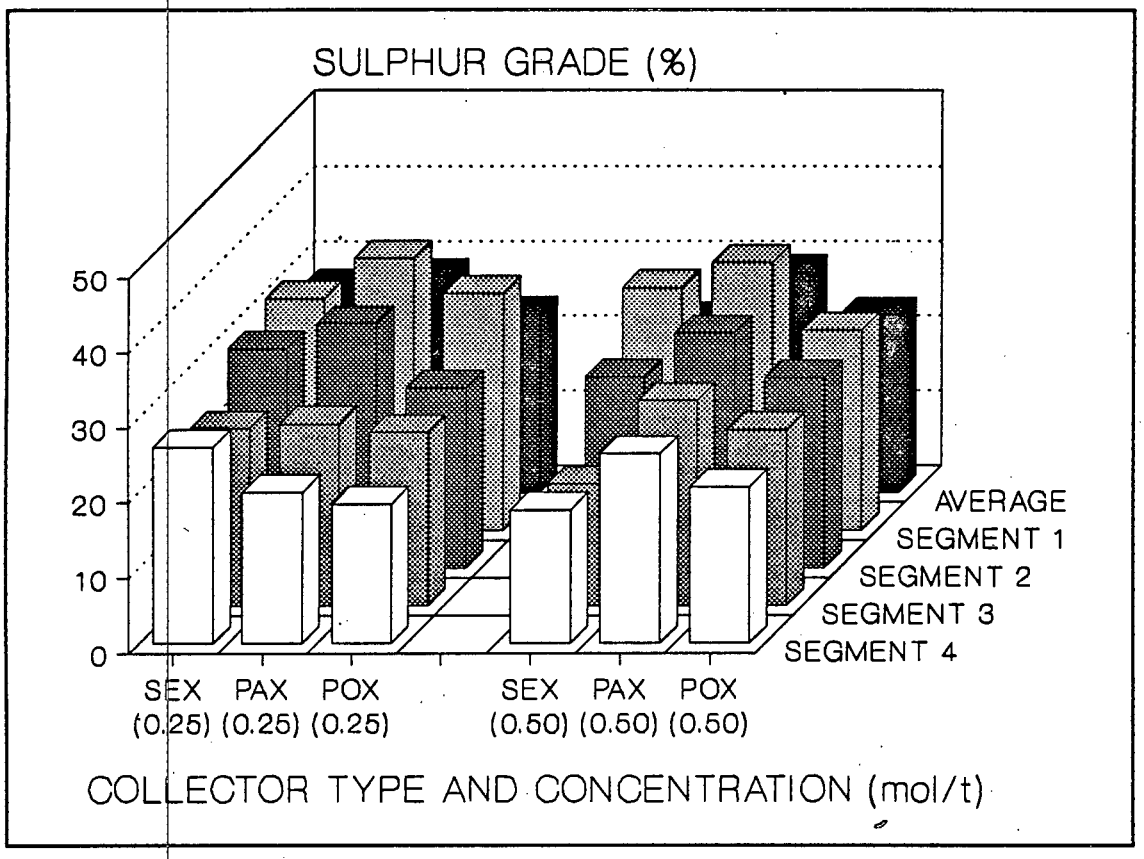

FIGURE 3.15 : Relationship Between Sulphur Grade and Height in the Froth

Figure 3.13 shows that the air hold-up increased, and hence the water hold-up decreased, as the hydrophobicity of the system increased. This confirms the theory that the greater the contact angle, the thinner the inter-bubble water lamellae because the bubble-particle bonds hold the bubbles closer together. This may cause some bubble breakage at high contact angles.

Figures 3.14 and 3.15 also reveal interesting trends about the way in which grade and recovery were affected by collector type and concentration. It can be seen that PAX (potassium amyl xanthate) gave the highest grades and recoveries. This was probably due to a contact angle effect. The hydrophobicity, and hence the contact angle, of the collectors increases as the length of the carbon chain increases and as the collector concentration

increases. If the contact angle was too low the bond between the bubble and the particle was weak and poor recoveries resulted. If the contact angle was too high then the froth built up quickly and had to be cut to prevent froth overflow. This resulted in a shorter time for the pyrite to float, and entrapment of gangue material in the tightly packed froth. Some bubble breakage may also have occurred due to excessive thinning of the inter-bubble lamellae.

It is also evident that overdosing with collector causes a reduction in overall recovery while the grade is unaffected. At higher collector concentrations the recovery at the top of the froth (segment 1) decreased while the recovery at the bottom of the froth (segment 4) increased. This indicates that the optimum contact angle for the system was being exceeded and the froth was too tightly packed. This is confirmed by the fact that at a collector dosage of 0.5 mol/ton SEX had the highest recovery at the top of the froth and POX the lowest, while at 0.25 mol/ton SEX had the lowest recovery at the top of the froth and PAX the highest.

3.4.2.iii TYPE AND CONCENTRATION OF FROTHER

Two different frothers (Dowfroth 200 and Dowfroth 250) were studied at three different concentrations, viz: 50 ppm, 75 ppm and 100 ppm. The results of these tests are shown in Table 3.6. The variation of sulphur grade and recovery at various heights in the froth are shown in Figures 3.16 and 3.17 respectively. It was found that the froth would not rise enough to fill the top segment at a frother concentration of 50 ppm.

It appears that there was an optimum frother concentration at about 75 ppm for Dowfroth 250. Below this dosage (50 ppm) the froth was not stable enough to achieve high recoveries, although the grades were good. Above this concentration (100 ppm) the recovery decreased with little change in the grade. The froth built up quickly and had to be cut allowing less time for the pyrite to float. This explains the high grade and recovery found at the bottom of the froth at the higher frother concentration. The froth also appeared to be more stable and it is likely that gangue particles were trapped in the upper levels of the froth. The grade and recovery profiles support theory.

TABLE 3.6 : Batch Froth Cutting Tests
Frother Type and Concentration

	SEGMENT	DOWFROTH 250			DOWFROTH 200		
		50 (ppm)	75 (ppm)	100 (ppm)	50 (ppm)	75 (ppm)	100 (ppm)
PARTICLE MASS (grams)	1		2.01	1.04		0.99	0.87
	2	1.36	0.90	0.70	0.77	0.62	0.72
	3	0.61	0.54	0.65	0.69	0.80	0.91
	4	0.92	1.03	1.37	1.16	1.24	1.16
	TOTAL	**2.89**	**4.48**	**3.76**	**2.62**	**3.35**	**3.66**
WATER MASS (grams)	1		7.1	8.2		5.0	7.8
	2	3.3	9.9	10.3	4.4	6.2	11.5
	3	8.9	14.7	14.8	10.0	13.1	12.9
	4	12.4	15.8	16.3	12.6	15.6	13.3
	TOTAL	**24.6**	**47.5**	**49.6**	**27.0**	**39.9**	**45.5**
PARTICLE/ WATER RATIO	1		0.283	0.127		0.198	0.112
	2	0.412	0.091	0.068	0.175	0.100	0.063
	3	0.069	0.037	0.044	0.069	0.061	0.071
	4	0.074	0.065	0.084	0.092	0.080	0.087
	AVERAGE	**0.117**	**0.094**	**0.076**	**0.097**	**0.084**	**0.080**
AIR HOLD-UP (%)	1		86.4	85.0		90.6	85.8
	2	93.4	82.0	81.4	91.8	88.7	79.3
	3	83.9	73.7	73.5	81.9	76.2	76.7
	4	77.5	71.5	70.4	77.1	71.7	75.9
	AVERAGE	**84.5**	**78.4**	**77.6**	**83.6**	**81.8**	**79.4**
GRADE (% S)	1		34.2	31.0		34.2	31.8
	2	36.3	23.6	29.3	36.2	30.6	29.8
	3	33.2	16.1	23.6	30.5	24.3	27.1
	4	29.8	18.2	26.1	26.1	21.2	28.2
	AVERAGE	**32.3**	**26.2**	**27.6**	**30.2**	**29.3**	**29.0**
RECOVERY (%)	1		44.6	20.9		22.0	18.0
	2	32.0	13.8	13.3	18.1	12.3	13.9
	3	13.1	5.6	10.0	13.7	12.6	16.0
	4	17.8	12.2	23.2	19.6	17.1	21.2
	TOTAL	**62.9**	**76.2**	**67.4**	**51.4**	**64.0**	**69.1**
PARTICLE SIZE (µm)	1		24.5	23.4		30.9	21.4
	2	22.3	18.9	27.1	16.4	14.8	19.1
	3	25.7	27.9	26.2	16.4	16.0	17.3
	4	23.3	27.6	28.3	13.7	22.7	21.1
	AVERAGE	**23.3**	**24.5**	**26.4**	**15.7**	**22.3**	**19.8**
FEED PART. SIZE (µm)		22.6	22.6	22.6	22.6	22.6	22.6
POOLED STD. DEV. (%)		7.8	7.8	6.5	7.4	7.6	7.6

For Dowfroth 200 the best conditions were at a frother concentration of 100 ppm, although the trends seen in the grade and recovery profiles are similar to those seen with Dowfroth 250. Dowfroth 200 and 250 are both polyoxypropylene glycols, the 200 and 250 referring to their approximate

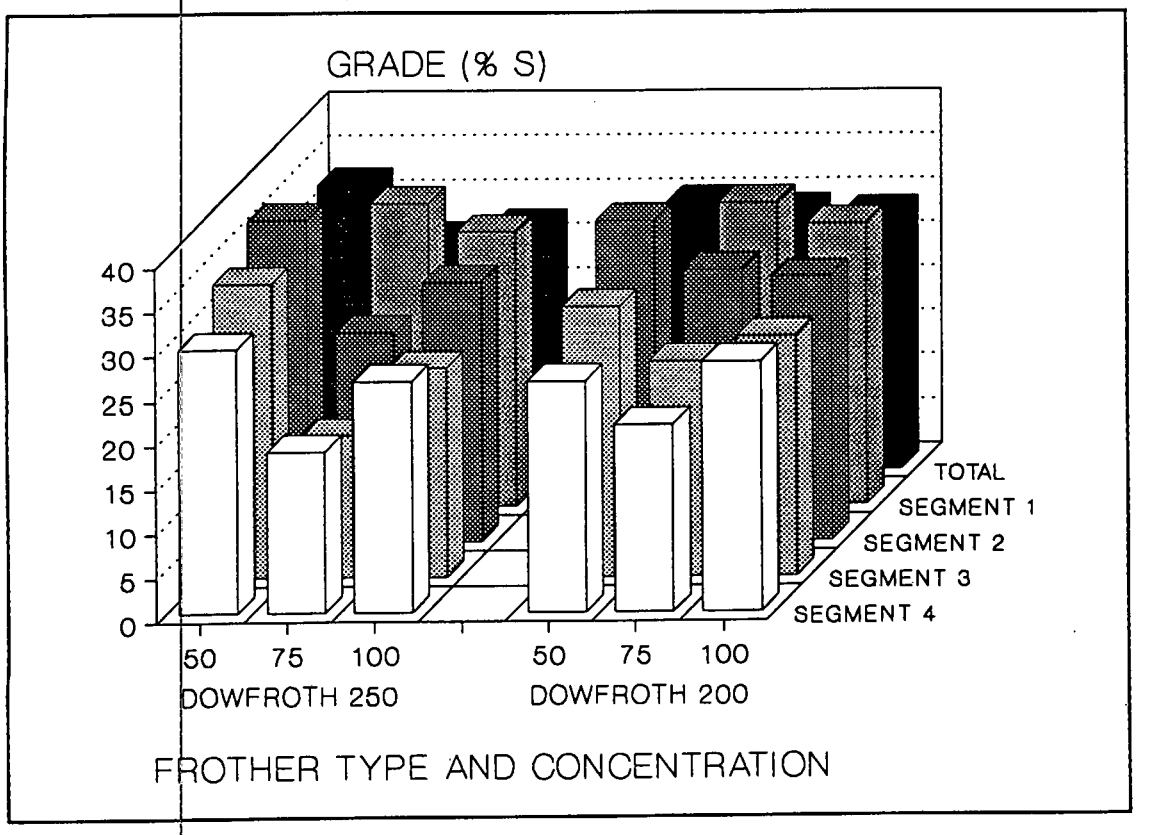

FIGURE 3.16 : Variation of Sulphur Grade with Frother Type and Concentration at Different Heights in the Froth

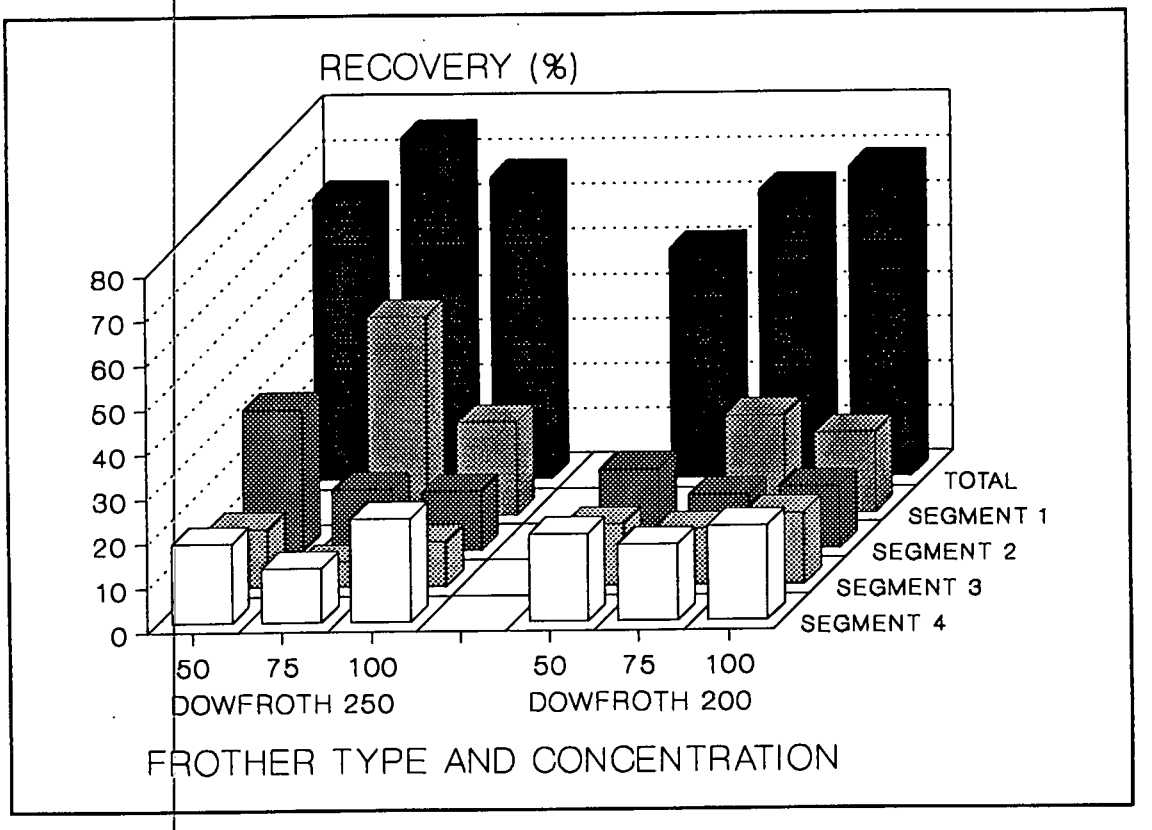

FIGURE 3.17 : Variation of Sulphur Recovery with Frother Type and Concentration at Different Heights in the Froth

molecular weights. In contrast to polyoxyethylene ether chains (Figure 2.10) the surface tension of solutions of compounds comprising polyoxypropylene ether chains (Dowfroth frothers) does not increase as the number of oxypropylene groups increases. The interfacial tension of the oil/water interface does however decrease as the number of oxypropylene groups increases (Leja 1982b). This explains the different optimum concentrations seen with the two frothers.

In the bubble sizing tests it was found that increasing the frother concentration above 10 ppm had little effect on the bubble size. This means that the variations observed in the froth with frother concentration must have been due to froth stability. Increasing the frother concentration must have made the bubbles more stable without affecting their size. As the frother concentration increased so did the water hold-up in the froth, indicating that the thickness of the water films around the bubbles must have increased. This means that there was less froth drainage and bubble coalescence.

3.4.2.iv PARTICLE SIZE

Three different particle size ranges were examined to quantify the effects of particle size at different heights in the froth. The three particle size ranges were a fine fraction (-38 μm), a coarse fraction (38 - 53 μm) and the unsized material used in all the other tests. It should be noted that in the fine and coarse fractions the pyrite and the quartz had the same particle size range, while in the unsized fraction the pyrite was finer than the quartz. The results for these tests can be seen in Table 3.7.

Figure 3.18 shows the variation of mass recovery and particle size and Figure 3.19, the variation of sulphur grade and recovery at different heights in the froth with the different particle size ranges. The fine particles gave a high mass pull because of the high degree of hydraulic entrainment. These fine particles formed a very stable froth with thin water films between bubbles. The result was that there was little elutriation of gangue material from the froth because there was little drainage of these films. This is confirmed by the grade plot, where the grade in all the segments was very low, and there was little upgrading between the bottom and the top of the froth. The particle size tended to increase slightly from the bottom to the

top of the froth. This indicates that the coarser pyrite tended to float first. The recovery with the fine material was low, even though the mass pull was high. This was because the degree of entrainment increases as particle size decreases, and hence there was little flotation occurring, making the selectivity poor. The froth built up very quickly with the fine particles, and thus there was only a short time available for the pyrite to float before the froth had to be cut. This was also a contributing factor to the low recoveries observed.

TABLE 3.7 : Batch Froth Cutting Tests : Feed Particle Size

	SEGMENT	FINE	UNSIZED	COARSE
PARTICLE MASS (grams)	1	1.29	1.04	1.47
	2	1.35	0.70	1.17
	3	1.48	0.65	1.01
	4	2.29	1.37	0.87
	TOTAL	**6.41**	**3.76**	**4.52**
WATER MASS (grams)	1	7.8	8.2	8.9
	2	13.1	9.3	9.2
	3	13.7	9.8	9.8
	4	14.5	16.3	13.7
	TOTAL	**49.1**	**43.6**	**41.6**
PARTICLE/ WATER RATIO	1	0.165	0.127	0.165
	2	0.103	0.075	0.127
	3	0.108	0.066	0.103
	4	0.158	0.084	0.064
	AVERAGE	**0.131**	**0.086**	**0.109**
AIR HOLD-UP (%)	1	85.5	85.0	83.4
	2	76.0	83.2	83.1
	3	74.9	82.3	82.2
	4	73.0	70.4	75.2
	AVERAGE	**77.3**	**80.2**	**81.0**
GRADE (% S)	1	14.2	31.0	25.9
	2	11.4	29.3	20.6
	3	10.4	23.6	18.3
	4	9.6	26.1	16.4
	AVERAGE	**11.1**	**27.6**	**23.7**
RECOVERY (%)	1	11.9	20.9	24.7
	2	10.0	13.3	15.7
	3	10.0	10.0	12.0
	4	14.3	23.2	9.3
	TOTAL	**46.2**	**67.4**	**61.7**
PARTICLE SIZE (µm)	1	14.0	23.9	42.6
	2	13.6	19.9	45.9
	3	12.6	25.2	37.2
	4	11.5	27.0	32.7
	AVERAGE	**12.7**	**24.5**	**40.2**
FEED PARTICLE SIZE (µm)		12.8	22.6	42.0
POOLED STD. DEV. (%)		4.0	6.5	7.3

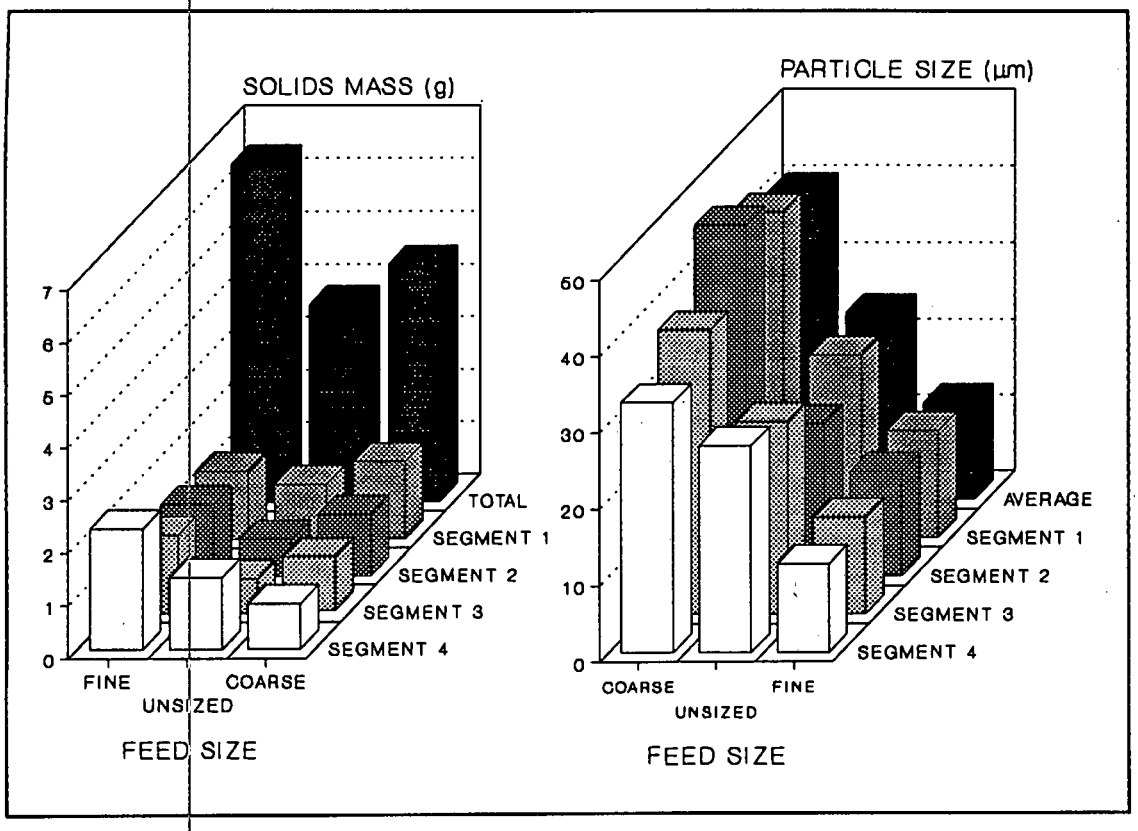

FIGURE 3.18 : Variation of Mass Pull and Particle Size with Feed Size at Different Heights in the Froth

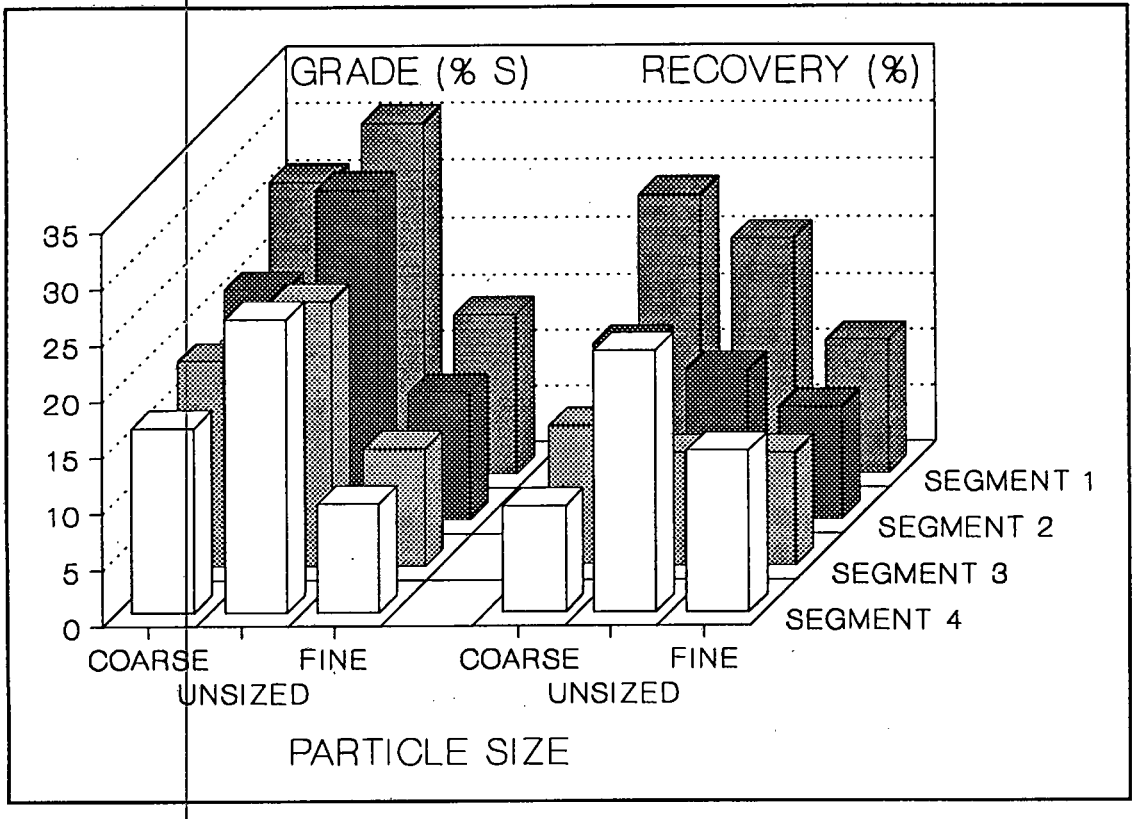

FIGURE 3.19 : Relationship Between Grade and Recovery for Different Particle Sizes and Height in the Froth

As the particle size increases the number of particles per unit mass decreases. The ratio of the number of particles of fine : unsized : coarse material was about 35:6:1 in the feed and about 45:4:1 in the froth. Thus the number of particles in the froth decreased sharply as the particle size increased.

The mass pull at the bottom of the froth indicates that the extent of entrainment decreased as the particle size increased. The grades for the coarse feed system were lower than those for the unsized system because any coarse gangue particles which were entrained into the froth would have been trapped and would not have been able to drain from the froth with the water. The recoveries found with the coarse fraction were higher than for the unsized material except for the bottom segment. This is because there was no fine pyrite to entrain into the bottom of the froth. Since pyrite is twice as dense as quartz, it is unlikely that the coarser pyrite would have been entrained.

3.4.2.v PULP TEMPERATURE

The results of the pulp temperature tests can be seen in Table 3.8. Five different temperatures were examined, viz: 5°C, 15°C, 25°C, 35°C and 45°C. It must be noted that at the higher temperatures the froth became less stable due to increased froth drainage, and the maximum froth height which could be attained was, thus, decreased. The viscosity of water decreases by a factor of 2.5 as the temperature increases from 5°C to 45°C (Table 3.8), and hence there must have been a corresponding increase in froth drainage. Thus, it would be expected that the highest mass pulls and recoveries would be recorded at the lower temperatures, while the best grades would occur at the higher temperatures.

Figure 3.20 shows the average grade and particle size and the overall recovery at the different temperatures. It can be seen, as expected, that the grade increased and the recovery decreased as the temperature increased. The decrease in particle size in the froth with increasing temperature indicates that the degree of entrapment of entrained gangue particles decreased with increasing temperature. It has also been shown that the bubble size decreases as the temperature increases. Entrainment

increases as the bubble size increases due to the increase in rise velocity of the bubbles, thus entrainment decreased as temperature increased.

TABLE 3.8 : Batch Froth Cutting Tests : Temperature

	SEGMENT	TEMPERATURE				
		5 (deg C)	15 (deg C)	25 (deg C)	35 (deg C)	45 (deg C)
PARTICLE MASS (grams)	1	2.96	1.84	1.04		
	2	1.00	1.02	0.70	0.80	
	3	0.58	0.72	0.65	0.72	0.96
	4	0.50	0.74	1.37	1.78	1.96
	TOTAL	**5.04**	**4.32**	**3.76**	**3.30**	**2.92**
WATER MASS (grams)	1	11.6	9.5	8.2		
	2	15.5	13.6	9.3	8.8	
	3	14.1	12.0	9.8	11.4	11.2
	4	11.7	14.0	16.3	12.0	16.5
	TOTAL	**52.9**	**49.1**	**43.6**	**32.2**	**27.7**
PARTICLE/ WATER RATIO	1	0.255	0.194	0.127		
	2	0.065	0.075	0.075	0.091	
	3	0.041	0.060	0.066	0.063	0.086
	4	0.043	0.053	0.084	0.148	0.119
	AVERAGE	**0.095**	**0.088**	**0.086**	**0.102**	**0.105**
AIR HOLD-UP (%)	1	77.9	82.2	85.0		
	2	72.1	75.4	83.2	84.0	
	3	74.8	78.4	82.3	79.5	79.7
	4	79.0	74.8	70.4	77.8	69.8
	AVERAGE	**75.9**	**77.7**	**80.2**	**80.4**	**74.7**
GRADE (% S)	1	26.5	28.9	31.0		
	2	25.1	26.6	29.3	36.3	
	3	24.2	24.3	23.6	29.6	39.9
	4	22.8	22.9	26.1	23.2	24.3
	AVERAGE	**25.5**	**26.5**	**27.6**	**27.8**	**29.4**
RECOVERY (%)	1	50.9	34.5	20.9		
	2	16.3	17.6	13.3	18.9	
	3	9.1	11.4	10.0	13.8	24.9
	4	7.3	11.0	23.2	26.8	30.9
	TOTAL	**83.6**	**74.5**	**67.4**	**59.5**	**55.8**
PARTICLE SIZE (µm)	1	26.9	25.2	23.4		
	2	27.6	26.4	27.1	20.9	
	3	27.9	26.7	26.2	23.6	17.2
	4	30.2	29.6	28.3	24.1	23.4
	AVERAGE	**27.5**	**26.5**	**26.4**	**23.2**	**21.4**
FEED PART. SIZE (µm)		22.6	22.6	22.6	22.6	22.6
POOLED STD. DEV. (%)		4.9	3.6	6.5	2.6	4.1
WATER VISCOSITY (cp)		1.52	1.14	0.89	0.72	0.60

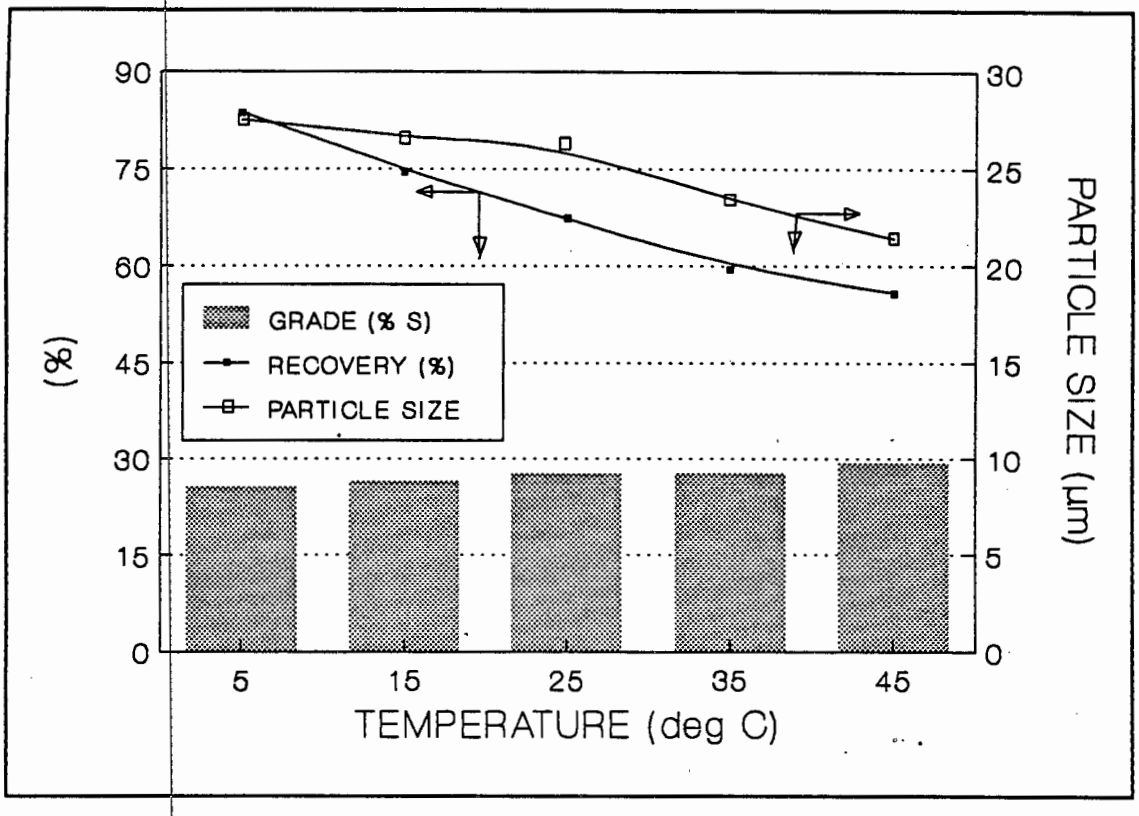

FIGURE 3.20 : Effect of Pulp Temperature on the Grade, Recovery and Particle Size in the Froth

3.4.2.vi FROTH HEIGHT TESTS

Tests were conducted at different froth heights with both pure pyrite, and the pyrite-quartz mixture used in the previous tests (Tables 3.9 and 3.10). Five different heights were examined (100 mm, 80 mm, 60 mm, 40 mm and 20 mm) so that a profile of the froth could be obtained as the froth built up. Any froth rearrangement which occurred would then become evident. The two different types of feed were used so that any differences in froth behaviour between a system with floatable particles only and a system with both floatable and non-floatable particles could be highlighted. It should be noted that the results for the same segment in different tests are not directly comparable. For example at a froth height of 40 mm segment 3 was at the top of the froth, while it was near the bottom when the froth height was 100 mm.

The trends in the mass recovery were the same for both the pyrite, and the pyrite-quartz systems. The mass recovery at different froth heights for the pyrite-quartz system is shown in Figure 3.21. The highest mass

recoveries occurred at the top and the bottom of the froth. The high mass recovery at the top of the froth was because the floatable (coarser) pyrite particles were found in this segment and pyrite is about twice as dense as quartz. The high particle mass at the bottom of the froth was due to entrainment. Entrained material was rejected at the pulp-froth interface due to the deceleration of the bubbles. The relatively high mass per segment at low froth heights was expected because little froth expansion had occurred, and only a short time had been allowed for froth drainage and elutriation of entrained material to occur.

TABLE 3.9 : Batch Froth Cutting Tests
Pyrite Air Rate and Froth Height Data

RUN	AIR RATE (cm/s)	TOTAL HEIGHT (mm)	TIME (sec)	SEGMENT	PARTICLE MASS (g)	WATER MASS (g)	PARTICLE/ WATER RATIO	AIR HOLD-UP (%)	d(50) (µm)
A	0.615	100	24	1	6.47	4.9	1.32	94.5	14.9
				2	4.51	5.6	0.81	88.5	14.3
				3	4.05	5.3	0.76	89.2	11.7
				4	6.80	5.5	1.24	87.9	7.5
				TOTAL	21.83	21.2	1.03	88.7	11.6
B	0.615	80	20	1	4.71	3.0	1.59	93.0	15.3
				2	5.15	3.9	1.32	91.3	14.4
				3	4.74	4.2	1.13	90.9	10.7
				4	7.00	4.5	1.56	89.6	7.7
				TOTAL	21.60	15.5	1.39	91.2	11.6
C	0.615	60	16	1					
				2	5.58	2.0	2.74	94.5	15.9
				3	6.03	4.6	1.33	89.7	13.1
				4	6.18	5.7	1.09	87.7	10.5
				TOTAL	17.79	12.3	1.45	90.6	13.0
D	0.615	40	13	1					
				2					
				3	6.24	1.9	3.30	94.4	16.6
				4	6.96	3.4	2.07	91.5	12.9
				TOTAL	13.20	5.3	2.51	93.0	14.6
E	0.615	20	10	1					
				2					
				3					
				4	8.78	1.6	5.49	94.1	17.3
				TOTAL	8.78	1.6	5.49	94.1	17.3
FEED					35.00				9.4

d(50) = 50% passing size.

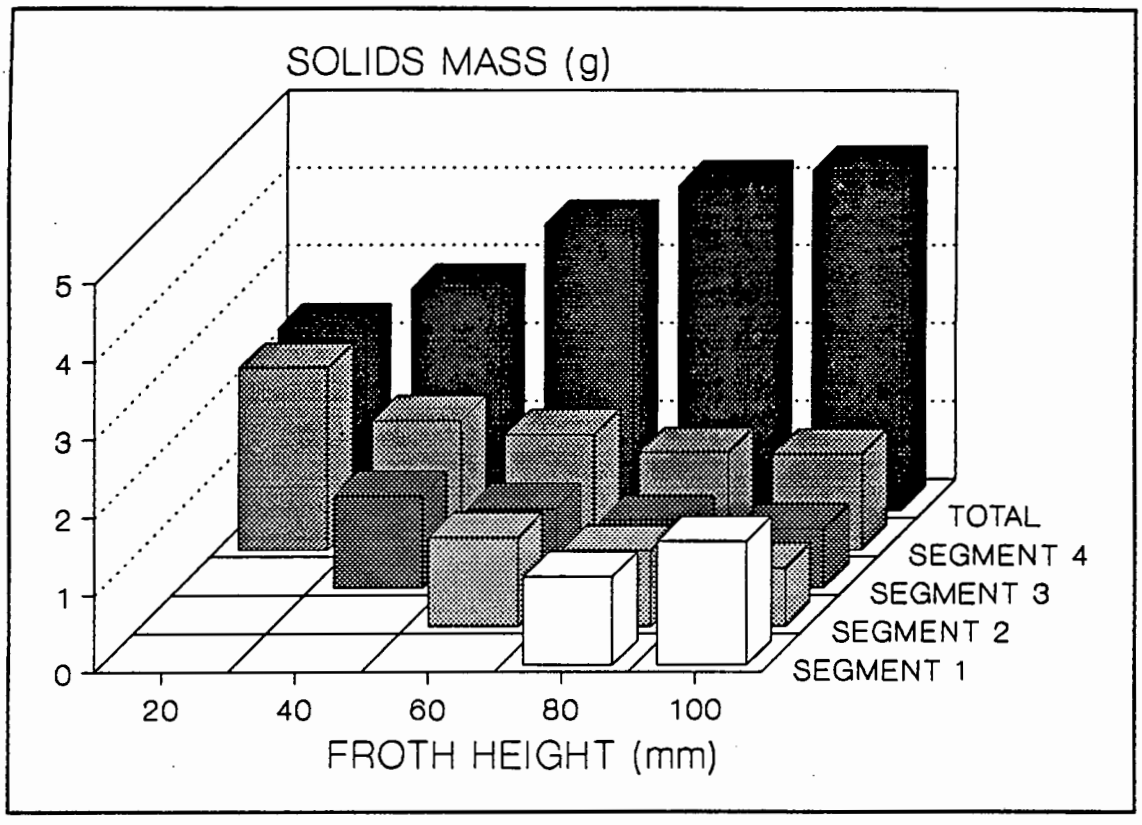

FIGURE 3.21 : Variation of Mass of Solids in the Froth with Froth Height for the Pyrite-Quartz System

If the pure pyrite, and the mixed system are compared it can be seen that the solids mass pull for the pure pyrite system was much greater than that of the mixed system. This is to be expected because there was ten times as much floatable material in the pyrite system as in the mixed system.

The water recovery for the mixed system was, however, higher. The reason for this was that the floated pyrite forms bridges between bubbles, effectively forcing the inter-bubble water lamellae to thin. In the mixed system, the larger quartz particles which were trapped in the froth could prevent this from happening by keeping the bubbles further apart and thus the froth was more hydrated. There were also less floated pyrite particles in the mixed system to form bridges between bubbles.

It can be seen from Tables 3.9 and 3.10 that the amount of water in the froth decreased as height in the froth increased. This means that the froth was best drained at the top, and that the amount of entrained material should have increased as height in the froth decreased.

TABLE 3.10 : Batch Froth Cutting Tests
Pyrite/Quartz Air Rate and Froth Height Data

RUN	AIR RATE (cm/s)	TOTAL HEIGHT (mm)	TIME (sec)	SEGMENT	PARTICLE MASS (g)	WATER MASS (g)	PARTICLE/ WATER RATIO	AIR HOLD-UP (%)	GRADE (% S)	REC (%)	d(50) (µm)
				1	1.71	10.7	0.160	90.1	32.9	37.0	18.6
				2	0.76	13.2	0.058	76.2	25.3	12.6	18.4
A	0.615	100	47	3	0.77	16.1	0.048	71.1	19.2	9.7	25.0
				4	1.13	17.6	0.064	68.0	26.5	19.7	30.8
				TOTAL	4.37	57.6	0.076	74.0	26.6	79.0	24.5
				1	1.15	9.1	0.126	83.3	31.4	23.7	24.3
				2	0.89	10.3	0.086	81.3	29.6	17.3	24.8
B	0.615	80	39	3	0.88	11.2	0.079	79.7	24.1	13.9	24.0
				4	1.25	17.9	0.070	67.7	29.2	24.0	29.6
				TOTAL	4.17	48.4	0.086	78.0	28.8	78.9	25.9
				1							
				2	1.16	12.3	0.094	77.7	31.8	24.3	26.8
C	0.615	60	31	3	1.03	13.0	0.084	76.5	30.0	20.3	26.3
				4	1.48	14.0	0.106	74.5	26.2	25.4	22.8
				TOTAL	3.67	39.4	0.093	76.2	29.0	70.0	25.0
				1							
				2							
D	0.615	40	25	3	1.19	7.8	0.153	85.6	39.3	30.7	31.8
				4	1.66	10.2	0.163	81.1	35.7	38.9	29.4
				TOTAL	2.85	18.0	0.158	83.4	37.2	69.6	30.4
				1							
				2							
E	0.615	20	20	3							
				4	2.33	9.7	0.240	81.7	42.4	64.8	32.0
				TOTAL	2.33	9.7	0.240	81.7	42.4	64.8	32.0
				1	1.04	13.7	0.076	75.4	31.6	21.5	21.9
				2	0.94	13.0	0.072	76.5	28.8	17.8	24.3
F	0.518	80	47	3	1.43	13.8	1.036	74.8	18.2	17.1	27.8
				4	1.61	16.6	0.097	69.7	15.9	16.8	26.3
				TOTAL	5.02	57.1	0.088	74.1	22.2	73.2	25.6
				1	1.00	15.6	0.064	71.9	29.9	19.6	23.6
				2	1.09	13.2	0.826	76.1	25.3	18.1	24.7
G	0.414	80	59	3	1.45	12.1	0.120	77.8	17.3	16.4	32.4
				4	2.00	17.1	0.117	68.6	12.1	15.8	26.8
				TOTAL	5.54	58.0	0.096	73.6	19.3	69.9	27.3
FEED					35.00				4.4		29.2

d(50) = 50% passing size.

The trends in particle size with froth height for both systems are shown in Figures 3.22 and 3.23. From Figure 3.22 it can be seen that the coarsest pyrite floated first. It should be noted all the pyrite used in these tests was finer than 38 µm with 57 percent being in the sub 10 µm range. The ultra-fine pyrite does not float well and tends to be entrained.

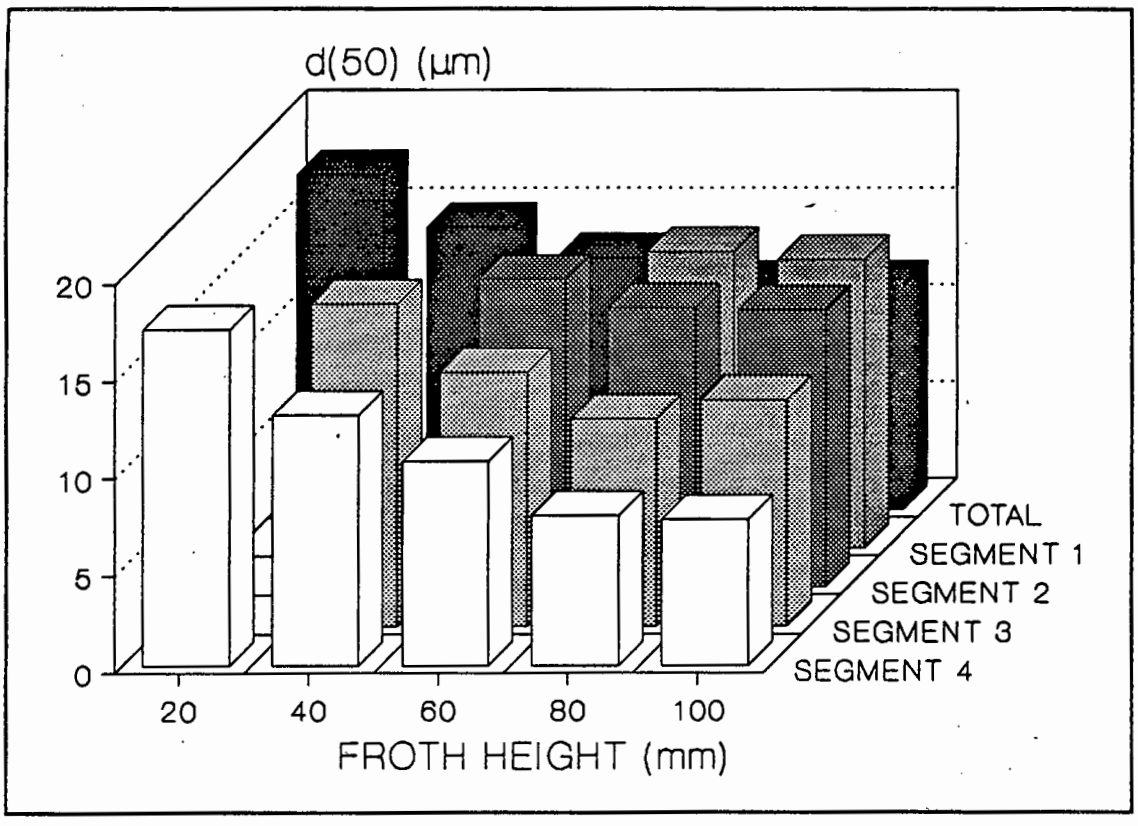

FIGURE 3.22 : Variation of Particle Size in the Froth with Froth Height for the Pure Pyrite System

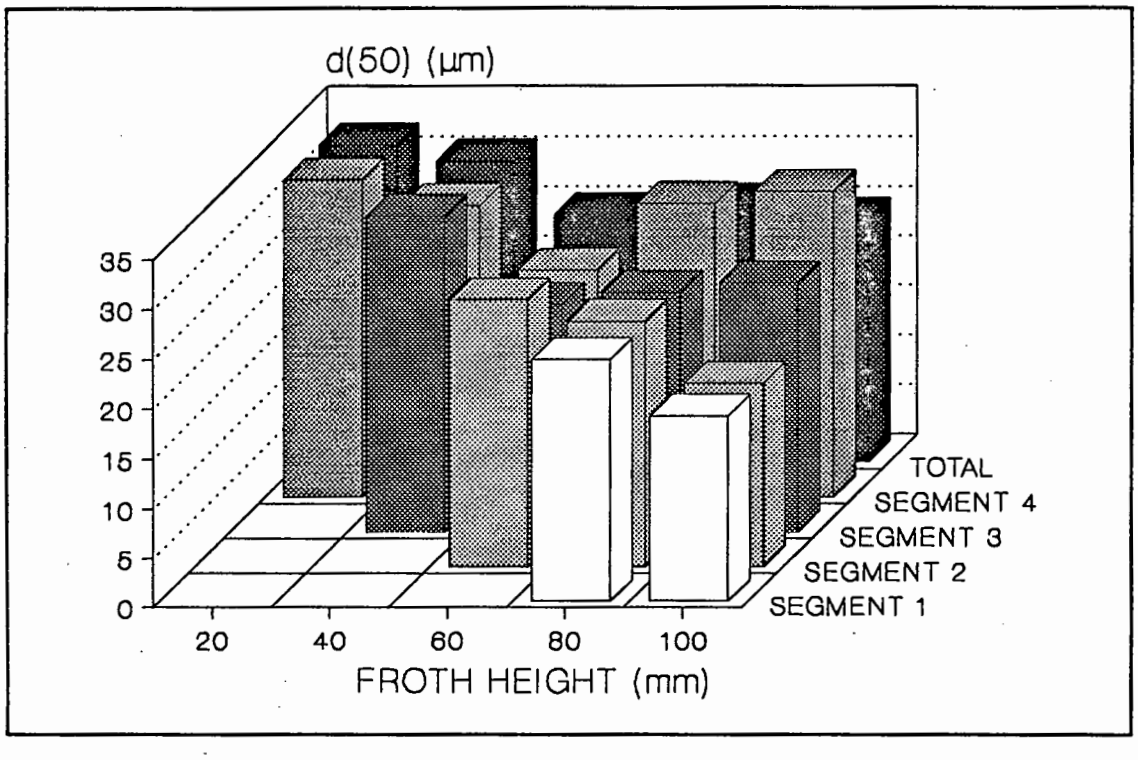

FIGURE 3.23 : Variation of Particle Size in the Froth with Froth Height for the Pyrite-Quartz System

For the pyrite-quartz system (Figure 3.23) the particle size decreased as height in the froth increased. This is because the amount of entrained material decreased as height in the froth increased. The quartz used in these tests was significantly larger than the pyrite, and so this result would be expected.

It can be seen from the grade-recovery data in Table 3.10 that the pyrite floated first and then an increasing amount of quartz was entrained into the froth. The small initial degree of entrainment indicates the bubbles were well loaded with pyrite, preventing quartz entrainment. Thus the 20 mm froth height test had the highest grade and the 100 mm test, the lowest. It can also be seen that the highest recoveries occurred in the top segment. The relatively high recoveries in the bottom segment were again due to entrainment of fine pyrite.

3.4.2.vii AIR RATE TESTS

Three sets of air flow rate tests were conducted with the pyrite-quartz ore at superficial air velocities of 0.414 cm/s, 0.518 cm/s and 0.615 cm/s (Table 3.10). The aim of these tests was to establish the effect of air flow rate on the froth. The air flow rate affects the bubble size and the bubble surface area, as well as the rate of flotation. Dobby and Finch (1985) propose the following relationship for the rate constant (k_r) in a column cell:

$$k_r = 1.5 \cdot E \cdot J_g / d_b$$

where E is the collision efficiency, J_g, the superficial gas velocity and d_b the bubble diameter. Dobby and Finch (1985) also state that:

$$d_b \propto J_g^x$$

The value of x varies between 0 and 1 depending on the way in which the bubbles are generated and the frother type and concentration. Therefore:

$$k_r \propto J_g^{1-x}$$

The collision efficiency (E) decreases as the bubble size increases. This means that there is an optimum air flow rate for flotation in the pulp. The

rate at which flotation occurs in the pulp affects the froth, so there must also be an optimum air flow rate for the froth. It does not appear that the air flow rates chosen for these tests straddled this optimum.

Table 3.10 shows that the solids mass pull tended to increase as the air flow rate decreased. This indicates one of two things: Either, the more tightly packed froth resulting from fine bubbles led to increased entrapment of gangue, or the major way in which particles were transferred into the froth was by flotation and not entrainment. The higher air rates would have given larger bubbles and would have favoured the entrainment mechanism. The smaller bubbles formed at low air rates would have favoured flotation, especially with fine material, because the streamlines around the bubbles are less pronounced and the chances of bubble-particle collision are greater.

The variations of sulphur grade and recovery with superficial air rate are shown in Figure 3.24. It can be seen that both the grade and the recovery increased as the air rate increased. This was not what would be expected, but it must be remembered that all the air rates chosen for these tests are low. Since the highest mass of solids was recovered at the lowest air rate there must have been a large degree of entrapment of gangue material at the lower air flow rates. This was probably due to poor froth drainage because the froth was more tightly packed due to the smaller bubbles. This is confirmed by the air hold-up profiles (Table 3.10). It can be seen from the grades in segment 4 that little ultra-fine pyrite was entrained into the bottom of the froth at the low air flow rates, but this increased as the air rate increased.

The recoveries at the different air flow rates follow the same trends as the grade. The probable reason for the increase in recovery as the air rate increases was the increased amount of bubble surface area available to float the pyrite particles.

There does not appear to be any marked trend in the particle size distributions as the air flow rate changed. There was, however, a general increase in the size of particles as the froth height decreased. This was, again, due to the different amounts of entrained quartz at different levels in the froth.

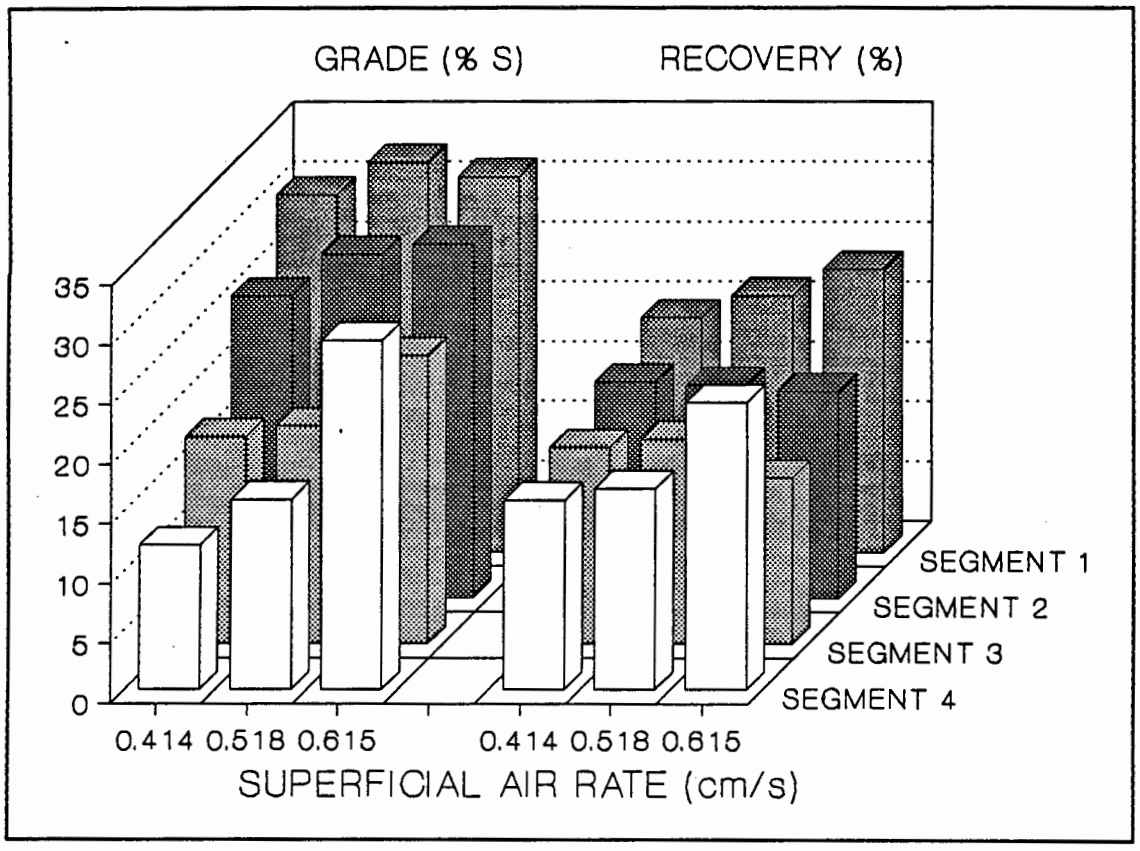

FIGURE 3.24 : Variation of Sulphur Grade and Recovery in the Froth with Superficial Air Rate

3.4.3 CONTINUOUS FROTH CUTTING TESTS

Froth cutting tests were carried under continuous conditions to determine the effects of four different flotation parameters on the froth at different heights in the froth. The four parameters were: pulp density, air rate, frother concentration, and froth height. Three different systems were studied:

- a pyrite-quartz mixture without wash water, to compare the results of the continuous and the batch systems and to highlight any differences between steady state and non-steady state operation;
- a pyrite-quartz mixture with wash water to quantify the effect that froth washing has at different levels in the froth, and to compare a system with a typical column froth to a system with a deep conventional froth; and
- the Unisel ore used in the residence time distribution studies so that the effects occurring at different levels in the froth could be

correlated with the froth residence time distribution, and to study a real ore and compare it to the synthetic ores used in the other tests.

Information was again gained about the solids mass, the water mass, the solid-to-water ratio, the air hold-up, the particle size and the grade at different levels in the froth, as well as the overall recovery.

3.4.3.i REPRODUCIBILITY

Six repeat runs, using the pyrite-quartz system with wash water, were conducted under identical conditions to establish the reproducibility of the system. The conditions were:

- a pulp density of 20% solids,
- a superficial air rate of 1.2 $cm \cdot s^{-1}$,
- a frother concentration of 25 ppm, and
- a froth height of 120 mm.

These data are given in Table 3.11. It was found that, at a 95% confidence limit, the mass of solids recovered was within 13% of the mean, and the water recovery within 26% of the mean. The precision of these values is significantly better than the batch system.

It was again decided to conduct three runs at the same conditions and to combine the froth from each segment for sulphur and particle size analyses. A similar criterion for the acceptance of a run was set to that used for the batch system; i.e. the masses of solids and water recovered must be within 1.5 standard deviations of the mean for the three runs. This meant that the solids recovery had to be within 7.5% of the mean and the water had to be within 14.8% of the mean for the run to be accepted. The increase in precision when the concentrates from each segment for the three run are combined can be seen in Table 3.12. The 95% confidence limits decreased from 12.8% to 3.3% for the solids recovery, and from 25.3% to 7.7% for the water recovery.

TABLE 3.11 : Reproducibility : Continuous Froth Cutting Tests

RUN	PARTICLE MASS (g)							
	CONC	*TAILS*	1	2	3	4	TOTAL	MEAN
1	25.9	288	1.19	1.33	1.71	2.24	6.47	*1.62*
2	28.6	281	1.24	1.42	1.71	2.12	6.49	*1.62*
3	26.6	292	1.20	1.34	1.77	2.25	6.57	*1.64*
4	28.0	303	1.11	1.60	1.87	2.26	6.84	*1.71*
5	28.5	284	1.27	1.38	1.72	2.23	6.60	*1.65*
6	25.1	300	1.13	1.33	1.61	2.02	6.10	*1.53*
AVERAGE	27.1	291	1.19	1.40	1.73	2.19	6.51	*1.63*
STD. DEV.	4.91%	2.69%	4.70%	6.65%	4.47%	4.03%	3.37%	*4.96%*
SIGNIFICANT VARIATION (95% CONFIDENCE LIMIT)								**12.76%**
RUN	WATER MASS (g)							
	CONC	*TAILS*	1	2	3	4	TOTAL	MEAN
1	532.7	1355	31.4	31.6	23.9	33.1	120.0	*30.0*
2	529.8	1339	28.1	28.6	33.9	33.2	123.8	*30.9*
3	452.6	1413	27.0	27.1	28.5	29.0	111.7	*27.9*
4	518.5	1293	31.2	34.9	34.3	27.5	127.9	*32.0*
5	462.2	1343	22.3	28.8	29.8	34.5	115.5	*28.9*
6	565.0	1213	29.2	28.4	32.6	30.5	120.7	*30.2*
AVERAGE	510.1	1326	28.2	29.9	30.5	31.3	119.9	*30.0*
STD. DEV.	7.84%	4.64%	10.77%	8.79%	11.85%	8.01%	4.09%	*9.86%*
SIGNIFICANT VARIATION (95% CONFIDENCE LIMIT)								**25.33%**
RUN	PARTICLE/WATER RATIO							
	CONC	*TAILS*	1	2	3	4	TOTAL	MEAN
1	0.049	0.213	0.038	0.042	0.071	0.068	0.055	*0.055*
2	0.054	0.210	0.044	0.050	0.050	0.064	0.052	*0.052*
3	0.059	0.207	0.044	0.049	0.062	0.078	0.058	*0.058*
4	0.054	0.234	0.036	0.046	0.054	0.082	0.055	*0.055*
5	0.062	0.211	0.057	0.048	0.058	0.065	0.057	*0.057*
6	0.044	0.247	0.039	0.047	0.049	0.066	0.050	*0.050*
AVERAGE	0.053	0.220	0.043	0.047	0.058	0.070	0.054	*0.054*
STD. DEV.	10.81%	6.84%	16.29%	5.51%	13.08%	9.96%	11.21%	*11.21%*
SIGNIFICANT VARIATION (95% CONFIDENCE LIMIT)								**28.80%**
RUN	AIR HOLD-UP							
	CONC	*TAILS*	1	2	3	4	TOTAL	MEAN
1			62.7	62.3	71.3	60.3	64.2	*64.2*
2			66.6	66.0	59.5	60.1	63.0	*63.0*
3			67.8	67.7	65.9	65.1	66.6	*66.6*
4			63.0	58.4	59.0	66.9	61.8	*61.8*
5			73.3	65.6	64.4	58.6	65.5	*65.5*
6			65.4	66.2	61.2	63.4	64.0	*64.0*
AVERAGE			66.5	64.4	63.6	62.4	64.2	*64.2*
STD. DEV.			5.36%	4.85%	6.71%	4.73%	2.43%	*5.41%*
SIGNIFICANT VARIATION (95% CONFIDENCE LIMIT)								*13.91%*
RUN	PARTICLE SIZE (μm)							
	CONC	*TAILS*	1	2	3	4	TOTAL	MEAN
1	19.6	22.6	19.9	20.0	22.6	23.9	22.0	*21.6*
2	19.3	23.5	18.7	20.4	23.0	23.5	21.7	*21.4*
3	18.1	23.1	20.4	19.7	22.1	23.0	21.6	*21.3*
4	18.9	23.4	18.4	19.7	22.4	23.3	21.5	*20.9*
5	18.2	22.5	19.4	20.7	22.3	23.0	21.6	*21.4*
6	18.4	22.9	20.2	20.9	22.2	24.2	22.2	*21.9*
AVERAGE	18.8	23.0	19.4	20.4	22.4	23.5	21.7	*21.4*
STD. DEV.	3.03%	1.74%	3.72%	2.35%	1.33%	1.83%	1.20%	*2.31%*
SIGNIFICANT VARIATION (95% CONFIDENCE LIMIT)								**5.06%**
RUN	GRADE (% S)							
	CONC	*TAILS*	1	2	3	4	TOTAL	MEAN
1	39.1	2.3	39.5	36.8	31.7	24.2	31.6	*33.0*
2	41.1	1.7	38.4	38.6	33.7	24.5	32.6	*33.7*
3	40.2	2.4	43.5	38.2	33.6	25.4	33.5	*35.1*
4	42.6	1.7	41.6	39.0	32.6	24.0	32.7	*34.3*
5	42.2	1.9	40.5	38.1	32.9	25.2	32.8	*34.1*
6	41.9	2.0	41.6	37.4	34.0	23.7	32.7	*34.1*
AVERAGE	41.2	2.0	40.9	38.0	33.1	24.5	32.7	*34.1*
STD. DEV.	2.95%	13.44%	4.05%	1.95%	2.31%	2.59%	1.75%	*2.73%*
SIGNIFICANT VARIATION (95% CONFIDENCE LIMIT)								**7.00%**

The raw data for all the subsequent runs is given in Appendix 2, Tables A2.1 to A2.12. The experimental conditions used were those specified in section 3.3.3 unless otherwise stated.

TABLE 3.12 : Continuous Froth Cutting Reproducibility Tests

SEGMENT			1	2	3	4	AVERAGE
SINGLE	SOLIDS MASS (g)	AVERAGE	1.19	1.40	1.73	2.19	*1.63*
		STD. DEV.	4.70%	6.65%	4.47%	4.03%	*4.96%*
		SIGNIFICANT VARIATION (95% CONFIDENCE LIMIT)					**12.76%**
	WATER MASS (g)	AVERAGE	28.2	29.9	30.5	31.3	*30.0*
		STD. DEV.	10.77%	8.79%	11.85%	8.01%	*9.86%*
		SIGNIFICANT VARIATION (95% CONFIDENCE LIMIT)					**25.33%**
	SOLIDS/ WATER RATIO	AVERAGE	0.043	0.047	0.058	0.070	*0.054*
		STD. DEV.	16.28%	5.50%	13.08%	9.95%	*11.21%*
		SIGNIFICANT VARIATION (95% CONFIDENCE LIMIT)					**28.80%**
	AIR HOLD-UP (%)	AVERAGE	66.5	64.4	63.6	62.4	*64.2*
		STD. DEV.	5.36%	4.85%	6.71%	4.73%	*5.41%*
		SIGNIFICANT VARIATION (95% CONFIDENCE LIMIT)					**13.91%**
	PARTICLE SIZE (μm)	AVERAGE	19.4	20.4	22.4	23.5	*21.4*
		STD. DEV.	3.72%	2.35%	1.33%	1.83%	*2.31%*
		SIGNIFICANT VARIATION (95% CONFIDENCE LIMIT)					**5.06%**
	GRADE (% S)	AVERAGE	40.9	38.0	33.1	24.5	*34.1*
		STD. DEV.	4.05%	1.95%	2.31%	2.59%	*2.73%*
		SIGNIFICANT VARIATION (95% CONFIDENCE LIMIT)					**7.00%**

SEGMENT			1	2	3	4	AVERAGE
GROUPED	SOLIDS MASS (g)	AVERAGE	1.19	1.40	1.73	2.19	*1.63*
		STD. DEV.	1.68%	2.62%	0.10%	0.76%	*1.29%*
		SIGNIFICANT VARIATION (95% CONFIDENCE LIMIT)					**3.32%**
	WATER MASS (g)	AVERAGE	28.2	29.9	30.5	31.3	*30.0*
		STD. DEV.	2.21%	2.70%	5.63%	1.48%	*3.00%*
		SIGNIFICANT VARIATION (95% CONFIDENCE LIMIT)					**7.71%**
	SOLIDS/ WATER RATIO	AVERAGE	0.043	0.047	0.058	0.070	*0.054*
		STD. DEV.	1.59%	0.25%	6.58%	0.83%	*2.31%*
		SIGNIFICANT VARIATION (95% CONFIDENCE LIMIT)					**5.94%**
	AIR HOLD-UP (%)	AVERAGE	66.5	64.4	63.6	62.4	*64.2*
		STD. DEV.	0.66%	0.91%	2.12%	0.71%	*1.10%*
		SIGNIFICANT VARIATION (95% CONFIDENCE LIMIT)					**2.82%**
	PARTICLE SIZE (μm)	AVERAGE	19.4	20.4	22.4	23.5	*21.4*
		STD. DEV.	0.79%	1.07%	0.62%	0.13%	*0.65%*
		SIGNIFICANT VARIATION (95% CONFIDENCE LIMIT)					**1.67%**
	GRADE (% S)	AVERAGE	40.9	38.0	33.1	24.5	*34.1*
		STD. DEV.	1.00%	0.44%	0.28%	0.86%	*0.65%*
		SIGNIFICANT VARIATION (95% CONFIDENCE LIMIT)					**1.67%**

3.4.3.ii EFFECT OF FLOTATION PARAMETERS ON MASS RECOVERY AT DIFFERENT LEVELS IN THE FROTH

The variation of the mass of solids recovered at different levels in the froth as the pulp density, superficial air rate, frother concentration and froth height were varied is shown in Figure 3.25. It can be seen that the mass recovery was always highest for the pyrite-quartz system without wash water, and lowest for the Unisel system. This would be expected because the wash water should wash entrained gangue material from the froth, and the Unisel ore contained less floatable material (pyrite) than the other systems (3.5% as opposed to 10%).

As the pulp density increased there was a steady increase in the mass of solids in the froth. This would be expected because there were more solids to float. It can also be seen that there was a general trend for the amount of solids in each froth segment to increase as height in the froth decreased. This indicates either that there was more entrained material in the lower levels of the froth or that the bubbles were coalescing at the top of the froth and material was being lost from this zone. In the system with no wash water it is likely that bubbles would coalesce at the top of the froth due to froth drainage, but this is less likely in the systems with wash water because the froth was well hydrated. The mass recovery profile in the froth for the system with no wash water is different to the batch system. The reason for this is that in the batch system there was a limited amount of floatable material, and this tended to float first giving a high mass pull at the top of the froth. In the continuous system, the pyrite was continuously being replaced as fresh feed entered the column, and thus the froth showed a decrease in the mass of ore as height in the froth increased because the entire froth was saturated with pyrite, and entrained material was being lost from the top of the froth by elutriation and bubble coalescence.

There was a trend for the mass pull to increase as the air rate decreased. This trend was also observed in the batch froth cutting tests and can only be ascribed to a bubble size effect. Smaller bubbles are produced at the lower air flow rates, and this leads to better flotation of the fine material and less entrainment. There is a possibility that material was trapped in the froth due to the more tightly packed froth in the system without wash water, but this was unlikely to be the case in the other systems. It was

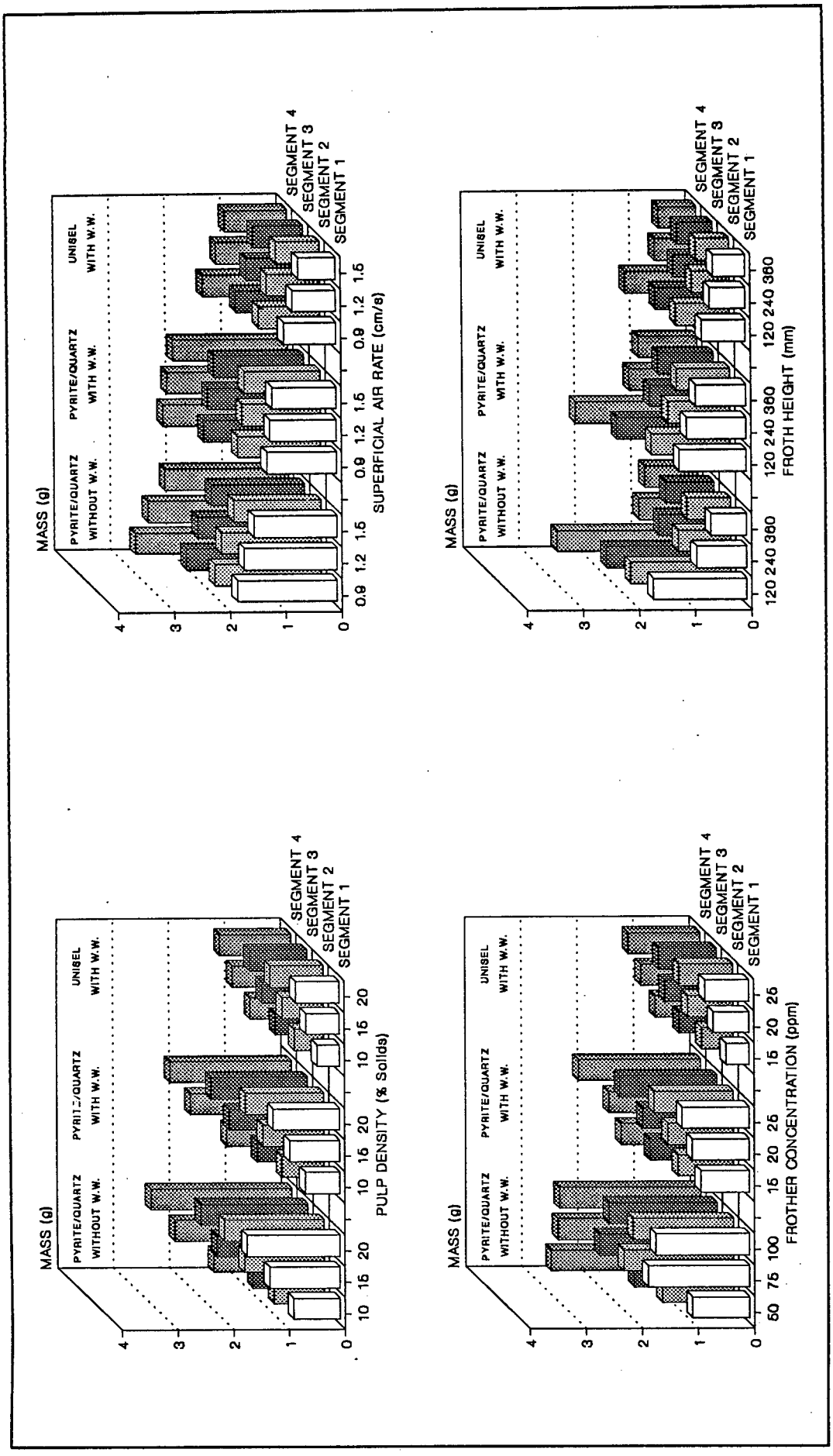

FIGURE 3.25 : Effect of Flotation Parameters on Mass Recovery at Different Heights in the Froth

found that the degree of mixing in the froth increased as the air rate increased. This could have led to floated material being lost at the bottom of the froth, and entrained material being circulated to the top of the froth. A decrease in grade with increasing air rate would then have been expected, and this was observed (Figure 3.29).

As the frother concentration increased the mass pull increased for the two systems with wash water. This was expected because the bubbles were more stable and hence there should have been less bubble coalescence. For the system without wash water significantly higher concentrations of frother were needed to produce a tall froth. This is because the froth was less hydrated, and hence there was more bubble coalescence. It can also be seen that a frother concentration of 75 ppm produced the highest overall mass recoveries. A similar trend was found in the batch froth cutting tests. The lower mass pull at the low frother concentration was due to the froth being less stable, and hence losing material. The lower recovery at the high frother concentration for the batch tests was ascribed to a short time for the pyrite to float before the froth had to be cut, but that was clearly not the case here. In the batch tests the biggest differences in mass recoveries were found in the top segment where the 75 ppm frother concentration had about double the mass pull of the 100 ppm test. In this system it can be seen that there was no segment in which the mass recoveries for the two cases were significantly different. If the grade profiles (Figure 3.29) are examined it can be seen that the 100 ppm system showed lower grades throughout the froth than the 75 ppm system. It is thus likely that more of the entrained material was trapped in the froth and that the froth residence time was decreased at the higher frother concentration. It must be remembered that pyrite is about twice as dense as quartz. The assumption of a shorter froth residence time is borne out by the rates of concentrate recovery for the two systems. The 100 ppm system had the higher mass pull (Table A2.3).

It must be noted that only the top 120 mm of the froth was sampled when the froth height was changed. This means that all of the froth was split at a froth height of 120 mm, half at 240 mm, and only the top third at a froth height of 360 mm. The trends observed in the mass recovery were expected, with a relatively large overall mass pull for the 120 mm froth and this decreased markedly as the froth height increased to 240 mm and then

decreased slightly further at 360 mm. This trend was most marked in the system without wash water because of the decrease in froth stability. If the pyrite-quartz systems are compared, it can be seen the mass recovery was the highest for the system with no wash water at 120 mm but the lowest at the other two froth heights. There was also a two fold decrease in concentrate mass flow as the froth height increased from 120 to 360 mm for the system with no wash water, compared a 1.36 time decrease for the system with wash water.

The other notable factor is that there was a large decrease in mass pull as the height in the froth increased for the 120 mm tests, and this trend was not nearly as marked for the other two froth heights (e.g. a factor of 1.83 for 120 mm compared to 1.17 for 360 mm; pyrite-quartz system with wash water.) This trend was expected because there should have been little entrained material in any of the segments with the deeper froths.

3.4.3.iii EFFECT OF FLOTATION PARAMETERS ON SOLIDS-TO-WATER RATIO AT DIFFERENT LEVELS IN THE FROTH

The variation of the mass ratio of solids-to-water at different levels in the froth as the pulp density, superficial air rate, frother concentration and froth height were varied is shown in Figure 3.26. It can be seen that in all cases the solids-to-water ratio for the system without wash water was significantly larger than for the two systems with wash water. This was expected. It can also be seen that the Unisel system always had a lower solids-to-water ratio than the pyrite-quartz system with wash water. There was little difference in the water masses recovered, so this was purely the effect of the different mass recoveries discussed in the previous section. The solids-to-water ratio also decreased as height in the froth increased due to the increasing amount of solids towards the bottom of the froth. This trend was not well marked in the system without wash water because of the drainage of the water from the upper levels in the froth.

In all cases the solids-to-water ratio increased as the pulp density increased because there were more particles in the froth and the amount of water in the froth changed little.

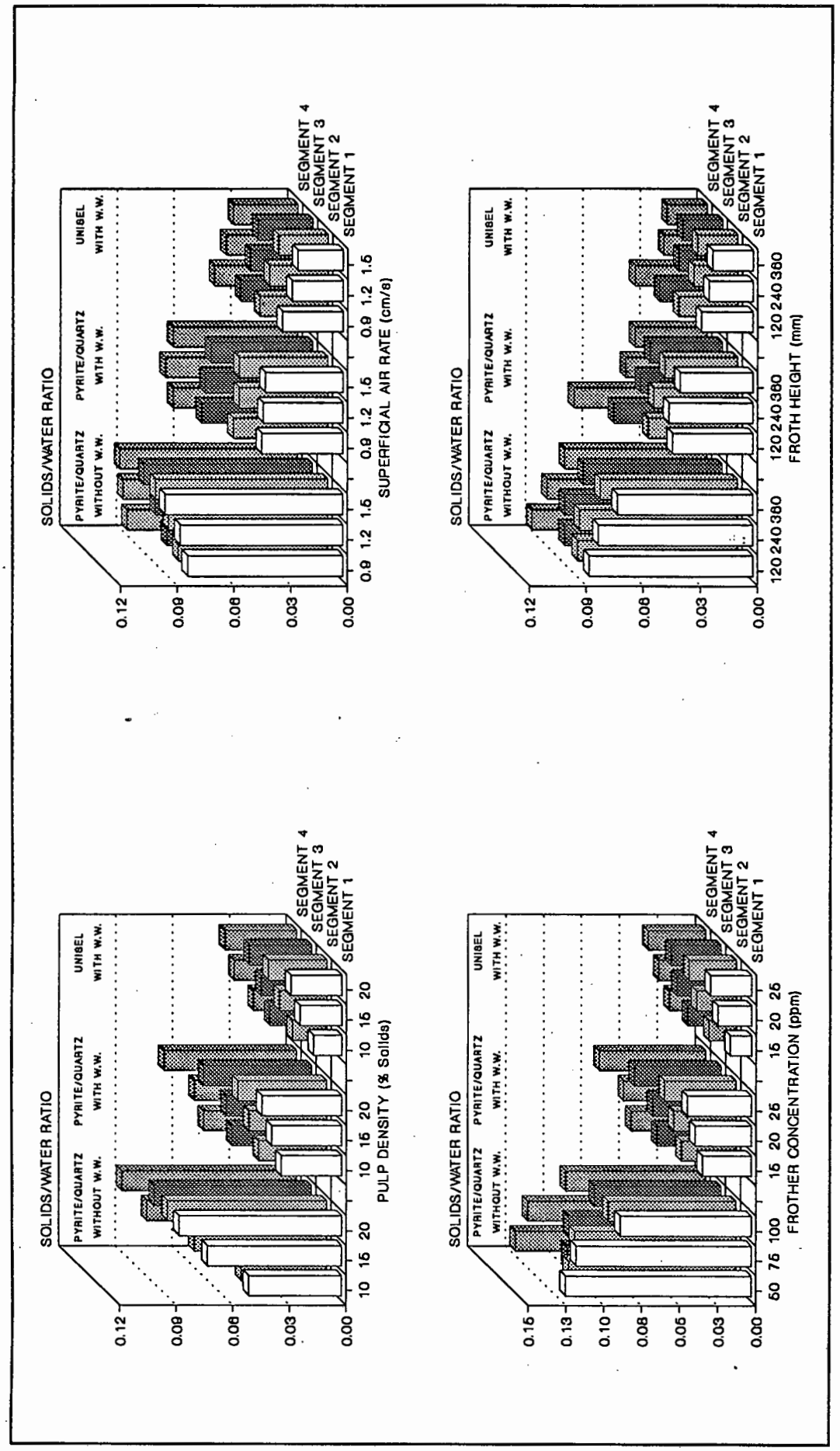

FIGURE 3.26 : Effect of Flotation Parameters on Solids/Water Ratio at Different Heights in the Froth

The solids-to-water ratio decreased as the air rate increased for the systems with wash water and increased as the air rate increased for the pyrite-quartz system without wash water. The reason for the trend in the systems with wash water was that the mass of solids collected increased as the air rate decreased while the water recovery remains reasonably constant. Although the mass of solids collected in the system with no wash water increased as the air rate decreased, the water recovery decreased sharply as the air rate increased. This was because the water drained from the froth more easily as the bubble size increased. The net result was an increase in solids-to-water ratio as the air rate decreased.

The solids-to-water ratio increased as the frother concentration increased for the systems with wash water, but decreased as the frother concentration increased for the pyrite-quartz system without wash water. Again, for the systems with wash water, there was an increase in the solids mass recovery while the water recovery remained relatively constant. For the system with no wash water, decreasing the frother concentration led to thinner water films around bubbles, and hence to a less hydrated froth. The relatively high values observed in the top sections of the froth were due to froth drainage, and it can clearly be seen that this was most prevalent in the 50 ppm test, confirming that higher frother concentrations inhibited the drainage of water from the froth.

There was a trend for the solids-to-water ratio to decrease as the froth height increased. This was a direct result of the mass recovery trends discussed in the previous section. The sharp increase in the solids-to-water ratio at the bottom of the froth (segment 4) for the systems with wash water at a froth height of 120 was due to the recycling of entrained material in this zone.

3.4.3.iv EFFECT OF FLOTATION PARAMETERS ON THE AIR HOLD-UP AT DIFFERENT LEVELS IN THE FROTH

The variation of the air hold-up at different levels in the froth as the pulp density, superficial air rate, frother concentration and froth height were varied is shown in Figure 3.27. The air hold-up in the froth is a good indication of the drainage of water from the froth. The higher the air hold-up, the

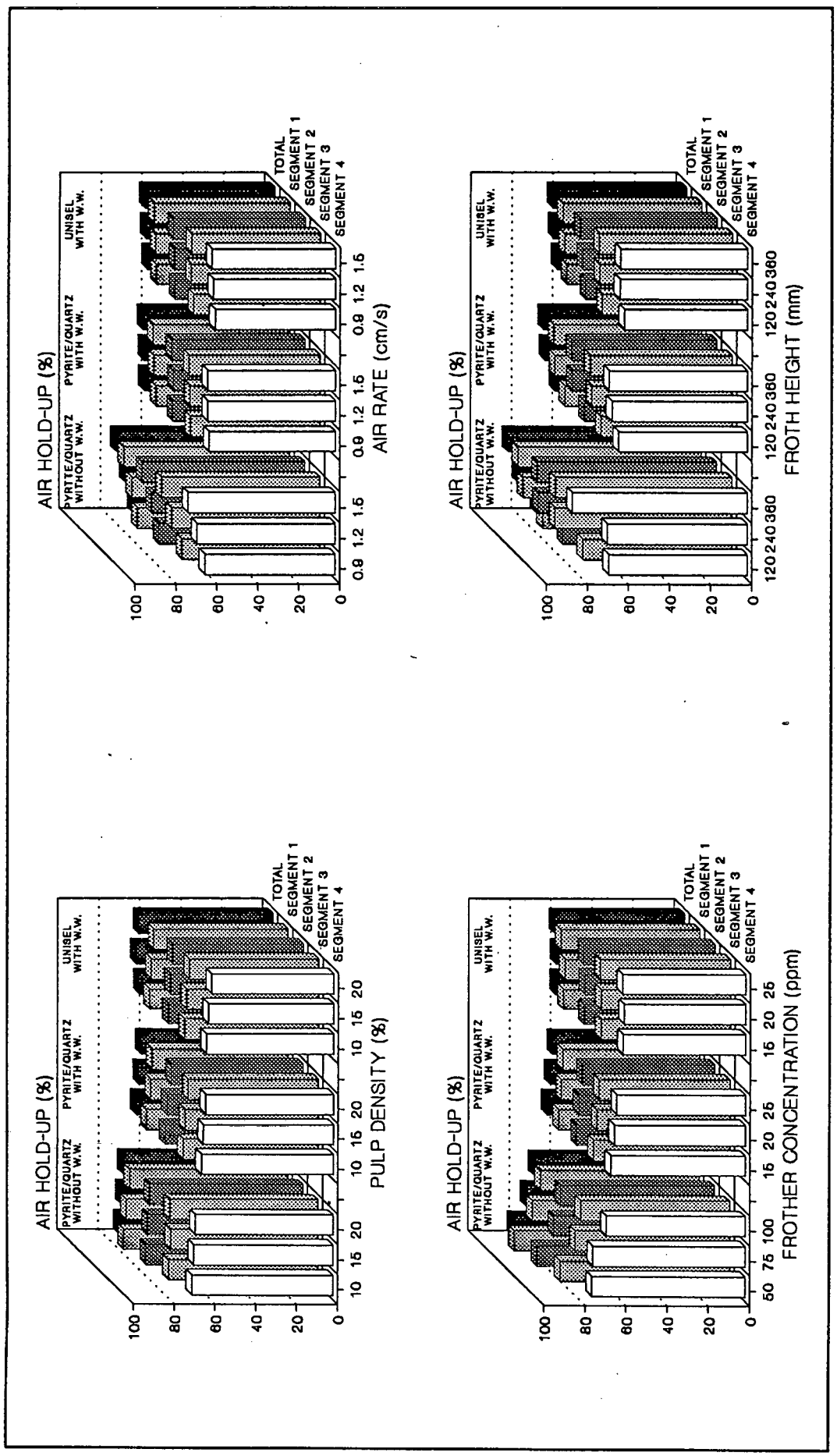

FIGURE 3.27 : Effect of Flotation Parameters on Air Hold-Up at Different Heights in the Froth

better drained the froth. If it is assumed that the entrained material follows the water in the froth, then the higher the air hold-up, the smaller the amount of entrained material in the froth.

Generally the air hold-up in the froth increased as height in the froth increased, as would have been expected. This trend, however, was not marked in the systems with wash water, as water was continuously added to the top of the froth, masking the froth drainage. It also appeared that none of the flotation parameters had much effect on the air hold-up when wash water is added.

Changing the pulp density had virtually no effect on the system without wash water. This was to be expected because the pulp density should have had little effect on the rate of froth drainage.

As stated before increasing the air rate, and hence the bubble size caused more water to drain from the froth, and so the air hold-up increased as the air rate increased for the system with no wash water.

Likewise, increasing the frother concentration inhibited froth drainage and bubble coalescence. This resulted in the lowest air hold-ups being recorded at the highest frother concentrations.

The froth height was the only parameter that appeared to have a major effect on the air hold-up in the system where no wash water was used. As would have been expected, the extent of froth drainage increased as the froth height increased.

3.4.3.v EFFECT OF FLOTATION PARAMETERS ON THE PARTICLE SIZE AT DIFFERENT LEVELS IN THE FROTH

The variation of particle size at different levels in the froth as the pulp density, superficial air rate, frother concentration and froth height were varied is shown in Figure 3.28. In general, the particle size in the froth and its water content are good indicators of the amount of entrained material in the froth, the smaller the particle size and the more water in the froth, the more entrainment. This should definitely have been true for the Unisel ore, but

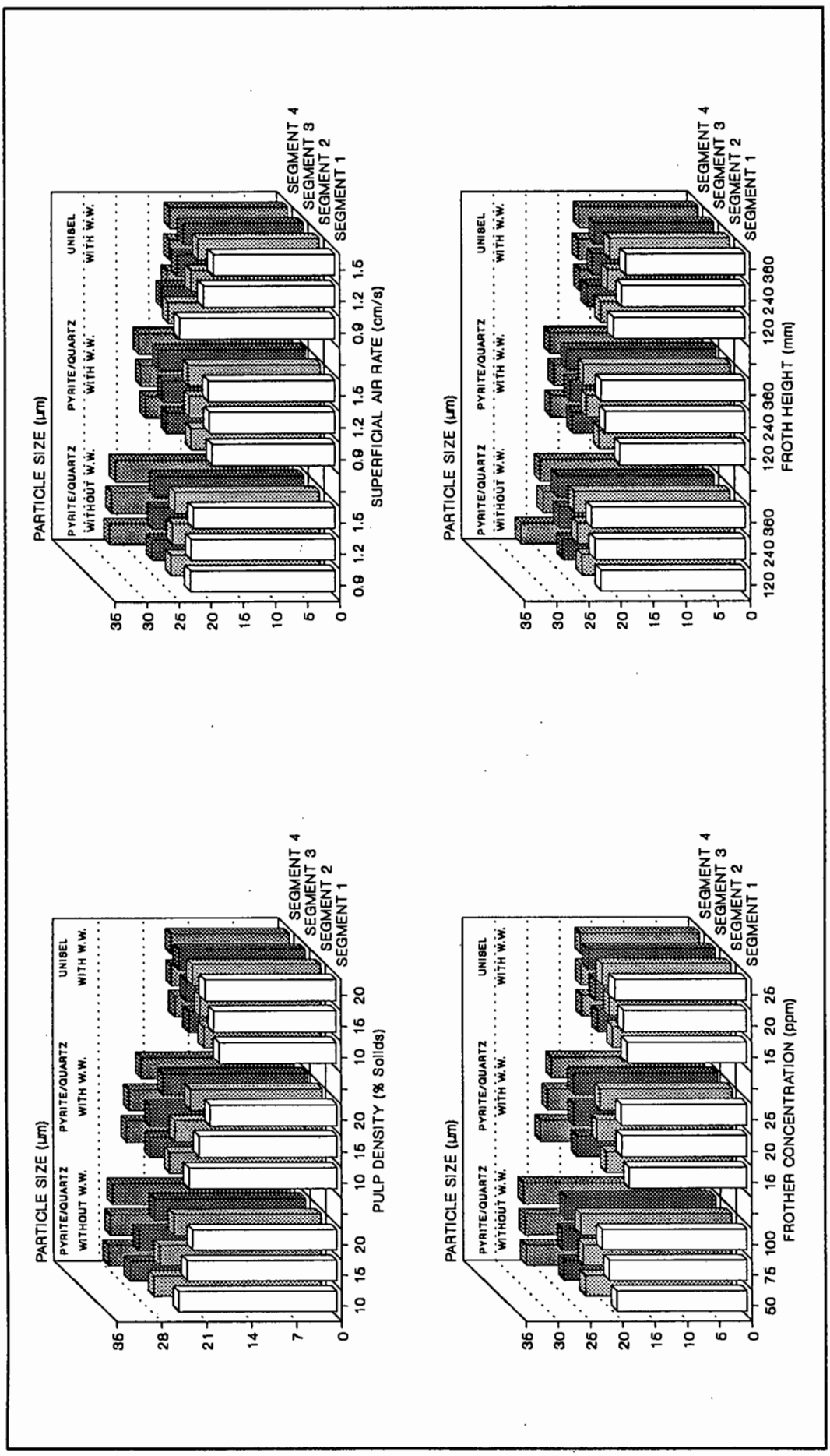

FIGURE 3.28 : Effect of Flotation Parameters on Particle Size at Different Heights in the Froth

not for the synthetic ore because the quartz was coarser than the pyrite. It can be seen, generally, that the average particle size increases as height in the froth increased for the Unisel ore and decreased as height in the froth increased for the synthetic ore. It can also be seen that the pyrite-quartz system with wash water had a smaller mean particle size in the froth than the system without wash water. This was expected because much of the coarser (gangue) material would have been elutriated from the froth by the wash water.

As the pulp density increased the proportion of entrained material in the froth decreased. This is evident because the particle size in the froth decreased for the pyrite-quartz systems and increased for the Unisel system as the pulp density increased. As the pulp density increased there were more floatable particles available in the pulp, and so the bubbles were likely to be more loaded with floated material. This would slow the rise rate of the bubbles and result in less entrainment. Thus ratio of floated-to-entrained particles in the froth would increase.

Changing the air rate had little effect on the pyrite-quartz systems, but the particle size in the Unisel system increased as the air flow rate decreased. As the air flow rate decreases the bubbles become smaller. The increase in the particle size for the Unisel system was either due to more efficient flotation due to the finer bubbles, or to less elutriation of the coarse gangue material from the froth because the smaller bubbles resulted in a more tightly packed froth. The small bubbles were unlikely to entrain much of the quartz in the pyrite-quartz systems because this material was relatively coarse.

It can generally be seen that the mean particle size in the froth increased as frother concentration increased. This was probably due to the froth being more tightly packed at the higher frother concentrations, and the larger particles being trapped in the froth.

The particle size tended to increase as the froth height increased for the pyrite-quartz systems and tended to decrease for the Unisel system. This was expected because the amount of entrained material in the froth should have decreased as froth height increases. In the system with no wash water, the large increase in the particle size at the bottom of the froth was testimony to the amount of entrained material in this zone.

3.4.3.vi EFFECT OF FLOTATION PARAMETERS ON SULPHUR GRADE AT DIFFERENT LEVELS IN THE FROTH

The variation of sulphur grade at different levels in the froth as the pulp density, superficial air rate, frother concentration and froth height were varied is shown in Figure 3.29. It can be seen, as expected, that grade increased as height in the froth increased. It can also be seen that the grade for the pyrite-quartz system with wash water was higher than for the system without wash water.

The grade tended to increase as the pulp density increased because there was less mixing in the froth. If there was macro-mixing in the froth then entrained particles from the bottom of the froth could have reported to the concentrate and floated material could have been lost.

There was an increase in grade as the superficial air velocity decreased because smaller bubbles were produced at the lower air flow rates. These smaller bubbles promoted more efficient flotation and less entrainment. These smaller bubbles were also more stable and less likely to coalesce, which resulted in less mixing in the froth.

For the pyrite-quartz system without wash water the highest grades were produced at a frother concentration of 75 ppm. At the lower frother concentration (50 ppm) there was more bubble coalescence, and hence more froth mixing. This was borne out by the high grades seen at the bottom of the froth (segment 4). At the higher frother concentration, the bubbles packed tightly together and elutriation of entrained gangue material was more difficult. For the systems with wash water, the highest grades were achieved at the highest frother concentration because the wash water helped to prevent the entrapment of entrained material in the froth. It can, however, again be seen that the highest grade occurred at the bottom of the froth for the pyrite-quartz system with the lowest frother concentration. This was again probably due to increased mixing in the froth.

The trends in the grade profiles seen as the height of the froth increased are expected. There was a significant increase in grade as height in the froth increases for the 120 mm froth height because the whole froth was sampled. The grade profiles for the other two froth heights were much

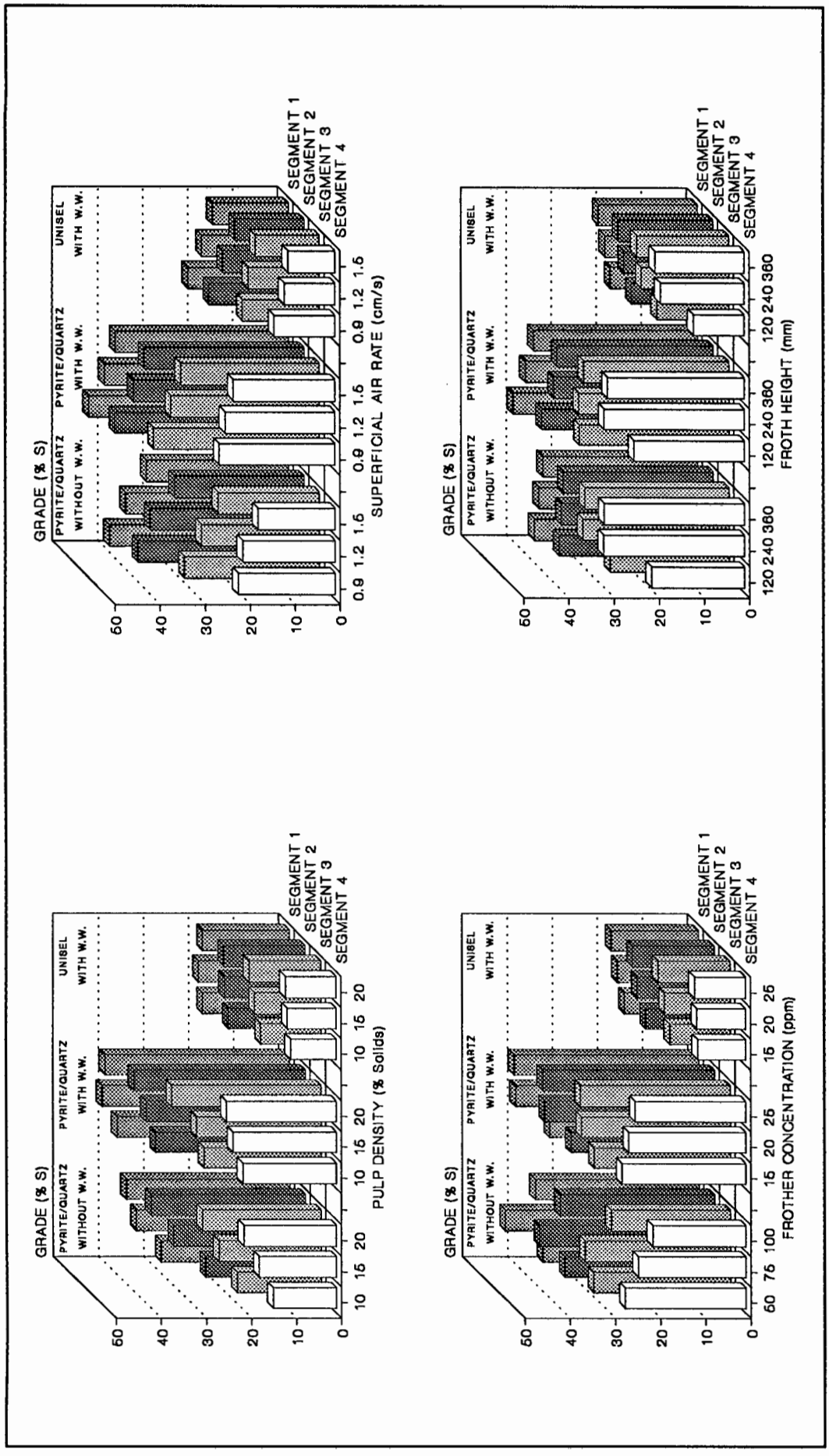

FIGURE 3.29 : Effect of Flotation Parameters on Sulphur Grade at Different Heights in the Froth

flatter because only the top zone of the froth was sampled. For the pyrite-quartz systems it can be seen that there was a slight decrease in grade at the top of the froth as the froth height increased. This was probably due to the loss of fine pyrite from this region.

3.4.3.vii EFFECT OF FLOTATION PARAMETERS ON RECOVERY

The effects of pulp density, superficial air rate, frother concentration and froth height on the recovery of pyrite for the three systems are shown in Figure 3.30. The sulphur grade and the mass pull for the top segment are shown in Figures 3.29 and 3.25 respectively. Since the recovery is proportional to the product of the mass pull and the grade, the trends seen in the recovery were expected.

As the pulp density increased the degree of mixing in the froth decreased and hence the recovery increased. The smaller bubbles produced at the lower air rates again led to a less mixed froth and hence better recoveries. This trend was not very marked because as the air rate increased the bubble surface area available for flotation also increases and hence more particles should have been floated.

The sharp decrease in recovery for the system with no wash water at the low and high frother concentrations was due to increased froth mixing on the one hand, and decreased froth residence time on the other. When wash water was added the best recoveries were seen at the highest frother concentrations. This was because the degree of mixing in the froth decreased as the frother concentration increased due to less bubble coalescence. This effect was clearly seen in the froth residence time distribution studies (section 3.4.4).

As the froth height increased, the recovery decreased. This was due to the loss of floated particles from the froth as froth drainage and bubble coalescence increased. This effect was most noticeable in the system without wash water because of the increased rates of froth drainage and bubble coalescence.

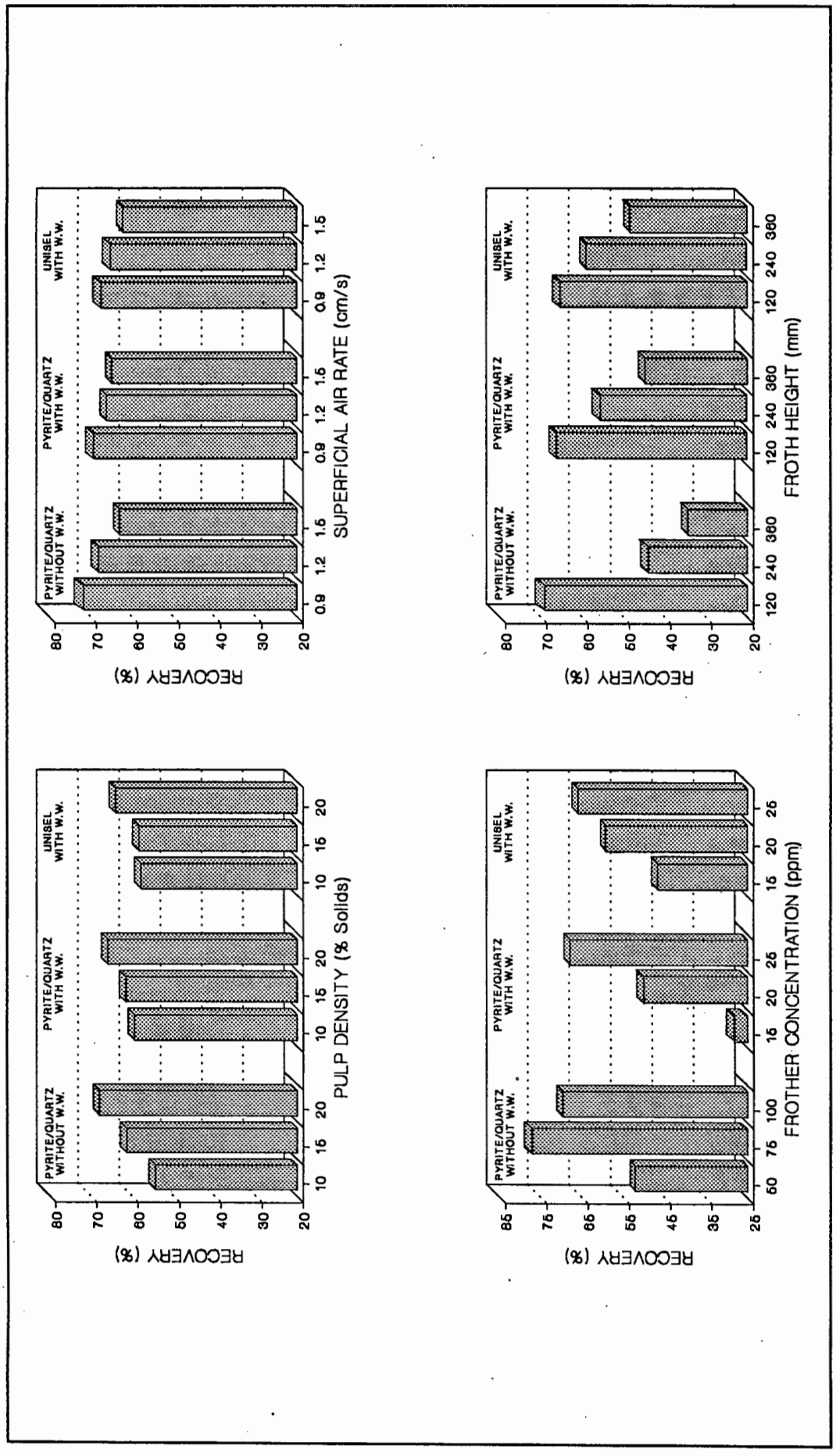

FIGURE 3.30 : Effect of Flotation Parameters on Sulphur Recovery

3.4.4 RESIDENCE TIME DISTRIBUTION STUDIES

3.4.4.i CHOICE OF MODEL

Several compartment models would be suitable for use in the modelling of the froth phase, such as a plug flow reactor with several sequential feed points, or plug flow reactors in parallel with different individual residence times, or a tanks-in-series model with recycle. A plug flow reactor with a recycle stream (Figure 3.31) was ultimately chosen to model the froth for two reasons: Firstly, any flow regime between plug flow (zero recycle) and mixed flow (infinite recycle) could be represented using this model, and, secondly, as will be shown, the model parameters (τ_i and r) have some physical significance. The reasons for the inclusion of the lag and step change in the model are discussed in section 2.4.2.i.

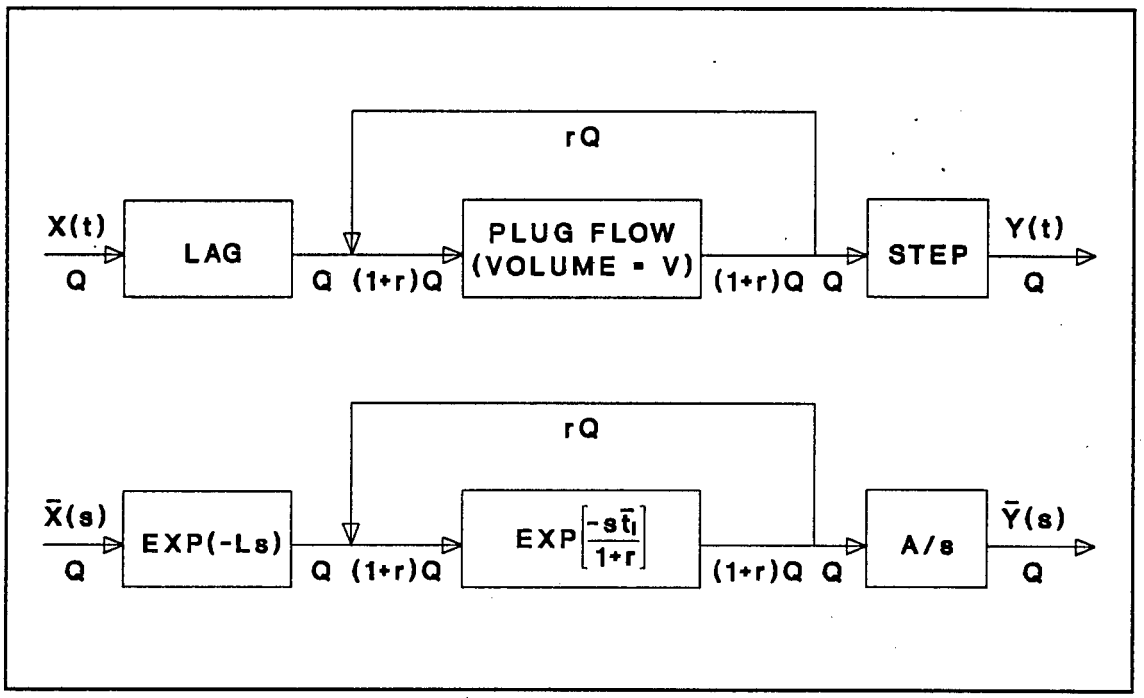

FIGURE 3.31 : Froth Model

3.4.4.ii CALCULATION OF MODEL PARAMETERS

Two methods of modelling the data are possible: The method of moments and the frequency response method (Wen and Fan 1962). The frequency response method, although more complex, was chosen because it gives

equal weight to all portions of the curve and deals effectively with long tails. Details of the model derivation are given in Appendix 3.

The methods of calculating τ, σ^2 and N were the same as in section 2.4.2.i. The D/uL value was calculated using an open inlet - open outlet system (Levenspiel, 1972):

$$\sigma^2/\tau^2 = 2(D/uL) + 8(D/uL)^2$$

The input signal for the froth zone was taken to be the signal measured at detector 3 at the bottom of the froth. It would have been totally inappropriate to use the column feed inlet signal because most of the material entering in the feed travels down into the pulp zone before flotation occurs. In order to use detector 3 as the proper inlet signal for the froth two assumptions had to be made: Firstly, all the isotopically labelled particles that floated must remain in the froth. The high pyrite recoveries that were obtained support this first assumption. And secondly, that a constant fraction of the material entering the froth was entrained. If the second assumption is true, then only the magnitude of the signal from detector 3, but not the shape of the curve, would be affected by the entrainment (Figure 3.32). The effects of entrainment would then be negated when the response curves were normalized.

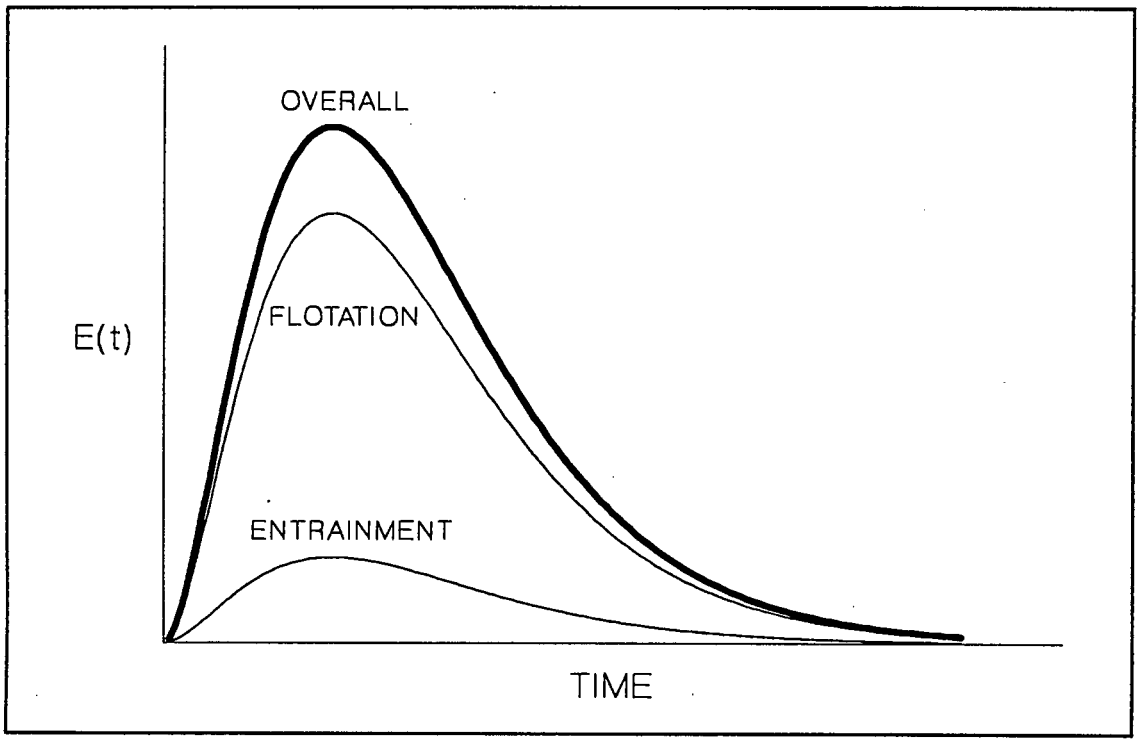

FIGURE 3.32 : Effect of Entrainment on Output Signals

3.4.4.iii REPRODUCIBILITY

Five runs were done at the standard conditions (run 3) to determine the reproducibility of the tracer studies. In all cases the mean absolute deviation between the experimental response curves and the mean response curve for all the runs was less than 9%.

TABLE 3.13 : Reproducibility Tests

TEST NO.	DETECTOR 1				DETECTOR 2			
	$\bar{t}$ (sec)	MAD (%)	VAR	MAD (%)	$\bar{t}$ (sec)	MAD (%)	VAR	MAD (%)
1	**139**	6.7	**0.431**	6.1	**125**	6.8	**0.469**	5.8
2	**137**	5.3	**0.440**	4.1	**125**	6.8	**0.475**	4.6
3	**120**	7.6	**0.489**	6.5	**107**	8.5	**0.512**	2.8
4	**119**	8.5	**0.498**	8.5	**108**	7.7	**0.520**	4.4
5	**135**	3.8	**0.437**	4.8	**120**	2.6	**0.514**	3.2
AVE	**130**	6.6	**0.459**	6.0	**117**	6.5	**0.498**	4.2

$\bar{t}$ = MEAN RESIDENCE TIME MAD = MEAN ABSOLUTE DEVIATION VAR = VARIANCE

3.4.4.iv MODEL DISCRIMINATION

Figures 3.33 and 3.34 show the age distribution curves [E(t)] for the froth for detectors 1 and 2 respectively for run 6 (Table 2.1). Also shown are the E(t) curves predicted by the plug flow recycle model, the tanks-in-series model and axial dispersion model. It was found that the mean absolute deviations from actual behaviour of the froth phase and the recycle model were less than 8% in all cases. From Figures 3.33 and 3.34 it can be seen that neither the tanks-in-series model nor the axial dispersion model could provide an acceptable fit for the froth phase and it was, thus, necessary to use a two parameter compartment model such as the one chosen.

An analysis was carried out to assess the sensitivity of the froth model to each of the model parameters and to ascertain the degree of inter-dependence of the model parameters (Box and Draper, 1987). One of the model parameters is plotted against the other showing error contours. The results of this analysis are shown in Figure 3.35 for run 6. The relative scales on the axes are related to the sensitivity of the model to each model parameter. This sensitivity is calculated by increasing and decreasing each model parameter in turn by a fixed amount (say 10%) from the optimum

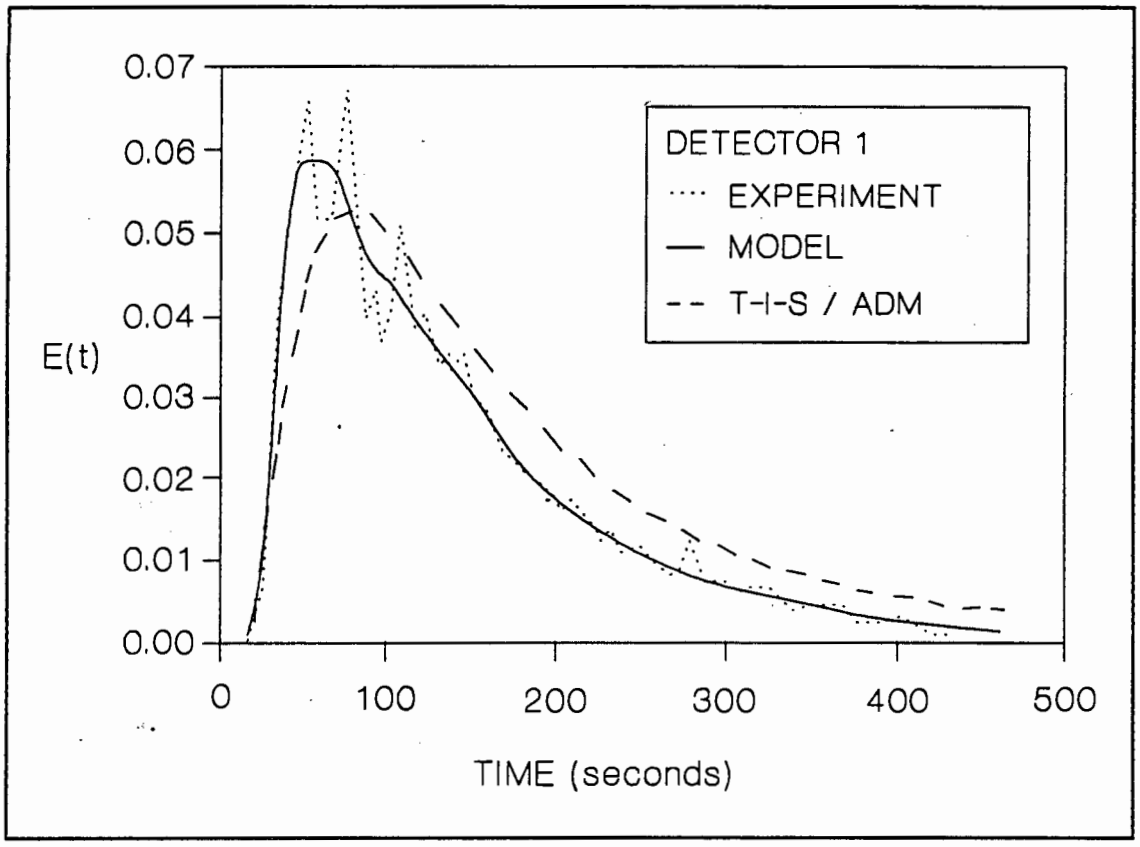

FIGURE 3.33 : E(t) Curve for Detector 1

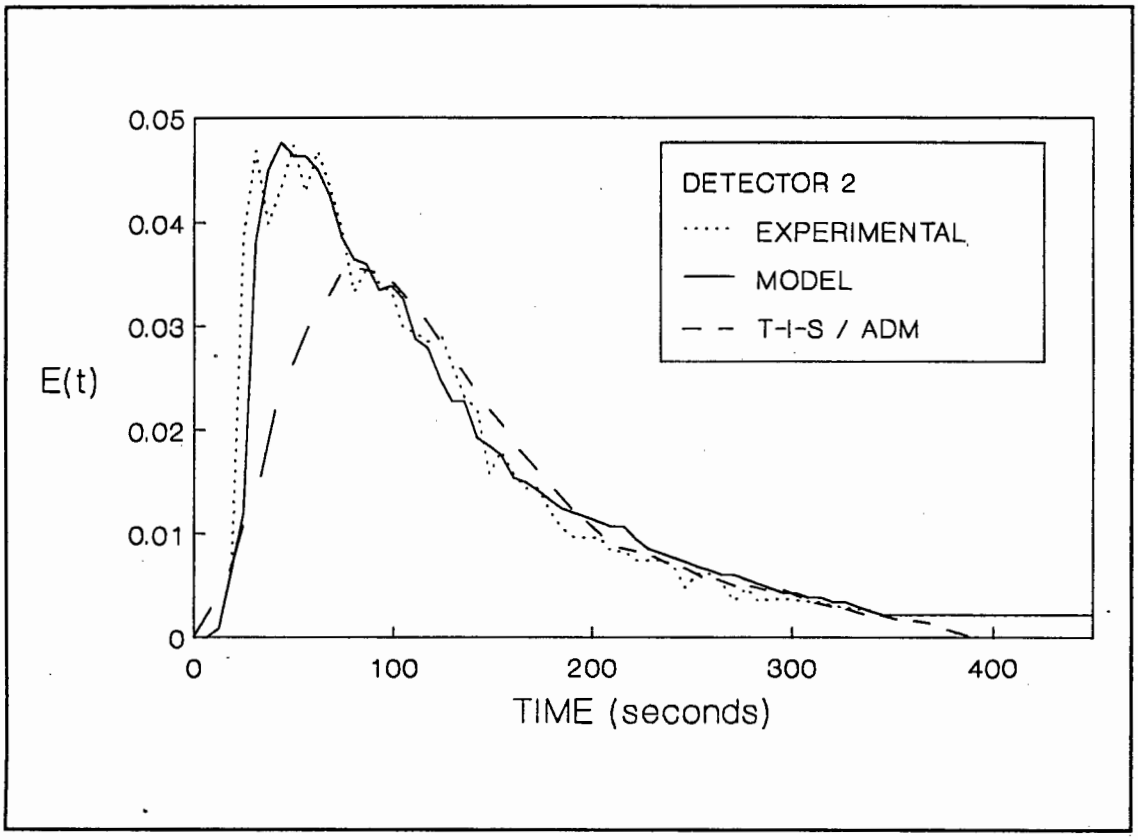

FIGURE 3.34 : E(t) Curve for Detector 2

value and noting the increase in the error. The ratio of the increase in error is then the ratio of the lengths of the axes, i.e.:

y	error(y)	x	error(x)
y_{opt}	E_{opt}	x_{opt}	E_{opt}
$0.9 \cdot y_{opt}$	E_{y1}	$0.9 \cdot x_{opt}$	E_{x1}
$1.1 \cdot y_{opt}$	E_{y2}	$1.1 \cdot x_{opt}$	E_{x2}

$$\Delta(E_y) = E_{y1} + E_{y2} - 2 \cdot E_{opt}$$

$$\Delta(E_x) = E_{x1} + E_{x2} - 2 \cdot E_{opt}$$

$$\frac{\Delta(E_y)}{\Delta(E_x)} = \frac{\text{Length of y axis (cm)}}{\text{Length of x axis (cm)}}$$

The relative lengths of the axes are important as they affect the shape of the error contours. If the axes are chosen incorrectly then the error contours will be flattened in either the x or the y direction. In the extreme this would lead to the assumption that the model was independent of one of the parameters.

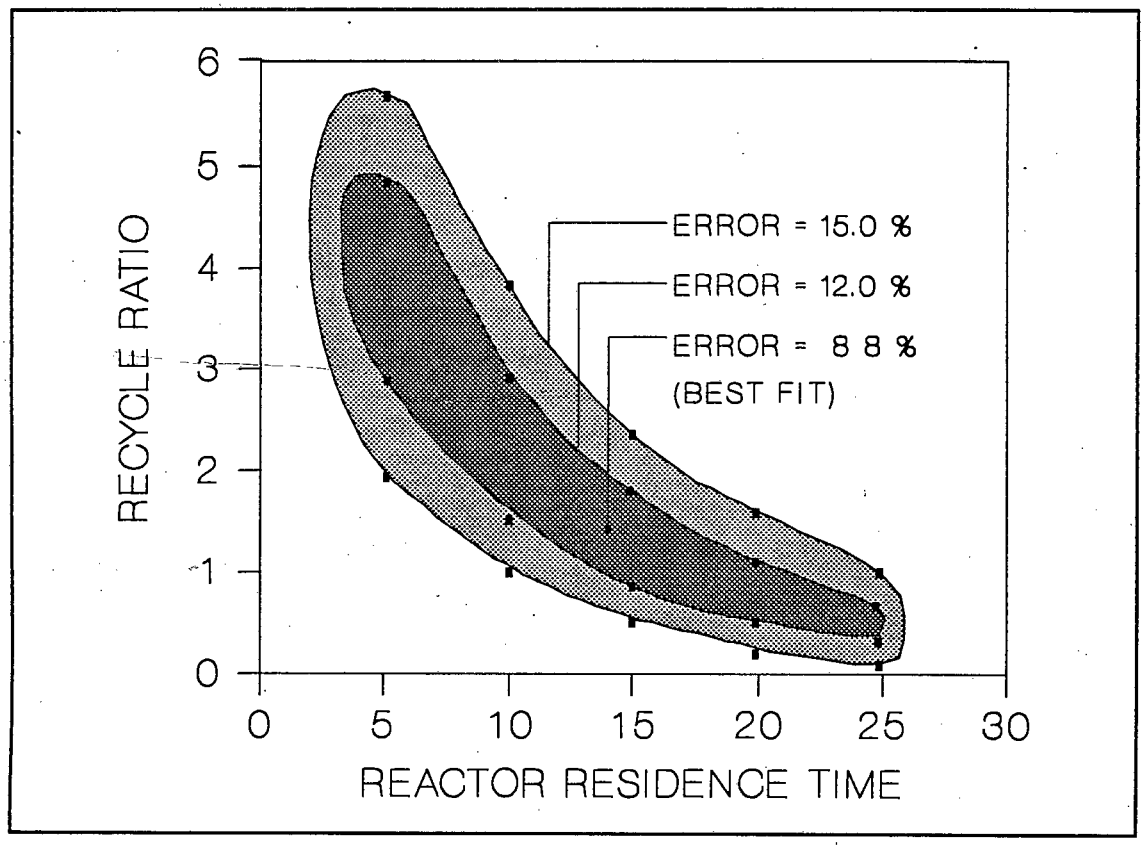

FIGURE 3.35 : Froth Model Error Analysis

The shape of the contours is indicative of the relationship between the parameters. If the two parameters were completely independent then the contours would be circular and if one parameter was directly proportional to the other, then 45 degree lines would result. Horizontal or vertical lines are obtained if the model is independent of one of the parameters.

Figure 3.35 clearly shows that the reactor residence time was essentially inversely proportional to the recycle ratio. This relationship was expected because an increase in the reactor recycle ratio would cause an increase in the volumetric flow rate through the reactor and thus a decrease in the reactor residence time. The unsymmetrical shape of the contours, however, indicates that there is a large degree of independence between the parameters, because if the parameters were dependent on each other, parallel contours would result. Figure 3.36 shows a plot of reactor residence time against recycle ratio for detector 1. The best fit for the data using a reciprocal equation is shown; the correlation coefficient was only 0.6.

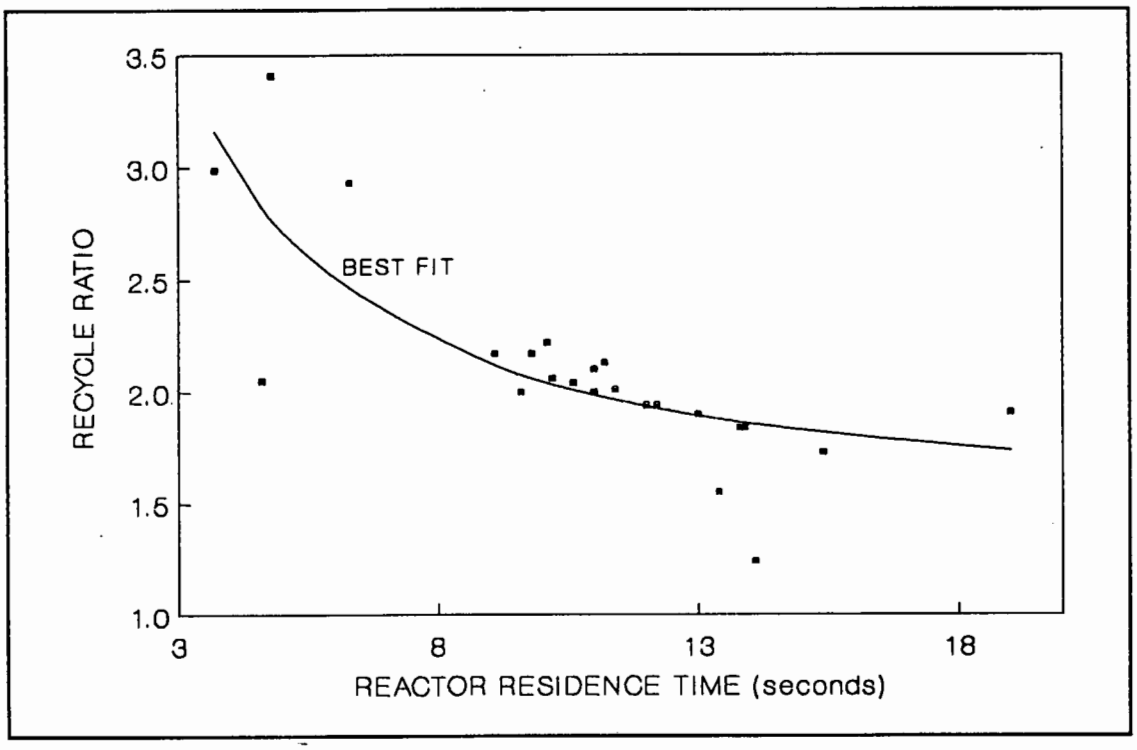

FIGURE 3.36 : Reactor Residence Time vs Recycle Ratio

The froth phase model parameters as well as the best fits for the tanks-in-series and the axial dispersion models are given in Table 3.14. The flotation parameters that were varied are shown in Table 2.1.

TABLE 3.14 : Froth Phase Model Data

RUN NO	PARAMETER VARIED	DETECTOR 1					DETECTOR 2				
		$\bar{t}$ (sec)	D/UL	N	$\bar{t}_i$ (sec)	r	$\bar{t}$ (sec)	D/UL	N	$\bar{t}_i$ (sec)	r
1		109	0.153	2.01	10.2	2.06	89	0.178	1.64	6.8	1.35
2	FEED	117	0.147	2.14	11.0	2.00	105	0.160	1.89	8.0	1.27
3	RATE	130	0.145	2.18	12.0	1.94	117	0.153	2.01	9.0	1.27
4		139	0.140	2.28	13.0	1.90	122	0.151	2.06	9.3	1.25
5		150	0.136	2.36	13.9	1.84	129	0.147	2.13	9.9	1.24
6		151	0.088	4.16	14.1	1.24	137	0.096	3.72	10.6	1.05
7	WASH	144	0.113	3.01	13.4	1.55	131	0.129	2.55	9.9	1.18
8	WATER	130	0.145	2.18	12.0	1.94	117	0.153	2.01	9.0	1.27
9	RATE	122	0.159	1.19	11.2	2.13	102	0.225	1.17	7.9	1.50
10		98	0.161	1.87	9.1	2.17	89	0.249	1.03	6.8	1.55
11		40	0.222	1.19	3.7	2.99	46	0.248	1.01	3.4	1.55
12	AIR	49	0.155	1.98	4.6	2.05	46	0.232	1.11	3.5	1.52
13	RATE	106	0.149	2.09	9.6	2.00	75	0.182	1.58	5.8	1.37
14		130	0.145	2.18	12.0	1.94	117	0.153	2.01	9.0	1.27
15		202	0.139	2.27	19.0	1.91	182	0.102	3.46	13.9	1.08
16		130	0.145	2.18	12.0	1.94	117	0.153	2.01	9.0	1.27
17	FROTHER	122	0.151	2.06	11.4	2.01	103	0.171	1.73	7.8	1.32
18	CONC	118	0.157	1.95	11.0	2.10	95	0.182	1.59	7.1	1.36
19		110	0.166	1.80	10.1	2.22	90	0.189	1.50	7.0	1.38
20	PULP	130	0.145	2.18	12.0	1.94	117	0.153	2.01	9.0	1.27
21	DENSITY	68	0.219	1.21	6.3	2.93	43	0.248	1.01	3.3	1.56
22		51	0.253	0.98	4.8	3.41	36	0.280	0.84	2.8	1.65
23	REPEATS	113	0.153	2.01	10.6	2.04	93	0.174	1.66	7.2	1.34
24		105	0.163	1.85	9.8	2.17	93	0.248	1.03	7.4	1.55
25	FROTH	165	0.128	2.58	15.4	1.73	148	0.139	2.31	11.3	1.22
26	HEIGHT	148	0.136	2.36	13.8	1.84	129	0.145	2.18	9.9	1.22
27		131	0.143	2.21	12.2	1.94	116	0.510	2.06	8.9	1.25

$\bar{t}$ = Mean Residence Time. R = Plug Flow Recycle Ratio (from model)

$\bar{t}_i$ = Plug Flow Residence Time (from model) D/UL = Vessel Dispersion Number

N = Number of Tanks in Series

Figures 3.37 and 3.38 show the relationships between the froth phase model parameters and the overall mean residence time (τ) and the variance (σ^2) respectively. There is a direct correlation between the mean residence time in the froth (τ) determined from the response curves and the reactor residence time (τ_i) determined from the model. It was expected that these two residence times would be related. A similar relationship exists between the variance (σ^2) and reactor recycle ratio (r). Again, this result was expected because the variance and the reactor recycle ratio are both measures of

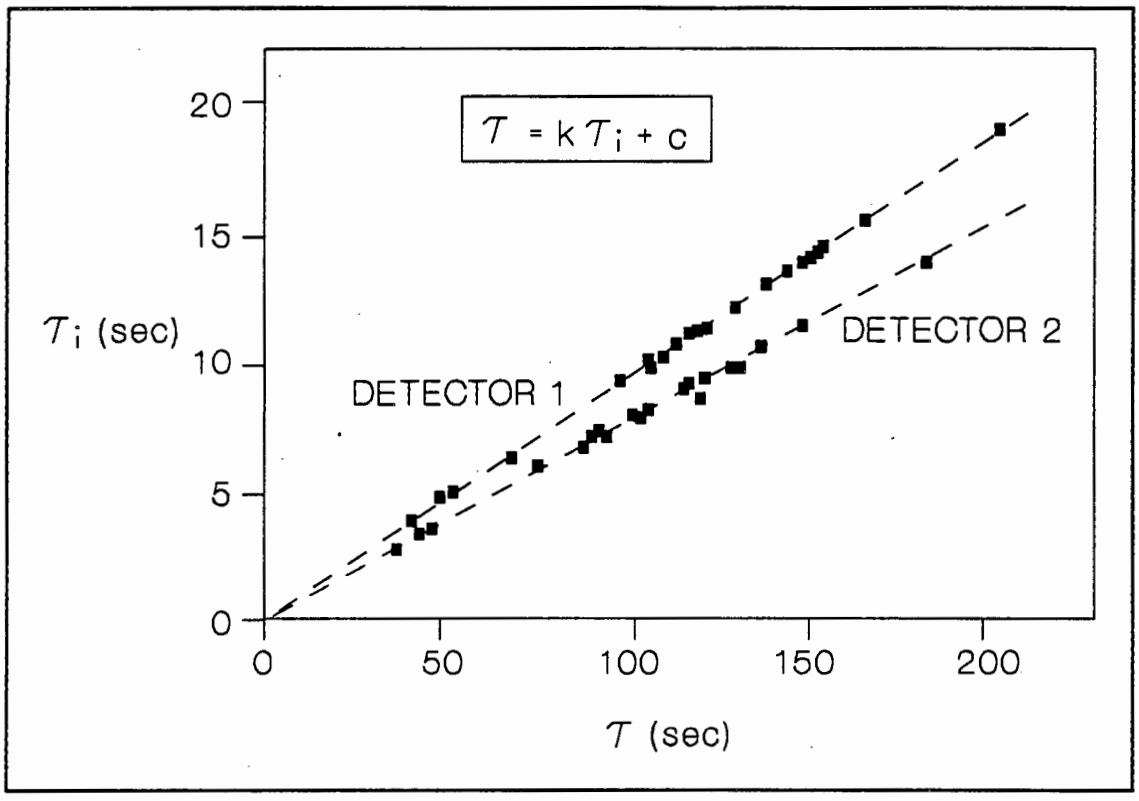

FIGURE 3.37 : Model Significance - Residence Time

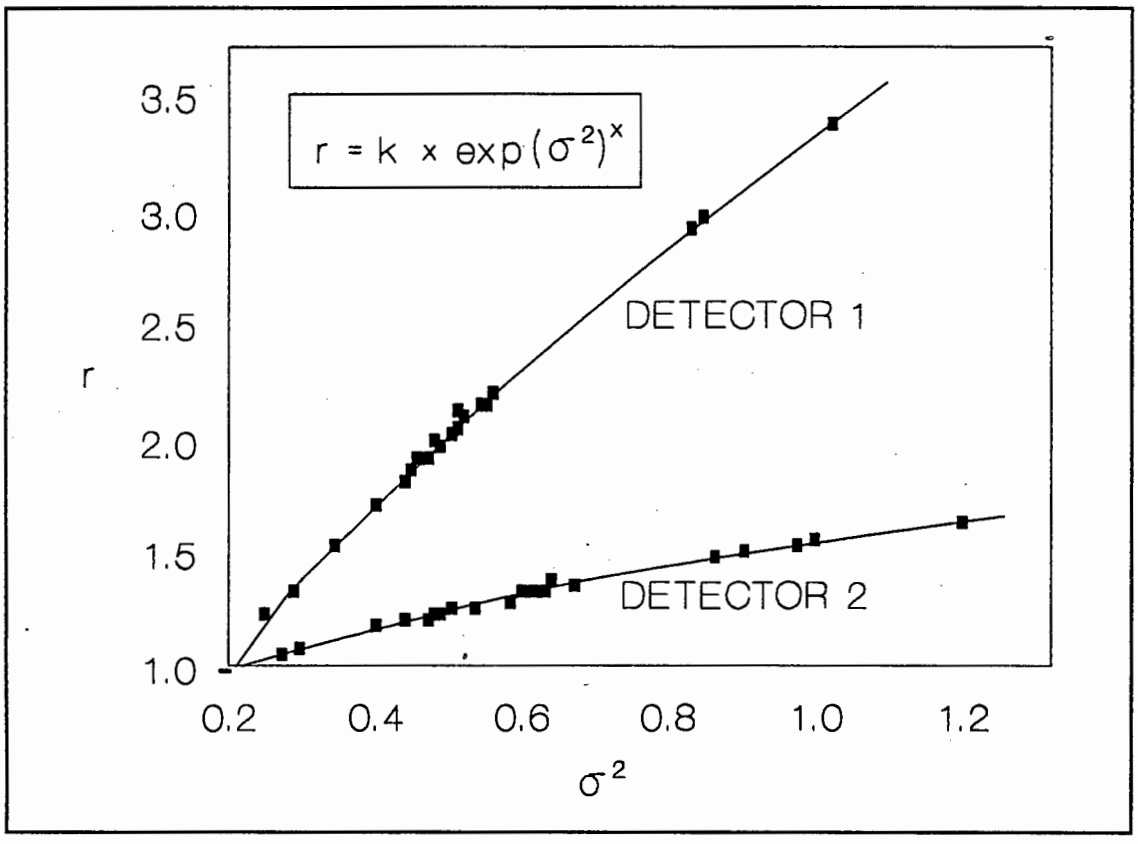

FIGURE 3.38 : Model Significance - Degree of Mixing

the mixing that occurred in the froth phase. These relationships confirm that the model parameters have actual physical significance. This further validates the choice of model.

It can also be seen that the values of the constants in these relationships varied with depth in the froth, especially the recycle ratio. The recycle ratio increased markedly as height in the froth increased, while there is only a small increase in the reactor residence time as height in the froth increased. This implies that the top half of the froth is better mixed than the bottom half. This increased mixing must be due either to bubble coalescence, or poor wash water distribution.

3.4.4.v EFFECT OF FLOTATION PARAMETERS ON RESIDENCE TIME IN THE FROTH

Figure 3.39 gives a qualitative impression of the effects of increasing the flotation parameters considered in this study on the reactor residence time (mean residence time) and the reactor recycle ratio (degree of mixing) in the froth. Since many of the effects are non-linear, this figure is merely designed to give an impression of the magnitude of the changes without putting any value to them.

It can be seen that parameters which increased the mean residence time in the froth were always accompanied by a decrease the degree of mixing. Figure 3.39 shows that increasing the wash water rate, the pulp density and the froth height all caused significant increases in the residence time in the froth, while increasing the air rate caused a sharp decrease in the froth residence time. Increasing the wash water rate, and to a lesser extent the pulp density and the froth height caused a decrease in the degree of mixing in the froth.

Increasing the feed rate caused a decrease in froth residence time because there were more particles to float, and hence more particles report to the froth and the froth rose more quickly. The slight increase in the mixing in the froth is difficult to explain, but may have been due to the development of circulation channels within the froth. It was noticed that, under some conditions, the froth was tightly packed, and the wash water was not evenly

distributed, but tended to flow down the walls of the column in channels along with some of the froth. This would lead to increased froth mixing. There was also a tendency for the bubbles near the walls to coalesce, and cause the froth to flow downwards near the walls.

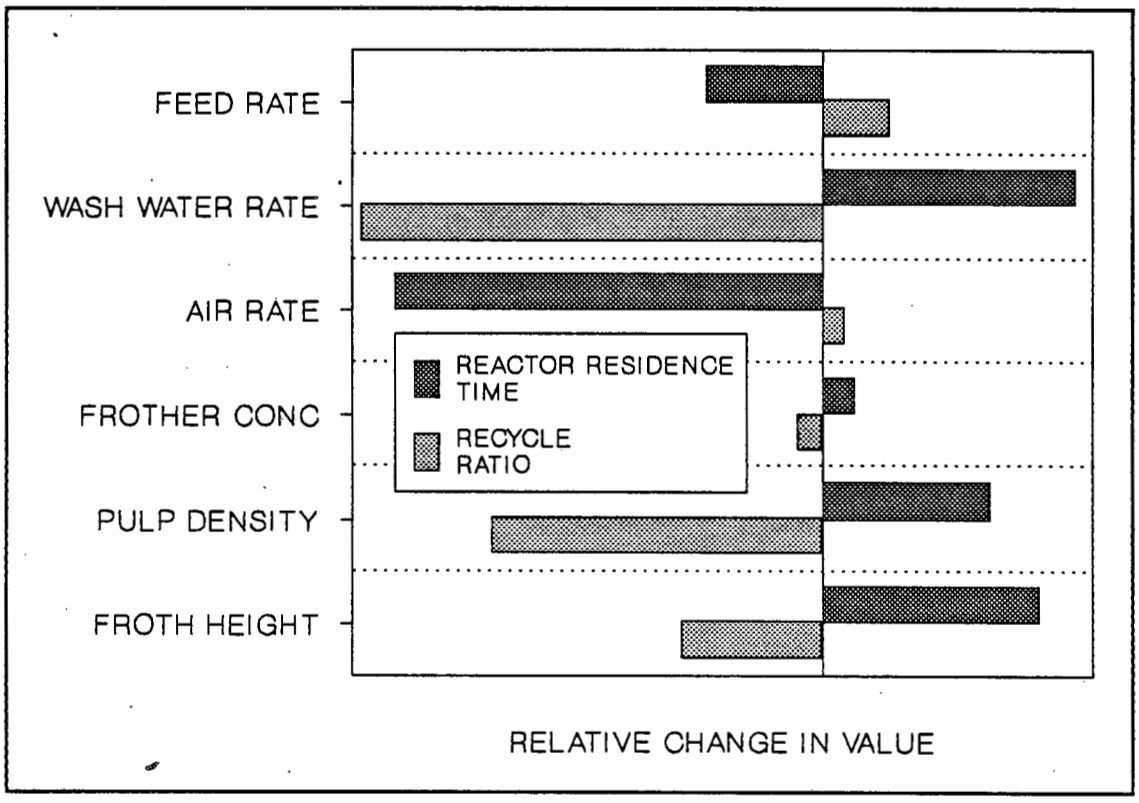

FIGURE 3.39 : Effect of Flotation Parameters on the Residence Time Distributions in the Froth

The increase in froth residence time as the wash water rate increased was due to the increased downward bias in the froth. Increasing the wash water rate increased the water hold-up in the froth and hence helped to prevent bubble coalescence. This in turn decreased the degree of mixing in the froth.

Increasing the air flow rate increased the bubble size and decreases the residence time of the air in the froth because the air hold-up in the froth increased. This caused a decrease in solids residence time in the froth. There was a very slight increase in the degree of mixing in the froth as the air velocity increased. There were two competing effects here: the increase in mixing due to bubbles coalescence, and the decrease in mixing due to the increased bubble rise velocity. Run 11 (Table 3.14), however shows

that there was a big increase in the degree of mixing if the bubbles were too large. The air rate in run 12 was higher than in run 11 (7.08 $cm \cdot s^{-1}$ as opposed to 5.07 $cm \cdot s^{-1}$) but the bubbles in run 11 were significantly larger because a different type of sparger was used. This effect was caused by the increase in the rate of bubble coalescence, without a corresponding decrease in air residence time.

Increasing the frother concentration had little effect on either the froth residence time or the recycle ratio. This is because increasing the frother concentration had little effect on the bubble size and, in the presence of wash water, the higher frother concentration should have had little effect on the rate of bubble coalescence.

As the pulp density increased the degree of mixing in the froth decreased. This was because there were more particles in the froth, and hence it was more stable. This increased froth stability resulted in a longer froth residence time because particles were not circulated from the bottom to the top of the froth due to macro-mixing.

It is not surprising that the froth residence time increased as the froth height increased because the froth volume increased. It was found that the superficial rise velocity of the solids in the froth was roughly constant. The decrease in the froth mixing was probably because the height to diameter ratio of the froth had increased and hence the flow regime was closer to plug flow.

3.5 SUMMARY

3.5.1 FROTH STABILITY TESTS

These tests showed that the stability of the froth was a function of both the size and the hydrophobicity of the particles in the froth. Fine hydrophobic particles stabilized the froth by inhibiting bubble coalescence, while coarse particles with a low hydrophobicity could destabilize the froth by allowing excessive froth drainage.

3.5.2 BATCH FROTH CUTTING TESTS

The froth-splitting apparatus provided a rapid and simple means by which the effect of flotation parameters on the froth zone could be investigated, and allowed data to be obtained on the variation, with height in the froth, of the following parameters:

- the masses of solids and water;
- the mass ratio of solids-to-water;
- the air hold-up;
- the grade and recovery of sulphur;
- the particle size distribution.

Although the small amount of concentrates collected decreased the precision of the results, it was found, at a 95% confidence limit, that experimental errors were below 6%.

The testwork done on the pyrite-quartz ore showed that:

- the particle size of the pyrite decreased with decreasing height in the froth; there was no marked trend in the particle size of the quartz.
- The air hold-up in the froth increased with increasing height in the froth.
- The sulphur grade decreased with decreasing height in the froth.

- the recovery of pyrite decreased with decreasing height in the froth, but increased again in the bottom segment as a result of the recycling of ultra-fine pyrite (< 10 μm) at the bottom of the froth.
- There was an optimum carbon chain length and collector dosage for xanthate collectors. Below this optimum there was a loss of recovery because the pyrite was not hydrophobic enough. Above this value the system became unselective.
- The was an optimum frother concentration for each frother type. The froth became unstable at low frother concentrations and floated material was lost. At high frother concentrations the froth became too tightly packed and entrained gangue material was trapped in the froth.
- Selectivity decreased as particle size decreased. The best grades and recoveries were achieved with a system with a range of particle sizes.
- Froth stability decreased as the temperature increased. The best grades were achieved at high temperature, and the best recoveries at low temperatures.
- An examination of the froth as it built up showed that the coarsest pyrite floated first and there was little entrainment initially. The amount of entrainment increased as the pyrite was depleted.
- The tightly packed froths achieved with small bubbles hindered the elutriation of entrained material from the froth and resulted in poor grades and recoveries.

3.5.3 CONTINUOUS FROTH CUTTING TESTS

The froth in a steady-state system has been partitioned into four horizontal segments so that the effects of flotation parameters could be examined as a function of height in the froth. Three systems were examined, viz: a pyrite-quartz system without wash water, a pyrite-quartz system with wash water, and a system using Unisel ore with wash water. The reproducibility of the system was found to be better than that of the batch system.

Four flotation parameters were examined: The pulp density, the air rate, the frother concentration, and the froth height, each at three different conditions.

For the system with no wash water it was found that most of the trends were the same as those observed for the batch system. Where there were differences, they were due to the depletion of floatable material in the batch system.

The trends seen for the pyrite-quartz system with wash water and the Unisel system were generally similar. The only significant differences were in the particle size distributions in the froth. These were caused by the quartz being coarser than the pyrite in the pyrite-quartz system. Thus entrainment of gangue increased the particle size for the pyrite-quartz system, and decreased it for the Unisel system.

It was found that the addition of wash water to the froth resulted in a higher water hold-up in the froth. This led to better elutriation of entrained material from the froth, and a more stable froth due to less bubble coalescence. The result of this was that the mass pull decreased with the addition of wash water, but the grade increased, and the recovery stayed roughly the same. The trends from the bottom to the top of the froth were more marked when no wash water was added.

3.5.4 FROTH RESIDENCE TIME DISTRIBUTION STUDIES

The residence time distribution of the solid phase in the froth zone of a column flotation cell has been modelled using an isotopically labelled tracer. The reproducibility of the system was better than 9% in all cases.

A plug flow reactor with recycle was used to model the froth zone in the flotation column. It was found that the mean absolute deviation between the experimental response curve and the response curve predicted by the model was less than 8% in all cases. One parameter models such as the tanks-in-series model and the axial dispersion model were found to the inadequate to model the froth.

A sensitivity analysis showed that the parameters chosen for the model, viz., the reactor recycle ratio (r) and the reactor residence time (τ_i) were largely independent of each other. Correlations were found between the mean residence time in the froth (τ) and the reactor residence time (τ_i) and between the variance in the froth (σ^2) and the reactor recycle ratio (r). These relationships were useful in establishing initial estimates of the model parameters.

The flotation parameters which had the biggest effect on the residence time distribution of the froth were the wash water rate, the air rate, the pulp density and the froth height.

3.5.5 PROCESSES OCCURRING IN THE FROTH

The major factors which determined the stability of the froth were the rates of water drainage from the froth and bubble coalescence. The particle size of the hydrophobic material in the froth had a large influence on the stability of the froth. Figure 3.40 shows the effects of different particle size ranges on water drainage from the froth and bubble coalescence. Assume a system where the mass of solids in the froth zone is constant. As the particle size doubles, the number of particles per unit mass decreases by a factor of 8. This means that the finer the particle size the more particles in the froth. A fine floated particle may either form a bond between two bubbles, or protrude into the water film between the bubbles and increase the drag in the water (Figure 3.40 A). In either case the rate of film drainage would be slowed and bubble coalescence inhibited.

If all the particles are all large, then there will be relatively few particles in the froth. A particle may again bond between two bubbles and keep them far enough apart to prevent coalescence, but there will be relatively few of these bonds as there are relatively few particles. This allows water to drain from the films between the bubbles where there are no particles keeping them apart and these bubbles will coalesce (Figure 3.40 B).

Ultra-fine particles are usually not floated due to bubble streamline effects. Most of them would thus remain in the water films between the bubbles and effectively increase the viscosity of the water. This slows the rate of

water drainage from the froth and inhibits bubble coalescence. If, however, a particle does form a bond between two bubbles it would force the inter-bubble water film to thin until it ruptured and the bubbles coalesced (Figure 3.40 C).

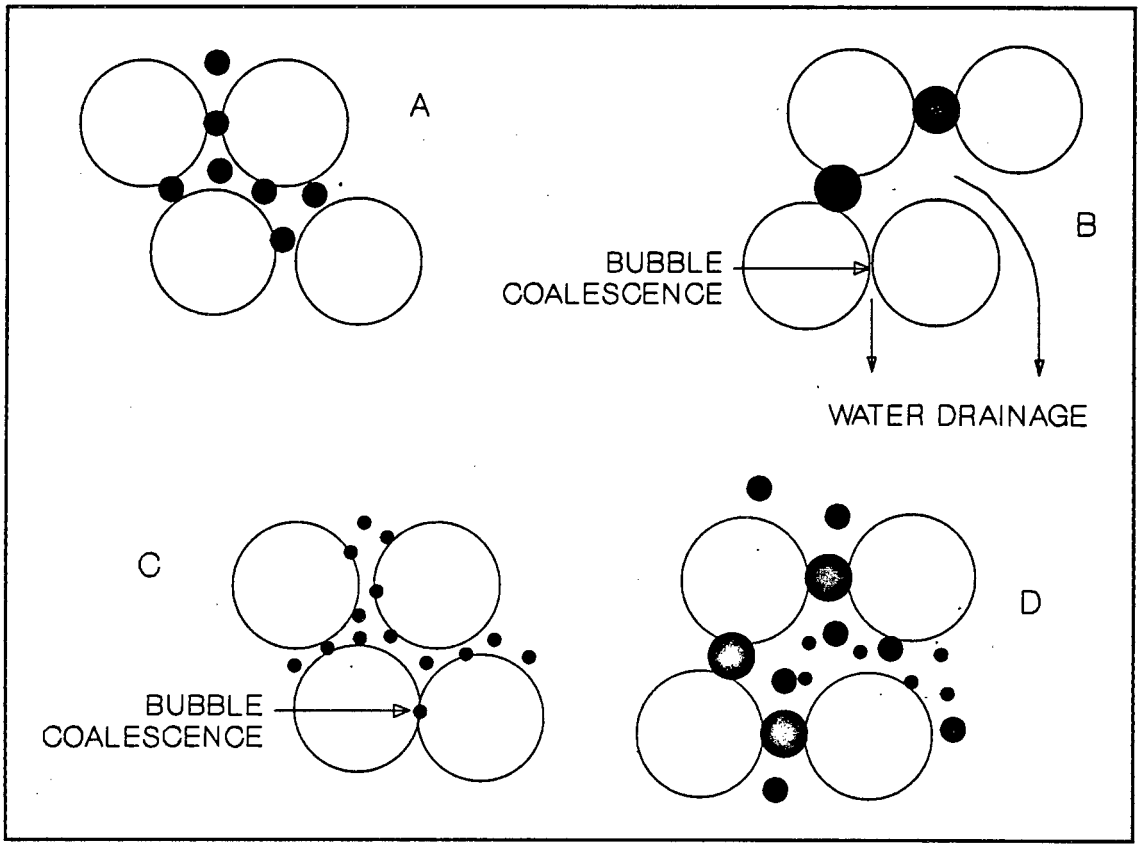

FIGURE 3.40 : Effect of Particle Size on Froth Stability

The optimum froth stability is achieved when a range of particle sizes is present in the froth. The larger particles form bonds between bubbles and stop the inter-bubble water films from reaching their rupture thickness, while the finer particles either remain bonded to just one bubble or are free in the water films, increasing the effective viscosity of the water. This slows the rate of water drainage from these films and contains the tendency for the bubbles to coalesce found when only large particles are present (Figure 3.40 D). Non-floated particles also stabilize the froth as they remain in the water films between the bubbles and inhibit froth drainage.

Figure 3.41 shows a schematic of the froth profiles with and without wash water. In the system with no wash water the froth is tightly packed with a high air hold-up, while the system with the wash wash water has a much

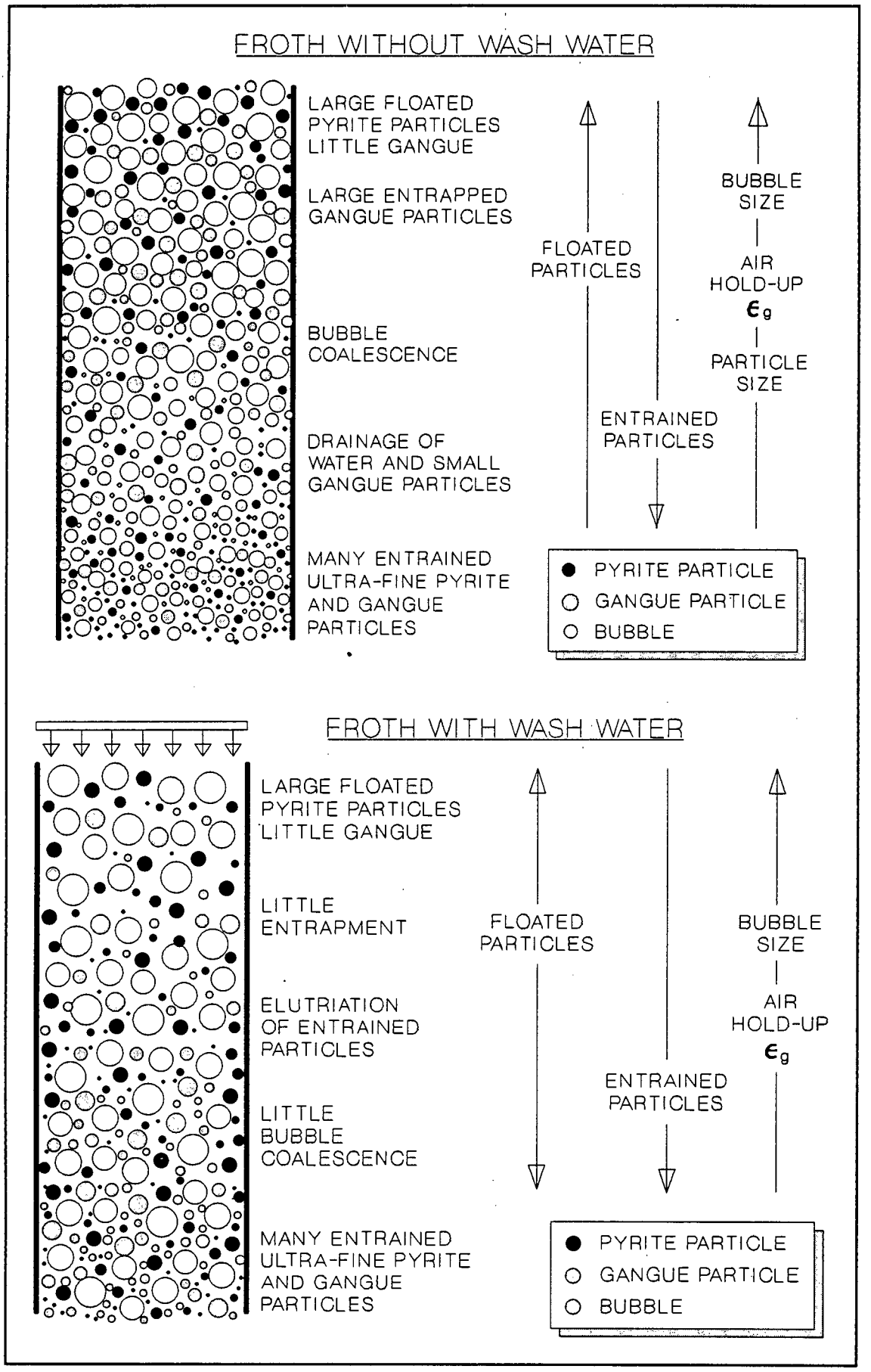

FIGURE 3.41 : Froth Profile With and Without Wash Water

higher liquid hold-up. In the system with no wash water some of the larger gangue particles are trapped in the froth and cannot drain with the water due to their size. Elutriation of entrained material is aided by the addition of wash water and the gangue particles are rejected at a much lower level in the froth. In both systems there is a crowded region at the bottom of the froth due to the rejection of entrained material at this level. There is a much higher degree of bubble coalescence when no wash water is added and hence there is a significant increase in bubble size from the bottom to the top of the froth.

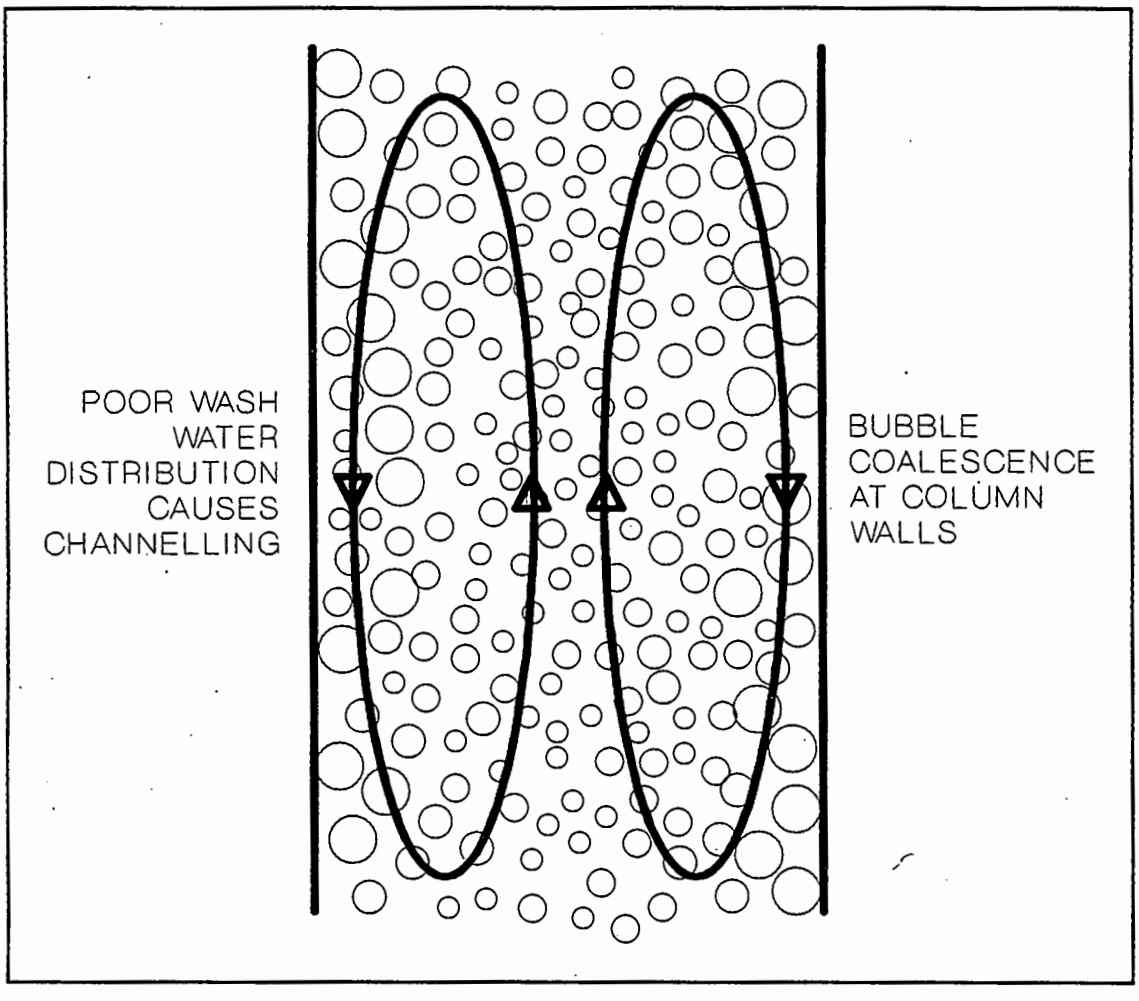

FIGURE 3.42 : Froth Recirculation

Figure 3.42 offers a proposal for circulation channels that may be set up in the froth under some conditions. There is a velocity profile across the froth caused by drag forces at the walls. This results in the bubbles in the centre of the froth rising faster than those near the sides. Also at low frother concentrations, wash water rates or pulp densities the bubbles near

the walls tend to coalesce as they come into contact with the walls. This results in a net downward flow of water in this region. This downward flow of water can also be caused by high wash water rates or poor wash water distribution which result in the wash water running down the walls of the column.

Due to these channels some of the froth tends to travel up in the centre and back down at the walls. This results in the return of floated particles to the base of the froth and the short circuiting of gangue material from the bottom of the froth directly into the concentrate. The froth thus becomes more mixed and less effective as a cleaning zone. As the column diameter increases the height to diameter ratio of the froth zone decreases. This would result in the froth zone becomming more mixed. There is also more scope for these circulation channels to develop in larger diameter columns due to poor air or feed distribution. This froth zone mixing is especially prominent in large unbaffled columns, or columns that are incorrectly baffled (Moys et. al., 1991).

Chapter 4

COLUMN METALLURGICAL PERFORMANCE

4.1 INTRODUCTION

The metallurgical performance of a column flotation cell is determined by the interaction of the pulp and froth zones. The major difference between a column flotation cell and a bank of mechanical flotation cells is the column has only one pulp-froth interface, whereas the bank of mechanical cells consists of a number of transfer units in series, each with its own pulp-froth interface. Thus in a bank of mechanical cells there is a grade profile across the bank of cells, and little change in grade in each cell's pulp zone due to the well mixed conditions. In a column cell the grade profile is from the bottom to the top of the pulp zone.

The design methodology for mechanical cells is not well defined with all of the cell supplier having their own concepts of which are the most important parameters in cell design, for example cell, rotor and stator geometry, power input, aeration type, etc. The design of columns has been quantified to a far greater extent, with all of the column suppliers using roughly the same design techniques. The higher degree of precision in column design allows studies of the effects of column variables on the metallurgical performance of the column to be applied more universally.

This chapter examines the effects of the following flotation parameters on the metallurgical performance of a laboratory column flotation cell:

- the feed rate,
- the wash water rate,
- the air rate,
- the frother concentration,
- the pulp density,

- the froth height,
- the mean residence time in both the pulp and froth zones, and
- the degree of mixing in the pulp and froth zones.

This chapter consists of a brief discussion of the literature on column performance, followed by the experimental methods. The results are discussed and a summary concludes the chapter.

4.2 THEORY

Finch and Dobby (1990) discuss the interactions of the pulp and froth zones and compare the recoveries achieved in mechanical cells with those achieved in columns. The schematic diagram shown in Figure 4.1 highlights the differences in the interactions between the pulp and froth zones for the two systems.

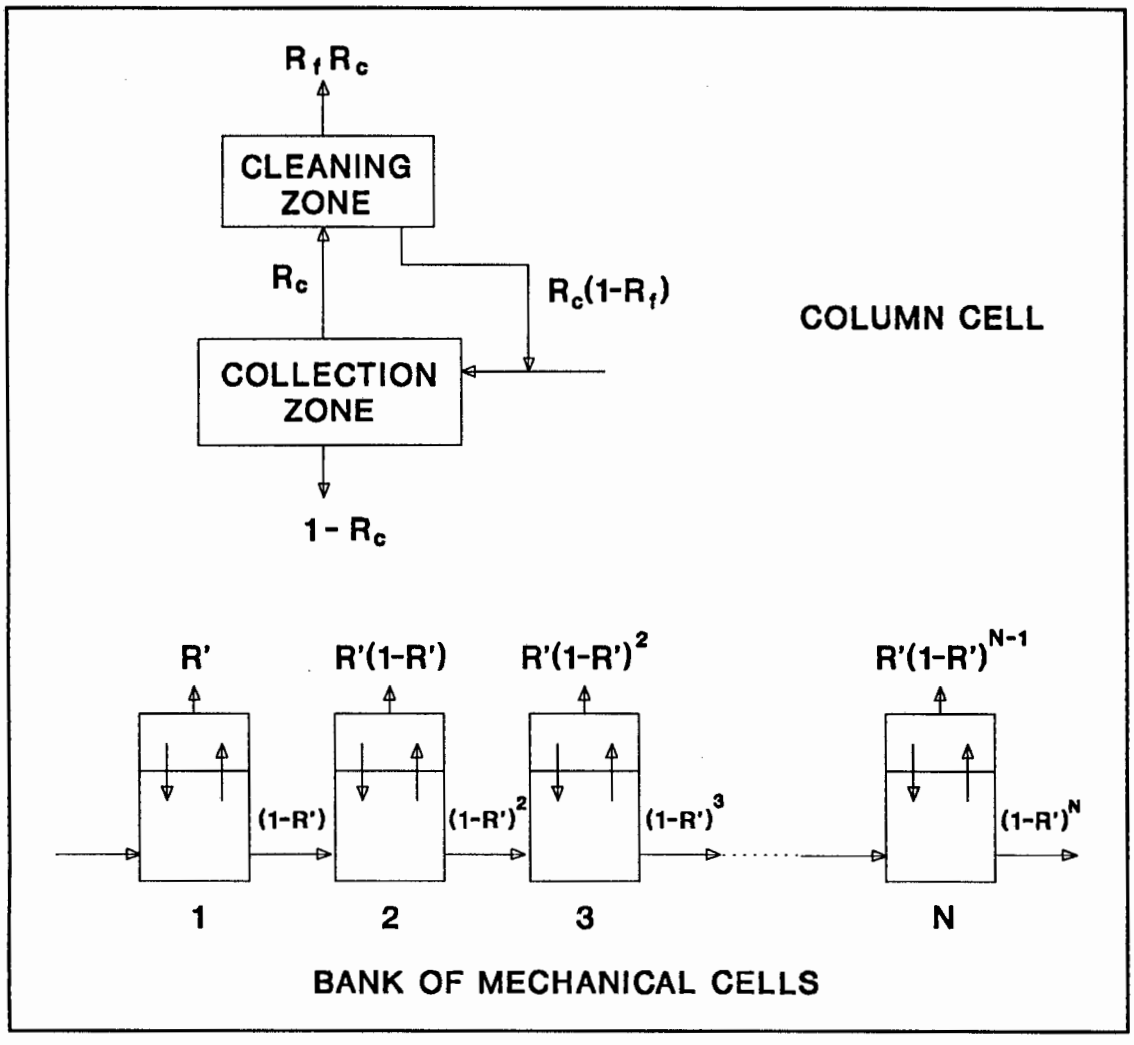

FIGURE 4.1 : Comparison Between the Interaction of the Pulp and Froth Zones of a Bank of Mechanical Cells and a Column Cell (After Finch and Dobby, 1990)

For the column cell the recovery is given by (Falutsu and Dobby, 1989):

$$R = \frac{R_f R_c}{R_f R_c + 1 - R_c}$$

and for a bank of mechanical cells (Harris, 1976):

$$R = 1 - (1 - R')^N$$

Some of the floated particles are always lost from the froth due to bubble coalescence. Finch and Dobby (1990) point out that the key difference between the two systems is the retention time of these particles which drop back out of the froth. In a column these particles have 100 percent of their original residence time, while in the bank of mechanical cells their average residence time is less than the original residence time. Thus the particles that are lost from the froth have more opportunity to be refloated in a column than in a bank of mechanical cells with the same overall residence time.

Initially it was assumed that the grade in the column was determined by the froth zone and the recovery by the dynamics occurring in the pulp zone (Dobby and Finch, 1986b assumed that the froth zone recovery was 100 percent). Ynchausti et al. (1988) showed that most of the upgrading in columns occurred at the pulp-froth interface because entrained material was dropped due to the deceleration of the bubbles and the downward bias. This suggests that the major functions of the froth are to provide a stable medium for the transport of the floated material into the concentrate and to ensure even distribution of the wash water. The equation above for the column recovery shows that the overall recovery is the product of the individual recoveries of the froth and pulp zones. Falutsu and Dobby (1989) found froth recoveries were always less than 60 percent.

A detailed discussion of the major column flotation parameters can be found in Section 1.2.1. Table 4.1 gives a summary of some of the column performance data found in the literature. The effects of an increase in the flotation parameter on the grade, recovery and concentrate mass pull are shown in this table.

It can be seen that an increase in concentrate grade is invariably accompanied by a decrease in recovery. Increasing the following parameters leads to an increase in grade and a decrease in recovery:

- the wash water rate and
- the froth height.

A decrease in grade and an increase in recovery are caused by an increase in the following parameters:

- the air rate and
- the frother concentration.

As the particle size, feed rate and the pulp density increase an optimum in the recovery curve is observed. It can also be seen that increasing the mean residence time in the system leads to an increase in both the grade and the recovery.

TABLE 4.1 : Effect of Flotation Parameters on Column Performance

Parameter	Grade	Recovery	Mass Pull	Mineral	Reference
Air Rate	-	+	+	Coal	Nicol et al., 1988
	-	+		Coal	Luttrell et al., 1988
	opt	nc		Coal	Perekh et al., 1988
	nc	opt		Zinc	Del Villar et. al., 1991
	-			Iron Ore	Sandvik et al., 1991
Wash Water Rate	+	-	-	Coal	Nicol et al., 1988
	+	-		Coal	Luttrell et al., 1988
	+	nc		Coal	Perekh et al., 1988
		-		Gold Ore	Ugarte and Reinoso, 1991
	+			Iron Ore	Sandvik et al., 1991
Residence Time	+	+		Gold Ore	Subramanian et al., 1988
	+	nc		Coal	Perekh et al., 1988
				Tin	Harris and Franzidis, 1989
Froth Height		-		Coal	Woodburn et al., 1988
	+	-		Flourite	Ynchausti et al., 1988b
	+	nc		Coal	Perekh et al., 1988
	+			Iron Ore	Sandvik et al., 1991
Feed Rate	-	+		Coal	Luttrell et al., 1988
			opt	Zinc	Del Villar et. al., 1991
Column Height		+		Coal	Perekh et al., 1988
Particle Size		opt		Tin	Harris and Franzidis, 1989
		opt		Base Metal	Espinosa-Gomez and Johnson, 1991
	-	opt		Chalcopyrite	Yianatos and Bergh, 1991
Frother Conc.	-	+		Coal	Olivera and Peres, 1991
		+		Gold Ore	Ugarte and Reinoso, 1991
	-			Iron Ore	Sandvik et al., 1991
Pulp Density	-	opt		Coal	Olivera and Peres, 1991
	+	-		Chromite	Guney et al., 1991

+ = increase - = decrease opt = optimum nc = no change

4.3 EXPERIMENTAL METHODS

A schematic diagram of the flotation column used in these tests is shown in Figure 4.2. The column is described in section 2.3.2. The ore and water were mixed in a 50 litre conditioning tank together with the collector and frother. The wash water used in these tests was a frother solution of the same concentration as that of the pulp. The feed and the wash water rates were controlled with variable speed peristaltic pumps. The level in the column was controlled by varying the tailings rate using a variable speed peristaltic pump.

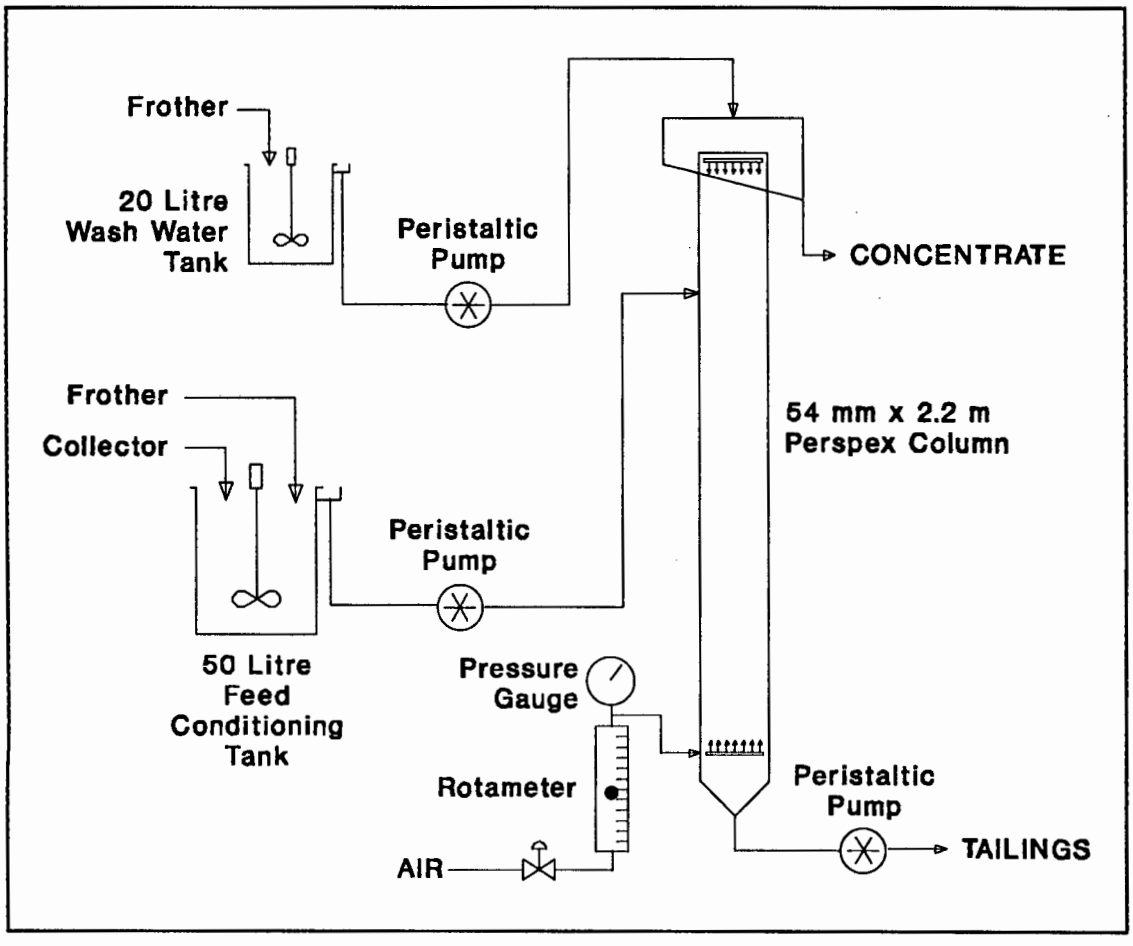

FIGURE 4.2 : Schematic Diagram of the Column Flotation Rig

The column was run for 20 minutes to allow steady state to be reached, and then samples of the concentrate and tailings were taken. These samples were dried and analysed for sulphur and particle size.

4.4 RESULTS AND DISCUSSION

Six flotation parameters were varied in this study, they were the feed rate, the wash water rate, the air rate, the frother concentration, the pulp density and the froth height. The data from these tests are given in Table 4.3.

4.4.1 REPRODUCIBILITY

Five runs were done at standard conditions to determine the reproducibility of the tests. The results of these repeat runs are given in Table 4.2. It can be seen that in all cases the mean absolute deviation from the average value was less than 9 percent, and it was considerably better (less than 5 percent) if the results of the tracer studies are not considered.

TABLE 4.2 : Reproducibility Tests

Test No.		1	2	3	4	5	AVE
Conc.	$\bar{t}$ (sec)	**139**	**137**	**120**	**119**	**135**	**130**
	MAD (%)	6.7	5.3	7.6	6.8	5.8	6.6
	N	**2.32**	**2.27**	**2.05**	**2.01**	**2.29**	**2.18**
	MAD (%)	6.1	4.1	6.5	8.5	4.8	6.0
	Grade (% S)	**20.0**	**19.0**	**19.6**	**19.9**	**20.5**	**19.8**
	MAD (%)	1.0	4.3	1.0	0.4	3.5	2.0
	Mass (g/min)	**11.8**	**12.6**	**12.1**	**12.8**	**12.7**	**12.4**
	MAD (%)	4.8	1.6	2.4	3.2	2.4	2.9
	Mass Pull(%)	**5.85**	**6.19**	**5.91**	**6.21**	**6.14**	**6.06**
	MAD (%)	3.5	2.2	2.5	2.5	1.3	2.4
	Recovery (%)	**66.3**	**70.9**	**68.5**	**67.2**	**67.1**	**68.0**
	MAD (%)	2.5	4.3	0.7	1.2	1.3	2.0
	d(50) (μm)	**24.6**	**25.8**	**24.7**	**25.1**	**24.8**	**25.0**
	MAD (%)	1.6	3.2	1.2	0.4	0.8	1.4
Tails	t (sec)	**136**	**131**	**143**	**145**	**135**	**138**
	MAD (%)	1.4	5.1	3.6	5.1	2.2	3.5
	N	**2.34**	**2.20**	**2.63**	**2.52**	**2.40**	**2.41**
	MAD (%)	2.8	9.4	8.4	4.6	0.4	5.1
	Grade (% S)	**0.6**	**0.6**	**0.6**	**0.6**	**0.6**	**0.6**
	MAD (%)	3.6	2.1	0.6	0.1	2.6	1.8
	Mass (g/min)	**189.9**	**191.0**	**192.6**	**193.3**	**194.1**	**192.2**
	MAD (%)	1.2	0.6	0.2	0.6	1.0	0.7
	d(50) (μm)	**17.1**	**17.0**	**17.1**	**17.0**	**17.1**	**17.1**
	MAD (%)	0.0	0.6	0.0	0.6	0.0	0.2
Feed	Mass (g/min)	**201.7**	**203.6**	**204.7**	**206.1**	**206.8**	**204.6**
	MAD (%)	1.4	0.5	0.0	0.7	1.1	0.7

$\bar{t}$ = Mean Residence Time N = Number of Tanks-in-Series
MAD = Mean Absolute Deviation d(50) = 50% Passing Particle Size

TABLE 4.2 : Column Metallurgical Performance Data

RUN NO	PARAMETER VARIED		CONCENTRATE							TAILINGS					FEED	
			$\bar{t}$ (sec)	N	GRADE (% S)	MASS (g/min)	MASS PULL (%)	REC (%)	d(50) (μm)	$\bar{t}$ (sec)	N	GRADE (% S)	MASS (g/min)	d(50) (μm)	MASS (g/min)	d(50) (μm)
1		0.93 cm/s	109	2.01	16.2	17.8	6.94	64.0	21.4	101	2.09	0.7	249.4	17.1	256.3	18.1
2	FEED	0.84 cm/s	117	2.14	17.4	15.2	6.62	67.6	23.1	118	2.28	0.6	223.0	17.1	229.6	18.1
3	RATE	**0.73 cm/s**	130	2.18	19.8	12.4	6.06	68.0	25.0	138	2.41	0.6	198.5	17.1	204.6	18.1
4		0.63 cm/s	139	2.28	20.9	9.8	5.66	67.4	26.7	163	2.52	0.6	167.8	17.2	173.5	18.1
5		0.53 cm/s	150	2.36	22.7	7.2	4.97	64.0	27.2	180	2.68	0.7	140.0	17.3	145.0	18.1
6		0.29 cm/s	151	4.16	22.8	10.4	5.12	66.1	28.0	107	1.94	0.6	198.2	17.1	203.3	18.1
7	WASH	0.27 cm/s	144	3.01	21.6	11.2	5.52	67.7	27.9	133	2.01	0.6	197.5	17.0	203.0	18.1
8	WATER	**0.25 cm/s**	130	2.18	19.8	12.4	6.06	68.0	25.0	138	2.41	0.6	198.5	17.1	204.6	18.1
9	RATE	0.23 cm/s	122	1.91	18.1	13.3	6.62	68.1	22.9	142	2.86	0.6	194.3	17.1	200.9	18.1
10		0.20 cm/s	98	1.87	14.7	15.6	7.82	65.3	18.8	150	3.27	0.6	191.8	17.3	199.6	18.1
11		5.07 cm/s	40	1.19	13.3	9.0	4.50	34.1	20.0	105	1.80	1.2	195.9	17.6	200.4	18.1
12	AIR	7.08 cm/s	49	1.98	14.7	15.9	7.89	66.0	16.5	131	2.20	0.6	193.6	17.5	201.5	18.1
13	RATE	4.51 cm/s	106	2.09	15.9	15.1	7.50	67.8	18.7	135	2.30	0.6	193.8	17.3	201.3	18.1
14		**2.31 cm/s**	130	2.18	19.8	12.4	6.06	68.0	25.0	138	2.41	0.6	198.5	17.1	204.6	18.1
15		1.69 cm/s	202	2.27	30.1	7.7	3.81	61.9	26.0	150	3.21	0.7	198.3	17.4	202.1	18.1
16		**25 ppm**	130	2.18	19.8	12.4	6.06	68.0	25.0	138	2.41	0.6	198.5	17.1	204.6	18.1
17	FROTHER	20 ppm	122	2.06	18.0	12.4	6.22	63.4	20.0	132	2.36	0.7	193.3	17.4	199.5	18.1
18	CONC.	15 ppm	118	1.95	16.9	10.1	5.07	48.5	18.2	129	2.26	0.9	194.3	17.6	199.4	18.1
19		10 ppm	110	1.80	15.5	6.4	3.18	28.2	18.8	123	2.24	1.3	197.8	17.8	201.0	18.1
20	PULP	**20 %**	130	2.18	19.8	12.4	6.06	68.0	25.0	138	2.41	0.6	198.5	17.1	204.6	18.1
21	DENSITY	15 %	68	1.21	20.2	7.7	5.77	66.6	19.2	98	1.58	0.6	127.6	17.8	133.4	18.1
22		10 %	51	0.98	19.9	5.4	5.35	60.0	17.9	81	1.50	0.7	95.6	18.1	100.9	18.1
23	REPEATS	0.93 cm/s	113	2.01	17.0	17.8	6.90	66.6	21.1	106	2.16	0.6	250.9	17.1	257.8	18.1
24		0.20 cm/s	105	1.85	14.4	15.7	7.74	65.0	19.1	153	3.30	0.6	195.0	17.3	202.7	18.1
25	FROTH	910 mm	165	2.58	24.5	9.0	4.49	62.5	17.2	97	1.24	0.7	196.1	17.7	200.6	18.1
26	HEIGHT	780 mm	148	2.36	22.0	11.0	5.49	68.9	18.3	98	1.36	0.6	194.8	17.6	200.3	18.1
27		680 mm	131	2.21	19.7	12.3	6.11	68.3	25.0	100	1.31	0.6	195.1	17.1	201.2	18.1

$\bar{t}$ = Mean Residence Time N = Number of Tanks-in-Series d(50) = 50% Passing Particle Size

4.4.2 EFFECT OF MEAN RESIDENCE TIME ON COLUMN PERFORMANCE

Figure 4.3 shows the effects of the mean residence time in both the pulp and the froth zones on the concentrate grade. It can be seen that there is a linear correlation between the mean residence time in the froth and the grade. The four spurious points were for tests where the froth was unstable, two at high air rates (viz: 7.08 and 5.07 $cm \cdot s^{-1}$), and the other two at low pulp densities (viz: 10 and 15 % solids) . The froth instability results in the froth being very well mixed and hence particles short circuiting from the bottom of the froth into the concentrate. This linear relationship indicates that the froth plays a major role in the cleaning process with the amount of entrained material in the concentrate decreasing as the froth residence time increases.

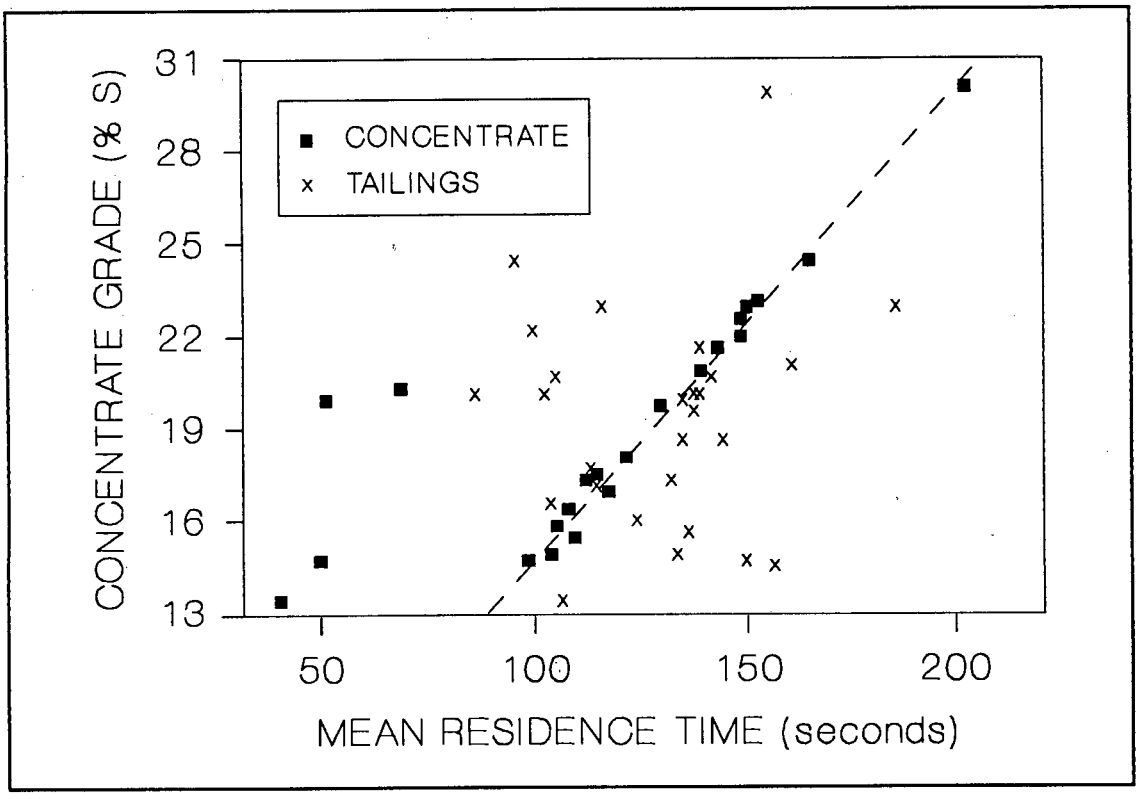

FIGURE 4.3 : Effect of the Mean Residence Time in the Column on the Concentrate Grade

It can be seen that there is no correlation between the mean residence time in the pulp zone and the grade. This would be expected because little upgrading occurs in the pulp zone.

Figures 4.4 and 4.5 show the effects of the mean residence time in the column on the concentrate mass pull and sulphur respectively. Figure 4.3 indicates that the mass pull to the concentrate shows a roughly linear decrease as the residence time in the froth increases. This is the opposite trend to that seen in the grades, and is the result of entrained material being cleaned from the froth. Again the points not near the straight line were due to froth instability.

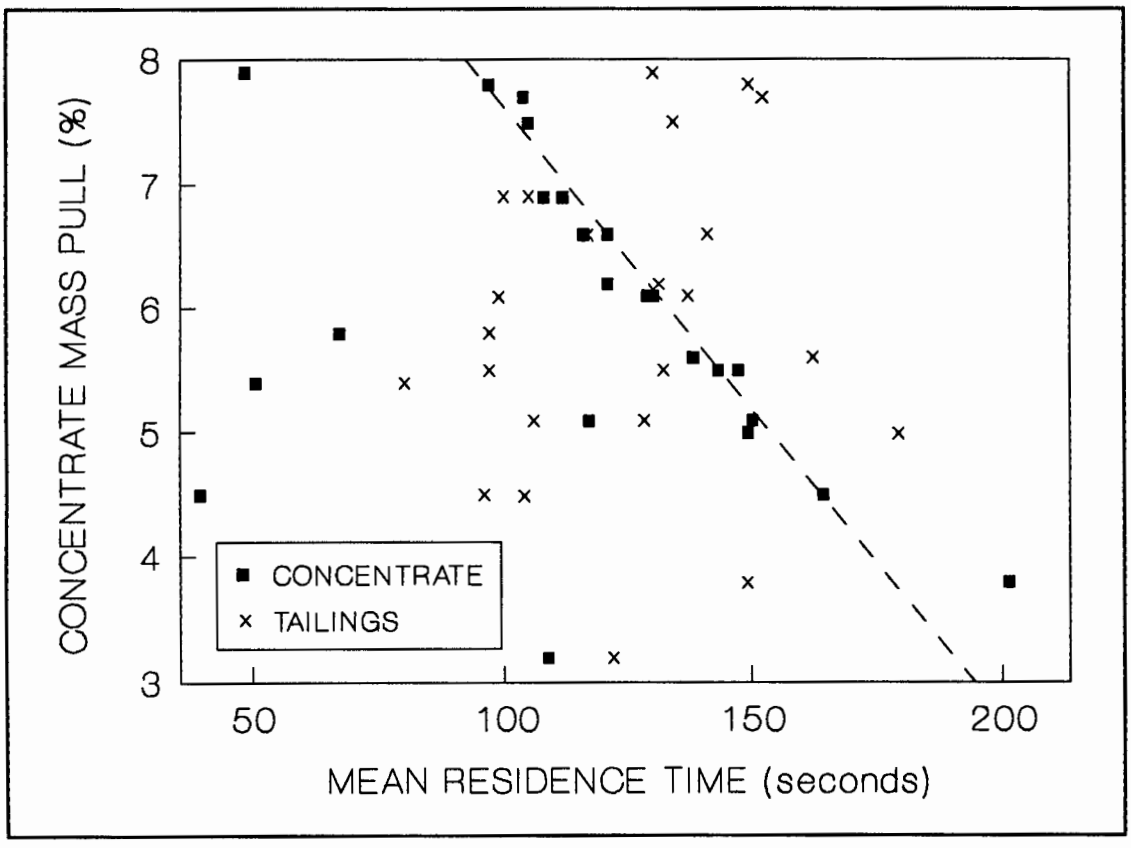

FIGURE 4.4 : Effect of the Mean Residence Time in the Column on Concentrate Mass Pull

There is, again, no correlation between the concentrate mass pull and the mean residence time in the pulp. This indicates that there was more than enough time for the flotation of particles in the pulp zone, and the loading of the bubbles in the pulp was at equilibrium. This is born out the recovery data shown in Figure 4.5. It can be seen that the recovery was virtually independent of the mean residence time in the pulp. It is likely that the recovery would have decreased if the column was shorter and there was insufficient time for complete particle collection to occur.

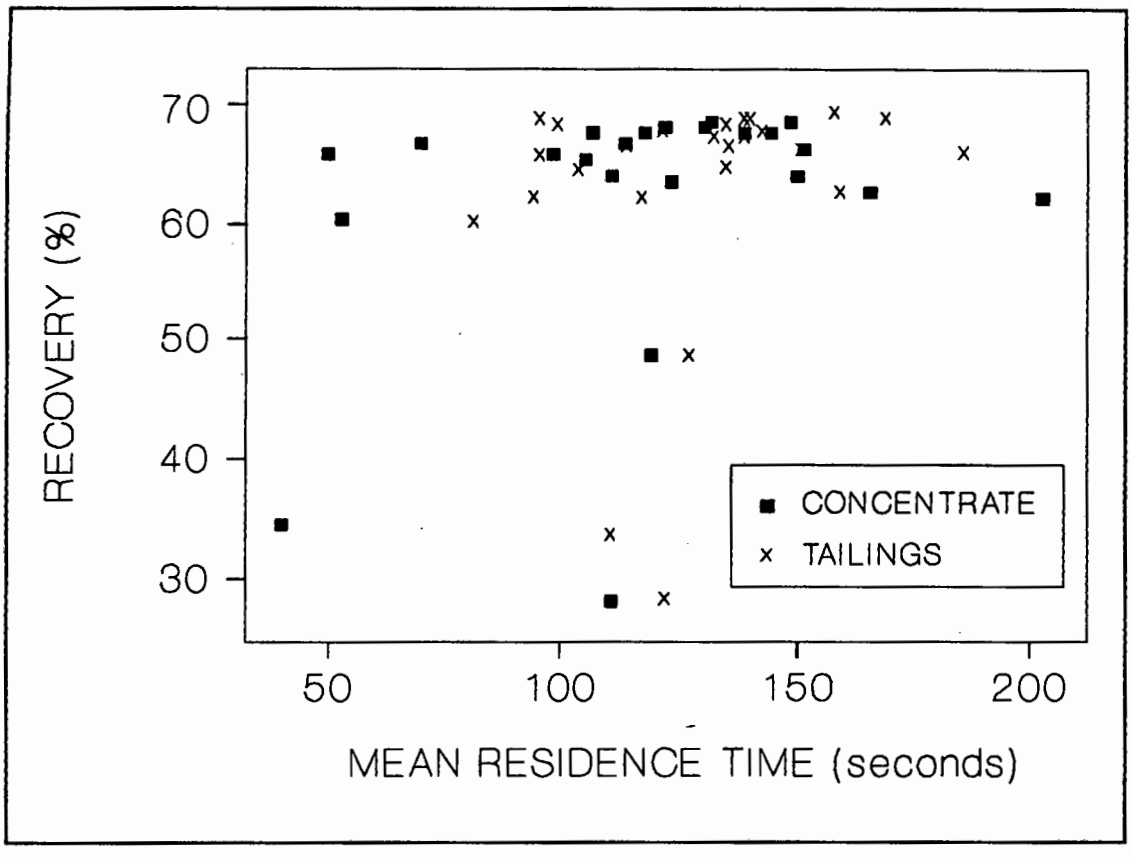

FIGURE 4.5 : Effect of the Mean Residence Time in the Column on Sulphur Recovery

Figure 4.5 shows that the recovery was unaffected for the residence time in the froth. The recovery is determined by the combination of the concentrate grade and mass pull, and since these show opposite trends they cancel each other out. At low froth residence times an increase in recovery would be expected, but this did not occur because the froth was well mixed (Table 4.3) and some of the floated material was dropped from the froth due to this mixing.

The effect of the mean residence time in the froth on the concentrate particle size (Figure 4.6) is not as marked as with the grade and mass pull, but there is a trend for the particle size to increase as residence time in the froth increases. This would be expected because the degree of entrainment increases as the particle size decreases. Increasing the mean residence time in the froth would lead to more elutriation of this fine material from the froth and hence the particle size in the concentrate would increase. There is, again, no trend in the relationship between particle size in the concentrate with mean residence time in the pulp.

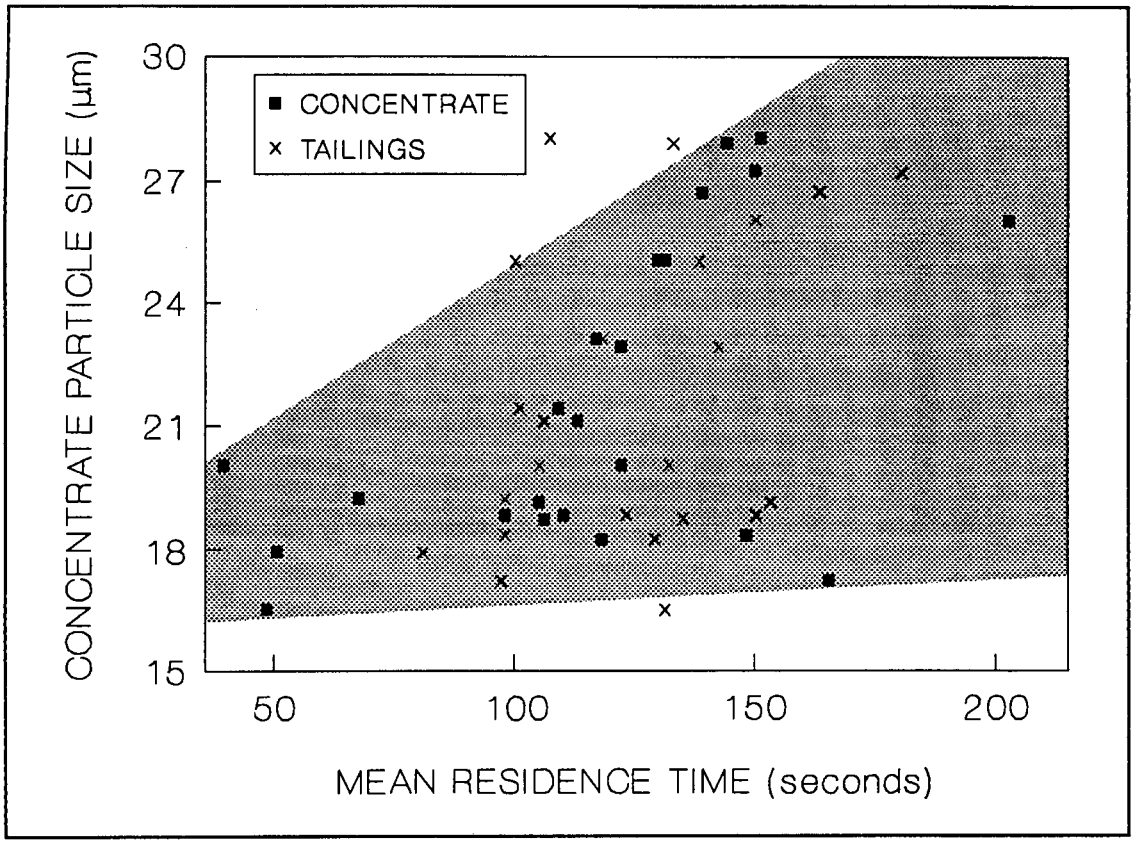

FIGURE 4.6 : Effect of the Mean Residence Time in the Column on Concentrate Particle Size

4.4.3 EFFECT OF MIXING ON COLUMN PERFORMANCE

It was shown in Section 3.4.4. that the degree of mixing in the froth was partly dependent on the mean residence time in the froth. This is due to the relationship:

$$\sigma_\theta^2 = \sigma^2/\tau^2 \equiv 1/N$$

Thus the number of tanks-in-series is related is related to the mean residence time for both the pulp and froth zones. It would therefore be expected that the trends seen as the mean residence time changed with the grade, the concentrate mass pull, the sulphur recovery, and the particle size would be repeated with the number of tanks-in-series (N). Figures 4.7 to 4.10 show these relationships. The increased scatter of the points for the concentrate is because the degree of mixing is not solely a function of the mean residence time in the froth as shown by Figure 3.36.

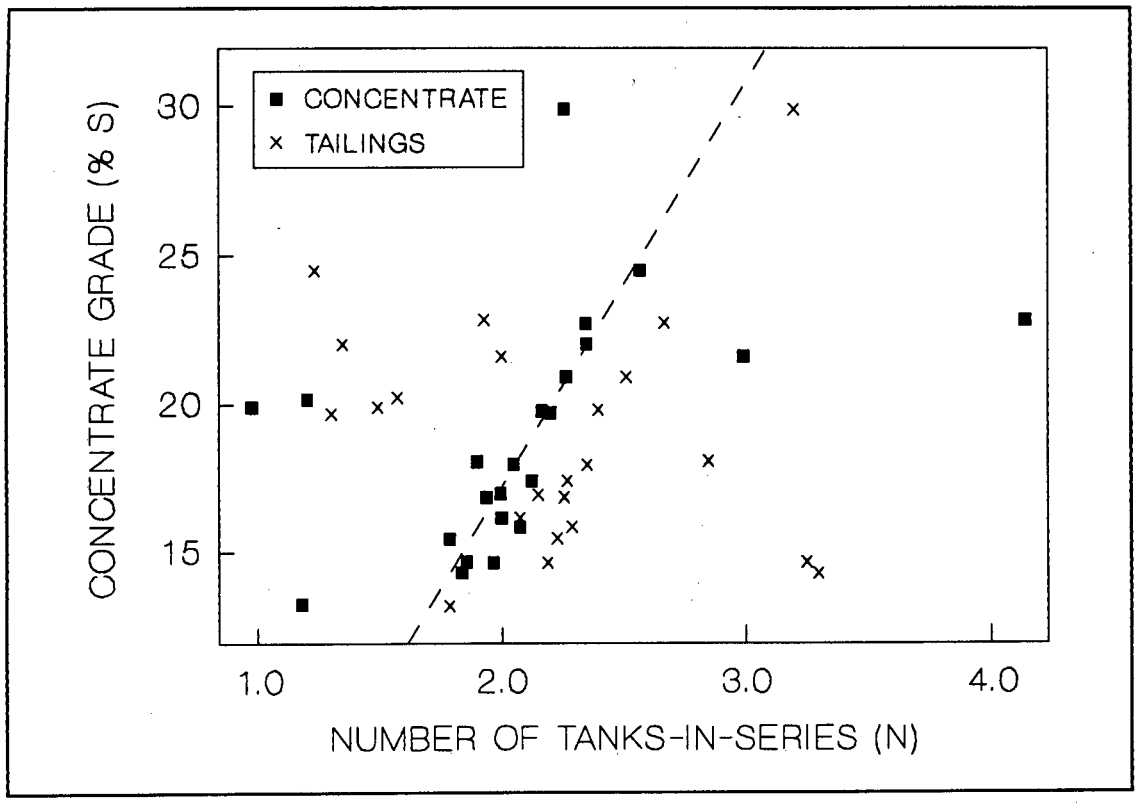

FIGURE 4.7 : Effect of the Degree of Mixing in the Column on the Concentrate Grade

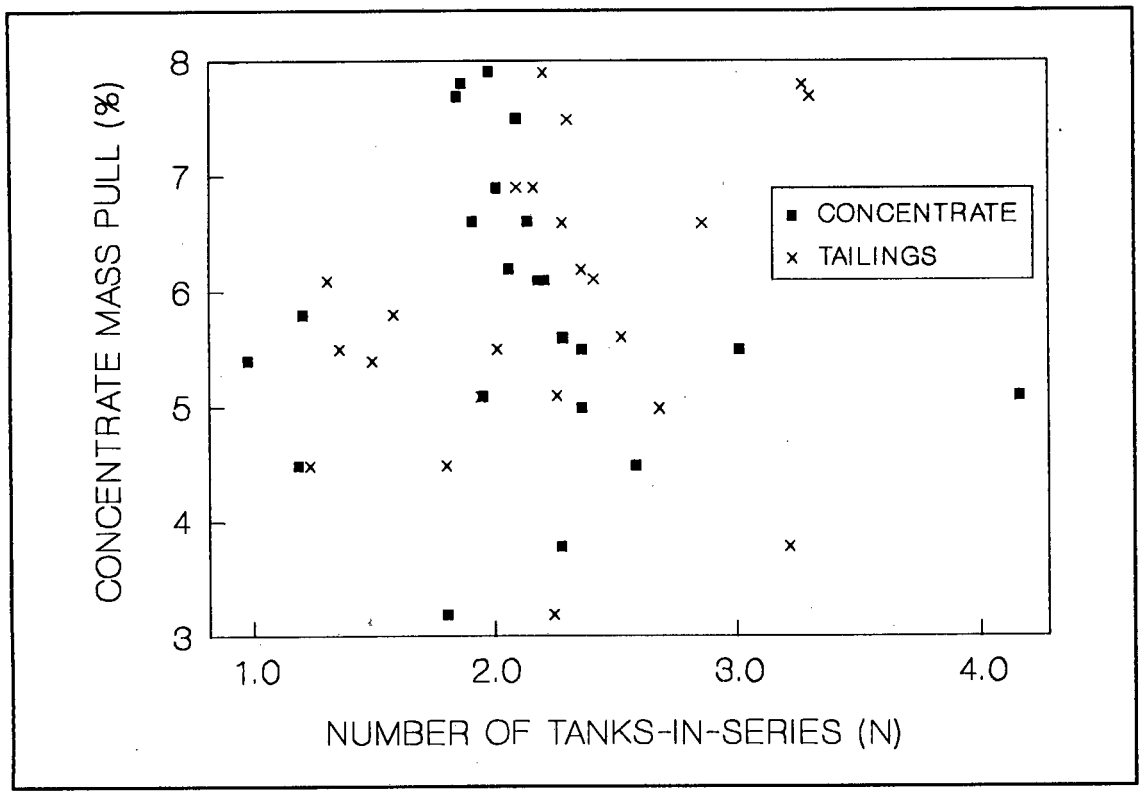

FIGURE 4.8 : Effect of the Degree of Mixing in the Column on the Concentrate Mass Pull

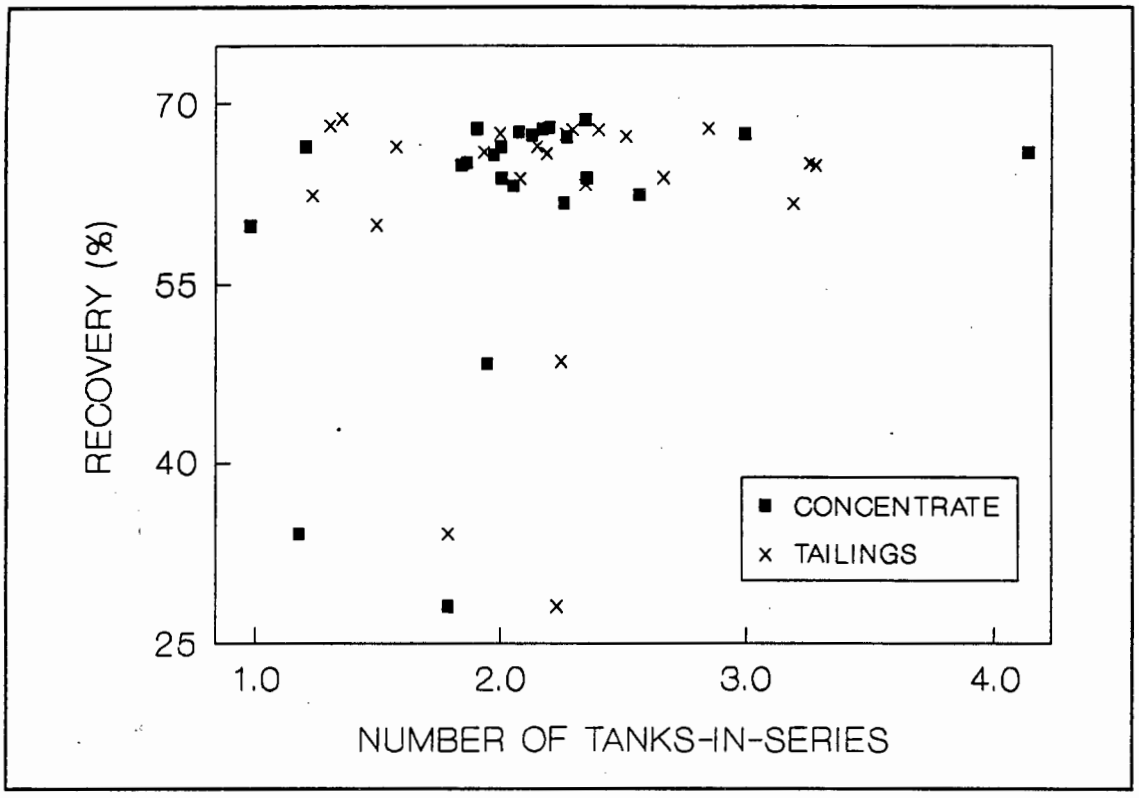

FIGURE 4.9 : Effect of the Degree of Mixing in the Column on the Sulphur Recovery

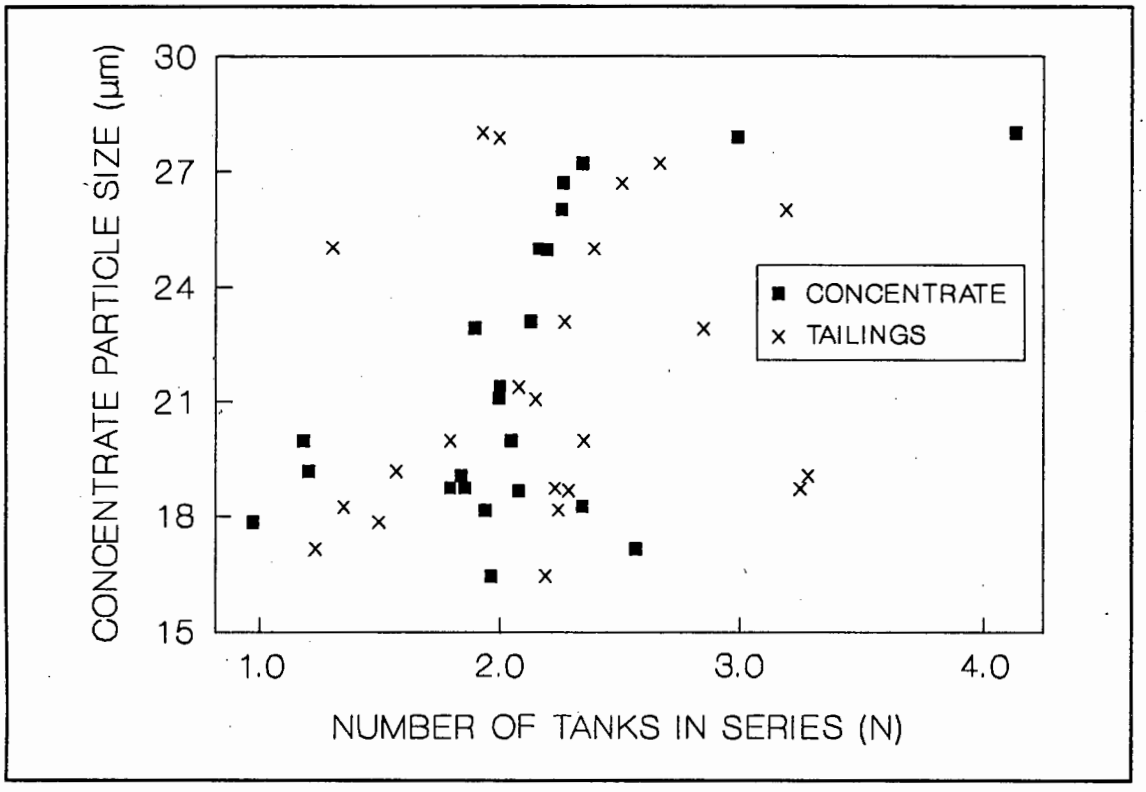

FIGURE 4.10 : Effect of the Degree of Mixing in the Column on the Concentrate Particle Size

As the degree of mixing in the froth increases particles can start to short circuit from the bottom to the top of the froth and so the froth becomes less effective at cleaning. This results in a decrease in grade and an increase in the amount of fine entrained material reporting to the concentrate. These trends can be seen in Figures 4.7 and 4.10. There was no marked trend for the concentrate mass pull to decrease as the degree of mixing (1/N) increased (Figure 4.8) as was seen with the residence time, but the sulphur recovery (Figure 4.9) was, again, generally unaffected by the degree of mixing.

4.4.4 EFFECT OF FLOTATION PARAMETERS ON THE CONCENTRATE GRADE

Figure 4.11 shows the effects of the feed rate, the wash water rate, the air rate, the frother concentration, the pulp density and the froth height on the concentrate grade.

As the volumetric feed rate decreases there is a decrease in the mass feed rate of the solids and the liquid, while a decrease in the pulp density results only in a decrease in the mass feed rate of solids, but not the liquid. From Figure 4.11 it can be seen that increasing the feed rate decreases the grade, but changing the pulp density has little effect on the grade. The major difference between these two parameters is that changing the feed rate changes the nominal residence time in the column, while changing the pulp density does not. This indicates that decreasing the residence time in the column decreases the grade. This is in conflict with the data shown in Figure 4.3, which indicates that there is no correlation between the grade and the mean residence time in the pulp. It must, however be remembered that the points for the low pulp densities do not lie on the straight line in Figure 4.3 because the froth was unstable and this would have led to a decrease in grade at the lower pulp densities.

As the mass feed rate of solids increases the probablity of floating the high grade, slow floating, fine particles decreases and this would lead to a decrease in grade. Also as the feed rate increases the residence time in the froth decreases and the degree of mixing increases. This also leads to a reduction in grade.

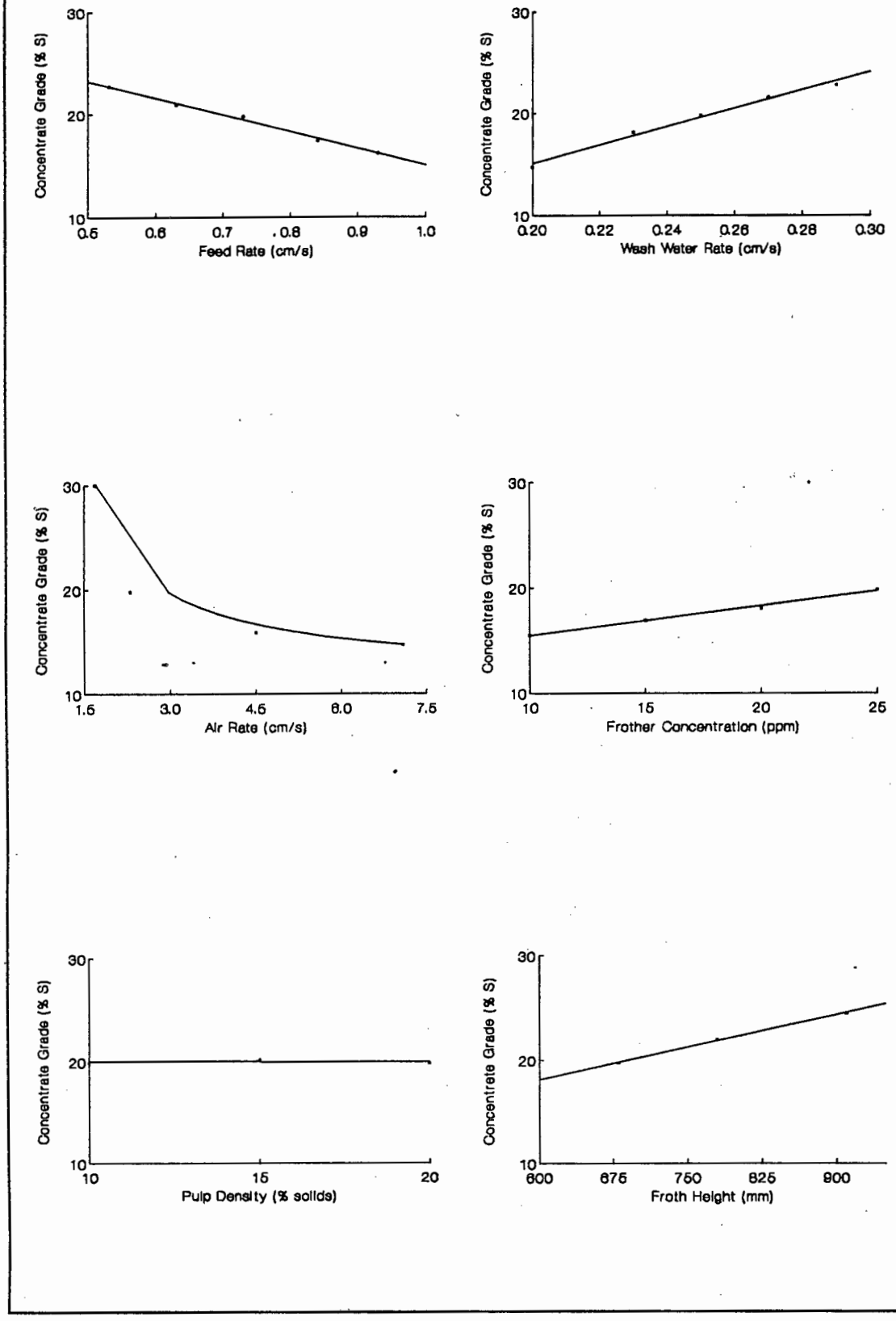

FIGURE 4.11 : Effect of Flotation Parameters on the Concentrate Grade

The trend for the grade to increase as the wash water rate increases is expected and is the result of better cleaning in the froth zone and less froth mixing. The increase in grade as the frother concentration increases can also be attributed to less mixing in the froth. As the frother concentration increases bubble coalescence in the froth is inhibited and so the froth is more stable.

As the air rate increases there is a sharp decrease in the grade due to the larger bubbles and the wider range of bubble sizes that are produced. Large bubbles rise faster than small bubbles promoting entrainment rather than flotation. Large bubbles coalesce more readily in the froth than small bubbles and this together with the wider range of bubble sizes leads to an increase in froth mixing. This allows more of the entrained material to report to the concentrate.

The increase in grade as the froth height increases is a direct result of an increase in the mean residence time in the froth. This allows more efficient cleaning in the froth.

4.4.5 EFFECT OF FLOTATION PARAMETERS ON THE CONCENTRATE MASS PULL

Figure 4.12 shows the effects of the feed rate, the wash water rate, the air rate, the frother concentration, the pulp density and the froth height on the concentrate mass pull. Again the opposite trends are seen to the grade curves shown in Figure 4.11 (except for the frother concentration curve). This is expected because increasing the mass pull increases the amount of entrained material in the froth.

As the feed rate increased there was more material available to float, and hence the mass pull would be expected to increase. It can again be seen that there was little change in the mass pull as the pulp density increased. Because the froth becomes unstable at the lower pulp densities the mass pull is higher than expected. A relatively high percentage of the material at the bottom of the froth is circulated directly to the top of the froth and into the concentrate due to the high degree of mixing in the froth.

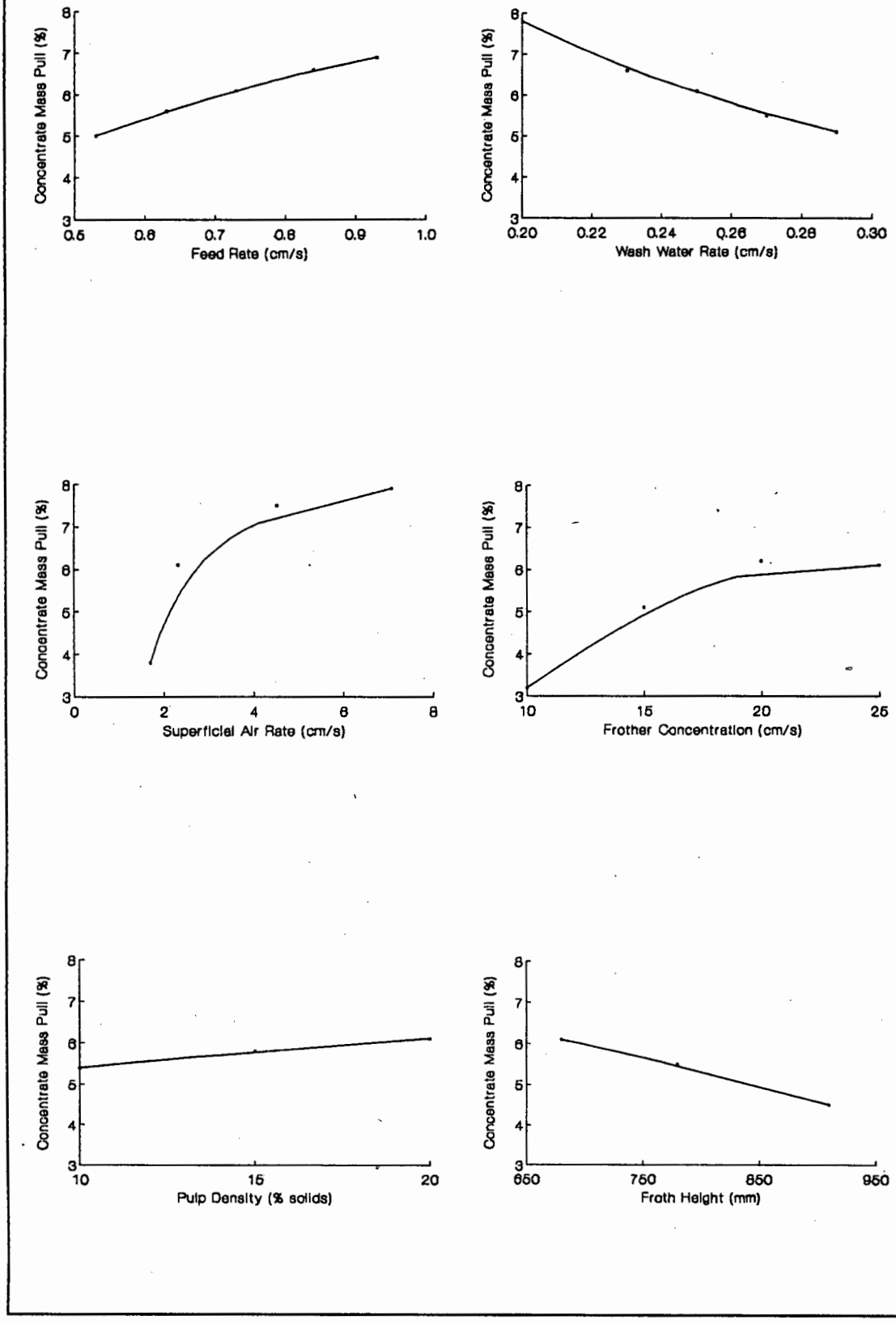

FIGURE 4.12 : Effect of Flotation Parameters on the Concentrate Mass Pull

The decrease in mass pull as the wash water rate increased was expected because the increased downward bias in the froth zone prevented much of the entrained material from reporting to the concentrate. Similarly by increasing the froth height the cleaning in the froth improved because there was less froth mixing. This prevented circulation channels from developing and particles short circuiting the froth. These circulation channels did develop as the air rate was increased because the bubble size in the pulp increased which led to the bubbles in the froth being less stable. The bubble size in the froth was observed to increase drastically because more bubble coalescence occurred. Thus the sharp increase in mass pull as the air rate increased was expected.

Both the grade and the mass pull increased as the frother concentration increased which seem anomalous, but again the points for the low frother concentrations do not lie on the straight line on the grade-mean residence time curve (Figure 4.3). This means that the froth was unstable and thus much of the material that was floated into the froth zone was dropped back into the pulp before it could report to the concentrate. The low grades observed at the low frother concentrations were due to macro-circulation from the bottom to the top of the froth which drastically reduced the cleaning efficiency of the froth. If the froth was stable the grade would be expected to decrease as the frother concentration increased because the froth would become more tightly packed and some of the entrained material would be trapped in the froth. This trend was seen in the froth cutting tests (sections 3.4.2 and 3.4.3) and is consistent with the trends reported in the literature (Table 4.1).

4.4.6 EFFECT OF FLOTATION PARAMETERS ON THE SULPHUR RECOVERY

Figure 4.13 shows the effects of the feed rate, the wash water rate, the air rate, the frother concentration, the pulp density and the froth height on the sulphur recovery. The recovery is determined by the combination of the concentrate grade and the mass pull, and so the trends observed were expected.

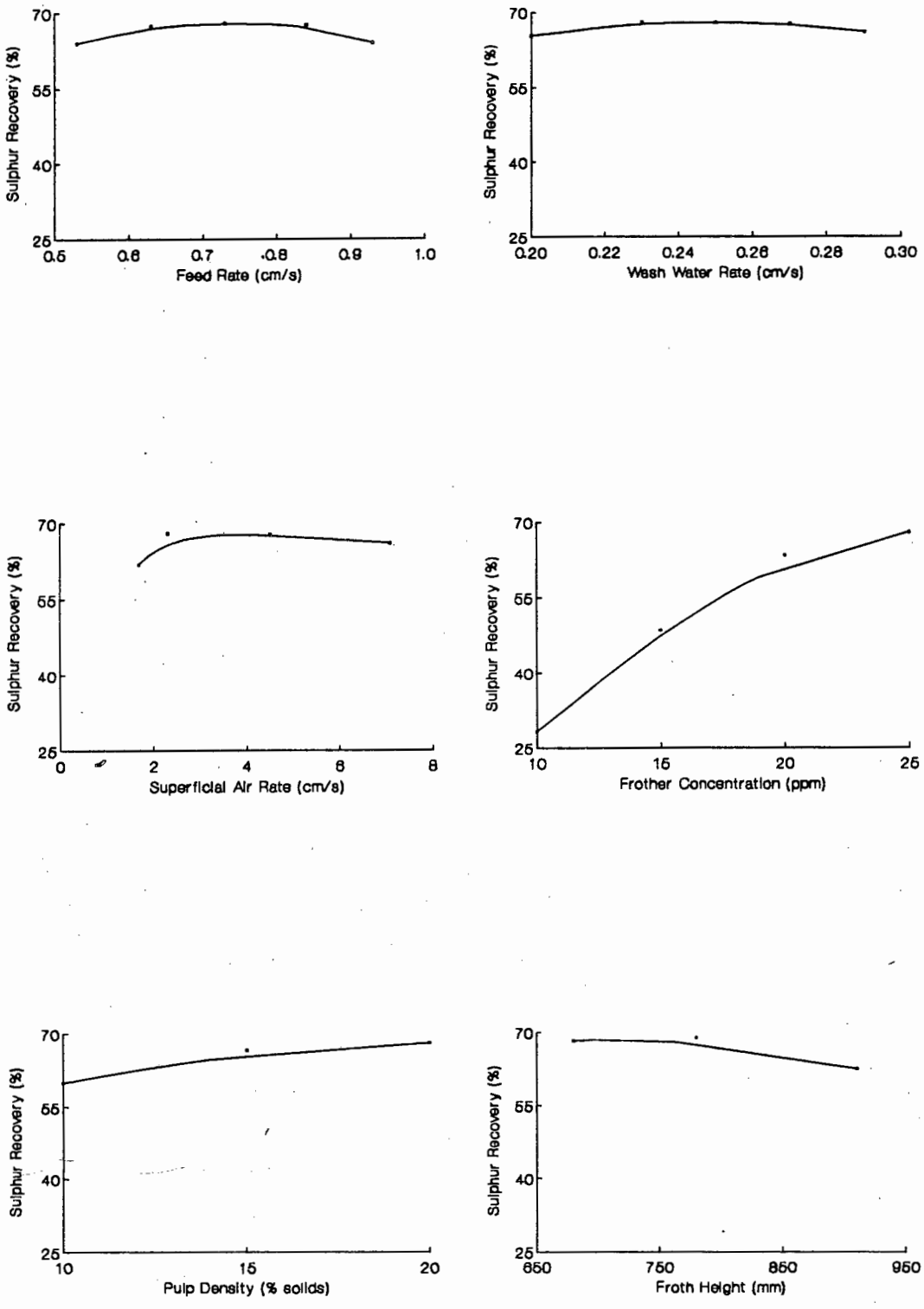

FIGURE 4.13 : Effect of Flotation Parameters on the Sulphur Recovery

The curves for the feed rate, the wash water rate and the air rate all show optimum values even though the curves are nearly flat. These optima were caused by a loss of grade due to froth mixing on one hand and a decrease in mass pull of entrained and slow floating fine pyrite particles on the other hand.

The recovery increased dramatically as the frother concentration increased. This trend was also seen to a lesser extent in the pulp density-recovery curve. These trends were due to the instability of the froth at the lower values, the effects of which have already been discussed. It would naturally be expected that the recovery would increase anyway as these two parameters increased due to more material being available for flotation as the pulp density increased, and the entrapment of entrained pyrite in the froth as the frother concentration increased.

There was no dramatic change in the degree of froth mixing as the froth height changed which resulted in the decrease in mass pull being greater than the increase in concentrate grade. Thus the sulphur recovery decreased as the froth height increased. This trend was also generally found in the literature (Table 4.1).

4.4.7 EFFECT OF FLOTATION PARAMETERS ON THE PARTICLE SIZE IN THE CONCENTRATE

Figure 4.14 shows the effects of the feed rate, the wash water rate, the air rate, the frother concentration, the pulp density and the froth height on the mean particle size in the concentrate. The particle size is a good indicator of the relative extents of flotation and entrainment. The finer the particle size the more entrainment.

All of the trends seen in Figure 4.14 except the froth height trend can be explained in terms of the amount of entrained material in the concentrate and the degree of mixing in the froth.

The froth height trend is anomalous because the residence time in the froth increases and the degree of mixing decreases as the froth height increases. Thus the concentrate particle size should increase as the froth

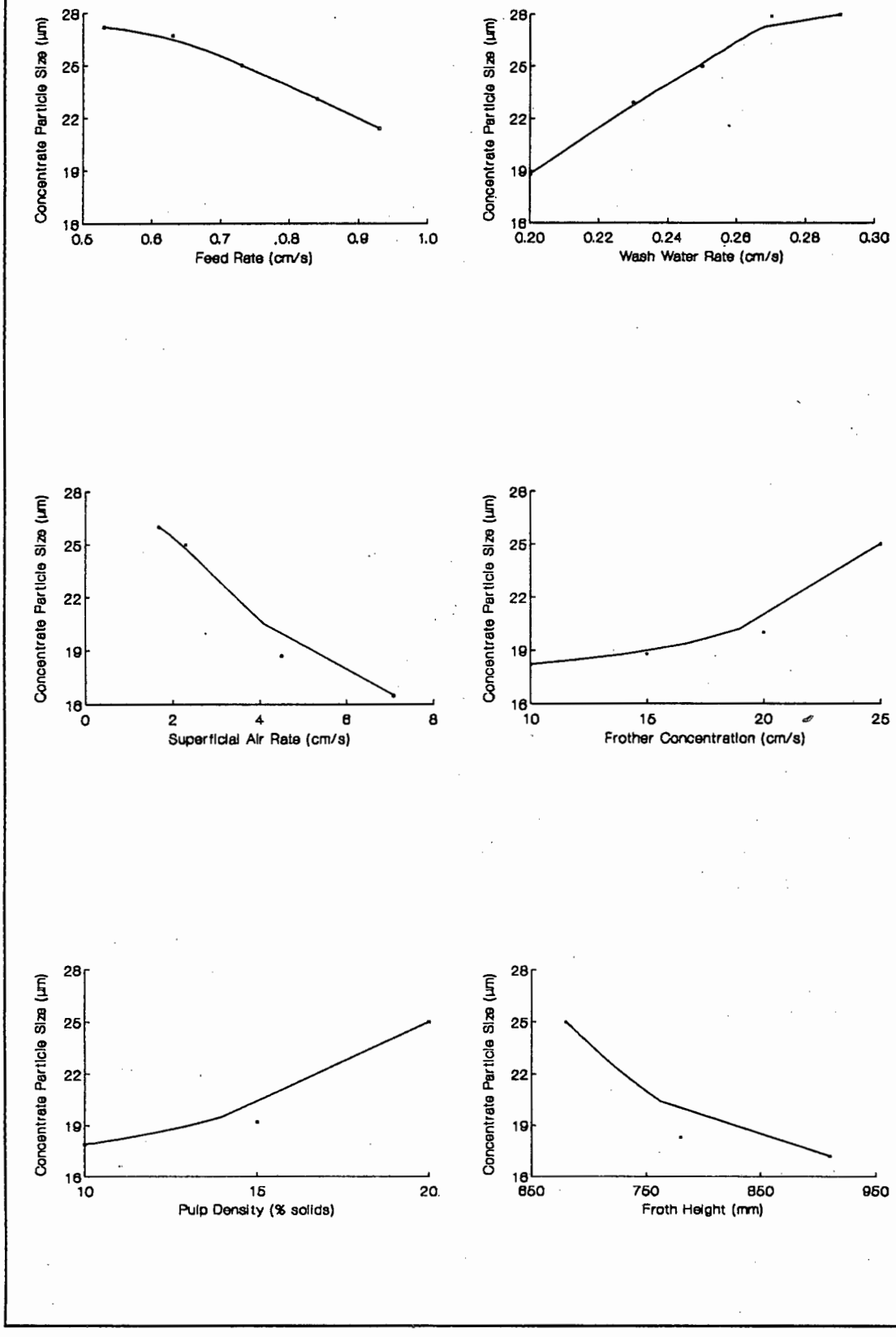

FIGURE 4.14 : Effect of Flotation Parameters on the Concentrate Particle Size

height increases. It is possible that the wash water was not as well distributed in the deeper froths and some of the fine entrained or slow floating material was trapped in the froth, although this should have been reflected in lower grades which were not observed.

4.5 SUMMARY

A qualitative summary of the effects of the flotation parameters studied on the metallurgical performance of the column is given in Table 4.4. It can be seen that the parameters which caused an increase in mean residence time resulted in less mixing. Parameters which resulted in lower concentrate grades generally resulted in a smaller mean particle size in the concentrate and a higher mass pull to the concentrate. For the systems where the froth was relatively stable the recovery tended to have an optimum value determined by the interaction of the grade and the mass pull. Where the froth was unstable recovery was lost.

TABLE 4.4 : Effect of an Increase in Flotation Variables on the Behaviour of the Solids in the Froth Phase

PARAMETER / VARIABLE	MEAN RESIDENCE TIME	DEGREE OF MIXING	GRADE	RECOVERY	MASS PULL	MEAN PARTICLE SIZE
FEED RATE	↓↓	↑	↓	∩	↑↑↑	↓↓
WASH WATER RATE	↑↑	↓↓↓	↑↑↑	∩	↓↓	↑↑↑
AIR RATE	↓↓↓	↑↑	↓↓↓	∩	↑↑	↓↓
FROTHER CONC	↑	↓	↑	↑↑↑	↑↑	↑↑
PULP DENSITY	↑↑	↓↓	↔	↑	↑↑↑	↑↑
FROTH HEIGHT	↑	↓	↑	↓	↓↓	↓↓

↑ INCREASE ↓ DECREASE ↔ NO CHANGE ∩ OPTIMUM

Chapter 5

CONCLUSIONS

A system has been developed to measure the sizes of bubbles in both two- and three phase systems in flotation cells. Bubbles are drawn up a capillary tube past two optical detectors and the signals are logged by a micro-processor system. The system can size up to 4000 bubbles in each test at a rate of 50 bubbles per second. The reproducibility of the results was excellent with the large number of bubbles sized providing good statistical confidence in the distributions obtained.

The bubble size generated in flotation columns is primarily a function of the type of sparger used, the viscosity of the pulp and the surface tension of the system. The size of the bubbles formed is determined by the rate at which a pocket of air can be surrounded by a film of slurry. The rate at which this film forms is in turn determined by the viscosity. The stability of the film around the bubble is a function of the surface tension of the system. The bubble generation system determines the volume and speed of air at each bubble formation site. Shock waves are generated as the air leaves some spargers systems which results in smaller bubbles.

An increase in bubble size was caused by the following parameters:

- an increase in air rate;
- an increase in particle size;
- an increase in viscosity;
- a decrease in temperature;
- an increase in pulp density;
- a decrease in frother concentration;
- an increase in pH; and
- a decrease in ionic strength.

All of these trends can be explained in terms of either the rate of formation of films around the bubbles, or the air-slurry surface tension. It was also found that the type of ore used and the presence of ultra-fine metal-xanthate precipitates affected the bubble size. The surface charge on the mineral and the metal-xanthate precipitates may have an effect on the viscosity and surface tension of the system.

Liquid and solid residence time distribution studies were carried out in a laboratory column flotation cell with a gold ore using isotopically labelled tracers for the solids and a salt solution for the liquid. The reproducibility was good.

There was a significant difference between the residence time distributions of the solid and the liquid phases in the pulp with the solids being more mixed than the liquid. This was because there is far more solid-bubble interaction than liquid-bubble interaction. The solids also have a greater settling rate than the liquid. Correlations predicting the solid phase behaviour from liquid phase data should therefore be avoided. An examination of the liquid phase residence time distributions showed that there was little difference between the two- and three-phase systems.

A tanks-in-series model was found to provide a good fit for both the solid and liquid phases in the pulp zone with the mean absolute deviation between the experimental data and the model always less than 5%.

The axial dispersion model and the tanks-in-series model were found to provide a similar fit for the residences time distributions of the solids in the pulp. The axial dispersion model was not used because some of the D/uL values found in this study were too large for the assumptions made in the model to be valid. The D/uL value would also increase as the column height-to-diameter ratio increases. This makes the axial dispersion model unsuitable for larger columns and could lead to errors in scale-up.

A perfect plug flow reactor with a recycle stream was used to model the residence time distribution of the solids in the froth zone of a laboratory flotation column. It was found that the mean absolute deviation between the experimental response curve and the curve predicted by the model was less than 8% in all cases. It was found that several two parameter

compartment models could have be used, but single parameter models such as the tanks-in-series model were found to be inadequate to model the froth. The liquid tracer studies showed that very little of the feed water reported to the concentrate and therefore the water in the froth must have come from the wash water.

A sensitivity analysis in which the model parameters were plotted against each other showed that the parameters chosen for the model, viz: the reactor residence time and recycle ratio were largely independent of each other. There were correlations between the mean residence time in the froth and the reactor residence time and between the degree of mixing in the froth and the reactor recycle ratio. These relationships were expected and validated the model choice because they showed that the model parameters were physically significant. These relationships were also useful in obtaining initial estimates of the model parameters.

A study of the effects of some flotation parameters on the metallurgical performance of the column showed that:

- The pulp density had the largest effect on the mean residence time in the pulp zone because the mass of solids in the column decreased as the pulp density decreased.
- The air rate had the largest effect on the mean residence time in the froth zone. As the air rate decreased the bubble size in both the pulp and froth zones decreased and the residence time in the froth increased because there was less short circuiting of material into the concentrate.
- The volumetric feed rate had the largest effect on the degree of mixing in the pulp zone As the feed rate increased the mean residence time in the pulp decreased and the amount of solids in the pulp increased. This led to more interaction between the particles and the bubbles, and hence more mixing.
- The wash water rate had the largest effect on the degree of mixing in the froth zone. Increasing the wash water rate decreased the amount of bubble coalescence in the froth and hence the froth became less mixed.

- The concentrate grade was most affected by the air rate. As the air rate increased, the bubble size increased and so did the amount of entrainment.
- The recovery was determined by the combination of the mass pull and the grade in the concentrate, and tended to have an optimum value caused by the loss of floatable material due to bubble coalescence on one hand and froth cleaning on the other. At low frother concentrations and pulp densities the froth was observed to be unstable and hence floatable material was lost causing a decrease in recovery.
- The volumetric feed rate had the largest affect on the concentrate mass pull because the amount of floatable material in the pulp increased as the feed rate increased. This trend was also observed as the pulp density increased.
- The particle size in the concentrate was most affected by the wash water rate. The smaller particles tend to be entrained into the froth rather than floated, and so are washed from the froth at higher wash water rates.

Generally it was found that the parameters which led to an increase in the mean residence time led to a decrease in the degree of mixing. This is a direct result of the fact that the variance of the residence time distribution curve is divided by the mean residence time to obtain the degree of mixing. Parameters which caused a decrease in the concentrate grade increased the concentrate mass pull because as the mass pull increases so does the amount of entrained material in the concentrate.

The batch froth splitting apparatus provided a rapid and simple means by which froth profiles could be investigated. The froth was split into four horizontal segments by the four froth splitting rings. A synthetic pyrite-quartz ore was used to simplify the interpretation of the results. Data on the masses of solids and water, the grade, the recovery, the air hold-up and the particle size was obtained as a function of height in the froth as flotation parameters were varied. The experimental error was found to be less than 6 percent at a 95 percent confidence limit.

The testwork on the pyrite-quartz ore showed that;

- The particle size of the pyrite decreased with decreasing height in the froth indicating that the coarser (> 10 μm) pyrite floated first. There was a slight increase in the particle size of the quartz from the bottom to the top of the froth due to entrapment of the coarser quartz particles.
- The air hold-up increased with increasing height in the froth due to froth drainage.
- The grade decreased with decreasing height in the froth. This was due to both a froth cleaning action and the fact that the pyrite that floated first was found at the top of the froth, and as the pulp became depleted of pyrite more entrainment occurred.
- The pyrite recovery decreased with decreasing height in the froth, but increased again in the bottom segment as a result of the recycling of ultra-fine pyrite (< 10 μm) at the bottom of the froth. This utlra-fine pyrite tend to be entrained, and hence is rejected at the bottom of the froth.
- There was an optimum carbon chain length and collector dosage for the xanthate collectors used in this study. Below this optimum there was a loss of recovery because the slow floating particles were not collected and above this value the froth became tightly packed and unselective.
- There was an optimum frother concentration for each type of frother. Below this value the froth was unstable, and above this value the froth was too tightly packed to be selective.
- Selectivity in the froth decreased as particle size decreased because the froth became tightly packed and entrained particles were trapped in the froth The concentrate mass pull decreased as the particle size increased due to excessive froth drainage and bubble coalescence giving poor recoveries. Also as the particle size in the froth doubles, the number of particles in the froth decreases by a factor of 8. The best grades and recoveries were achieved with a range of particle sizes present because a stable, well drained froth was formed.

- Froth stability decreased as temperature increased due to a decrease in water viscosity as temperature increases. The best grades were thus achieved at high temperatures and the best recoveries at low temperatures.

The continuous froth splitting apparatus worked on the same principle as the batch froth splitting apparatus, but it was fitted to a continuous laboratory column cell. This system was used to obtain froth profiles of steady-state froths for comparison with the batch froth splitting data. Both a synthetic pyrite-quartz ore and a gold ore were tested. Tests were done with and without wash water. The reproducibility of this system was found to be better than that of the batch system.

The trends in the batch and continuous systems with no wash water were generally the same and differences can be ascribed to the depletion of pyrite in the batch system.

It was found that the addition of wash water to the froth resulted in a higher water hold-up in the froth. This led to better elutriation of entrained material from the froth, and a more stable froth zone due to less bubble coalescence. The addition of wash water resulted in a decrease in concentrate mass pull and an increase in concentrate grade, with little change in recovery. The trends from the bottom to the top of the froth were more marked when no wash water was added because more froth drainage and bubble coalescence occurred.

REFERENCES

AHMED, N. and JAMESON, G.S., 1985. *The Effect of Bubble Size on the Flotation of Fine Particles.*, Int. J. Miner. Process., Vol 14, pp 195 - 215.

ALFORD, R.A., BAGULEY, P.J., ARTONE, E. and BIJOK, A., 1991. *The Oracle Ridge Column Flotation Circuit from Concepts to Production.*, Proc. Int. Conf. Column Flot., Sudbury, Ontario, Canada, Vol. 1, pp 123 - 136.

AMELUNXEN, R.L., LLERENA, R. DUNSTAN, P. and HULS, B., 1988. *Mechanics of Column Flotation Operation.*, Proc. Int. Column Symp., Phoenix, Arizona, Chapter 16, pp 149 - 156.

AMELUNXEN, R.L., 1991. *Lip Loading Considerations in Flotation Columns.*, Proc. Int. Conf. Column Flot., Sudbury, Ontario, Canada, Vol. 2, pp 661 - 672.

ANFRUNS, J.P. and KITCHENER, J.A., 1976. *The Absolute Rate of Capture of Single Particles by Single Bubbles.*, In M.C. Fuerstenau (Editor), Flotation, A M Gaudin Memorial Volume, AIME, New York, N.Y., Vol. 2, pp 632.

ARBITER, N. and HARRIS, C.C., 1962. *Flotation Kinetics.*, In: D.W. Fuerstenau (Ed.) Froth Flotation., 50th Anniversary Volume, AIME., New York, pp 215 - 262.

BAHR, A., LÜDKE, H. and MEHRHOFF, F.W., 1982. *The development and Introduction of a New Coal Flotation Cell.*, CIM XIV Int. Miner. Process. Cong., Toronto, Canada, October 17 - 23, pp VII-5.1 - VII-5.4.

BAIRD, M.H.I. and RICE, R.G., 1975. *Axial Dispersion in Large Unbaffled Columns.*, Chem. Engng. J., Vol. 9, pp 171 - 174.

BALL, B. and FUERSTENAU, D.W., 1974. *The Determination of Rate Constants from Semi-Batch Flotation Tests.*, Quart. Colorado School of Mines, Vol. 69, pp 27 - 40.

BARKER, L.M., 1986. *The Effect of Electrolytes on the Flotation of Pyrite.*, MSc Thesis, University of Cape Town, Cape Town, South Africa.

BASCUR, A.D. and HERBST, J.A., 1982. *Dynamic Modelling of a Flotation Cell with a View Toward Automatic Control.*, CIM. XIV Int. Min. Process. Cong., Oct. 17 - 23, Toronto, Canada, pp III-11.1 - III-11.22.

BEAUMONT, E., McDONALD, G., CONTINI, N. and WELLS, J., 1991. *The Commissioning and Operation of Two 3.6 Metre Diameter Columns for Zinc Cleaning at the Faro Concentrator.*, Proc. Int. Conf. Column Flot., Sudbury, Ontario, Canada, Vol. 2, pp 539 - 556.

BERGH, L.G. and YIANATOS, J.B., 1991. *Advances in Flotation Column Dynamics and Measurements.*, Proc. Int. Conf. Column Flot., Sudbury, Ontario, Canada, Vol. 2, pp 409 - 422.

BISCHOFF, K.B. and LEVENSPIEL, O., 1962. *Fluid Dispersion-Generalisation and Comparison of Mathematical Models - I. Generalisation of Models.*, Chem. Engng. Sci., Vol. 17, pp 245 - 255.

BISSHOP, J.P. and WHITE, M.E., 1976. *Study of Particle entrainment in Flotation Froths.*, Trans. Inst. Min. Metall. Section C., Vol. 85, pp C191 - C194.

BOLIN, N.J. and SÖDERBERG, L., 1991. *Experience from Installations of Column Flotation in Sweden.*, Proc. Int. Conf. Column Flot., Sudbury, Ontario, Canada, Vol. 2, pp 573 - 584.

BOUTIN, P. and WHEELER, D.A., 1988. *Column Flotation.*, Mining World, Vol. 20, No. 3, pp 47 - 50.

BOX, G.E.P. and DRAPER, N.R., 1987. *Empirical Model Building and Response Surfaces.*, Wiley, New York, New York, Chap 3, pp 34 - 103.

BROMLEY, E.H., EGAN, J.R. and SHARP, G.R., 1991. *Column Flotation at Cominco.*, Proc. Int. Conf. Column Flot., Sudbury, Ontario, Canada, Vol. 2, pp 585 - 594.

BRYSON, A.W., 1970. *Non-Ideal Flow Models and Pulse Testing.*, Unpublished Report, University of the Witwatersrand, Johannesburg, South Africa.

BUFFHAM, B.A. and GIBILARO, L.G., 1968. *A Generalization of the Tanks-in-Series Mixing Model.,* AIChE Journal, Vol. 14, No. 5, pp 805 - 806.

BURGER, A.J., 1989. *A Model for the Evaluation of the Composition of the Pulp Phase in a Flotation Column.*, S. Afr. Instn. Min. Metall. Int. Colloq.: Developments in Froth Flotation., Gordon's Bay, Cape Town., Vol. 2.

BURGER, A.J., 1991. *The Performance of a Flotation Column in the Recovery of Gold and Pyrite from Backfill Material.*, Proc. Int. Conf. Column Flot., Sudbury, Ontario, Canada, Vol. 2, pp 595 - 608.

BUSHELL, C.H.G., 1962. *Kinetics of Flotation.*, Trans. AIME., Vol. 233, pp 226 - 273.

CASTILLO, D.I. and DOBBY, G.S., 1991. *Simulation of Flotation Column Circuits.*, Proc. Int. Conf. Column Flot., Sudbury, Ontario, Canada, Vol. 1, pp 109 - 122.

CHOWDHURY, S., FLEMMING, I.T.R., FRANCIS, A.D. and TEMBO, E., 1991. *Development of Column Flotation at the Nchanga Concentrator of Zambia Consolidated Copper Mines Limited.*, Proc. Int. Conf. Column Flot., Sudbury, Ontario, Canada, Vol. 2, pp 495 - 510.

CLIFT, R., 1991. *Private Communication,* University of Surrey, Guildford, England.

CLINGAN, B.V. and McGREGOR, D.R., 1987. *Column Flotation Experience at Magma Copper Company, with Related Experience of Other Mineral Processors.*, 116th Annual AIME-SME Meeting, Denver Colorado, February.

CONTINI, N.J., WILSON, S.W. and DOBBY, G.S., 1988. *Measurement of Rate Data in Flotation Columns.*, Proc. Int. Column Symp., Phoenix, Arizona, Chap. 10, pp 81 - 90.

COVA, D.R., 1966. *Catalyst Suspension in Gas Agitated Tubular Reactors.*, I&EC Proc. Design Dev., Vol 5, pp 20.

CUTTING, G.W. and DEVENISH, M., 1975. *A Steady-State Model of Froth Flotation Structures.*, SME Annual Meeting, New York, Preprint No. 75-B-56.

CUTTING, G.W., WATSON, D., WHITEHEAD, A. and BARBER, S.P., 1981. *Froth Structure in Continuous Flotation Cells: Relation to the Prediction of Plant Performance from Laboratory Data using Process Models.*, Int. J. Miner. Process., Vol. 7, pp 347 - 369.

CUTTING, G.W., BARBER, S.P. and WATSON, D., 1982. *Prediction of Flotation Plant Performance from Batch Tests Using Process models: Effect of Froth Structure.*, CIM. XIV Int. Min. Proc. Congr., Oct. 17 - 23, Toronto, Canada, pp IV-14.1 - IV-14.20.

CUTTING, G.W., BARBER, S.P. and NEWTON, S., 1986. *Effects of Froth Structure and Mobility on Performance and Simulation of Continuously Operated Flotation Cells.*, Int. J. Miner. Process., Vol. 16, pp 43 - 61.

DAVIDSON, J.F. and SCHULER, B.O.G., 1960a. *Bubble Formation at an Orifice in an Inviscid Liquid.*, Trans. Inst. Chem. Engnrs., Vol. 38, pp 144.

DAVIDSON, J.F. and SCHULER, B.O.G., 1960b. *Bubble Formation at an Orifice in an Viscous Liquid.*, Trans. Inst. Chem. Engnrs., Vol. 38, pp 335.

DECKWER, W.-D. and SCHUMPE, 1987. *Bubble Columns - the State of the Art and Current Trends.*, Int. Chem. Eng., Vol. 27, No. 3, pp 405 - 422.

DEGNER, V.R. and SABEY, J.B., 1988. *WEMCO/Leads Flotation Column Development.*, Proc. Int. Column Symp., Phoenix, Arizona, Chapter 29, pp 267 - 281.

DEL VILLAR, R., FINCH, J.A., YIANATOS, J.B. and LAPLANTE, A.R., 1988. *Column Flotation Simulation.*, Computer Applications in the Mineral Industry, K. Fytas, J.L. Collins and R. Singhal (Eds.), Balkema, Rotterdam, pp 233 - 239.

DEL VILLAR, R., SOTO, H. and LACOMBE, P., 1991. *Column Flotation Circuit Design at Les Mines Selbaie.*, Proc. Int. Conf. Column Flot., Sudbury, Ontario, Canada, Vol. 1, pp 149 - 164.

DERJAGUIN, B.V. and DUKHIN, S.S., 1961. *Theory of Flotation of Small and Medium Size Particles.*, Trans. IMM, Vol 70, pp 221 - 246.

DIMOU, A., 1986. *The Flotation of Pyrite Using Xanthate Collectors.*, MSc Thesis, University of Cape Town, Cape Town, South Africa.

DIPPENAAR, A., 1982a. *The destabilization of froth by solids: 1. The Mechanism of Film Rupture.*, Int. J. Miner. Process., Vol. 9, pp 1 - 14.

DIPPENAAR, A., 1982b. *The destabilization of froth by solids: 2. The Rate-Determining Step.*, Int. J. Miner. Process., Vol. 9, pp 15 - 27.

DOBBY, G.S. and FINCH, J.A., 1985. *Mixing Characteristics of Industrial Flotation Columns.*, Chem Engng. Sci., Vol. 40(7), pp 1061 - 1068.

DOBBY, G.S. and FINCH, J.A., 1986a. *Particle Collection in Columns - Gas Rate and Particle Size Effects.*, Can. Metall. Q., 25(1), pp 9 - 13.

DOBBY, G.S. and FINCH, J.A., 1986b. *Flotation Column Scale-Up and Modelling.*, CIM Bulletin, May, pp 89 - 96.

DOBBY, G.S. and FINCH, J.A., 1987. *Particle Size Dependence in Flotation Derived from a Fundamental Model of the Capture Process.*, Int. J. Miner. Process., Vol. 21, pp 241 - 260.

DOBBY, G.S., YIANATOS, J.B. and FINCH, J.A., 1989. *Estimation of Bubble Diameter in Flotation Columns from Drift Flux Analysis.*, Can. Metall. Quart., Vol. 27(2), pp 85 - 90.

DUNNE, R.C., FORBES, A.W., HARRIS, P.J., HULSE, N.D., and MOYS, M.H., 1976. *The Measurement of Bubble Size Distributions in Flotation Pulps.*, MINTEK Tech. Mem. No. 14032, Randburg.

EGAN, J.R., FAIRWEATHER, M.J. and MEEKEL, 1988. *Application of Column Flotation to Lead and Zinc Beneficiation at Cominco.*, Proc. Int. Column Symp., Phoenix, Arizona, Chapter 4, pp 19 - 26.

EISSA, S.H., EL-HALWAGI, M.M. and SALEH, M.A., 1971. *Axial and Radial Mixing in a Cocurrent Bubble Column.*, Ind. Eng. Chem. Process Des. Develop., Vol. 10, No. 1, pp 31 - 36.

ESPINOSA-GOMEZ, R., 1987. *Recovery of Pyrochlore from Slimes Discarded at Niobec by Column Flotation.*, PhD Thesis, McGill University, Montreal, Canada.

ESPINOSA-GOMEZ, R., YIANATOS, J.B., FINCH, J.A. and JOHNSON, N.W., 1988. *Carrying Capacity Limitations in Flotation Columns.*, Proc. Int. Column Symp., Phoenix, Arizona, Chapter 15, pp 143 - 148.

ESPINOSA-GOMEZ, R. and JOHNSON, N.W., 1991. *Technical Experiences with Conventional Columns at Mount Isa Mines Limited.*, Proc. Int. Conf. Column Flot., Sudbury, Ontario, Canada, Vol. 2, pp 511 - 524.

EWERS, W.E., 1984. *A Retrospective View of Flotation.*, In: M.H. Jones and J.T. Woodcock (Editors), Principles of Mineral Flotation, Australasian Inst. Min. Metall. Symp. Ser., No. 40, Melbourne, pp 57 - 64.

FAIRWEATHER, and EGAN, 1991. *Froth Phase Mixing by Multi-Point Temperature Analysis in Industrial Flotation Columns.*, Proc. Int. Conf. Column Flot., Sudbury, Onterio, Canada, Vol. 1, 235 - 260

FALUTSU, M. and DOBBY, G.S., 1989. *Direct Measurement of Froth Drop Back and Collection Zone Recovery in a Laboratory Flotation Column.*, Miner. Engng., Vol. 2, No. 3, pp 377 -386.

FINCH, J.A. and DOBBY, G.S., 1990. *Column Flotation.*, Pergamon Press, 1st Edition, Oxford.

FLINT, L.R. and HOWART, W.J., 1971. *The Collection Efficiency of Small Particles with Spherical Air Bubbles.*, Chem. Engng. Sci., Vol. 26, pp 1155 - 1168.

FLYNN, S.A. and WOODBURN, E.T., 1987. *An Ultra-Fine Froth Model for the Selective Separation of Ultra-Fine Coal from Mineral in a Dispersed Air Flotation Cell.*, Powder Technology, Vol. 49, No. 2, pp 127 - 142.

FORD, M.A. and KING, R.P., 1983. *The Simulation of Ore Dressing Plants.*, Int. J. Miner. Process., Vol. 12, pp 285 - 304.

FRANZIDIS, J.-P., HARRIS, M.C. and O'CONNOR, C.T., 1991. *Review of Column Flotation Practice on South African Mines.*, Proc. Int. Conf. Column Flot., Sudbury, Ontario, Canada, Vol. 2, pp 479 - 495.

FREW, J.A. and TRAHAR, W.J., 1982. *Roughing and Cleaning Flotation Behaviour and the Realistic Simulation of Complete Plant Performance.*, Int. J. Miner. Process., Vol. 9, pp 101 - 120.

FUERSTENAU, M.C., 1882. *Sulphide Mineral Flotation.*, In P.R. King (Editor), Principles of Flotation., S. Afr. Instn. Min. Metall. Monogr. Ser., No. 3, pp 159 - 182.

FUREY, J.T. and MOON, K.S., 1991. *Unit Column Flotation.*, Proc. Int. Conf. Column Flot., Sudbury, Ontario, Canada, Vol. 1, pp 15 - 30.

GLASSER, D., BRYSON, A.W. and KARSTAEDT, N.E., 1980. *The numerical inversion of the Laplace Transform by its Reduction to a Fourier Series.*, Unpublished Report, University of the Witwatersrand, Johannesburg, South Africa.

GOODALL, C.M. and O'CONNOR, C.T., 1989. *Residence Time Distribution Studies of the Solid and Liquid Phases in a Laboratory Column Flotation Cell.*, S. Afr. Instn. Min. Metall. Int. Colloq.: Developments in Froth Flotation., Gordon's Bay, Cape Town., Vol. 2.

GOODALL, C.M. and O'CONNOR, C.T., 1991. *Residence Time Distribution Studies in a Flotation Column. Part 1: The Modelling of Residence Time Distributions in a Laboratory Column Flotation Cell.*, Int. J. Miner Process., Vol. 31, pp 97 - 113.

GORZITZKE, W.G. and MACPHAIL, N.G., 1989. *Pneumatic Flotation of Some South African Coals.*, S. Afr. Instn. Min. Metall. Int. Colloq.: Developments in Froth Flotation., Gordon's Bay, Cape Town., Vol. 2.

GREAVES, M. and ALLEN, B.W., 1974. *Steady-State and Dynamic Characteristics of Flotation in a Single Cell.*, Trans. Inst. Chem. Eng., Vol. 52, pp 136 - 148.

GREEN, J.C.A., 1984. *The Optimisation of Flotation Networks.*, Int. J. Miner. Process., Vol. 13, pp 83 - 103.

GÜNEY, A., ÖNAL, G. and DOGAN, M.Z., 1991. *Beneficiation of Üçköprü Chromite Gravity Tailings by Free Jet Type Flotation System.*, Proc. Int. Conf. Column Flot., Sudbury, Ontario, Canada, Vol. 2, pp 609 - 618.

HANSFORD, G.S., LEVY, C.D. and DE KOCK, J.W., 1976. *Rheological Measurements on the Pulps from South African Gold Mines.*, J. S. Afr. Instn. Min. Metall., Vol. 76, pp 363 - 369.

HARRIS, C.C. and RIMMER, H.W., 1966. *Study of a Two-Phase Model of the Flotation Process.*, Trans. Inst. Min. Metall. Section C, Vol. 75, pp C153 - C162.

HARRIS, C.C., 1976. *A Recycle Flow Flotation Machine Model: Response of Model to Parameter Changes.*, Int. J. Miner. Process., Vol. 3, pp 9 - 25.

HARRIS, M.C. and FRANZIDIS, J.-P., 1989. *Flotation Trials at Rooiberg Tin Mine Using a Portable Column Cell.*, S. Afr. Instn. Min. Metall. Int. Colloq.: Developments in Froth Flotation., Gordon's Bay, Cape Town., Vol. 2.

HARRIS, P.J., 1992. *Private Communication.*, Mintek, Randburg, South Africa

HIRAJIMA, T., TAKAMORI, T., TSUNEKAWA, M., MATSUBARA, T., OSHIMA, K., IMAI, SAWAKI, K. and KUBO, S., 1991. *The Application of Fuzzy Logic to Control Concentrate Grade in Column Flotation at Toyoha Mines.*, Proc. Int. Conf. Column Flot., Sudbury, Ontario, Canada, Vol. 2, pp 375 - 390.

HOH, Y.C, CHUNG, W.Y. and WANG, W.K., 1986. *Interfacial Tension Studies on the Extraction of Lanthanum by D2EHPA.*, Hydrometallurgy, Vol. 15(3), pp 381 - 390.

HULS, B.J., HYMA, D.B., DOBBY, G.S. and LACHANCE, C.D., 1991. *Scaleup and Installation of Flotation Columns at Falconbridge Ltd.*, Proc. Int. Conf. Column Flot., Sudbury, Ontario, Canada, Vol. 1, pp 119 - 210.

IMAFUKU, K., WANG, T., KOIDE, K. and KUBOTA, H., 1968. *Behaviour of Suspended Solid Particles in the Bubble Column.*, Jap. Chem. Engng. J., Vol. 2, pp 153 -158.

JAMESON, G.J., 1984. *Physics and Hydrodynamics of Bubbles.*, In: The Scientific Basis of Flotation., K.J. Ives (Editor), Martinus Nijhoff Publishers, The Hague, pp 53 - 78.

JAMESON, G.J., 1988. *A New Concept in Flotation Column Design.*, Proc. Int. Column Symp., Phoenix, Arizona, Chapter 30, pp 281 - 286.

JIANG, E.W. and HOLTHAM, P.N., 1986. *Theoretical Model of Collision Between Particles and Bubbles in Flotation.*, Trans. Inst. Min. Metall. Section C, Vol. 9b, pp C187.

JOSHI, J.B. and SHARMA, M.M., *1979. A Circulation Cell Model for Bubble Columns.*, Trans. IChemE., Vol. 57, pp 244 - 251.

JOSHI, J.B., 1980. *Axial Mixing in Multi-Phase Contactors - A Unified Correlation.*, Trans. IChemE., Vol. 58, pp 155 - 165.

JOWETT, A., 1966. *Gangue Mineral Contamination of Froth.*, Brit. Chem. Eng., Vol. 2, pp 330 - 333.

JOWETT, A., 1980. *Formation and Disruption of Particle-Bubble Agglomerates in Flotation.*, P. Somasundaran (Editor), Fine Particle Processing Int. Symp., AIME, Vol. 1, Chap. 37, New York.

KING, R.P., TE RIELE, W.A.M. and BUCHALTER, E., 1970. *An Improved Distribution Parameter Model for Flotation Kinetics of Mineral Flotation.*, National Institute of Metall. Report No. 966., Johannesburg, South Africa.

KING, R.P., 1975. *Simulation of Flotation Plants.*, Trans. Soc. Min. Eng., AIME., Vol. 258, pp 286 - 293.

KING, R.P., 1982. *Flotation of Fine Particles.*, In R.P. King (Editor), Principles of Flotation., S. Afr. Inst. Min. Metall. Monogr. Ser., No. 3,pp 215 - 225.

KIRCHBERG, H. and TOPPER, E., 1964. *The Mineralisation of Air Bubbles in Flotation.*, 7th Int. Min. Proc. Congress.

KOSICK, G.A., DOBBY, G.S. and YOUNG, P.D., 1991. *ColumnEX: A Powerful and Affordable Control System for Column Flotation.*, Proc. Int. Conf. Column Flot., Sudbury, Ontario, Canada, Vol. 2, pp 359 - 375.

KRAMERS, H. and ALBERDA, G., 1953. *Frequency Response Analysis in Continuous Flow Systems.*, Chem. Engng. Sci., Vol. 2, pp 173.

LAOHAPANIT, R., LAPLANTE, A.R. and BOULET, A., 1991. *Column Flotation Testwork at Les Mines Camchib Inc., Chibougamau, Quebec.*, Proc. Int. Conf. Column Flot., Sudbury, Ontario, Canada, Vol. 1, pp 181 - 198.

LAPLANTE, A.R., YIANATOS, J. and FINCH, J.A., 1988. *On the Mixing Characteristics of the Collection Zone in Flotation Columns.*, Proc. Int. Column Symp., Phoenix, Arizona, Chapter 9, pp 69 - 79.

LEE, K.Y., PATE, W.T., OBLAD, A.E. and HERBST, J.A., 1991. *Methodology for Selecting a Control Strategy for a Column Flotation Unit.*, Proc. Int. Conf. Column Flot., Sudbury, Ontario, Canada, Vol. 2, 423 - 436

LEJA, J., 1982a., *Flotation Froths and Foams.*, Surface Chemistry of Froth Flotation., Plenum Press, New York, N.Y., Chap 9, pp 549 - 609.

LEJA, J., 1982b., *Flotation Surfactants.*, Surface Chemistry of Froth Flotation., Plenum Press, New York, N.Y., Chap 5, pp 205 - 340.

LEJA, J. and HE, B.Q., 1984. *The Role of Flotation Frothers in the Particle-Bubble Attachment Process.*, In: M.H. Jones and J.T. Woodcock (Editors), Principles of Mineral Flotation, Australasian Inst. Min. Metall. Symp. Ser., No. 40, Melbourne.

LEVENSPIEL, O., 1961. *Comparison of the Tanks-in-Series and the Dispersion Model for Non-Ideal Flow.*, Chem. Engng. Sci., Vol 16, pp 576 - 577.

LEVENSPIEL, O., 1972. *Non-Ideal Flow.*, Chemical Reaction Engineering., 2nd Ed., Wiley, New York, N.Y., Chap. 9, pp 253 - 315.

LEVENSPIEL, O., 1979. *The Chemical Reactor Omnibook.*, OSU Book Stores Inc., Corvallis, Oregon, pp 61-1 - 66-9.

LIVSHITZ, A.K. and DUDENKOV, S.V., 1965. *Some Factors in Flotation Froth Stability.*, Proc. VIII Int. Min. Proc. Conf., New York, N.Y., pp 367 - 371

LUTTRELL, G.H., WEBER, A.T., ADEL, G.T. and YOON, R.H., 1988. *Microbubble Flotation of Fine Coal.*, Proc. Int. Column Symp., Phoenix, Arizona, Chapter 21, pp 205 - 212.

LYNCH, A.J., JOHNSON, N.W., McKEE, D.J. and THORNE, G.C., 1974. *The Behaviour of Minerals in Sulphide Flotation Processes with Special Reference to Simulation and Control.*, J. S. Afr. Inst. Min. Metall., Vol. 74, pp 349 - 361.

MARSDEN, D.D., 1962. *The Effect of pH, Temperature and Density on The Kinematic Viscosity of some South African Mine Pulps.*, J. S. Afr. Instn. Min. Metall., Vol 62, pp 391 - 398.

MAVROS, P., LAZARIDIS, N.K., and MATIS, K.A., 1989. *A Study and Modelling of Liquid-Phase Mixing in a Flotation Column.*, Int. J. Miner. Process., Vol. 26, pp 1 - 16.

McKAY, J.D., FOOT, D.G. and SHIRTS, M.B., 1988. *Column Flotation and Bubble Generation Studies at the Bureau of Mines.*, Proc. Int. Column Symp., Phoenix, Arizona, Chapter 18, pp 173 - 186.

MEYER, W.C., and KLIMPEL, R.R., 1982. *Rate Limitations in Froth Flotation.* SME Annual Meeting, Dallas, Texas, Feb. 14 - 18, SME Preprint No. 82-35.

MIKA, T.S. and FUERSTENAU, D.W., 1969. A *Microscopic Model of the Flotation Process.*, 8th Int. Miner. Process. Cong., Institute Mekhanobre, Lenningrad, pp 246 - 269.

MILLER, R.S., 1985. *Photographic Observations of Bubble Formation in Flashing Nozzle Flow.*, Trans. ASME, Vol. 107, pp 750 - 755.

MILLS, P.J. and O'CONNOR, C.T., 1990. *The Modelling of Liquid and Solids Mixing in a Flotation Column.*, Miner. Engng. Vol. 3, No. 6, pp 567 - 576.

MILLS, P.J.T., YIANATOS, J.B. and O'CONNOR, C.T., 1992. *The Mixing Characteristics of Solid and Liquid Phases in a Flotation Column.*, Miner. Engng., Vol 5, No 10 - 12.

MISZCZAK, J., 1987. *Private Communication.*, McGill University, Montreal, Canada.

MOON, K.S. and SIROIS, L.L., 1988. *Theory and Industrial Application of Column Flotation in Canada.*, Proc. Int. Column Symp., Phoenix, Arizona, Chapter 11, pp 91 - 102.

MOONEY, J., 1951. *The Viscosity of a Concentrated Suspension of Spherical Particles.*, J. Colloid Sci., Vol. 6, pp 162 - 170.

MORIZOT, G., SAVE, M., CONIL, P. and McKAY, J., 1991. *Shrinkage of Roughing and Cleaning Stage with Column Flotation: The Chessy Case.*, Proc. Int. Conf. Column Flot., Sudbury, Ontario, Canada, Vol. 1, pp 75 - 88.

MOYS, M. H. 1978. *A Study of a Plug Flow Model for Flotation Froth Behaviour.*, Int. J. Miner. Process., Vol. 5, pp 21 - 38.

MOYS, M. H., 1979. *A Study of Processes Occuring in Flotation Froths.*, PhD Thesis, University of Natal, Durban, South Africa.

MOYS, M. H. 1984. *Residence Time Distributions and Mass Transport in the Froth Phase of the Flotation Process.*, Int. J. Miner. Process., Vol. 13, pp 117 - 142.

MOYS, M.H. and FINCH., J.A., 1988. *The Measurement and Control of Level in Flotation Columns.*, Proc. Int. Column Symp., Phoenix, Arizona, Chap. 12, pp 103 - 112.

MOYS, M.H., 1989. *Further Developments in the Control of Level in Flotation Columns.*, S. Afr. Instn. Min. Metall. Int. Colloq.: Developments in Froth Flotation., Gordon's Bay, Cape Town., Vol. 2.

MOYS, M.H., ENGELBRECHT, J.A., and TERBLANCHE, N., 1991. *The Design of Baffles to Reduce Axial Mixing in Flotation Columns.*, Proc. Int. Conf. Column Flot., Sudbury, Ontario, Canada, Vol. 1, pp 275 - 288.

MULAR, A.L. and MUSARA, W.T., 1991. *A Batch Flotation Column for Rate Data Measurement.*, Proc. Int. Conf. Column Flot., Sudbury, Ontario, Canada, Vol. 1, pp 63 - 74.

NARASIMHAN, K.S., SINGH, R.N., BHATIA, R.K. and MADHUSUDHANAN, K., 1988. *Column Flotation for Fine Coal Recovery in India - A Techno Economic Assessment.*, Proc. Int. Column Symp., Phoenix, Arizona, Chapter 26, pp 243 - 248.

NELDER, J.A. and MEAD, R., 1965. *A Stepwise Non-Derivative Hill-Climbing Algorithm.*, Computer J., Vol. 7, pp 308 - 313.

NICOL, S.K., ROBERTS, T., BENSLEY, C.N., KIDD, G.W. and LAMB, R., 1988. *Column Flotation of Ultrafine Coal: Experience at BHP-Utah Coal Limited's Riverside Mine.*, Proc. Int. Column Symp., Phoenix, Arizona, Chapter 2, pp 7 - 12.

NORTON, J., 1991. *Private Communication.*, Pering Mine, Reivelo, South Africa.

O'CONNOR, C.T., 1991. *Private Communication.*, University of Cape Town, Cape Town, South Africa.

OHKI, Y. and INOUE, H., 1970. *Longditudinal Mixing of the Liquid Phase in Bubble Columns.*, Chem. Engng. Sci., Vol. 25, pp 1 - 16.

OLIVEIRA, M.L.M. and PERES, A.E.C., 1991. *Column Flotation Applied to Brazilian Coal.*, Proc. Int. Conf. Column Flot., Sudbury, Ontario, Canada, Vol. 1, pp 3 - 14.

OLSEN, T. and MEIK, S., 1991. *The Oracle Ridge Column Flotation Circuit from Concepts to Production.*, Proc. Int. Conf. Column Flot., Sudbury, Ontario, Canada, Vol. , pp 137 - 148.

OUNPUU, M. and TREMBLAY, R., 1991. *Investigation into the Effect of Column Height on the 1200 mm Diameter Column at Matagami.*, Proc. Int. Conf. Column Flot., Sudbury, Ontario, Canada, Vol. 1, pp 313 - 316.

PAL, R. and MASLIYAH, J., 1990. *Flow in Froth Zone of A Flotation Column.*, Can. Metall. Quart., Vol. 29, No. 2, pp 97 - 103.

PAREKH, B.K., GROPPO, J.G., STOTTS, W.F. and BLAND, A.E., 1988. *Recovery of Fine Coal from Preparation Plant Refuse Using Column Flotation.*, Proc. Int. Column Symp., Phoenix, Arizona, Chap. 24, pp 227 - 234.

PRYOR, E.J., 1965. *Mineral Processing.*, Elsevier, Amsterdam, 3rd ed., pp 501 - 503.

RANDALL, E.W., GOODALL, C.M., FAIRLAMB, P.M., DOLD, P.L. and O'CONNOR, C.T., 1988. *A Method of Determining the Sizes of Bubbles in Two- and Three-Phase Systems.*, J. Phys. E. Sci. Instrum., Vol. 22, pp 827 - 833.

REIS, J.B. and PERES, A.E.C., 1991. *Industrial Application of Flotation Columns in the Concentration of a Sulphide Ore at Mineração Manati Ltda. - Brazil.*, Proc. Int. Conf. Column Flot., Sudbury, Ontario, Canada, Vol. 2, pp 525 - 538.

REITH, T. RENKEN, S. and ISRAEL, B.A., 1968, *Gas Hold-Up and Axial Mixing in the Fluid Phase of Bubble Columns.*, Chem. Engng. Sci., Vol. 23, pp 619 - 629.

RIQUARTS, H.P., 1981. *Fluid Mechanical Modelling of Bubble Column Reactors.*, Ger. Chem. Eng., Vol. 4, pp 18.

ROSS, V.E., 1988. *Mass Transport in Flotation Froths.*, PhD Thesis, University of Stellenbosch, Stellenbosch, South Africa.

ROSS, V.E. and VAN DEVENTER, J.S.J., 1988. *Mass Transport in Flotation Column Froths.*, Proc. Int. Column Symp., Phoenix, Arizona, Chap. 14, pp 129 - 140.

SADA, E., YASUMISHI, A., KATOH, S. and NISHIOKA, M., 1978. *Bubble Formation in a .Flowing Liquid.*, Can. J. Chem. Engng., Vol. 56, pp 669 - 672.

SADLER, L.Y., 1973. *Dynamic Response of Continuous Mechanical Froth Flotation Cell.*, Trans. Soc. Min. Eng., AIME., Vol 254, pp 336 - 342.

SALAMA, A.I.A, MIKHAIL, M.W., ZHOU, G. and HYMA, D., 1991. *The Role of Computer Controlled Column Flotation In Fine Coal Recovery Optimization.*, Proc. Int. Conf. Column Flot., Sudbury, Ontario, Canada, Vol. 2, pp 455 - 466.

SANCHEZ-PINO, S.E. and MOYS, M.H., 1991. Characterisation of a Co-Current Downwards Flotation Column., Proc. Int. Conf. Column Flot., Sudbury, Ontario, Canada, Vol. 1, pp 341 - 356.

SANDVIK, K.L., NYBO, A.S. and RUSHFELDT, O., 1991. *Reverse Flotation to Low Impurity Levels.*, Proc. Int. Conf. Column Flot., Sudbury, Ontario, Canada, Vol. 1, pp 317 - 326.

SASTRY, K.V.S. and FUERSTENAU, D.W., 1970. *Theoretical Analysis of a Counter-Current Flotation Column.*, Trans. SME-AIME, Vol. 247, pp 46 - 52.

SASTRY, K.V.S. and LOFFTUS, K., 1988. *Mathematical Modelling and Computer Simulation of Column Flotation.*, Proc. Int. Column Symp., Phoenix, Arizona, Chap. 8, pp 57 - 68.

SCHOMMARZ, K.H., 1991. *The Design of a Column Cell to Beneficiate Pyrite.*, MSc Thesis, University of Cape Town, Cape Town, South Africa.

SCHULZE, H.J., 1977. *New Theoretical and Experimental Investigations on Stability of Bubble-Particle Agglomerates in Flotation: A Theory on the Upper Particle Size of Floatability.*, Int. J. Miner. Process., Vol. 4, pp 241 - 259.

SCHNEIDER, J.C. and VAN WEERT, G., 1988. *Design and Operation of the Hydrochem Flotation Column.*, Proc. Int. Column Symp., Phoenix, Arizona, Chapter 31, pp 287 - 292.

SMITH, C.A., 1984. *Dynamic simulation of Sulphide Flotation Circuits.*, PhD Thesis, University of Queensland, Australia.

SMITH, S., 1989. *Private Communication.*, Atomic Energy Corporation, Pelendaba, South Africa.

SMITHSON, E.P., JOHN, C.I.A., REA, T.E. and MWENYA, W.M., 1991. *Improving Concentrate Quality in the Concentrators of Zambia Consolidated Copper Mines Limited Using Column Cells.*, Proc. Int. Conf. Column Flot., Sudbury, Ontario, Canada, Vol. 2, pp 557 - 572.

SUBRAMANIAN, K.N., CONNELLY, D.E.G., and WONG, K.Y., 1988. *Commercialization of a Column Flotation Circuit for Gold Sulphide Ore.*, Proc. Int. Column Symp., Phoenix, Arizona, Chapter 3, pp 13 - 18

SUGANUMA, T. and YAMANISHI, T., 1966. *Behaviour of Solid Particle in Bubble Columns.*, J. Chem. Engng. J., Vol. 30, pp 1136.

SUTHERLAND D.N. and WARK I.K., 1955. *Frothing.*, In: Principles of Flotation, Australasian Inst. Min. Metall., Chapter 18, Melbourne.

SUTHERLAND, D.N., 1977. *An Appreciation of Galena Concentration Using a Steady-State Flotation Model.*, Int. J. Miner. Process., Vol. 4, pp 149 - 162.

TAGGART, A.F., 1921. *Manual of Flotation Processes.*, John Wiley and Sons Inc., New York, Chap 1, pp 1 - 22.

TRAMBOUZE, P., 1960. *Design of a Reactor for Reaction Between Two Liquid Phases.*, Rev. Inst. Franc. Petrole., Vol. 15, pp 1648.

TSUGE, H., TANAKA, Y. and HIBERIO, S., 1981. *Effect of the Physical Properties of Gas on Volume of Bubble Formed from a Single Submerged Orifice.*, Can. J. Chem. Engng., Vol 59., pp 569 - 572.

TUCKER, J.P., FRANZIDIS, J.-P., and O'CONNOR, C.T., 1991. *The Effect of Physical and Chemical Parameters on Bubble Size Distributions in a Cominco Air Sparging Test Rig.*, Proc. Int. Conf. Column Flot., Sudbury, Ontario, Canada, Vol. 1, pp 289 - 312.

UGARTE, P. and REINOSO, J.H., 1991. *Column Flotation Testing For Gold Upgrading in a Very Fine Low Grade Stream.*, Proc. Int. Conf. Column Flot., Sudbury, Ontario, Canada, Vol. 1, pp 31 - 44.

ULBRECHT, J.J. and BAYKARA, Z.S., 1981. *Significance of the Central Plume Velocity for the Correlation of Liquid Phase Mixing in Bubble Columns.*, Chem. Engng. Commum., Vol. 10, pp 619 - 629.

VIANA, P.R.M., SILVA, J.P., RABELO, P.J.B., COELHO, A.G. and SILVA, V.C., 1991. *Column Flotation for the Expansion of the Flotation Circuit at SAMARCO Mineração, Brazil.*, Proc. Int. Conf. Column Flot., Sudbury, Ontario, Canada, Vol. 1, pp 89 - 98.

WATSON, D. and GRAINGER-ALLEN, T.J.N., 1973. *Study of Froth Flotation by Use of a Steady-State Technique.*, Trans. Inst. Min. Metall. Section C, Vol. 82, pp C103 - C105.

WEAST, R.C. and ASTLE, M.J., 1982. *Handbook of Chemistry and Physics.*, Chemical Rubber Company Press Inc., 63rd Ed., Boca Raton, Florida.

WEBBER, C., BHARADWAJ, B. and MOON, K.S., 1991. *Zinc Cleaning Using Column Flotation at Ruttan Operation HBM&S.*, Proc. Int. Conf. Column Flot., Sudbury, Ontario, Canada, Vol. 1, pp 45 - 62.

WEN, C.Y. and FAN, L.T., 1975. *Models for Flow Systems and Chemical Reactors.*, Marcel Dekker Inc., New York, New York, Chap 6., pp 209 - 250.

WHEELER, D.A., 1988. *Historical View of Column Flotation Development.*, Proc. Int. Column Symp., Phoenix, Arizona, Chapter 1, pp 3 - 4.

WILSON, S.W. and STRATTON-CRAWLEY, R., 1991. *Design of Production Scale Flotation Columns Using a First Order Kinetic Model.*, Proc. Int. Conf. Column Flot., Sudbury, Ontario, Canada, Vol. 1, pp 165 - 180.

WOODBURN, E.T., KROPHOLLER, H.W., GREEN, J.C.A. and CRAMER, L.A., 1976. *The Utility and Limitations of Mathematical Modelling in the Prediction of the Properties of Flotation Networks.*, In: M.C. Fuerstenau (Ed.), Flotation., A.M. Gaudin Memorial Volume II, AIME., New York, pp 638 - 674.

WOODBURN, E.T. and WALLIN, P.J., 1984. *Decoupled Kinetic Model for Simulation of Flotation Networks.*, Trans. Inst. Min. Metall. Section C, Vol. 93, pp C153 - C161.

WOODBURN, E.T., STOCKTON, J.B. and ROBBINS, D.J., 1988. *Factors Influencing the Structure of a 3-Phase Coal Flotation Froth.*, Proc. Int. Column Symp., Phoenix, Arizona, Chap. 13, pp 113 - 128.

WOODBURN, E.T., STOCKTON, J.B. and ROBBINS, D.J., 1989. *Vision-Based characterisation of phase froths.*, S. Afr. Instn. Min. Metall. Int. Colloq.: Developments in Froth Flotation., Gordon's Bay, Cape Town., Vol. 1.

XU, M. and FINCH, J.A., 1991a. *Estimating Vessel Dispersion Number in Flotation Column Studies.*, Proc. Int. Conf. Column Flot., Sudbury, Ontario, Canada, Vol. 2, pp 437 - 454.

XU, M. and FINCH, J.A., 1991b. *The Axial Dispersion Model in Flotation Column Studies.*, Miner. Engng., Vol. 4, No. 5/6, pp 553 - 562.

YANG, D.C., 1988. *A New Packed Column Flotation System.*, Proc. Int. Column Symp., Phoenix, Arizona, Chapter 28, pp 257 - 266.

YASUMISHI, A., FUJKUMA, M. and MUROYAMA, K., 1986. *Measurement of Behaviour of Gas Bubbles and Gas Holdup in a Slurry Bubble Column by a Dual Electroresistivity Probe Method.*, J. Chem Engng. J., 19(5), pp 444 - 449

YE, Y., GOPALAKRISHNAN, S., PACQUET, E. and MILLER, J.D., 1988. *Development of the Air-Sparged-Hydrocyclone - A Swirl-Flow Flotation Column.*, Proc. Int. Column Symp., Phoenix, Arizona, Chapter 34, pp 305 - 314.

YIANATOS, J.B., LAPLANTE, A.R. and FINCH, J.A., 1985. *Estimation of Local Holdup in the Bubbling and Froth Zones of a Gas-Liquid Column.*, Chem. Engng. Sci., Vol. 40, No. 10, pp 1965 - 1968.

YIANATOS, J.B., FINCH, J.A. and LAPLANTE, A.R., 1986a. *Holdup Profile and Bubble Size Distribution of Flotation Column Froths.*, Can. Metall. Quart., Vol. 25, No. 1, pp 23 - 29.

YIANATOS, J.B., FINCH, J.A. and LAPLANTE, A.R., 1986b. *Apparent Hindered Settling in a Gas-Liquid-Solid Countercurrent Column.*, Int. J. Miner. Process., Vol. 18, pp 155 - 165.

YIANATOS, J.B., 1987. *Column Flotation Froths.*, PhD Thesis, McGill University, Montreal, Canada.

YIANATOS, J.B., FINCH, J.A. and LAPLANTE, A.R., 1987. *Cleaning Action in Column Flotation Froths.*, Trans. Inst. Min. Metall. Section C, Vol. 96, pp C199 - C205.

YIANATOS, J.B., FINCH, J.A. and LAPLANTE, A.R., 1988a. *Selectivity in Column Flotation Froths.*, Int. J. Miner Process., Vol 23., pp 279 - 292.

YIANATOS, J.B., ESPINOSA-GOMEZ, R., FINCH, J.A., LAPLANTE, A.R. and DOBBY, G.S., 1988b. *Effect of Column Height on Flotation Column Performance.*, Miner. Metall. Process., Feb., pp 11 - 14.

YIANATOS, J.B., 1989. *Column Flotation Modelling and Technology.*, S. Afr. Instn. Min. Metall. Int. Colloq.: Developments in Froth Flotation., Gordon's Bay, Cape Town., Keynote Address.

YIANATOS, J.B. and LEVY, A.R., 1989. *Estimation of Gas Hold-Up, Diameter and Apparent Density of Mineralised Bubbles in Industrial Flotation Columns.,* S. Afr. Instn. Min. Metall. Int. Colloq.: Developments in Froth Flotation., Gordon's Bay, Cape Town., Vol. 2.

YIANATOS, J.B. and FINCH, J.A., 1990. *Gas Hold-Up vs Gas Rate in Bubbly Flow Regime.,* Int. J. Miner. Process., Vol. 29, pp 141 - 146.

YIANATOS, J.B. and BERGH L.G., 1991. *RTD Studies in an Industrial Flotation Column: Use of Radioactive Tracer Technique.*, Proc. Int. Conf. Column Flot., Sudbury, Ontario, Canada, Vol. 1, pp 221 - 234.

YNCHAUSTI, R.A., HERBST, J.A. and HALES, L.B., 1988a. *Unique Problems and Opportunities Associated with Automation of Column Flotation Cells.*, Proc. Int. Column Symp., Phoenix, Arizona, Chap. 5, pp 27 - 34.

YNCHAUSTI, R.A., McKAY, J.D. and FOOT, D.G., 1988b. *Column Flotation Parameters, Their Effects.*, Proc. Int. Column Symp., Phoenix, Arizona, Chap. 17, pp 157 - 172.

YU, S. and FINCH, J.A., 1990. *Froth Zone Recovery in a Flotation Column.*, Can. Metall. Quart., Vol. 29, No. 3., pp 237 - 238.

ZHOU, Z., PLITT, L.R. and EGIERBOR, N.O., 1991. *On Bubble Size Determination in a Flotation Column.*, Proc. Int. Conf. Column Flot., Sudbury, Ontario, Canada, Vol. 1, 249 - 263.

ZIPPERIAN, D.E. and SVENSSON, U., 1988. *Plant Practice of the FLOTAIRE Column Machine for Metallic, Nonmetallic and Coal Flotation.*, Proc. Int. Column Symp., Phoenix, Arizona, Chapter 7, pp 43 - 53.

Appendix 1

BUBBLE SIZING SYSTEM

This hardware can be divided into four main parts: the optical detectors, the detector electronics, the microprocessor system and a personal computer (PC). The signals are obtained as a bubble travelling up the capillary tube passes the detectors. These signals are amplified and squared by the detector electronics and are used to produce a period and a velocity pulse for each bubble. The function of the microprocessor system is to time and store these pulses in memory together with the real time of the event. At the end of the measurement cycle this data is transmitted to the PC. A program on the PC receives these data and stores them in a disc file. The data analysis is described later.

A1.1 OPTICS AND DETECTOR ELECTRONICS

The optical detectors are two LED/photo-transistor pairs. Each detector signal is amplified and squared by the circuit shown in Figure A1.1, and the shapes of these signal are shown in Figure A1.2. The two detector pairs are mounted 5 mm apart in a machined brass block through which the capillary passes. Adjustment screws allow the capillary to be aligned precisely in the optical paths. Capillary tubes with bores ranging from 0.5 to 3 mm have been successfully used to detect bubbles ranging in diameter from 0.5 to 8 mm. To facilitate bubble capture, the end of the capillary is belled out to between 1 and 1.5 times the mean bubble diameter.

The signal voltages obtained at the phototransistor collector depend on the optical characteristics of the slurry or liquid being used, the LED current and the size of the collector resistor. A plot of collector voltage against slurry density is shown in Figure A1.3. The voltages for pure water, air (i.e. bubble) and black (100% opaque medium) are also indicated on the graph. It is interesting to note that water is a better transmitter of light than

the bubble because of the different refractive indices of the water-glass and air-glass boundaries. From Figure A1.4 it is evident that the choice of the correct LED current and collector resistor for the system in question is vital to achieve the biggest collector voltage, and hence the best signals. It can be seen that two-phase systems work best with a low LED current and a small collector resistor, while high LED currents and large collector resistors are best for higher slurry densities.

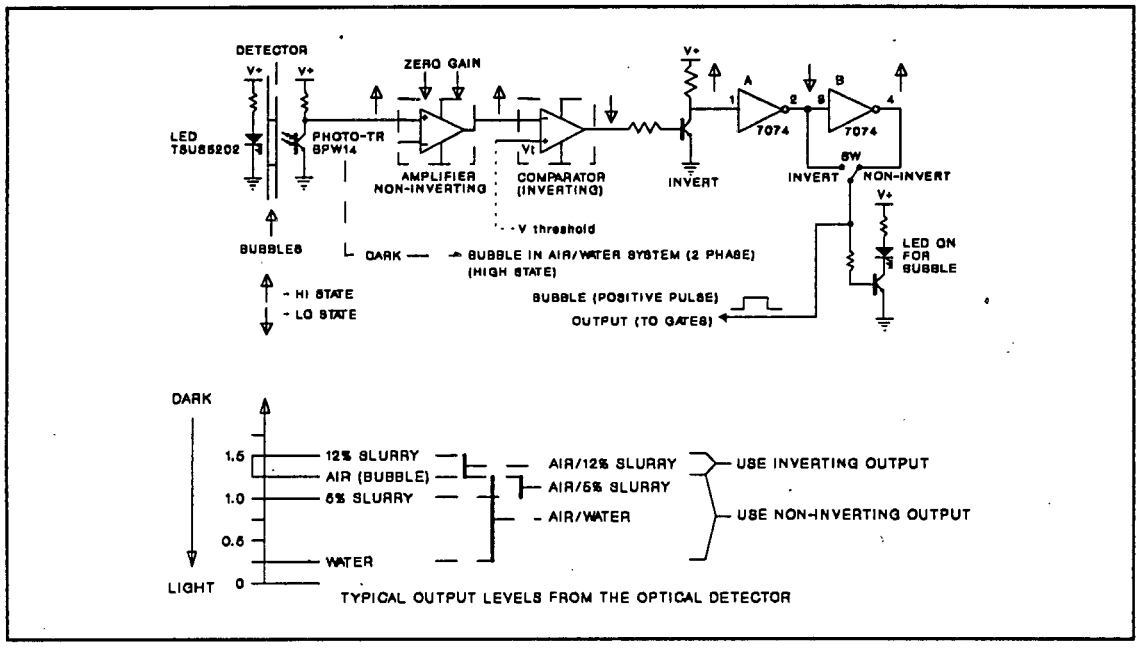

FIGURE A1.1 : Electronic Circuit for Optical Detectors

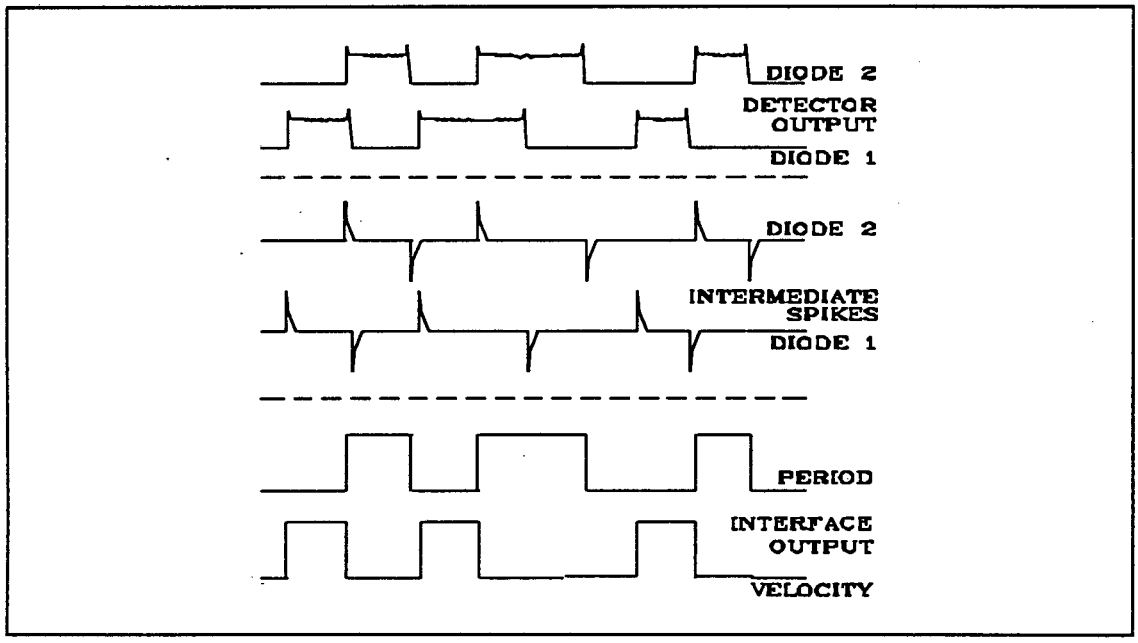

FIGURE A1.2 : Detector Signals

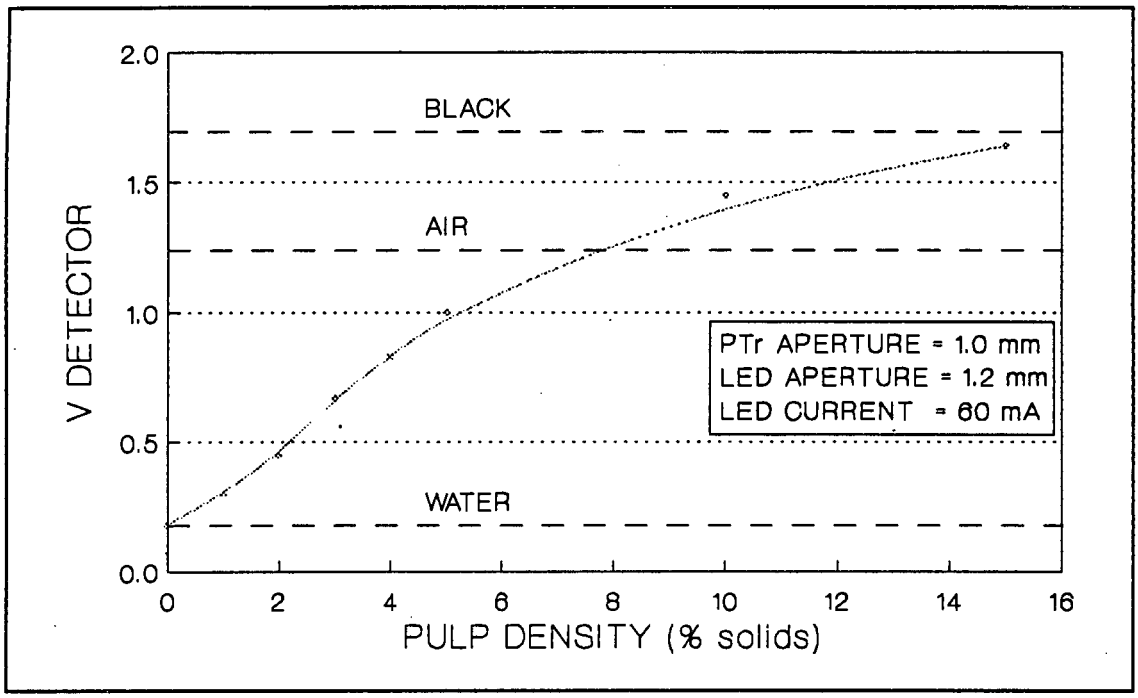

FIGURE A1.3 : Collector Voltage vs Slurry Density

When a slurry (three-phase system) is used it must be determined whether the detectors register a higher or lower light intensity for the slurry than for air. For correct operation of the 'gate' circuit (Figure A1.5) the bubble must result in a high going pulse at the detector amplifier output. For this reason the optional inversion of the signal at this stage in the circuit is provided for. The detector amplifiers may be either AC or DC coupled (switch selectable) and are provided with both gain (1 to 10) and zero offset adjustments. The smaller the differential between bubble and liquid phase signals the higher the gain required. The zero offset is adjusted such that bubble detection is indicated by the flashing of the panel indicator LEDs. Experience has shown that DC, rather than AC, amplifier coupling gives more reliable operation. This mode also allows static measurements to be made for the liquid and air phases.

The primary function of the 'gate' circuit is to generate a bubble velocity pulse. This is done by toggling a flip-flop on, on the leading edge of the pulse from the first (lower) detector and off as from the leading edge of the pulse from the second (upper) detector. The flip-flop output pulse width represents the velocity of the bubble provided that the two leading edges mentioned were created by the same bubble travelling up the tube. In the case of very small (broken) bubbles or bubbles not properly detected by

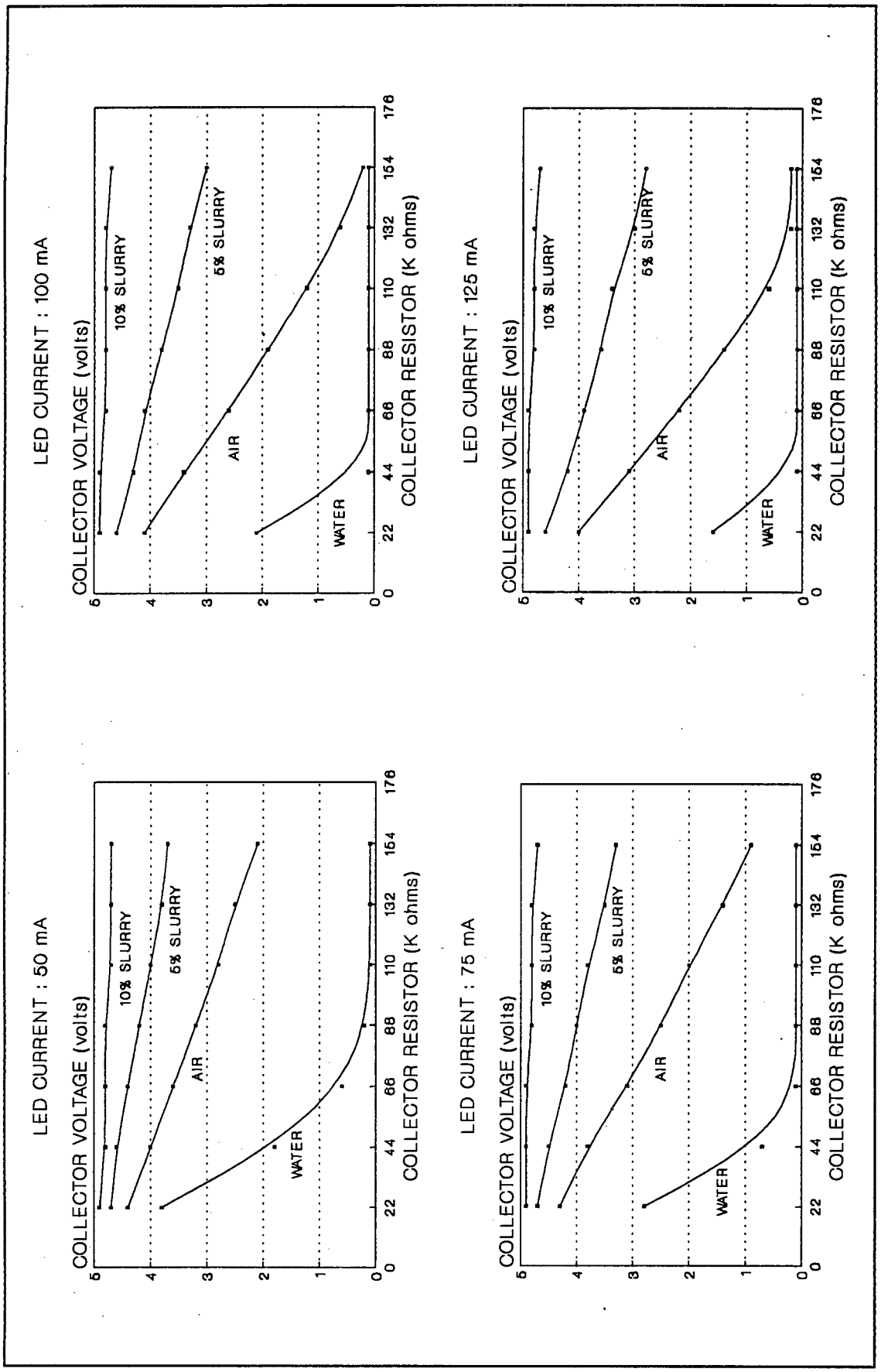

FIGURE A1.4 : Detector Characteristics

the optics, incorrect values will be recorded. Analysis of large amounts of data has shown this to occur in less than 2% of the readings, provided that the optics have been properly aligned. These spurious values are rejected by the data processing software.

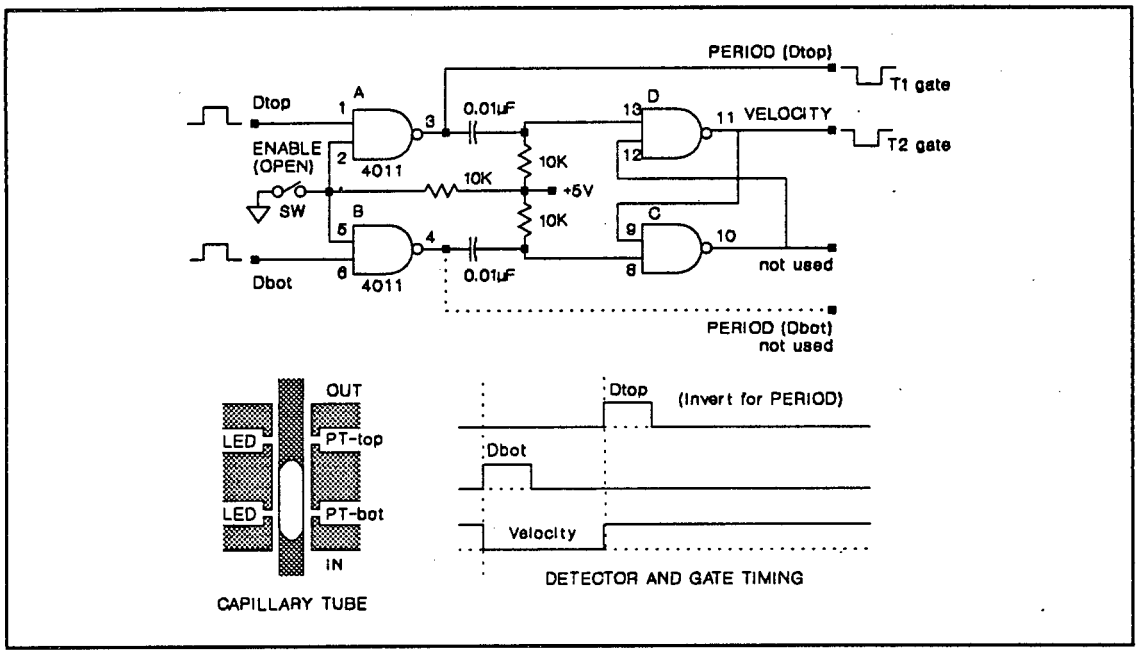

FIGURE A1.5 : Velocity Pulse Generation Circiut

A1.2 MPU DATA CAPTURE SYSTEM

The single board computer, designed in-house and used for the high speed data capture is based on the Motorola 6809 processor. The unit transmits the data to a PC at the end of the measurement period.

The program is permanently installed in the EPROM (erasable programmable read-only memory). Progress through the following measurement / data-transmission sequence is indicated by the successive illumination of 6 LEDs.

LED 1	: Ready	Waiting for first bubble
LED 2	: Sampling	Data logging active
LED 3	: Buffer Warning	Buffers 3/4 full
LED 4	: End of Measurement	Buffers full (or terminated)
LED 5	: Data Transmission	Data to PC
LED 6	: End of Job	Data acknowledged by the PC

Only two push button inputs are provided, one to initialize the system to the 'Ready' state and a second to manually terminate data collection (during phase 2 or 3).

The pulse timing functions are performed by the M6840 programmable timer chip. This device has three independent, 16 bit timers. Timers 1 and 2 are initialized in the 'period measurement mode', with interrupt generation enabled, and are used to measure the period and velocity pulse widths respectively. In this mode the timers are pre-loaded to maximum count (2^{16}) and decremented at the system clock frequency (1.5 Mhz) during the low going gate pulses. At the end of the gate pulse an interrupt is generated and the interrupt service routine reads and stores the current state of that counter. This read operation automatically reloads the counter for the next timing operation. The 1.5 Mhz clock frequency gives a resolution of 65.1 μs/count. The period of the measured pulse is therefore as follows;

$$\text{Period} = (2^{16} - \text{Count}) \times 65.1\ \mu s.$$

Timer 3 is initialized to 'continuous' mode counting with an external clock (from 150 baud clock). This results in a count rate of 3 ms and it is read and stored at each interrupt to establish the real time of the measuring events.

The measured data is stored in 32K bytes of RAM. As each bubble requires 8 bytes of storage (4 x 16 bit values : Period and Real time + Velocity and Real time), a total of about 4000 bubbles may be recorded. At a typical bubble rate of 20 s^{-1} this measurement cycle takes 200 seconds.

In addition to the memory and timer a peripheral interface adaptor (PIA) is installed to drive the LED indicators and read the input push switches. An asynchronous communication interface adaptor (ACIA) (serial port) is installed to allow communications with the PC.

A1.3 SOFTWARE

The system software comprises of three sections; the EPROM resident data capture routines for the M6809 processor, the file creation program which

accepts the data transmitted by the microprocessor unit (MPU) system, and data processing program which analyses the data files. All PC programs were written in Borland's Turbo Pascal (Version 5). This compiler produces fast and efficient code and has excellent graphics functions, which were essential for the data processing program.

A1.3.1 MPU SYSTEM

The M6809 routines were written in Assembler code as it was I/O intensive and speed was of primary importance. This code comprises of two distinct sections:

- The main line initializes the hardware, executes an idling loop during the data collection operation and subsequently transmits the contents of the data buffers to the PC via a simple send and acknowledge protocol.
- The actual timer measurements are recorded by the interrupt service routine. The task of this routine is to poll the timer to determine which channel generated the interrupt, read and store that channel together with the real time as read from timer 3. The recording of the bubble period and velocity pulse lengths are therefore treated as completely independent events by the program.

A1.3.2 PC DATA CAPTURE

The data capture program receives the timing data from the MPU system and stores it in record files for subsequent processing.

At start up the program verifies communications with the MPU system and then prompts for a data file 'core' name e.g. BUBDAT. Files are then sequentially created as BUBDAT1.BUB, BUBDAT2.BUB etc. Once the program is thus initialized all subsequent control is effected remotely from the MPU system

The buffers (period, velocity, time-period, time-velocity) are received sequentially and the block sizes indicated on the screen. The size of the

period block usually exceeds the size of the velocity block (for the reasons previously mentioned) by a few per cent. An abnormally large discrepancy is a indication of poorly aligned optics, a slurry system with unfavourable optical characteristics or a dilute system with large particles which are being detected as bubbles.

A1.3.3 DATA PROCESSING

The 16 bit data stored in record files by the data-capture system, are used by the data analysis program to create four sets of calibrated data. These values are stored in memory resident arrays to increase the speed of data manipulation, which necessitates the installation of 640K RAM in the PC used for data analysis. The four data arrays represent the period and velocity pulse widths (μs) and their real times (ms).

A1.3.4 DATA-MATCHING TECHNIQUE

The data-matching technique associates the independently measured bubble periods and velocities, which is essential for the calculation of bubble volumes. On completion of this matching procedure, spurious velocity measurements are rejected on the basis of a specified number of standard deviations from the mean velocity. The rejected values in the velocity array are replaced by the mean velocity value.

As previously discussed, small or broken bubbles may result in the number of volume pulses exceeding the number of velocity pulses. The real time of each measurement is also recorded and this is used as a means of assigning a velocity to each period pulse recorded. The technique for doing this is outlined below.

i.) The difference (N) between the number of period and the number of velocity pulses is determined. As mentioned previously if a good experimental technique is employed this difference (N) should be reasonably small.

ii.) In order to find a velocity measurement which was made at the same real time as a specific period measurement, a search of the bubble velocity measurements is made in the range N as shown in Figure A1.6.

iii.) If a velocity pulse within 5 ms (± 1 count) of the period pulse is found no further comparisons are made. This was found to increase the speed of data processing. If no velocity pulse could be found in this range, then the velocity pulse which occurred closest to the time at which the period pulse occurred was used.

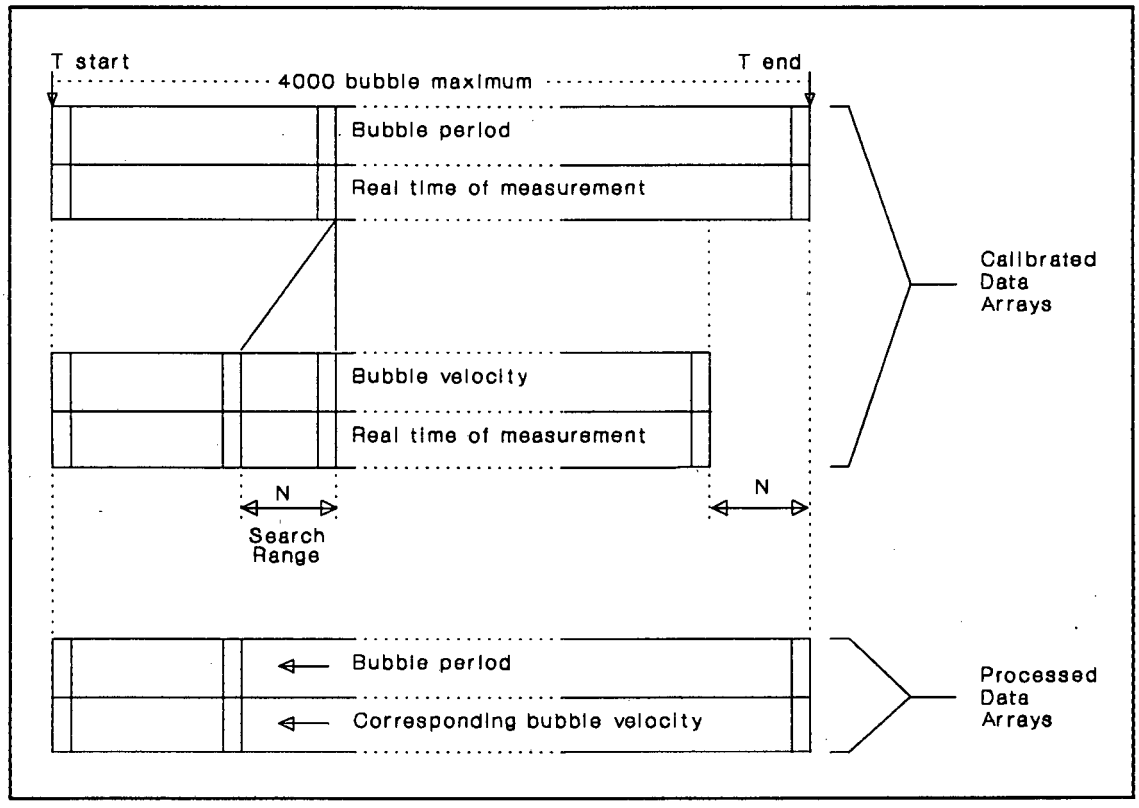

FIGURE A1.6 : Data Matching Technique

A1.3.5 VOLUME CALCULATIONS

While the bubble is in the capillary it is assumed to be cylindrical. This assumption is usually quite valid provided that the cylinders are significantly larger than the capillary bore. Thus the following calculations can be made. For a single bubble

$$u_i = L_d/T_i$$

where u_i = velocity of the bubble in $mm \cdot s^{-1}$, L_d = length between the detectors in mm and T_i = period of the velocity pulse in s, and

$$V_i = u_i \cdot P_i \cdot A$$

where V_i = volume of the bubble, P_i = measured bubble period and A = cross-sectional area of the capillary. By substituting we get:

$$V_i = (L_d/T_i)P_i \cdot A$$

and by rearrangement

$$V_i = L_d \cdot A \cdot (P_i/T_i)$$

where $L_d \cdot A$ is a constant dependent on the dimensions of the capillary and detectors.

Accurate determination of A is not easy to made. However the constant product ($L_d \cdot A$) may be calculated from the known data as follows:

$$\Sigma V_i = \Sigma L_d \cdot A(P_i/T_i)$$

$$\Sigma V_i = L_d \cdot A \times \Sigma (Pi/Ti)$$

$$L_d \cdot A = \Sigma V_i / \Sigma (P_i/T_i)$$

where ΣV_i = total bubble volume (burette) and P_i and T_i = data measured by the system for each bubble.

The volume of each individual bubble may therefore be calculated from the following equation:

$$V_i = (P_i/T_i) \times L \cdot dA$$

The results obtained for V_i yield the volume distribution of the bubbles at the pressure and temperature in the capillary tube. This will also be the distribution at normal pressure and temperature conditions. Hence the

number of bubbles of a particular volume at normal conditions, i.e. the conditions at which the total volume is measured in the gas burette, is obtained. Indeed the individual bubble volumes can be obtained at any set of pressure/temperature conditions (e.g. the conditions at the point of capture) by adjusting the total gas volume using the ideal gas law. In making the volume calculations, no account has been taken of the head of water/slurry at the point of capture. This difference has been shown to be insignificantly small under normal operating conditions. The bubble diameters are calculated assuming the bubbles to be spherical.

A1.3.6 GRAPHICAL OUTPUT

The large number of bubbles sampled means that the results of the above analysis are most conveniently presented graphically. The data is presented graphically in two forms.

1.) Variable vs variable. This form allows the user to plot any of the following variables against any other.

- Time
- Velocity pulse
- Period pulse
- Bubble volumes
- Bubble diameters

These plots can be used for experimental diagnostics, or for transient experiments.

2.) Frequency distributions. A frequency distribution of any of the above variables is possible. The most useful are bubble volume and diameter distributions, for which the mean and standard deviation are calculated and presented.

An example of a bubble size distribution histogram is shown in Figure A1.7. This was obtained using a 10% quartz slurry. Also indicated are the mean bubble size and the standard deviation.

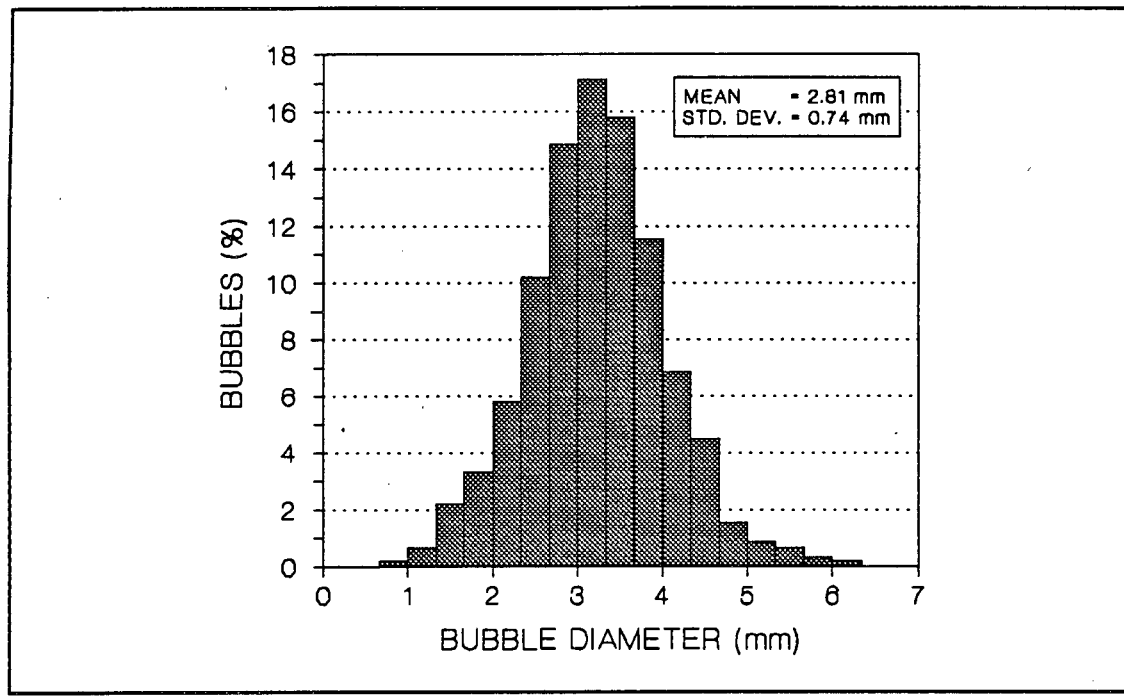

FIGURE A1.7 : Bubble Size Distribution Histogram

A1.4 OPERATING PROCEDURES

A flowsheet of the operating procedures for the bubble sizing system is shown in Figure A1.8.

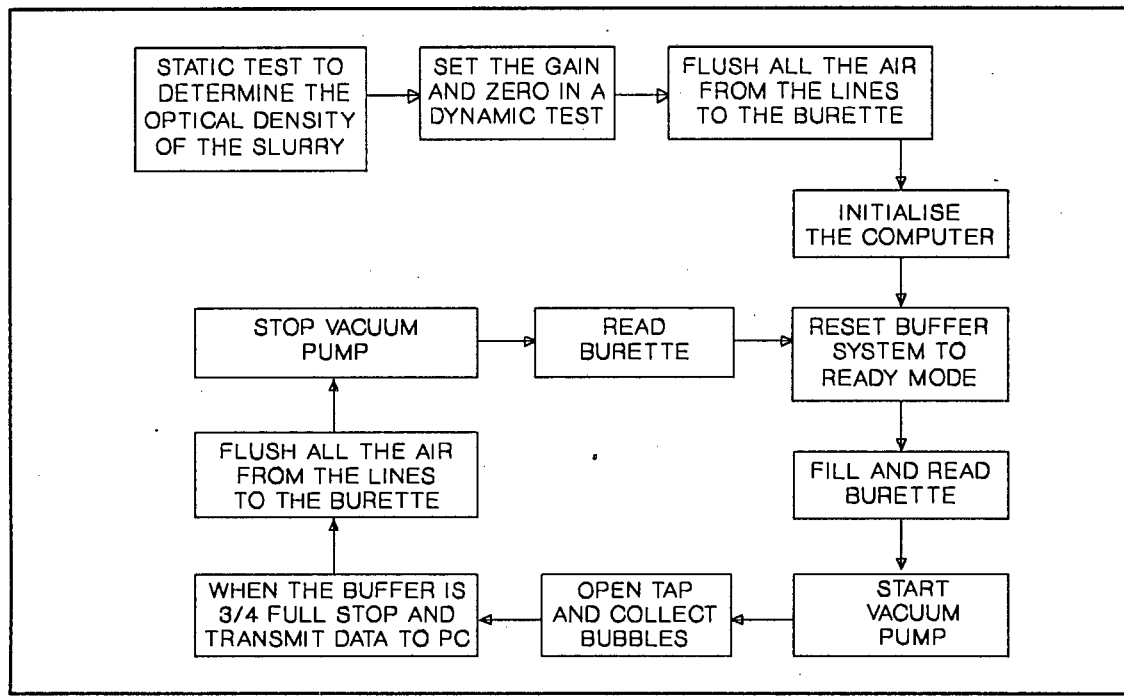

FIGURE A1.8 : Bubble System Operating Procedures

A1.5 OPERATING CONDITIONS

In order to determine the operating conditions under which reliable measurements could be made, a series of tests was performed in which capillaries with three different bell inlet diameters were used under varying vacuums. For these experiments all other conditions were kept constant, thus ensuring constant bubble sizes. The results are summarized in Table A1.1 and are plotted in Figure A1.9. Each diameter value shown represents the average of three separate experiments. Similarly each standard deviation value represents the average of three standard deviations of bubble diameter values. For each bell diameter the results were considered valid if the data point lay on the flat region of the bubble diameter vs vacuum curve shown in Figure A1.9, i.e. the region in which the measured diameter is independent of the applied vacuum. For the 5 mm bell, which was slightly larger than the recommended size, there was no flat region and the results were considered invalid for the particular bubbles generated in this experiment.

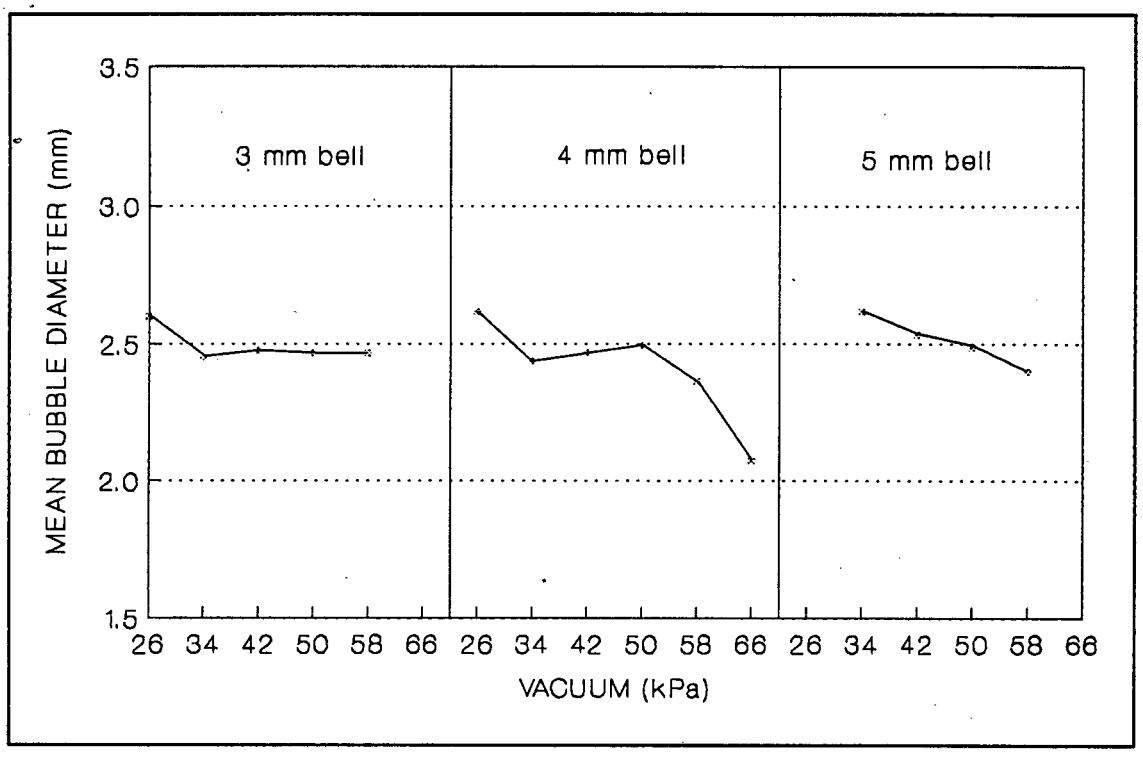

FIGURE A1.9 : Vacuum and Bell Size vs Bubble Size

Further evidence of the validity of the data may be obtained by examining the size distribution histograms. The valid data have an approximately normal distribution whereas poor experimental conditions show a skewed

distribution. Under extreme conditions two peaks may be obtained due to either coalescence (large bell and/or low vacuum) resulting in 'double bubbles', or breakage (small bell and/or high vacuum) resulting in 'half bubbles'.

The results in Table A1.1 show that the bubble diameters obtained were independent of the bell size and applied vacuum over a wide range of conditions.

TABLE A1.1 : Effect of Applied Vacuum and Inlet Bell Diameter on Mean Bubble Size

BELL SIZE (mm)	VACUUM (kPa)	AVERAGE DIAMETER (mm)	DIFFERENCE (%)	AVERAGE STD. DEV. (mm)	VALID (?)	VALID DIAMETER (mm)
5	34	2.617	0.3	0.623	NO	
5	42	2.533	0.4	0.613	NO	
5	50	2.490	0.5	0.617	NO	
5	58	2.400	0.8	0.743	NO	
4	26	2.617	0.5	0.613	NO	
4	34	2.437	1.1	0.657	YES	2.467
4	42	2.470	1.7	0.660	YES	2.467
4	50	2.493	1.1	0.630	YES	2.467
4	58	2.363	7.9	0.727	NO	
4	66	2.073	20.8	0.903	NO	
3	26	2.600	0.3	0.680	NO	
3	34	2.453	0.3	0.677	YES	2.466
3	42	2.477	0.3	0.713	YES	2.466
3	50	2.467	0.3	0.707	YES	2.466
3	58	2.467	0.3	0.687	YES	2.466

Appendix 2

CONTINUOUS FROTH CUTTING TESTS - RAW DATA

TABLE A2.1 : Continuous Froth Cutting Tests. Effect of Pulp Density for Pyrite/Quartz Without Wash Water

	PULP DENSITY (% sol)	CONC (/min)	TAILS (/min)	SEGMENT 1	2	3	4	TOTAL
PARTICLE	20	30.6	287.8	1.66	1.78	1.92	2.52	7.88
MASS	15	22.8	216.6	1.26	1.42	1.63	2.10	6.41
(g)	10	16.1	142.7	0.83	0.90	0.99	1.40	4.12
WATER	20	347.5	926	19.2	21.1	23.1	27.3	90.7
MASS	15	317.9	1038	17.8	20.4	23.6	26.7	88.5
(g)	10	291.1	1138	16.9	19.8	22.9	26.2	85.8
SOLIDS/	20	0.088	0.311	0.086	0.084	0.083	0.092	0.087
WATER	15	0.072	0.209	0.071	0.070	0.069	0.079	0.072
RATIO	10	0.055	0.125	0.049	0.045	0.043	0.053	0.048
AIR	20			77.2	74.9	72.5	67.4	73.0
HOLD-UP	15			78.9	75.8	72.0	68.2	73.7
(%)	10			80.1	76.6	73.0	69.0	74.7
	20	21.9	22.7	22.4	22.9	23.5	27.5	24.4
d50 (µm)	15	22.7	22.6	23.0	25.1	25.9	27.9	25.8
	10	23.1	22.5	24.6	26.0	27.3	28.2	26.8
GRADE	20	37.6	1.9	36.2	34.2	26.3	20.6	28.3
(% S)	15	34.3	2.3	34.0	29.2	22.6	17.2	24.7
	10	28.6	2.7	28.5	22.1	18.6	14.1	19.8
RECOVERY	20	67.8						
(%)	15	61.3						
	10	54.4						

TABLE A2.2 : Continuous Froth Cutting Tests. Effect of Air Rate for Pyrite/Quartz Without Wash Water

	AIR RATE cm/s)	CONC (/min)	TAILS (/min)	SEGMENT 1	2	3	4	TOTAL
PARTICLE	1.5	31.7	287.1	1.48	1.56	1.68	2.22	6.94
MASS	1.2	30.6	287.8	1.66	1.78	1.92	2.52	7.88
(g)	0.9	29.7	288.3	1.78	1.90	2.12	2.75	8.55
WATER	1.5	329.8	946	15.8	17.2	18.9	23.6	75.5
MASS	1.2	347.5	926	19.2	21.1	23.1	27.3	90.7
(g)	0.9	358.1	913	21.6	24.1	27.5	30.6	103.8
SOLIDS/	1.5	0.096	0.304	0.094	0.091	0.089	0.094	0.092
WATER	1.2	0.088	0.311	0.086	0.084	0.083	0.092	0.087
RATIO	0.9	0.083	0.315	0.082	0.079	0.077	0.090	0.082
AIR	1.5			81.2	79.5	77.4	71.8	77.5
HOLD-UP	1.2			77.2	74.9	72.5	67.4	73.0
(%)	0.9			74.4	71.4	67.3	63.5	69.1
	1.5	21.6	22.7	22.0	22.5	23.2	26.9	24.0
d50 (µm)	1.2	21.9	22.7	22.4	22.9	23.5	27.5	24.4
	0.9	22.3	22.6	22.5	23.1	23.6	27.8	24.6
GRADE	1.5	32.7	2.3	31.6	28.8	22.6	17.2	24.2
(% S)	1.2	37.6	1.9	36.2	34.2	26.3	20.6	28.4
	0.9	40.8	1.7	39.8	36.9	30.1	21.6	30.9
RECOVERY	1.5	61.0						
(%)	1.2	67.8						
	0.9	71.5						

TABLE A2.3 : Continuous Froth Cutting Tests. Effect of Frother Concentration for Pyrite/Quartz Without Wash Water.

	FROTHER CONC (ppm)	*CONC (/min)*	*TAILS (/min)*	SEGMENT 1	2	3	4	TOTAL
PARTICLE	100	*30.6*	*287.8*	1.66	1.78	1.92	2.52	**7.88**
MASS	75	*29.3*	*289.4*	1.80	1.95	2.09	2.55	**8.39**
(g)	50	*24.2*	*293.9*	1.01	1.26	1.48	2.67	**6.42**
WATER	100	*347.5*	*926*	19.2	21.1	23.1	27.3	**90.7**
MASS	75	*245.7*	*1029*	15.7	18.4	20.9	21.8	**76.8**
(g)	50	*180.7*	*1092*	8.3	11.5	14.7	21.4	**55.9**
SOLIDS/	100	*0.088*	*0.311*	0.086	0.084	0.083	0.092	**0.087**
WATER	75	*0.119*	*0.281*	0.115	0.106	0.100	0.117	**0.109**
RATIO	50	*0.134*	*0.269*	0.122	0.110	0.101	0.125	**0.115**
AIR	100			77.2	74.9	72.5	67.4	**73.0**
HOLD-UP	75			81.2	78.0	75.1	73.8	**77.0**
(%)	50			90.0	86.2	82.4	74.3	**83.2**
	100	*21.9*	*22.7*	22.4	22.9	23.5	27.5	**24.4**
d50 (µm)	75	*19.9*	*22.9*	21.3	22.7	23.5	27.2	**24.0**
	50	*18.2*	*23.0*	20.1	22.6	23.4	26.9	**24.2**
GRADE	100	*37.6*	*1.9*	36.2	34.2	26.3	20.6	**28.4**
(% S)	75	*43.6*	*1.5*	42.9	38.7	32.1	23.8	**33.5**
	50	*35.1*	*2.9*	34.6	33.1	30.2	26.7	**30.0**
RECOVERY	100	*67.8*						
(%)	75	*75.2*						
	50	*50.1*						

TABLE A2.4 : Continuous Froth Cutting Tests. Effect of Froth Height for Pyrite/Quartz Without Wash Water

	FROTH HEIGHT (mm)	*CONC (/min)*	*TAILS (/min)*	SEGMENT 1	2	3	4	TOTAL
PARTICLE	360	*15.4*	*302.1*	0.63	0.77	0.87	0.95	**3.22**
MASS	240	*20.3*	*298.3*	0.89	0.93	0.98	1.06	**3.86**
(g)	120	*30.6*	*287.8*	1.66	1.78	1.92	2.52	**7.88**
WATER	360	*217.8*	*1052*	8.9	10.7	11.9	12.6	**44.1**
MASS	240	*253.1*	*1021*	11.0	11.2	11.8	27.3	**46.6**
(g)	120	*347.5*	*926*	19.2	21.1	23.1	27.1	**90.7**
SOLIDS/	360	*0.071*	*0.287*	0.071	0.072	0.073	0.075	**0.073**
WATER	240	*0.080*	*0.292*	0.081	0.083	0.083	0.084	**0.083**
RATIO	120	*0.088*	*0.311*	0.086	0.084	0.083	0.092	**0.087**
AIR	360			89.4	87.3	85.9	85.0	**86.9**
HOLD-UP	240			86.9	86.7	86.0	67.9	**81.9**
(%)	120			77.2	74.9	72.5	67.3	**73.0**
	360	*23.6*	*22.5*	23.8	24.1	24.3	24.5	**24.2**
d50 (µm)	240	*23.0*	*22.6*	23.3	23.6	24.0	24.1	**23.8**
	120	*21.9*	*22.4*	22.4	22.9	23.5	27.5	**24.4**
GRADE	360	*34.5*	*2.0*	34.3	33.2	31.9	31.1	**32.4**
(% S)	240	*35.3*	*2.2*	35.2	33.7	32.3	31.2	**33.0**
	120	*37.6*	*2.4*	36.2	34.2	26.3	20.6	**28.4**
RECOVERY	360	*31.4*						
(%)	240	*42.2*						
	120	*67.8*						

TABLE A2.5 : Continuous Froth Cutting Tests. Effect of Pulp Density for Pyrite/Quartz With Wash Water

	PULP DENSITY (% sol)	CONC (/min)	TAILS (/min)	SEGMENT 1	2	3	4	TOTAL
PARTICLE	20	*27.1*	*291.3*	1.19	1.40	1.73	2.18	**6.50**
MASS	15	*18.7*	*220.3*	0.90	1.09	1.41	1.82	**5.22**
(g)	10	*12.9*	*146.8*	0.62	0.75	0.91	1.17	**3.45**
WATER	20	*510.1*	*1323*	28.2	29.9	30.5	31.3	**119.9**
MASS	15	*507.6*	*1407*	27.6	28.2	29.1	30.4	**115.3**
(g)	10	*502.3*	*1495*	26.1	27.4	28.6	29.8	**111.9**
SOLIDS/	20	*0.053*	*0.220*	0.042	0.047	0.057	0.070	**0.054**
WATER	15	*0.037*	*0.157*	0.033	0.039	0.048	0.060	**0.045**
RATIO	10	*0.026*	*0.098*	0.024	0.027	0.032	0.039	**0.031**
AIR	20			66.5	64.4	63.6	62.4	**64.2**
HOLD-UP	15			67.2	66.5	65.3	63.6	**65.6**
(%)	10			69.1	67.5	66.0	64.5	**66.8**
	20	*18.8*	*23.0*	19.4	20.4	22.4	23.5	**21.8**
d50 (µm)	15	*21.1*	*22.7*	21.4	22.8	24.1	25.4	**23.9**
	10	*22.8*	*22.6*	22.9	23.7	24.4	25.8	**24.5**
GRADE	20	*41.2*	*2.0*	40.9	38.0	33.1	24.5	**32.7**
(% S)	15	*41.9*	*2.2*	41.6	35.3	27.6	23.0	**30.0**
	10	*39.2*	*2.4*	38.2	33.2	26.0	20.8	**28.0**
RECOVERY	20	*65.8*						
(%)	15	*61.5*						
	10	*59.4*						

TABLE A2.6 : Continuous Froth Cutting Tests. Effect of Air Rate for Pyrite/Quartz With Wash Water

	AIR RATE (cm/s)	CONC (/min)	TAILS (/min)	SEGMENT 1	2	3	4	TOTAL
PARTICLE	1.5	*28.2*	*290.2*	1.15	1.36	1.62	2.07	**6.20**
MASS	1.2	*27.1*	*291.3*	1.19	1.40	1.73	2.18	**6.50**
(g)	0.9	*26.1*	*291.6*	1.25	1.49	1.81	2.25	**6.80**
WATER	1.5	*513.3*	*1320*	27.8	29.1	30.0	31.3	**118.2**
MASS	1.2	*510.1*	*1323*	28.2	29.9	30.5	31.3	**119.9**
(g)	0.9	*501.4*	*1329*	29.0	29.7	30.6	31.9	**121.2**
SOLIDS/	1.5	*0.055*	*0.220*	0.041	0.047	0.054	0.066	**0.052**
WATER	1.2	*0.053*	*0.220*	0.042	0.047	0.057	0.070	**0.054**
RATIO	0.9	*0.052*	*0.219*	0.043	0.050	0.059	0.071	**0.056**
AIR	1.5			66.9	65.3	64.2	62.4	**64.7**
HOLD-UP	1.2			66.5	64.4	63.6	62.4	**64.2**
(%)	0.9			65.5	64.6	63.4	61.7	**63.8**
	1.5	*19.1*	*22.9*	19.7	20.6	23.0	23.9	**22.2**
d50 (µm)	1.2	*18.8*	*22.9*	19.4	20.4	22.4	23.5	**21.8**
	0.9	*18.4*	*22.9*	19.1	20.2	21.7	22.8	**22.8**
GRADE	1.5	*39.0*	*2.1*	38.5	35.6	30.9	22.7	**30.6**
(% S)	1.2	*41.2*	*2.0*	40.9	38.0	33.1	24.5	**32.7**
	0.9	*44.9*	*1.8*	44.4	42.1	36.9	25.8	**35.8**
RECOVERY	1.5	*64.8*						
(%)	1.2	*65.8*						
	0.9	*69.2*						

TABLE A2.7 : Continuous Froth Cutting Tests. Effect of Frother Concentration for Pyrite/Quartz With Wash Water

	FROTHER CONC (ppm)	*CONC (/min)*	*TAILS (/min)*	SEGMENT 1	2	3	4	TOTAL
PARTICLE	25	*27.1*	*291.3*	1.19	1.40	1.73	2.18	**6.50**
MASS	20	*20.0*	*298.8*	1.01	1.16	1.33	1.64	**5.14**
(g)	15	*13.7*	*303.5*	0.86	0.98	1.19	1.42	**4.45**
WATER	25	*510.1*	*1323*	28.2	29.9	30.5	31.3	**119.9**
MASS	20	*507.4*	*1327*	27.6	28.6	29.7	30.5	**116.4**
(g)	15	*503.5*	*1325*	26.5	27.6	28.3	29.1	**111.5**
SOLIDS/	25	*0.053*	*0.220*	0.042	0.047	0.057	0.070	**0.054**
WATER	20	*0.039*	*0.225*	0.037	0.041	0.045	0.054	**0.044**
RATIO	15	*0.027*	*0.229*	0.032	0.036	0.042	0.049	**0.040**
AIR	25			66.5	64.4	63.6	62.4	**64.2**
HOLD-UP	20			67.2	66.0	64.6	63.5	**65.3**
(%)	15			68.5	67.2	66.3	65.3	**66.8**
	25	*18.8*	*22.9*	19.4	20.4	22.4	23.5	**21.8**
d50 (µm)	20	*18.1*	*22.9*	19.3	20.9	22.3	24.1	**21.9**
	15	*17.0*	*22.9*	18.2	19.5	21.8	23.5	**22.5**
GRADE	25	*41.2*	*2.0*	40.9	38.0	33.1	24.5	**32.7**
(% S)	20	*40.7*	*3.0*	40.6	37.6	32.9	25.9	**33.2**
	15	*33.2*	*4.1*	33.0	31.7	30.1	27.4	**30.2**
RECOVERY	25	*65.8*						
(%)	20	*47.9*						
	15	*26.9*						

TABLE A2.8 : Continuous Froth Cutting Tests. Effect of Froth Height for Pyrite/Quartz With Wash Water

	FROTH HEIGHT (mm)	*CONC (/min)*	*TAILS (/min)*	SEGMENT 1	2	3	4	TOTAL
PARTICLE	360	*19.9*	*297.8*	0.90	0.94	0.99	1.05	**3.88**
MASS	240	*23.9*	*293.9*	1.06	1.10	1.15	1.22	**4.53**
(g)	120	*27.1*	*291.3*	1.19	1.40	1.73	2.18	**6.50**
WATER	360	*483.6*	*1347*	23.7	24.7	26.1	27.6	**102.1**
MASS	240	*493.9*	*1337*	24.1	24.9	26.7	28.7	**104.4**
(g)	120	*510.1*	*1323*	28.2	29.9	30.5	31.3	**119.9**
SOLIDS/	360	*0.041*	*0.221*	0.038	0.038	0.038	0.038	**0.038**
WATER	240	*0.048*	*0.220*	0.044	0.044	0.043	0.043	**0.043**
RATIO	120	*0.053*	*0.220*	0.042	0.047	0.057	0.070	**0.054**
AIR	360			71.8	70.6	69.0	67.2	**69.6**
HOLD-UP	240			71.3	70.3	68.2	65.8	**68.9**
(%)	120			66.5	64.4	63.6	62.4	**64.2**
	360	*21.8*	*22.6*	22.4	22.8	23.2	23.7	**23.0**
d50 (µm)	240	*21.3*	*22.7*	21.7	22.4	22.8	23.0	**22.5**
	120	*18.8*	*22.9*	19.4	20.4	22.4	23.5	**21.8**
GRADE	360	*36.5*	*3.2*	36.3	34.6	32.1	30.3	**33.2**
(% S)	240	*38.2*	*2.7*	38.1	35.3	33.2	31.1	**34.3**
	120	*41.2*	*2.0*	40.9	38.0	33.1	24.5	**32.7**
RECOVERY	360	*42.9*						
(%)	240	*53.9*						
	120	*65.8*						

TABLE A2.9 : Continuous Froth Cutting Tests. Effect of Pulp Density for Unisel With Wash Water

	PULP DENSITY (% sol)	*CONC (/min)*	*TAILS (/min)*	SEGMENT 1	2	3	4	**TOTAL**
PARTICLE	20	*19.9*	*299.2*	0.78	0.95	1.03	1.28	**4.04**
MASS	15	*13.0*	*227.6*	0.60	0.74	0.81	1.06	**3.21**
(g)	10	*9.0*	*151.6*	0.40	0.52	0.58	0.74	**2.24**
WATER	20	*519.9*	*1317*	28.9	30.4	31.0	33.8	**124.1**
MASS	15	*513.7*	*1410*	27.9	29.5	29.9	32.6	**119.9**
(g)	10	*509.1*	*1497*	27.2	28.7	29.1	31.9	**116.9**
SOLIDS/	20	*0.038*	*0.227*	0.027	0.031	0.033	0.038	**0.033**
WATER	15	*0.025*	*0.161*	0.022	0.025	0.027	0.033	**0.027**
RATIO	10	*0.018*	*0.101*	0.015	0.018	0.020	0.023	**0.019**
AIR	20			65.7	63.9	63.1	59.7	**63.1**
HOLD-UP	15			66.9	65.0	64.5	61.2	**64.4**
(%)	10			67.8	66.0	65.5	62.1	**65.4**
	20	*20.8*	*17.9*	20.4	19.9	19.6	18.4	**19.4**
d50 (µm)	15	*19.1*	*18.0*	19.0	18.7	18.5	18.3	**18.6**
	10	*18.2*	*18.1*	18.2	18.1	18.1	17.9	**18.1**
GRADE	20	*19.5*	*0.7*	19.3	18.1	15.9	11.3	**15.6**
(% S)	15	*20.5*	*0.8*	20.2	17.9	14.7	10.9	**15.2**
	10	*19.6*	*0.8*	19.3	17.1	13.4	10.2	**14.3**
RECOVERY	20	*64.0*						
(%)	15	*58.3*						
	10	*57.8*						

TABLE A2.10 : Continuous Froth Cutting Tests. Effect of Air Rate for Unisel With Wash Water

	AIR RATE (cm/s)	*CONC (/min)*	*TAILS (/min)*	SEGMENT 1	2	3	4	**TOTAL**
PARTICLE	1.5	*21.4*	*299.3*	0.67	0.78	0.90	1.12	**3.47**
MASS	1.2	*19.9*	*299.2*	0.78	0.95	1.03	1.28	**4.04**
(g)	0.9	*18.5*	*302.2*	0.93	1.10	1.22	1.53	**4.78**
WATER	1.5	*521.9*	*1321*	28.2	30.0	31.1	33.2	**122.5**
MASS	1.2	*519.9*	*1317*	28.9	30.4	31.0	33.8	**124.1**
(g)	0.9	*514.6*	*1328*	29.1	30.6	31.9	34.5	**126.1**
SOLIDS/	1.5	*0.041*	*0.227*	0.024	0.026	0.029	0.034	**0.028**
WATER	1.2	*0.038*	*0.227*	0.027	0.031	0.033	0.038	**0.033**
RATIO	0.9	*0.036*	*0.228*	0.032	0.036	0.038	0.044	**0.038**
AIR	1.5			66.5	64.4	63.0	60.5	**63.6**
HOLD-UP	1.2			65.7	63.9	63.1	59.7	**63.1**
(%)	0.9			65.4	63.6	62.0	58.8	**62.4**
	1.5	*18.9*	*18.0*	18.8	18.8	18.7	18.3	**18.6**
d50 (µm)	1.2	*20.8*	*18.0*	20.4	19.9	19.6	18.4	**19.4**
	0.9	*24.7*	*17.9*	24.1	23.5	22.1	18.8	**21.8**
GRADE	1.5	*17.2*	*0.8*	16.9	15.4	14.3	10.5	**13.8**
(% S)	1.2	*19.5*	*0.7*	19.3	18.1	15.9	11.3	**15.6**
	0.9	*22.1*	*0.7*	22.4	21.1	17.2	13.6	**17.9**
RECOVERY	1.5	*60.4*						
(%)	1.2	*64.0*						
	0.9	*67.1*						

TABLE A2.11 : Continuous Froth Cutting Tests. Effect of Frother Concentration for Unisel With Wash Water

	FROTHER CONC (ppm)	*CONC (/min)*	*TAILS (/min)*	SEGMENT 1	2	3	4	**TOTAL**
PARTICLE	25	*19.9*	*299.2*	0.78	0.95	1.03	1.28	**4.04**
MASS	20	*12.5*	*307.6*	0.63	0.80	0.92	1.06	**3.41**
(g)	15	*8.7*	*313.4*	0.41	0.56	0.68	0.81	**2.46**
WATER	25	*519.9*	*1317*	28.9	30.4	31.0	33.8	**124.1**
MASS	20	*507.1*	*1333*	29.1	30.9	31.3	34.5	**125.8**
(g)	15	*497.9*	*1350*	28.5	30.6	31.4	34.2	**124.7**
SOLIDS/	25	*0.038*	*0.227*	0.027	0.031	0.033	0.038	**0.033**
WATER	20	*0.025*	*0.231*	0.022	0.026	0.029	0.031	**0.027**
RATIO	15	*0.017*	*0.232*	0.014	0.018	0.022	0.024	**0.020**
AIR	25			65.7	63.9	63.1	59.7	**63.1**
HOLD-UP	20			65.5	63.3	62.8	59.0	**62.6**
(%)	15			66.3	63.7	62.8	59.4	**63.0**
	25	*20.8*	*17.9*	20.4	19.9	19.6	18.4	**19.4**
d50 (µm)	20	*19.2*	*18.1*	19.0	18.8	18.6	18.3	**18.6**
	15	*18.5*	*18.1*	18.5	18.3	18.2	18.2	**18.3**
GRADE	25	*19.5*	*0.7*	19.3	18.1	15.9	11.3	**15.6**
(% S)	20	*18.1*	*1.2*	18.0	17.1	14.5	10.8	**14.6**
	15	*16.6*	*1.5*	16.4	15.2	13.3	10.6	**13.4**
RECOVERY	25	*64.0*						
(%)	20	*37.2*						
	15	*23.6*						

TABLE A2.12 : Continuous Froth Cutting Tests. Effect of Froth Height for Unisel With Wash Water

	FROTH HEIGHT (mm)	*CONC (/min)*	*TAILS (/min)*	SEGMENT 1	2	3	4	**TOTAL**
PARTICLE	360	*12.5*	*308.4*	0.57	0.59	0.63	0.68	**2.47**
MASS	240	*16.8*	*302.2*	0.63	0.66	0.70	0.75	**2.74**
(g)	120	*19.9*	*299.2*	0.78	0.95	1.03	1.28	**4.04**
WATER	360	*491.3*	*1352*	27.4	28.1	29.9	32.4	**117.8**
MASS	240	*503.3*	*1333*	28.0	29.3	30.0	32.0	**119.3**
(g)	120	*519.9*	*1317*	28.9	30.4	31.0	33.8	**124.1**
SOLIDS/	360	*0.025*	*0.228*	0.021	0.021	0.021	0.021	**0.021**
WATER	240	*0.033*	*0.227*	0.023	0.023	0.023	0.023	**0.023**
RATIO	120	*0.038*	*0.227*	0.027	0.031	0.033	0.038	**0.033**
AIR	360			67.5	66.7	64.6	61.6	**65.1**
HOLD-UP	240			66.8	65.3	64.4	62.0	**64.6**
(%)	120			65.7	63.9	63.1	59.7	**63.1**
	360	*18.6*	*18.1*	18.5	18.5	18.4	18.4	**18.4**
d50 (µm)	240	*19.3*	*18.0*	19.1	18.9	18.7	18.6	**18.8**
	120	*20.8*	*17.9*	20.4	19.9	19.6	18.4	**19.4**
GRADE	360	*22.0*	*1.1*	21.9	21.0	20.4	19.8	**20.7**
(% S)	240	*20.6*	*0.9*	20.5	19.8	19.3	18.6	**19.5**
	120	*19.5*	*0.7*	19.3	18.1	15.9	11.3	**15.6**
RECOVERY	360	*45.1*						
(%)	240	*57.1*						
	120	*64.0*						

Appendix 3

FROTH MODEL PARAMETER CALCULATION

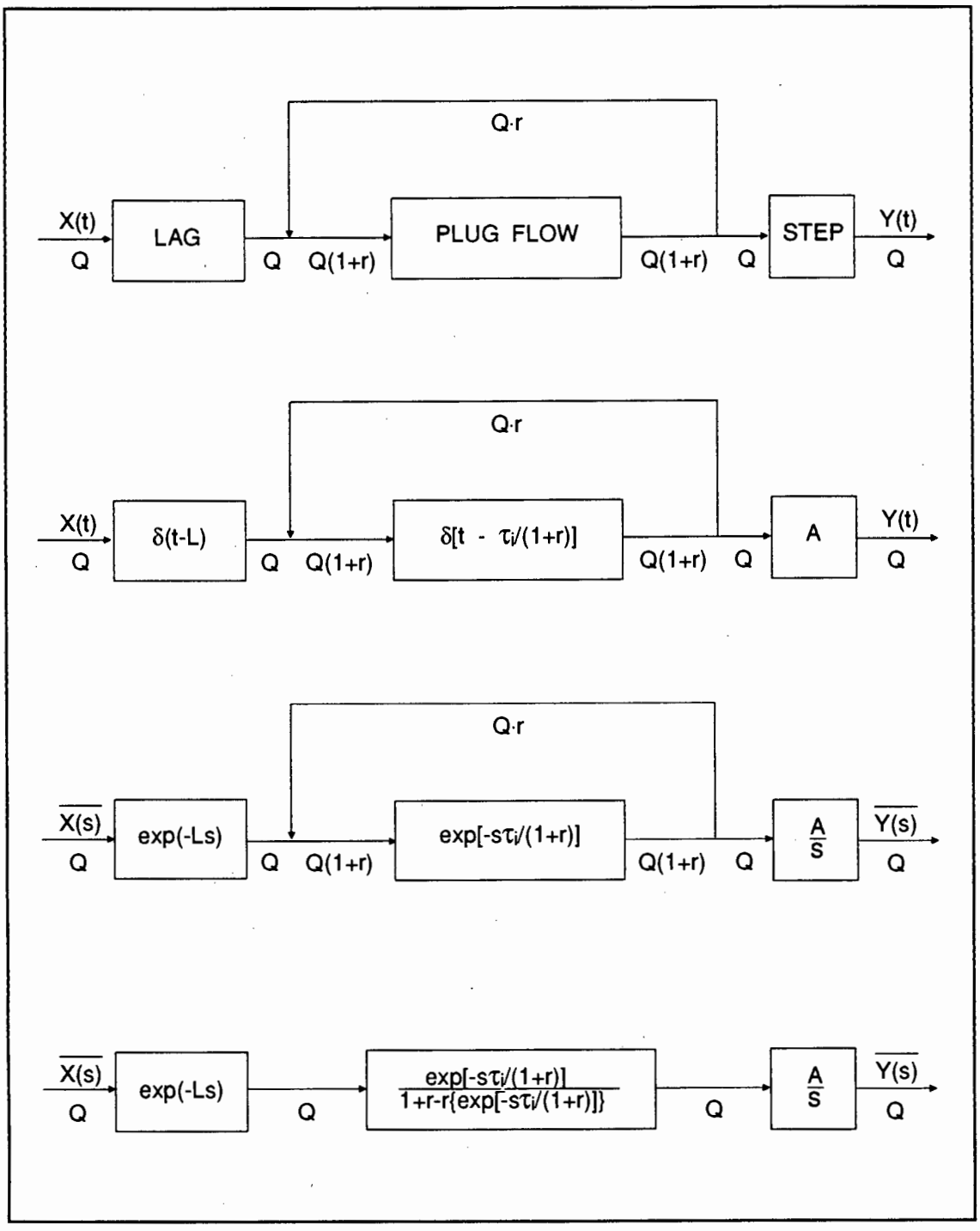

FIGURE A3.1 : Froth Phase Model

For the model:

Mass balance over the reactor with recycle yields the transfer function of the reactor:

$$\overline{W}(s) = \exp(-Ls) \times \frac{\exp[-s\tau i/(1+r)]}{1+r-r\cdot\exp[-s\tau i/(1+r)]} \times \frac{A}{s}$$

Let $K = \tau i/(1+r)$

$$\overline{W}(s) = \frac{A\cdot\exp[-s(L+K)]}{s[1+r-r\cdot\exp(-sK)]}$$

Let $s = \beta + i\omega$

$$\overline{W}(\beta+i\omega) = \frac{A\cdot\exp[-(\beta+i\omega)\cdot(L+K)]}{(\beta+i\omega)\cdot[1+r-r\cdot\exp(-(\beta+i\omega)K)]}$$

For the Laplace transform to exist the integral must be bounded. This condition allows β to be set to 0 (Glasser et al., 1980).

$$\overline{W}(i\omega) = \frac{A\cdot\exp[-i\omega(L+K)]}{i\omega[1+r-r\cdot\exp(-i\omega K)]}$$

But $\exp(-i\theta) = \cos\theta - i\cdot\sin\theta$

$$\overline{W}(i\omega) = \frac{A[\cos\ \omega(L+K) - i\cdot\sin\ \omega(L+K)]}{i\omega[1+r-r\cdot(\cos\ \omega K - i\cdot\sin\ \omega K)]}$$

$$\overline{W}(i\omega) = \frac{A[\cos\,\omega(L+K) - i\cdot\sin\,\omega(L+K)]}{\omega[i(1+r-r\cos\,\omega K) + r\sin\,\omega K]}$$

$$\overline{W}(i\omega) = \frac{A[\cos\,\omega(L+K) - i\cdot\sin\,\omega(L+K)][r\sin\,\omega K - i(1+r-r\cos\,\omega K)]}{\omega[i(1+r-r\cos\,\omega K) + r\sin\,\omega K][r\sin\,\omega K - i(1+r-r\cos\,\omega K)]}$$

$$\overline{W}(i\omega) = \frac{A[r\cos\,\omega(L+K)\sin\,\omega K - \sin\,\omega(L+K)(1+r-r\cos\,\omega K)]}{\omega[(1+r-r\cos\,\omega K)^2 + r^2\sin^2\omega K]}$$

$$- \frac{Ai[r\sin\,\omega(L+K)\sin\,\omega K + \cos\,\omega(L+K)(1+r-r\cos\,\omega K)]}{\omega[(1+r-r\cos\,\omega K)^2 + r^2\sin^2\omega K]}$$

Rearranging and grouping into Real (Re) and Imaginary (Im) parts:

$$\text{Re}\ \overline{W}(i\omega) = \frac{A[r\cos\omega(L+K)\sin\omega K - (1+r)\sin\omega(L+K) + r\sin\omega(L+K)\cos\omega K)]}{\omega[1 +2r +r^2 - 2r\cos\,\omega K - 2r^2\cos\,\omega K +r^2\cos^2\omega K +r^2\sin^2\omega K]}$$

$$\text{Im}\ \overline{W}(i\omega) = \frac{A[r\cos\omega(L+K)\cos\omega K - (1+r)\cos\omega(L+K) - r\sin\omega(L+K)\sin\omega K)]}{\omega[1 +2r +r^2 - 2r\cos\,\omega K - 2r^2\cos\,\omega K +r^2\cos^2\omega K +r^2\sin^2\omega K]}$$

But $\cos A\cdot\sin B + \sin A\cdot\cos B = \sin(A+B)$

$\cos A\cdot\cos B - \sin A\cdot\sin B = \cos(A+B)$

$\sin^2 A + \cos^2 A = 1$

$$\text{Re}\ \overline{W}(s) = \frac{A\cdot[r\cdot\sin\,\omega(L+2K) - (1+r)\cdot\sin\,\omega(L+K)]}{\omega[1 +2r + r^2 - 2r(1 +r)\cos\,\omega K + r^2]}$$

$$\text{Im}\ \overline{W}(s) = \frac{A\cdot[r\cdot\cos\,\omega(L+2K) - (1+r)\cdot\cos\,\omega(L+K)]}{\omega[1 +2r + r^2 - 2r(1 +r)\cos\,\omega K + r^2]}$$

$$\text{Re } \overline{W}(s) = \frac{A\cdot[r\cdot\sin\,\omega(L+2K) - (1+r)\cdot\sin\,\omega(L+K)]}{\omega[1 + 2r(1 + r)(1 - \cos\,\omega K)]} = RW$$

$$\text{Im } \overline{W}(s) = \frac{A\cdot[r\cdot\cos\,\omega(L+2K) - (1+r)\cdot\cos\,\omega(L+K)]}{\omega[1 + 2r(1 + r)(1 - \cos\,\omega K)]} = IW$$

For experimental data; Taking Laplace transforms:

$$\overline{H}(s) = \frac{\overline{Y}(s)}{\overline{X}(s)} = \frac{\int_0^\infty Y(t)\cdot\exp(-st)\,dt}{\int_0^\infty X(t)\cdot\exp(-st)\,dt}$$

Let $s = \beta + i\omega$

$$\overline{H}(\beta+i\omega) = \frac{\overline{Y}(\beta+i\omega)}{\overline{X}(\beta+i\omega)} = \frac{\int_0^\infty Y(t)\cdot\exp[-(\beta+i\omega)t]\,dt}{\int_0^\infty X(t)\cdot\exp[-(\beta+i\omega)t]\,dt}$$

Again let $\beta = 0$

$$\overline{H}(s) = \frac{\int_0^\infty Y(t)\cdot\exp(-i\omega t)\,dt}{\int_0^\infty X(t)\cdot\exp(-i\omega t)\,dt}$$

$$\overline{H}(i\omega) = \frac{\int_0^\infty Y(t)\cdot\cos\,\omega t\,dt - i\cdot\int_0^\infty Y(t)\cdot\sin\,\omega t\,dt}{\int_0^\infty X(t)\cdot\cos\,\omega t\,dt - i\cdot\int_0^\infty X(t)\cdot\sin\,\omega t\,dt}$$

Choose T such that $\int_0^T F(t)\,dt \gg \int_\tau^\infty F(t)\,dt$

$$T = 4(\tau + \sigma^2/\tau) \qquad \text{(Bryson, 1970)}$$

$$\bar{H}(i\omega) = \frac{{}_0\int^T Y(t)\cdot\cos\ \omega t\ dt - i\cdot{}_0\int^T Y(t)\cdot\sin\ \omega t\ dt}{{}_0\int^T X(t)\cdot\cos\ \omega t\ dt - i\cdot{}_0\int^T X(t)\cdot\sin\ \omega t\ dt}$$

Let $a = {}_0\int^T Y(t)\cdot\cos\ \omega t\ dt \qquad b = {}_0\int^T Y(t)\cdot\sin\ \omega t\ dt$

$$c = {}_0\int^T X(t)\cdot\cos\ \omega t\ dt \qquad d = {}_0\int^T X(t)\cdot\sin\ \omega t\ dt$$

$$\bar{H}(i\omega) = \frac{a - ib}{c - id} = \frac{(ac + bd) + i(ad - bc)}{c^2 + d^2}$$

$$\text{Re}\quad \bar{H}(s) = \frac{ac + bd}{c^2 + d^2} = RH$$

$$\text{Im}\quad \bar{H}(s) = \frac{ad - bc}{c^2 + d^2} = IH$$

$$a \cong \sum_{n=1}^{N} \bar{Y}(t)_n \cdot \int_{t(n-1)}^{tn} \cos\ \omega t\ dt$$

$$b \cong \sum_{n=1}^{N} \bar{Y}(t)_n \cdot \int_{t(n-1)}^{tn} \sin\ \omega t\ dt$$

$$c \cong \sum_{m=1}^{M} \bar{X}(t)_m \cdot \int_{t(m-1)}^{tm} \cos\ \omega t\ dt$$

$$d \cong \sum_{m=1}^{M} \bar{X}(t)_m \cdot \int_{t(m-1)}^{tm} \sin\ \omega t\ dt$$

$\bar{Y}(t)_n = [Y(t_n) + Y(t_{n-1})]/2$ and $\bar{X}(t)_m = [X(t_m) + X(t_{m-1})]/2$

$${}_{t(n-1)}\int^{tn} \cos\ \omega t\ dt = (1/\omega)[\sin\ \omega t]_{t(n-1)}^{tn} = (1/\omega)[\sin\ \omega t_n - \sin\ \omega t_{n-1}]$$

$$\int_{t(n-1)}^{tn} \sin \omega t \, dt = -(1/\omega)[\cos \omega t]_{t(n-1)}^{tn} = -(1/\omega)[\cos \omega t_n - \cos \omega t_{n-1}]$$

but $\sin A - \sin B = 2\cos[(A+B)/2]\cdot\sin[(A-B)/2]$

$\cos A - \cos B = -2\sin[(A+B)/2]\cdot\sin[(A-B)/2]$

$$\int_{t(n-1)}^{tn} \cos \omega t \, dt = (2/\omega)[\cos \frac{\omega(t_n+t_{n-1})}{2} \sin \frac{\omega(t_n-t_{n-1})}{2}]$$

$$\int_{t(n-1)}^{tn} \sin \omega t \, dt = (2/\omega)[\sin \frac{\omega(t_n+t_{n-1})}{2} \sin \frac{\omega(t_n-t_{n-1})}{2}]$$

$$a = \sum_{n=1}^{N} \frac{Y(t_n) + Y(t_{n-1})}{\omega} [\sin \frac{\omega(t_n - t_{n-1})}{2} \cdot \cos \frac{\omega(t_n + t_{n-1})}{2}]$$

$t_n - t_{n-1} = \Delta t_n$ and $t_n + t_{n-1} = (2n - 1)\cdot\Delta t_n$

$$a = \sum_{n=1}^{N} \frac{Y(t_n) + Y(t_{n-1})}{2} [\sin \frac{\omega\Delta t_n}{2} \cos \frac{\omega(2n - 1)\Delta t_n}{2}]$$

$$b = \sum_{n=1}^{N} \frac{Y(t_n) + Y(t_{n-1})}{\omega} [\sin \frac{\omega\Delta t_n}{2} \sin \frac{\omega(2n - 1)\Delta t_n}{2}]$$

$$c = \sum_{m=1}^{M} \frac{X(t_m) + X(t_{m-1})}{\omega} [\sin \frac{\omega\Delta t_m}{2} \cos \frac{\omega(2m - 1)\Delta t_m}{2}]$$

$$d = \sum_{m=1}^{M} \frac{X(t_m) + X(t_{m-1})}{\omega} [\sin \frac{\omega\Delta t_m}{2} \cos \frac{\omega(2m - 1)\Delta t_m}{2}]$$

For a fit, the model and experimental data transfer functions must agree over a range of frequencies i.e.:

$$\overline{W}(i\omega_j) \cong \overline{H}(i\omega_j) \qquad \text{for } j = 1, 2, 3, \text{ etc.}$$

For higher frequencies the errors become large and the largest value of j should be chosen such that the error is less than the experimental error. A least squares technique is used to find the best model fit.

$$\varphi = \sum_{j=1}^{J} [(RW - RH)^2 + (IW - IH)^2] = \text{minimum}$$

A Nelder-Mead algorithm (Nelder and Mead, 1965) was used to find φ.

NOMENCLATURE

Roman Symbols

a	Fn(ω,t,Y(t))	
A	Step Change	
A_c	Cross-Sectional Area of the Cell	$[L^2]$
A_{cf}	Cleaning Factor	
A_{xs}	Capillary Cross-Sectional Area	$[L^2]$
b	Fn(ω,t,Y(t))	
c	Fn(ω,t,X(t))	
C	Concentration	$[ML^{-3}]$
C_0	Initial Tracer Concentration	$[ML^{-3}]$
C_f	Concentration in the Froth	$[ML^{-3}]$
C_{fi}	Concentration of Species i in the Froth	$[ML^{-3}]$
C_{Fi}	Classification Function	
C_l	Concentration in the Feed	$[ML^{-3}]$
C_{li}	Concentration of Species i in the Feed	$[ML^{-3}]$
C_{pi}	Solids Concentration of Particle Size i in the Pulp	$[ML^{-3}]$
C_{ti}	Tailings Concentration of Gangue of Particle Size i	$[ML^{-3}]$
C_T	Concentration in the Pulp	$[ML^{-3}]$
C_{Ti}	Concentration of Species i in the Pulp	$[ML^{-3}]$
d	Fn(ω,t,X(t))	
d_b	Bubble Diameter	[L]
d_c	Column Diameter	[L]
d_f	Film Thickness	[L]
d_p	Particle Diameter	[L]
d_{95}	95% Passing Particle Diameter	[L]
D/uL	Vessel Dispersion Number	
D	Dispersion Coefficient	$[L^2T^{-1}]$
D_l	Dispersion Coefficient for Liquid	$[L^2T^{-1}]$
D_p	Dispersion Coefficient for Solids	$[L^2T^{-1}]$
D_r	Radial Dispersion Coefficient	$[L^2T^{-1}]$
D_x	Axial Dispersion Coefficient	$[L^2T^{-1}]$
E	Collision Efficiency	
E_{opt}	Minimum Error	
E_{x1}	Error at x_1	
E_{x2}	Error at x_2	

E_{y1}	Error at y_1	
E_{y2}	Error at y_2	
E(t)	Normalised Concentration at Time t	
E(θ)	Exit Age Distribution Curve.	
g	Acceleration Due to Gravity	$[LT^{-2}]$
G	Air Flow Rate	$[L^3T^{-1}]$
h	Froth Height	[L]
$\overline{H}(s)$	Transfer Function for Experimental Data	
IH	Imaginary Part of $\overline{H}(s)$	
IW	Imaginary Part of $\overline{W}(s)$	
J_d	Downward Bias	$[LT^{-1}]$
J_{df}	Froth Drainage Flux	$[LT^{-1}]$
J_g	Superficial Gas Velocity	$[LT^{-1}]$
J_l	Superficial Liquid Velocity	$[LT^{-1}]$
J_u	Upward Bias	$[LT^{-1}]$
k	Constant	
k'	Effective Rate of Particle Entry into the Froth	$[MT^{-1}]$
k_{b-p}	Particle-Bubble Size Factor	
k_{b-pc}	Critical Particle-Bubble Size Factor	
k_{ci}	Proportionality Constant	$[LM^{-3}]$
k_{cw}	Proportionality Constant	$[LM^{-3}]$
k_f	Fraction of Particles Entering the Froth that are Returned to the Pulp	
k_f''	$k_f/(V_fC_l)$	
k_{fi}	Rate of Particles of Species i Entering the Pulp from the Froth	$[MT^{-1}]$
k_{fi}'	$k_{fi}V_f$	$[ML^3T^{-1}]$
k_{fi}''	$k_{fi}r_o$	$[L^2T^{-1}]$
k_{fw}	Rate of Water Entry into the Froth	$[L^3T^{-1}]$
k_{fw}''	$k_{fw}r_o$	$[L^2T^{-1}]$
k_i	Detachment Rate Constant	$[T^{-1}]$
k_p	Actual Rate of Particle Entry into the Froth	$[MT^{-1}]$
k_p'	k_p/V_p	$[ML^{-3}T^{-1}]$
k_{pi}	Rate of Particles of Species i Entering the Froth	$[MT^{-1}]$
k_r	Rate Constant	$[T^{-1}]$
K	$\tau_i/(1+r)$	
K_c	Dimensionless Constant	
K_s	Particle-Bubble Size Factor	

l	Primary Length Parameter	[L]
L	Lag	
L_c	Column Length	[L]
L_d	Distance Between the Detectors	[L]
L_p	Height in the Pulp Zone of the Column	[L]
m	$Fn(Re_b,d_b,d_c)$	
m_c	Flow Rate of Particles in the Concentrate	$[MT^{-1}]$
$m_{ei}(z_w)$	Mass Flow Rate of Entrained Species i at the Froth Surface	$[MT^{-1}]$
$m_{fi}(z_w)$	Mass Flow Rate of Floated Species i at the Froth Surface	$[MT^{-1}]$
m_i	Mass of Species i	[M]
$m_i(0)$	Mass Flow Rate of Species i into the froth	$[MT^{-1}]$
$m_i(z)$	Mass Flow Rate of Species i at Height z	$[MT^{-1}]$
M_{fi}	Mass of Species i in the Froth	[M]
M_i	Mass of Gangue of Particle Size i in the Froth	[M]
M_{pi}	Mass of Species i in the Pulp	[M]
M_w	Mass of water in the Froth	[M]
n	Constant	
N	Number of Tanks-in-Series	
N_4	Number of Tanks-in-Series for the Top Half of the Pulp Zone	
N_5	Number of Tanks-in-Series for the Whole of the Pulp Zone	
N_B	Number of Particles Colliding with Bubbles	
N_T	Maximum Number of Particles Colliding with Bubbles if Streamlines did not divert particles	
P	$Fn(u,d_c,D_x,D_r)$	
P_i	Period of the Length Pulse	[T]
P_m	Primary Energy Dissipation Rate	$[L^2T^{-3}]$
q_c	Flow Rate of Water in the Concentrate	$[L^3T^{-1}]$
$q_c(z_w)$	Flow Rate of Water at the Froth Surface	$[L^3T^{-1}]$
Q	Volumetric Flow Rate	$[L^3T^{-1}]$
Q_D	Rate of Drainage from the Froth	$[L^3T^{-1}]$
Q_{Di}	Rate of Drainage of Particles of Size i from the Froth	$[L^3T^{-1}]$
Q_{DW}	Rate of Drainage of Water from the Froth	$[L^3T^{-1}]$
Q_f	Volumetric Flow Rate of Froth	$[L^3T^{-1}]$
Q_{Fi}	Concentrate Flow Rate of Particle Size i	$[L^3T^{-1}]$

Q_{Fw}	Concentrate Flow Rate of Water	$[L^3T^{-1}]$
Q_i	Rate of Particles of Size i Entering the froth from the Pulp	$[L^3T^{-1}]$
Q_I	Volumetric Flow Rate of Feed	$[L^3T^{-1}]$
Q_T	Volumetric Flow Rate Tailings	$[L^3T^{-1}]$
Q_W	Volumetric Flow Rate Water in the Concentrate	$[L^3T^{-1}]$
r	Reactor Recycle Ratio	
r_0	Proportionality Constant	$[L^2]$
r_p	Radial Position	[L]
R	Ultimate Recovery	
R'	Stage Recovery	
R_c	Recovery in the Collection Zone	
R_f	Recovery in the Froth Zone	
R_{fc}	Overall Recovery	
R_g	Gangue Recovery	$[MT^{-1}]$
R_t	Recovery at time t	
Re	Reynolds Number	
Re_b	Reynolds Number for a Bubble	
Re_{bs}	Reynolds Number for a Bubble Relative to the Slurry	
RH	Real Part of $\overline{H}(s)$	
RW	Real Part of $\overline{W}(s)$	
s	Laplace Transform Operator	
S	Solids Concentration	$[ML^{-3}]$
S'	$Fn(r_p,d_c,Z)$	
t	Time	[T]
$\bar{t}$	Mean Residence Time	[T]
$\bar{t}_i$	Residence Time in Plug Flow Reactor	[T]
t_{peak}	Normalised Peak Time	
T_i	Period of Velocity Pulse	[T]
u	Superficial Velocity (Solids or Liquid)	$[LT^{-1}]$
u_d	Velocity of the Dispersed Phase	$[LT^{-1}]$
u_i	Velocity of the Bubble	$[LT^{-1}]$
U_b	Bubble Velocity	$[LT^{-1}]$
$U_i(z)$	Drainage Velocity for Species i	$[LT^{-1}]$
U_{sg}	Bubble Velocity Relative to the Slurry	$[LT^{-1}]$
v_i	Velocity of Species i	$[LT^{-1}]$
v(z)	Bubble Rise Velocity	$[LT^{-1}]$
v_∞	Terminal Bubble Rise Velocity	$[LT^{-1}]$

V	Total Bubble Volume	$[L^3]$
V_f	Volume of Froth	$[L^3]$
V_i	Bubble Volume	$[L^3]$
V_p	Volume of Pulp	$[L^3]$
$W(s)$	Transfer Function for Model	
x	Dimensionless Constant	
x_{opt}	Value of x at which the Minimum Error Occurs	
x_p	Axial Position	[L]
$\overline{X}(s)$	Input Laplace Transform	
$X(t)$	Input Function in the Time Domain	
y_{opt}	Value of y at which the Minimum Error Occurs	
$\overline{Y}(s)$	Output Laplace Transform	
$Y(t)$	Output Function in the Time Domain	
z	Height in the Froth	[L]
z_{di}	Level at which Detachment Starts	[L]
z_f	Distance from the Top of the Film	[L]
z_w	Distance from the Froth Surface	[L]
Z	$Fn(x_p,d_c,D_r,D_x)$	

Greek Symbols

α	Fraction of Froth Removed in the Concentrate	
α_f	Liquid Holdup in the Froth	
α_s	Relative Froth Stability	
β	Real Part of s	
γ	Surface Tension	$[MT^{-2}]$
$\Gamma(N)$	Gamma Function	
ε	Gas Holdup	
η	Viscosity	$[ML^{-1}T^{-1}]$
θ	t/τ	
λ	Back Mixing Parameter	
μ	Liquid Viscosity	$[ML^{-1}T^{-1}]$
ρ	Density	$[ML^{-3}]$
ρ_c	Density of the Continuous Phase	$[ML^{-3}]$
ρ_d	Density of the Dispersed Phase	$[ML^{-3}]$
ρ_i	Density of Species i	$[ML^{-3}]$
ρ_l	Density of Liquid	$[ML^{-3}]$

ρ_l	Density of Liquid	$[ML^{-3}]$
σ^2	Variance	
σ_θ^2	σ^2/τ^2	
τ	Mean Residence Time (Pulp or Froth)	[T]
τ_i	Residence Time in Plug Flow Reactor	[T]
φ	Least Squares Function	
ω	Imaginary Part of s	

Abbreviations

AC	Alternating Current
ACIA	Asynchronous Communication Interface Adaptor
ADM	Axial Dispersion Model
CSTR	Continuous Stirred Tank Reactor
DC	Direct Current
EPROM	Erasable Programmable Read Only Memory
I/O	Input/Output
LED	Light Emitting Diode
MPU	Microprocessor Unit
PC	Personal Computer
PIA	Peripheral Interface Adaptor
PTr	Photo Transmitter
PZC	Point of Zero Charge
RAM	Random Access Memory
T-I-S	Tanks-in-Series